1991-09

Study of the transition to turbulence within a curved rectangular channel with 40 to 1 aspect ratio.

Fuqua, Steven Jay

Monterey, California. Naval Postgraduate School

NAVAL POSTGRADUATE SCHOOL
Monterey, California

THESIS

STUDY OF THE TRANSITION TO TURBULENCE WITHIN A CURVED RECTANGULAR CHANNEL WITH 40 TO 1 ASPECT RATIO

by

Steven J. Fuqua

September 1991

Thesis Advisor: Phillip M. Ligrani
Thesis Co-Advisor: Chelakara S. Subramanian

Approved for public release; distribution is unlimited.

REPORT DOCUMENTATION PAGE

1a. REPORT SECURITY CLASSIFICATION Unclassified	1b. RESTRICTIVE MARKINGS
2a. SECURITY CLASSIFICATION AUTHORITY	3. DISTRIBUTION/ AVAILABILITY OF REPORT Approved for public release; distribution is unlimited.
2b. DECLASSIFICATION/DOWNGRADING SCHEDULE	
4. PERFORMING ORGANIZATION REPORT NUMBER(S)	5. MONITORING ORGANIZATION REPORT NUMBER(S)
6a. NAME OF PERFORMING ORGANIZATION Naval Postgraduate School 6b. OFFICE SYMBOL *(If Applicable)* 34	7a. NAME OF MONITORING ORGANIZATION Naval Postgraduate School
6c. ADDRESS *(city, state, and ZIP code)* Monterey, CA 93943-5000	7b. ADDRESS *(city, state, and ZIP code)* Monterey, CA 93943-5000
8a. NAME OF FUNDING/SPONSORING ORGANIZATION Propulsion Directorate 6b. OFFICE SYMBOL *(If Applicable)*	9. PROCUREMENT INSTRUMENT IDENTIFICATION NUMBER MIPR C-30030-P
8c. ADDRESS *(city, state, and ZIP code)* US Army Aviation R/T Act. AVSCOM NASA-Lewis; Cleveland, OH 45433	10. SOURCE OF FUNDING NUMBERS PROGRAM ELEMENT NO. / PROJECT NO. / TASK NO. / WORK UNIT ACCESSION NO.

11. TITLE *(Include Security Classification)*
STUDY OF THE TRANSITION TO TURBULENCE WITHIN A CURVED RECTANGULAR CHANNEL WITH 40 TO 1 ASPECT RATIO

12. PERSONAL AUTHOR(S)
Fuqua, Steven Jay

13a. TYPE OF REPORT	13b. TIME COVERED	14. DATE OF REPORT *(year, month,day)*	15. PAGE COUNT
Master's Thesis	FROM 1/91 TO 9/91	September 1991	178

16. SUPPLEMENTARY NOTATION
The views expressed in this thesis are those of the author and do not reflect the official policy or position of the Department of Defense or the U.S. Government.

17. COSATI CODES			18. SUBJECT TERMS *(continue on reverse if necessary and identify by block number)*
FIELD	GROUP	SUBGROUP	Dean vortices, centrifugal instabilities, turbulence, rectangular curved channel, laminar/turbulent transition

19. ABSTRACT *(Continue on reverse if necessary and identify by block number)*

Longitudinal turbulence intensity and streamwise mean velocity variations are studied from measurements using single-sensor hot-wire probes at Dean numbers from 50 to about 450 in a curved rectangular channel with 40 to 1 aspect ratio, mild curvature, and an inner to outer radius ratio of 0.979. Measured results show significant increases in the longitudinal turbulence intensity as the Dean number increases above 150. These increases are first apparent near the concave surface in upwash regions between individual vortices which make up each vortex pair. Such increases correspond closely with twisting vortex motions, which is important in regard to transition from laminar to turbulent flow because these variations provide evidence that twisting results in the first important increases in turbulence energy at a given location as the Dean number increases.

20. DISTRIBUTION/AVAILABILITY OF ABSTRACT [X] UNCLASSIFIED/UNLIMITED [ ] SAME AS RPT. [ ] DTIC USERS	21. ABSTRACT SECURITY CLASSIFICATION Unclassified
22a. NAME OF RESPONSIBLE INDIVIDUAL Professor Ligrani	22b. TELEPHONE (Include Area Code) (408) 646-3382 22c. OFFICE SYMBOL

Approved for public release; distribution is unlimited.

Study of the Transition to Turbulence Within a Curved Rectangular Channel with 40 to 1 Aspect Ratio

by

Steven Jay Fuqua
Lieutenant, United States Navy
B.S., Tennessee Technological University, 1984

Submitted in partial fulfillment of the
requirements for the degree of

MASTER OF SCIENCE IN MECHANICAL ENGINEERING

from the

NAVAL POSTGRADUATE SCHOOL

September 1991

ABSTRACT

Longitudinal turbulence intensity and streamwise mean velocity variations are studied from measurements using single-sensor hot-wire probes at Dean numbers from 50 to about 450 in a curved rectangular channel with 40 to 1 aspect ratio, mild curvature, and an inner to outer radius ratio of 0.979. Measured results show significant increases in the longitudinal turbulence intensity as the Dean number increases above 150. These increases are first apparent near the concave surface in upwash regions between individual vortices which make up each vortex pair. Such increases correspond closely with twisting vortex motions, which is important in regard to transition from laminar to turbulent flow because these variations provide evidence that twisting results in the first important increases in turbulence energy at a given location as the Dean number increases.

TABLE OF CONTENTS

LIST OF FIGURES

NOMENCLATURE

C	Temperature Correction Function
CCPF	Curved Channel Poiseuille Flow
d	Channel Height, $(r_o\text{-}r_i)$
De	Dean Number, $(Re_d)\sqrt{d/r_i}$
e	Streamwise Velocity Perturbation
E, E_{meas}	Mean Output Voltage from Anemometer Bridge
E_{corr}	Temperature Corrected Bridge Output Voltage
E_{oc}	Zero Velocity Intercept of Best-Line Fit of Calibration Data
OHR	Overheat Ratio
R_c	Hot-Wire Cold Resistance
Re_d	Reynolds Number Based on Channel Height
Re_τ	Reynolds Number Based on Friction Velocity and Channel Half-Height
R_H	Hot-Wire Hot Resistance
r_i	Curved Channel Inside Radius
r_o	Curved Channel Outside Radius
T_{cal}	Freestream Temperature at Time of Calibration
T_∞	Freestream Temperature at Commencement of Surveys
T_{meas}	Freestream Temperature as it Varies with Time
U_{bulk}	Bulk Mean Velocity Used to Determine De
u_{CCPF}	Streamwise Velocity Assuming CCPF
$\overline{u}$	Streamwise Mean Velocity
U	Instantaneous Velocity, $\overline{u} + u'$

u_τ	Friction Velocity
u^+	Wall Coordinate for Streamwise Mean Velocity, u / u_τ
$\overline{u'^2}$	Longitudinal Reynolds Normal Stress
X/d	Normalized Streamwise Direction
y^+	Wall Coordinate in Radial Direction, $Y u_\tau / \nu$
Y/d	Normalized Radial Direction
Z/d	Normalized Spanwise Direction

Greek Symbols

α	Temperature Coefficient of Resistance for Hot-Wire Probe
δ	Channel Half-Height, $d/2$
ρ	Density
ν	Kinematic Viscosity
θ	Streamwise Location from Start of Curvature
τ_w	Shear Stress at the Wall

ACKNOWLEDGMENT

I would like to express my appreciation to those who made this work possible. Particularly, Professor Ligrani who provided inspiration and guidance from the very beginning and Professor Subramanian who never hesitated in coming to my aid, providing the technical know-how needed to get me through. Most of all, I would like to thank my family, Kathi, Steven and Matthew, without whose support and encouragement none of this would have been possible. Thank you.

I. INTRODUCTION

Curved channels with rectangular cross-sections are important in regard to a number of components of interest to the U.S. Navy. Such channels exist within heat exchangers used in applications ranging from gas turbine engines to steam power plants. Curved cooling passages with rectangular cross-sections are also present within interior portions of gas turbine blades. Results from the curved channel study are also applicable to situations in which unbounded flows move over concave surface curvature (i.e., concave sides of gas turbine blades and airfoils) because the physical phenomena in the two situations are very similar. The present work is important for these applications first, because it provides information to designers constructing such facilities, secondly, because it provides basic information needed by researchers who are developing prediction schemes for these channels, and thirdly, because it provides new physical insight into the behavior of fluid dynamics and heat transfer phenomena in these practical applications.

A. BACKGROUND

Flow in a curved rectangular channel is characterized by the Dean number, defined as the Reynolds number based on channel height d and bulk streamwise velocity times a curvature factor equal to $(d/r_i)^{1/2}$, where r_i is the radius of the convex surface.

$$De = Re_d \sqrt{\frac{d}{r_i}} \qquad \{1.1\}$$

At a given streamwise location, flow is two-dimensional and laminar at low Dean numbers. This is curved channel Poiseuille flow. Dean [Ref. 1], using analytical means, first demonstrated that curved channel flow is unstable to small amplitude disturbances for $De > 36$. Above this critical Dean number, pairs of counter-rotating vortices develop in

the laminar flow as the primary instability. Brewster *et al.* [Ref. 2] experimentally found pairs of steady counter-rotating vortices for conditions when the channel is unstable to small amplitude disturbances, providing experimental verification of the theoretical work by Dean. Numerical work by Finlay [Ref. 3] predicts these vortices become unstable at higher *De* to two types of travelling waves, resulting in two kinds of wavy vortex flows, referred to as undulating Dean vortex flow and twisting Dean vortex flow. The first photographic evidence of vortex motions believed to be twisting is presented by Ligrani and Niver [Ref. 4]. However, the first mention of experimentally observed waviness is given by Kelleher *et al.* [Ref. 5]. Additional evidence of wavy vortex flow is given by Matsson and Alfredsson for a curved channel, with and without rotation [Refs. 6, 7]. Ligrani *et al.* [Ref. 8] present additional experimental evidence of wavy vortex motions associated with undulating and twisting and compare these results with numerical predictions. Numerical simulations by Moser and Moin [Ref. 9] predict the behavior of longitudinal turbulence intensity in a curved channel with fully turbulent flow. A recent work by Bottaro *et al.* [Ref. 10] considers the spatial development of the flow in a curved channel from experimental measurements and using three-dimensional finite-volume simulations.

The present study continues efforts by Niver [Ref. 11], Baun [Ref. 12], Longest [Ref. 13], Fields [Ref. 14] and Kendall [Ref. 15] on the same curved channel. Niver's flow visualization results provided the first photographic evidence of twisting and undulating vortex flow. Baun continued this work by studying the time-averaged flow field and power spectra for Dean numbers from 50 to 250. Longest's flow visualization results provided photographic evidence of vortex pair merging and splitting at Dean numbers of 75 and 100. Fields conducted a comprehensive study in a cleaner, or less disturbed flow, for Dean numbers from 35 to 425 that showed evidence of vortex pairs to a

higher Dean number than previously observed by Baun. Kendall conducted a detailed analysis of merging and splitting phenomena for Dean numbers from 60 to 150. Kendall also focussed on unsteady Dean vortex pair behavior as evidenced by spectra and correlation measurements.

The present study is motivated by the fact that little is known about the character of longitudinal turbulence intensity in laminar and transitioning curved channel flows. Of particular interest is the relationship between twisting and local increases of the longitudinal Reynolds normal stress.

B. OBJECTIVES

The primary objective of this study is to investigate the variations in the longitudinal turbulence intensity as they occur at different locations in the channel over a range of Dean numbers. These data are intended to give insight into transition to a fully turbulent flow from a laminar flow containing a spanwise array of vortex pairs. Particular attention is devoted to twisting and its relation to local increases of longitudinal normal Reynolds stress.

C. ORGANIZATION

The material in this thesis is organized as follows. Chapter II describes the curved channel and equipment used for measurement of surveys and near wall profiles. Chapter III describes the experimental procedures used. Experimental results are presented in Chapter IV. Summary and conclusions are presented in Chapter V. Figures are presented in Appendix A and Appendix B presents a software directory of the programs used. Appendix C provides a directory of the data files generated in support of this work.

II. EXPERIMENTAL APPARATUS

The apparatus used in this study are located in the laboratories of the Mechanical Engineering Department of the Naval Postgraduate School. They primarily consist of a transparent curved channel, a data acquisition system and a traversing mechanism.

A. CURVED CHANNEL

The curved channel is described in detail by Ligrani and Niver [Ref. 4]. A schematic illustration and photograph of the facility are shown in Figures 1 and 2, respectively. A brief discussion of the facility follows.

1. Description of the Facility

The channel is an open-circuit suction facility developed to study transitional flows. At the inlet, an aluminum honeycomb and three screens reduce spatial non-uniformities in the flow. These are followed by a two-dimensional nozzle with a 20 to 1 contraction ratio that accelerates the flow into a 2.44 meter long straight duct [Ref. 8]. The duct is followed by a curved test section shown schematically in Figure 3. The 180 degree curved section is followed by another 2.44 meter long straight duct, a honeycomb, several screens, a diffuser, then an outlet plenum. The outlet plenum is connected to a second plenum using 50.8 mm diameter tubing. This second plenum is maintained at a low pressure by a 1/3 horsepower blower manufactured by ICG Industries, Inc. The blower is connected to the second plenum using a flexible coupling to prevent motor vibrations from affecting the upstream flow. A globe valve between the plenums is used to adjust the flow rate.

The test probe is inserted into the flow through a slot in the convex wall of the test section at a streamwise location 120° from the start of curvature. The slot is 0.32 cm

wide, 7.62 cm long and is aligned in the spanwise direction 5.08 cm from the channel centerline. A support block (see Figures 4 and 5) made of polycarbonate (15.24 cm by 6.35 cm by 2.22 cm) is joined using epoxy to the wall surrounding the slot to maintain the wall's dimensional integrity and to minimize the deflection of the curved wall in the vicinity of the slot. Foam is used to line the slot to allow probe insertion with no air leakage into the test section [Ref. 8]. This arrangement allows the probe to be positioned at different locations within a spanwise/radial plane.

2. Cleaning the Channel

The small scale disturbances leading to transition are believed to be initiated at the nozzle inlet or in the boundary layers developing along the nozzle. Dust buildup on the walls of the flow management unit and on the walls of the channel itself are thus a concern because these may create disturbances which affect transition behavior. According to Saric [Ref. 16], wall discontinuities with heights of 0.3-0.6 microns can have severe effects on transition development in a channel. To minimize this problem, the channel and inlet section were cleaned using a commercial glass cleaner with ammonia (Windex) and a lint free cloth. Changes to the flow resulting from this cleaning are described in Section IV D.

B. PROBES, ELECTRONICS AND DATA ACQUISITION SYSTEM

The present study employs hot-wire anemometry for the measurement of turbulence and unsteady laminar flows. Perry [Ref. 17] describes principles of hot-wire anemometer operation. According to him, an electric current is passed through a fine filament that is exposed to a cross flow. As the flow rate varies, the heat transfer from the filament varies. This, in turn, causes a variation in the heat balance of the filament. There are two modes of operation of a hot-wire system, constant current and constant temperature. The constant temperature mode is used in this study. Here, the filament is placed in a feedback circuit that tends to maintain the wire at a constant resistance, and hence, constant temperature.

Fluctuations in the cooling of the filament are then seen as variations in wire current. The current is sensed by placing the filament in a resistance bridge so that variations in current result in changes in the bridge output voltage. Using appropriate calibration relationships, this voltage is related to the flow velocity.

The data acquisition system and probe traverse are shown schematically in Figure 6. Specific components are described in detail in the following section.

1. Hot-wire Probes

DANTEC type 55P14 and DANTEC type 55P04 probes are used in these experiments. These probes are shown in Figure 7 [Ref. 18]. The sensors of these probes are 90% platinum - 10% rhodium wire with a 5 μm diameter. The active length of each wire is 1.25 mm. The overall length of the sensors and plated end wires of type 55P14 probes is 1.25 mm and the overall wire length of type 55P04 probes is 3 mm. The cold resistance of each wire is about 4 - 5 ohms and an overheat ratio of 1.8 is used in all experiments. The temperature coefficient of resistance, α, is 0.0036 ohms/°C. Each probe is mounted using a DANTEC type 55H21 probe support, and is positioned in the channel as shown in Figure 4.

2. Hot-wire Anemometer Bridge

A DANTEC model 55M10 constant temperature bridge is used to operate the hot-wires with a HF FILTER setting of 2 and GAIN ADJUST setting of 4. The hot-wire is connected to the bridge using a 5 meter long BNC cable. Dynamic response is verified using the .3 kHz square wave generator within the bridge. Typically, the "-3 dB" point (frequency at which mean square response has fallen to half its nominal value) is about 125 kHz. Actual system response is less, however, because frequency response is most often limited by the spatial resolution of the probe [Ref. 19]. The anemometer has two BNC cable connectors for analog signal output. One output is connected as an input to the

signal conditioner and the second output is connected directly to an oscilloscope to provide a visual indication of the voltage signal from the hot-wire bridge.

3. Signal Conditioner

A DANTEC model 56N20 signal conditioner is used to amplify and low pass the bridge output prior to analog-to-digital (A/D) conversion. A gain of 2 (with 0 offset voltage) is used to provide a dynamic signal within the ± 10 V range of the analog-to-digital converter. The high pass filter is set to DC, and the low pass filter is set to 1 kHz for Dean numbers up to 275 and to 3 kHz for Dean numbers beyond 275. The LP filter was used to remove spurious electronic noise from the bridge output and to prevent aliasing. To minimize attenuation of the data signal, the low pass filter setting was changed at Dean number of 275 based on power spectra for similar flow conditions from Fields [Ref. 14]. At the higher Dean numbers, the turbulence energy levels are insignificant at frequencies beyond 3 kHz.

4. Analog-to-Digital Converter

The analog signal from the signal conditioner is digitized using a Hewlett-Packard 6944A Series 200 Multiprogrammer with a buffered 69759A A/D card capable of 12-bit binary resolution. As configured, the multiprogrammer can support two channels, however only one channel is used for this study. Sample size and sampling frequency for each data point are specified so that accurate time-averaged magnitudes of flow properties are obtained. Throughout this experiment, a total of 20,000 samples are acquisitioned at each data point. At low Dean numbers (less than 275), a total sampling frequency of 5,000 Hz is used for two channels (2,500 Hz per channel), resulting in a total of 8 seconds of sampled data at each measurement point. For higher Dean numbers (275 and above), a total sampling frequency of 5,000 Hz per channel is used, resulting in 4 seconds of data at each measurement point.

The gain and offset of the data acquisition system are measured using procedures described by Green [Ref. 20]. The offset for the channel employed is found by shorting the signal conditioner input and then recording the output from the analog-to-digital converter. The system gain for a particular channel is found by inputting a 1.5 kHz sinusoidal signal of known RMS voltage and comparing this value to the RMS voltage at the output of the analog-to-digital converter. Typical values for gain and offset are 1.918 and -0.006, respectively.

5. Microcomputer

A HP series 9000 Model 310 computer is used to collect and process data from the A/D converter. With the available memory, the computer is capable of storing and processing only about 5000 samples of data. To obtain 20,000 samples for each measured point, the data acquisition software collects data in batches of 5000, processes them, stores intermediate results, and then repeats this process four times. The HP series 9000 Model 310 computer is also used to control the probe traversing equipment. Data processing is done using the software HOTWIREu described in Appendix B.

6. Temperature Measurement

The temperature of the flow entering the curved channel is measured using a T-type copper-constantan thermocouple connected to a low-speed data acquisition system, which is shown schematically in Figure 8. This system is entirely independent from the high-speed system mentioned above. The calibration characteristics of the thermocouple are shown in Figure 9. From this calibration, the relationship between voltage and temperature is approximated using a third-order polynomial given by:

$$T(°C) = 9.5767 - 1.0241e{+}4\,E(V) + 4.5290e{+}7\,E(V)^2 - 1.9205e{+}10\,E(V)^3 \quad \{2.1\}$$

Temperatures are measured at 10 minute intervals during most of the experiments using the program TEMPMEAS run on a second HP series 9000 Model 310 computer.

C. PROBE TRAVERSING DEVICES

1. Survey Apparatus

Surveys of streamwise mean velocity and longitudinal Reynolds stress are made over a 0.35 inch by 2.0 inch spanwise/radical plane normal to the streamwise direction. This plane is divided into 328 grid locations (8 radial by 41 spanwise) spaced 0.05 inch apart in both directions. During a survey, the probe is positioned at each of these positions using an automated two-dimensional traversing mechanism shown in Figures 10 and 11. Within this mechanism, the probe is attached to a mount which is secured to a travelling block that is moved in the radial and spanwise directions by two lead screws, each with 20 threads-per-inch pitch. The lead screws are rotated using D.C. stepping motors (SLO-SYN M092-FD310) that are controlled by a MODULYNX MITAS type PMS085-C2AR controller and driven by a MODULYNX MITAS type PMS085-D050 drive [Ref. 20]. The controller is linked to the microcomputer through a built-in RS-232 interface. The motor controller is operated in the remote mode, which allows probe traversing commands to be executed from the data acquisition software program HOTWIREu.

2. Near Wall Apparatus

Near wall profiles are obtained using the same data acquisition system mentioned above, and a slightly modified version of the same traverse. The 20 thread-per-inch rod for the radial component of motion is replaced with one with 100 threads-per-inch pitch. The hardware components are shown in Figures 12 and 13. Additionally, the travelling block used to mount the probe is constructed as to minimize the effect of backlash, and software is altered to account for the new threaded rod. With these modifications, the resolution of the radial position is increased by a factor of 5.

The near-wall profiles are difficult to obtain due to the proximity of probes to the channel wall and the fragile nature of the hot-wire probes. The sensors of the probes employed for this part of the study were constructed in-house. To accomplish this, DANTEC 55P04 probe mounts were employed, to which silver-plated platinum (90%)-rhodium (10%) wire was soldered. The silver coating was then etched to expose a 1.25 mm active length using a 40% nitric acid solution in distilled water. During the etching process, a current of about 100 mA was passed through the sensing wire.

III. EXPERIMENTAL PROCEDURES

A. HOT-WIRE CALIBRATION

The hot-wire probes are calibrated in an open circuit subsonic wind tunnel using procedures for low velocity measurement described by Ligrani and Bradshaw [Ref. 19]. The velocity calibration is performed by placing hot-wire probes in the flow with individual wires oriented normal to the flow. The mean velocity, U, is varied from 1 to 10 m/s and the corresponding bridge output voltage is then recorded.

Typical results are shown in Figure 14. Here the data is shown with $E^2 - E_{oc}^2$ plotted against $U^{0.45}$, where E is the mean voltage and E_{oc} is the zero velocity intercept of the best-fit line (not the actual zero-flow voltage). At moderate velocities, the relationship is linear and may be approximated by:

$$U^{0.45} = \frac{1}{B}\left(E^2 - E_{oc}^2\right) \qquad \{3.1\}$$

where B is a calibration constant.

At lower velocities, the calibration data is assumed to be non-linear. Ligrani and Bradshaw [Ref. 19] have found that hot-wires of this type exhibit linear behavior for $Re_d \geq 0.07$, where Re_d is the Reynolds number based on wire diameter. For velocities below this limit, they propose a third-order polynomial relationship of the form:

$$\alpha = a_0 + a_1\beta + a_2\beta^2 + a_3\beta^3 \qquad \{3.2\}$$

where $\alpha = U^{0.45}$, $\beta = E^2 - E_{oc}^2$ and a_0, a_1, a_2 and a_3 are calibration constants. The calibration constants are determined so that equations {3.1} and {3.2} form a continuous

function as α varies. When data are processed, only equation {3.1} is employed in the form of a look-up table as the lowest Re_d encountered was greater than 0.07.

Before each calibration, the electronics are allowed to warm up to steady-state condition. The cold resistance is obtained with flow past the probe, then an overheat ratio of 1.8 is applied. During calibration, the HF FILTER and GAIN ADJUST of the DANTEC 55M01 bridge are adjusted to optimize frequency response of the probe. A HF FILTER setting of 2 and GAIN ADJUST of 4 were determined to be the best choice for optimal response.

B. DEAN NUMBER DETERMINATION

The flow rate or Dean number is set by referring to the pressure drop across a standard 1.5 inch ASME orifice plate. The details of this procedure are presented by Fields [Ref. 14]. For all runs prior to run number 070391.2145[1], the pressure drop was measured with a 0 - 0.5 inch range Meriam model 40GD10WM inclined tube manometer or a 0 - 4 inch range Meriam model 40HE35WM inclined tube manometer. For run number 070391.2145, and all runs thereafter, the pressure drop was measured with a 0 - 2 inch Validyn model PS309 digital manometer. The digital manometer is preferred because it yields good accuracy over all Dean numbers of interest.

C. MEASUREMENT OF DEAN NUMBER SURVEYS

1. Procedures

Details of the measurement procedures used to obtained the surveys are now discussed. At the beginning of these procedures, the DANTEC probe holder is placed into

---

[1]Run numbers are specified in a MMDDYY.hhmm format, where MM, DD, and YY indicate the month, day and year of the run and hh and mm indicate the hour and minute of the run. This convention is used throughout this study.

the probe mounting block which is attached to a travelling block on the traverse. The travelling block is then located as close to the curved channel as possible. This probe holder is visually aligned with the slot with the foam removed. Foam is ordinarily located in the slot located in the convex wall to prevent air leakage around the probe as it traversed through the spanwise/radial plane. The hot-wire probe is then inserted into the holder and then carefully guided through the slot and positioned so that the probe is located at a radial location of $Y/d = 0.1$. Continuity of the wire is subsequently verified using the DANTEC bridge. Afterwards, the foam is replaced into the convex wall slot.

With the probe now in the flow, the cold resistance, R_c, is measured using the DANTEC bridge. The hot resistance, R_H, may then be calculated using an equation of the form:

$$R_H = R_c \times OHR \qquad \{3.3\}$$

where OHR is the overheat ratio. This operating resistance is set on the bridge and the bridge is placed in the "operate" mode.

Data collection begins with the probe 0.05 inches from the concave wall ($Y/d = 0.1$) at the first spanwise position which is at $Z/d = 4.0$ or 2.0 inches from the spanwise centerline of the channel. As the survey continues, the probe moves towards the convex wall in 0.05 inch steps. Eight radial steps are made at each spanwise location. To move to the next spanwise position the probe is moved 0.1 inch in the negative spanwise direction, then 0.05 inch in the reverse (or positive) spanwise direction, and then it is repositioned radially to a location 0.05 inches from the concave surface. This positioning procedure is used to reduce the effects of leadscrew backlash and ensure repeatable data regardless of the direction of spanwise probe movements [Ref. 4].

At each probe position within the channel, 20,000 samples are taken. Afterwards, the data are processed and the probe is moved to the next station. After the probe is moved to each new station, measurements are delayed 10 seconds to allow any unsteadiness introduced into the flow by the probe movements to dissipate. Approximately 8 hours are required to complete a survey of 328 points. During the survey, the temperature of the air entering the channel is recorded so that corrections can be made later to account for ambient temperature variations.

2. Data Reduction

a. Calculation of Turbulence Statistics

As previously mentioned, the collection of 20,000 samples at each node is done in 4 loops, each containing 5000 samples. Turbulence statistics are calculated and averaged for each loop; the averages from the four loops are then averaged. The turbulence statistics are calculated as follows:

$$\bar{u} = S_u$$

$$\overline{u'^2} = S_{uu} - S_u S_u \qquad \{3.4\}$$

where:

$$S_u = \frac{1}{20{,}000} \sum_{loop=1}^{4} \sum_{sample=1}^{5{,}000} U$$

$$S_{uu} = \frac{1}{20{,}000} \sum_{loop=1}^{4} \sum_{sample=1}^{5{,}000} UU \qquad \{3.5\}$$

In these equations, U is the instantaneous velocity ($U = \bar{u} + u'$).

b. Temperature Drift Correction

According to Perry [Ref. 17], one of the most important sources of error in hot-wire measurements is the failure to account correctly for mean ambient temperature variations. Ideally, measurements should be taken at the same temperature as the calibration (i.e., if variations are within ±1/2°C throughout calibration and measurement procedures, corrections are unnecessary).

The velocity surveys were performed days, sometimes weeks, following calibration and the surveys themselves require about 8 hours to complete. Because the laboratory facility does not have an effective temperature control system a temperature correction was thus necessary. Green [Ref. 20] recommends a correction be applied to this measured bridge voltage, E_{meas}, which is given by:

$$E_{corr} = E_{meas}(1 + C) \qquad \{3.6\}$$

where E_{corr} = corrected voltage and C = Temperature correction function given by:

$$C = \frac{\alpha}{2(OHR - 1)}(T_{\infty} - T_{cal}) \qquad \{3.7\}$$

where α = temperature coefficient of resistance, OHR = overheat ration, T_{∞} = freestream temperature and T_{cal} = freestream temperature at time of calibration.

The correction given by equation {3.6} and {3.7} is applied to the look-up table which is constructed for data reduction using equations {3.1} and {3.2} at the start of each survey [Ref. 20]. Applying the temperature correction in this manner accounts for the differences in temperature between T_{∞} measured at the start of a survey and T_{cal}. Because of variations in T_{∞} during a survey, a second correction was sometimes necessary. This correction was applied to the data by first determining the corrected voltage from the mean velocity $\bar{u}$ using the equation given by:

$$E_{corr}^2 = E_{oc}^2 + B\,\bar{u}^{0.45} \qquad \{3.8\}$$

This voltage was then corrected for variations between T_∞ and T_{meas} using:

$$E_{corr}^* = E_{corr}\left(1 + C^*\right) \qquad \{3.9\}$$

where T_{meas} is the freestream temperature as it varies with time, and where:

$$C^* = \frac{\alpha}{2\left(OHR - 1\right)}\left(T_{meas} - T_\infty\right) \qquad \{3.10\}$$

Velocities corrected to account for temperature drift during a run may then be calculated using the equation given by:

$$\bar{u}^{0.45} = \frac{1}{B}\left(E^{*2}_{corr} - E^2_{oc}\right) \qquad \{3.11\}$$

Temperature drift was most apparent in the surveys of streamwise mean velocity. The measured quantity $\overline{u'^2}$ did not show significant evidence of temperature drift during a survey, and therefore, this correction was not applied to measurements of $\overline{u'^2}$.

D. PROCEDURES FOR MEASUREMENT OF NEAR WALL PROFILES

Near wall profiles are obtained using procedures similar to those used in obtaining surveys with several exceptions. First, the probe is initially placed at a radial position 0.015 inches from the concave wall. This is done in the following manner. First, an expendable, or *dummy*, probe (with no usable sensor) is placed in the channel in contact with the concave wall. This establishes a reference, or zero, position. Using the MITAS controller, this *dummy* probe is then positioned at the channel centerline. The *dummy* probe is then replaced with a calibrated probe using procedures previously discussed. Using the zero reference, the new probe is carefully positioned to the 0.015 inch position while monitoring bridge output voltage and probe response on the oscilloscope trace. To

account for any difference in the positions of the dummy probe and the actual measuring probe, additional correction was deemed necessary. This type of correction to the radial position is determined from data at a Dean number of 125 and is discussed in detail in the results.

During data acquisition, the probe is moved radially in steps of 0.005 inch for a total of 28 radial positions. Changes in spanwise position are done manually using the MITAS controller. When positioning in the spanwise direction, the probe is first moved to the channel centerline (Y/d = 0.5) then positioned to the desired spanwise location, as a precaution against probe damage due to unevenness in the concave wall surface. The probe is then positioned at a radial location of 0.015 inches away from the concave wall. A new radial traverse then begins.

A complete near wall profile requires less than 40 minutes. During this short period of time, variations in ambient temperature were generally insignificant, and consequently no temperature drift corrections were necessary.

IV. EXPERIMENTAL RESULTS

Streamwise mean velocity and longitudinal Reynolds normal stress as measured in a radial/spanwise plane located 120° from the start of curvature for Dean numbers from 50.2 to 451.5 are presented in this section. Each contour plot presented is obtained from a radial/spanwise plane survey of a grid 8 by 41 points spaced 0.05 inch apart in each direction. In these plots, Y and Z are normalized by the channel height, d, so that $Y/d = 0.0$ represents the concave surface and $Y/d = 1.0$ represents the convex surface. Z/d is measured with respect to the channel centerline.

Near wall profiles of streamwise mean velocity and longitudinal Reynolds normal stress are presented for three distinct spanwise locations for Dean numbers of 125, 170 and 240, and at one spanwise location for a Dean number of 401. Each profile plot was obtained from a radial survey of 28 grid locations spaced 0.005 inch apart.

Also presented in this chapter are results from turbulence intensity measurements taken at the exit of the channel nozzle.

A. INLET TURBULENCE INTENSITY

The longitudinal turbulence intensity at the nozzle exit is measured using a DANTEC type 55P01 single-sensor hot-wire probe mounted normal to the flow direction and operated in constant temperature mode. The probe is located at $X/d = 4.0$, $Y/d = 0.5$ and $Z/d = 5.75$, where X/d is measured from the nozzle exit. The bridge output signal is high-pass filtered at 10 Hz and low-pass filtered at 1 kHz. These filter settings are chosen to obtain the turbulence intensity magnitudes representative of conditions at the inlet of the facility without contamination by low frequency laboratory disturbances and without contamination of any high frequency electronic noise.

Data obtained from these measurements are presented in Figure 15. Presented are values of longitudinal turbulence intensity normalized by the local mean velocity for Dean numbers of 223.5, 326.8 and 425.7. Also included in this figure are values obtained by Smith [Ref. 22] obtained from a straight channel with an inlet very similar to that used in this study (the only difference is that Smith's channel had cheese cloth over the inlet as an additional dust precipitator). Both facilities have the same nozzle design and dimensions, and same flow management apparatus consisting of three screens and a honeycomb. In the present study, the turbulence intensity varies from 0.0013 to 0.0015 compared values in the straight channel of 0.0011 to 0.0024. It should be noted the present data are contaminated by 60 Hz electronic noise, and therefore, the values presented in Figure 15 are higher than actual longitudinal turbulence intensities in the flow.

Removing all of the electronic noise from the signal is difficult because signal levels are so low. Ligrani and Niver [Ref. 4] give the turbulence intensities of the streamwise velocity at Dean numbers of 290 and 450 as 0.0006 and 0.0010, respectively. The results of Ligrani and Niver are believed to be more representative of the flow than ones measured presently because they used additional electronic filters to remove the 60 Hz electronic noise from the signal.

B. SURVEYS

Surveys of time-averaged quantities are presented in Figures 16 through 42 and in Figures 64 through 119. Of these, contour plots of normalized streamwise mean velocity are presented in Figures 16 through 19. Velocity perturbation contours are presented in Figures 22 through 25. Normalized longitudinal Reynolds normal stress contours are presented in Figures 27 through 34. Figures 64 through 89 present individual contour plots of the dimensional streamwise mean velocity, and Figures 90 through 115 present individual contour plots of the dimensional longitudinal Reynolds normal stress. Figures

116 through 119 also present individual contour plots of the dimensional streamwise mean velocity and individual contour plots of the dimensional longitudinal Reynolds normal stress at De = 125 and 175, however these data were obtained prior to channel cleaning. All other survey data were obtained just after the channel was thoroughly cleaned.

1. Normalized Streamwise Mean Velocity

Normalized streamwise mean velocity surveys obtained with the single-sensor hot-wire probe are presented in Figures 16 through 19 for De = 50.2 to 451.5. These data are normalized by the bulk velocity, U_{bulk} (the same bulk velocity as that used to determine the Dean number).

At De = 50.2, Figure 16 shows that the flow is spanwise uniform, as expected. No local disturbances to the mean velocity are evident due to the presence of vortex pairs. However, there is evidence of vortex pairs in data for De = 60.2 presented in the same figure. At this De, there are two significant velocity deficits within the survey: the first at Z/d = 6.0 and the second at Z/d = 7.2. These deficits extend over approximately half the channel height from Y/d = 0.1 to 0.5. As the Dean number increases from 70.2 to 150.6, the velocity deficits span the entire channel height. The presence of these deficits span the entire flow and appear to be *spanwise periodic*. Each deficit indicates the location of an *upwash* region between the two vortices (with respect to the concave wall) within each vortex pair. The time-averaged flow field also shows a vortex pair merging between De = 100.4 and 125.4. This is evident when the two deficits at Z/d = 7.5 and 8.0 merge into one deficit at Z/d = 7.9. A similar occurrence is observed from De = 190.7 to 200.7.

Compared to results for De from 70.2 to 150.6, the character of deficit regions changes as the Dean number varies from 160.5 to 250.8. They become smaller in the radial direction and extend over larger spanwise distances. At De = 263.3 through 451.5 the flow is more or less *spanwise uniform*, indicated by almost no evidence of vortex pairs

in the time averaged flow field. Vortex pairs may be present at these Dean numbers, however, if they are there, they are not apparent in time-averaged measurements because of considerable vortex pair unsteadiness in the spanwise and radial directions.

Some important features of these surveys are summarized in Figures 20 and 21. Figure 20 presents the minimum and maximum mean velocity measured in each survey grid. The maximum value is the actual maximum for the 120° spanwise/radial plane at each Dean number whereas the minimum value is only the minimum within Y/d = 0.1 to 0.8. The minimum and maximum bracket the bulk velocity, as expected. At Dean numbers from about 60.2 to 250.8, the location of the minimum velocity is in the upwash regions where velocity deficits are present.

Figure 21 presents the same data as Figure 20 compared with similar results obtained by Fields [Ref. 14]. Fields data was obtained using a miniature five-hole pressure probe and is presented here to show that agreement between the two sets of results is reasonably good. Contour plots are also in excellent agreement with those obtained by Fields, particularly, in regard to the detailed characteristics of individual velocity deficits. There are differences, however, in the spanwise position of vortex pairs between the present study surveys and ones from Fields. This is believed to be due to inlet channel disturbances caused by dirt accumulating on the walls and inlet flow management sections of the channel. This effect is discussed in greater detail later in this chapter.

2. Velocity Perturbation

At small values of Dean number, the fluid motion in the curved channel is two-dimensional and laminar, without secondary flows. The velocity profile is nearly parabolic with the maximum shifted slightly toward the concave surface compared to flow in a straight channel. This velocity profile then corresponds to *curved channel Poiseuille flow* (CCPF) [Refs. 23, 24]. When the primary flow instability sets in at higher *De*, the velocity

profile is altered from the CCPF profile. To show deviations from curved channel Poiseuille flow, values of velocity corresponding to CCPF are subtracted from the streamwise mean velocity. The resulting velocity perturbation ($\bar{u}$ - u_{CCPF}) contours are presented in Figures 22 through 25 to illustrate perturbations to curved channel Poiseuille flow caused by time-averaged secondary flows.

In Figure 22 at De = 50.2, there are no observable variations in the mean velocities from CCPF. At De = 60.2, differences from CCPF become apparent. In particular, there are two circular shaped deficits at Z/d = 6.0 and 7.5 that correspond to upwash regions (these also correspond to deficits in the streamwise mean velocity). As the Dean number increases from 70.2 to 150.6, the deficits take the shape of upside down triangles. As the Dean number increases further from 170.6 to 250.8, the deficit regions continue to change shape until the flow finally becomes spanwise uniform for Dean numbers from 263.3 to 451.5. Results for De = 263.3 to 451.5 from Figures 24 and 25, show significant deviations in the mean velocity from CCPF. This is because the flow is approaching a more turbulent flow profile.

From results like the ones presented in Figures 22 through 25, magnitudes of e, the streamwise velocity perturbation across the spanwise/radial measurement plane can be determined. This quantity e is given by:

$$e = \sqrt{\frac{1}{A}\int_A (u - u_{CCPF})^2 \, dA} \qquad \{4.1\}$$

where A is the area of the cross-section and u_{CCPF} is the velocity assuming curved channel Poiseuille flow. This quantity represents the cumulative effect of variations of the streamwise mean velocity from CCPF due to the primary instability in the channel for a particular Dean number. Magnitudes of e as they vary with De are presented in Figure 26.

A steadily increasing trend with Dean number is evident. When compared with results from Bottaro, *et al.* [Ref. 10] for the same *De* and approximately same streamwise location, the present results are slightly lower. This is probably because of a slightly smaller measurement plane in the present study.

3. Longitudinal Reynolds Normal Stress

Variations of the longitudinal Reynolds normal stress with Dean number are presented in Figures 27 through 34. In Figures 27 through 30, the data is presented normalized by the local mean velocity squared whereas in Figures 31 through 34 the data is normalized by the bulk mean velocity squared. These data were obtained simultaneously with the mean velocity results presented earlier.

At low *De* (*De* < 150.6), the values of longitudinal Reynolds normal stress are very low. This is because the values of turbulence intensity at the exit of the nozzle are also very low as previously discussed. In Figures 27 to 30, increases in Reynolds stress first occur at locations corresponding to inflow regions near the concave surface that are present between the two vortices which makeup each vortex pair. These stress regions first become apparent at *De* = 60.2 and become more apparent as the Dean number increases. For some Dean numbers, as is seen at *De* = 90.4, two side by side regions of localized increased turbulence intensity are present within the location corresponding to one upwash region. This corresponds to regions of high mean shear on either side of an upwash. Here the mean velocity gradients in spanwise and radial directions are high.

For *De* above 150.6, the stress magnitude continuously increases with the highest intensity levels occurring within the upwash regions. Above *De* = 250.8, the intensity contours appear less periodic in the spanwise direction. Finally, at *De* = 263.3 through 451.5 the contours become spanwise uniform. Such behavior corresponds to spanwise uniform streamwise mean velocity contours and velocity perturbation contours.

Results presented in Figures 27 through 30 are qualitatively similar to results presented in Figures 31 through 34. Normalizing by the local mean velocity tends to magnify Reynolds normal stress variations in regions of low velocity, such as exist near the concave wall in upwash regions.

Some notable features of these surveys are presented in Figures 35 through 42, where Reynolds normal stress variations are presented in dimensional form. Figure 35 presents the minimum and maximum values from each survey. Minimum values are representative of the flow for the range of Y/d from 0.1 to 0.8. For De = 50.2 through 125.4, the values are initially very low. At De = 150.6, the magnitude of the maximum value increases dramatically in magnitude. This corresponds to the start of the twisting mode, a phenomena that appears as vortex patterns that rock [Ref. 4]. At a Dean number of 250.8, the magnitude of the maximum turbulence intensity again increases drastically and continues to increase through De = 451.5. The same trend is observed in the minimum value for $De \geq 250.8$.

Figures 36 through 39 present values of the dimensional longitudinal turbulence intensity for specific locations within vortex pair structures. These locations were selected to correspond to specific locations within the left most upwash region seen in the survey shown in Figure 16. Values of the longitudinal normal stress are given in Figure 36 for locations where this quantity is a maximum. Values of the longitudinal normal stress are given in Figure 37 for Y/d = 0.1 at the same Z/d position where the maximum occurs. Values of the longitudinal normal stress are given in Figure 38 for the channel centerline (Y/d = 0.5) at the same spanwise locations as Figures 36 and 37. Figure 39 presents the value at a fixed radial and spanwise location (Y/d = 0.1 and Z/d = 5.2). This location corresponds to the location of the maximum intensity for De = 100.4. The general trends are similar to those observed in Figure 35.

Figures 40 through 42 present composites of the data shown previously in Figures 36 through 38. The dimensional longitudinal Reynolds stress variations in these figures are given for three different locations within the vortex pair structure: within an inflow region near the local streamwise mean velocity minima at Y/d = 0.1, within an inflow region at Y/d = 0.5 and the same Z/d position, and at the location where the longitudinal normal stress is maximum. The data in these figures thus correspond to specific locations within the vortex pair structure and not to fixed Z/d locations as De is changed.

Figure 40 indicates that dimensional normal stress magnitudes increase with De, and are quite low for De < 150. For De from 50 to 75, magnitudes at Y/d = 0.5 are higher than ones for Y/d = 0.1, whereas the opposite trend is generally present for higher De up to 125. When normalized using U_{bulk}, maximum $\overline{u'^2}$ magnitudes vary between 0.019 and 0.028.

As De increases above about 150, Figure 41 (which includes the Figure 40 data plotted using different abscissa and ordinate scales) shows that $\overline{u'^2}$ magnitudes are much higher than those at lower De for all three locations within the vortex pair structure. Compared to results at De = 125, longitudinal normal stress magnitudes are about 30 times greater. According to Ligrani, *et al.* [Ref. 8], these higher stresses at 150 ≤ De ≤ 185-200 are probably mostly due to twisting motions of the vortex pairs, as well as a partial result of fluid that, in some cases, may be agitated by twisting. Twisting is believed to be associated with turbulent energy increases because both occur at the same locations within a vortex pair structure and over nearly the same range of Reynolds numbers.

C. NEAR WALL PROFILES

Near wall profiles of the streamwise mean velocity and the longitudinal Reynolds normal stress are presented in Figures 43 through 63. These results were obtained using single-sensor hot-wire probes mounted on DISA type 55P04 probe mounts. At the beginning of each profile, each probe is initially located at an approximate radial position of Y = 0.015 inches (i.e., 0.015 inches from the concave wall). Individual probes are then moved away from the concave wall in 0.005 inch steps, as previously discussed. Measurements are taken at three spanwise locations (Z/d = 5.25, 5.50 and 6.00) for De = 125, 170, 240 and 401.

These spanwise locations and De were selected based upon the surveys presented earlier in Figures 16 to 19. The first spanwise position, Z/d = 5.25, was chosen because it corresponds to a position near the center of the left most upwash region for De = 125.4 in Figure 16. The second spanwise position, Z/d = 5.50, corresponds to a position just to the right of the same upwash region. The third and final spanwise position, Z/d = 6.00, corresponds to a downwash region. Of course, these positions with respect to vortex pair structure were expected to be slightly different for other De of 170, 240 and 400.

The lowest velocity measured in these profiles is above values corresponding to Re_d = 0.07, the mixed convection limit for hot-wire probes given by Ligrani and Bradshaw [Ref. 19]. This Re_d is based on local mean velocity and sensor wire diameter. For the presently employed sensors, the Re_d value corresponds to a fluid velocity of approximately 0.2 m/s. Above this mean velocity, the probe is subject to forced convection only.

1. Streamwise Mean Velocity

Near wall streamwise mean velocity profiles are presented in Figures 43 through 49. Data for De = 125 are presented in Figures 43 and 44, for De = 170 in Figure

45, for De = 240 in Figure 46 and for De = 401 in Figures 47 through 49. For De = 125, 170 and 240, data are presented for all three spanwise positions. For De = 401, data are presented for Z/d = 5.25 only because the flow at this De is spanwise uniform.

Magnitudes of the streamwise mean velocity given in Figure 43 are not in full agreement with surveys presented for the same De in Figure 16. These differences are not presently fully understood. They may be a result of movement of the vortex pairs relative to positions evident in the surveys or because of data scatter resulting from the difficulties in measuring the very low flow velocities at this De.

The data of Figure 43 are also plotted in wall coordinates in Figure 44. The wall coordinates are given by:

$$u^+ = \frac{u}{u_\tau} \qquad \{4.2\}$$

and:

$$y^+ = \frac{Y\, u_\tau}{\nu} \qquad \{4.3\}$$

where:

$$u_\tau = \sqrt{\frac{\tau_w}{\rho}} \qquad \{4.4\}$$

where τ_w is the shear stress at the wall, u_τ is the friction velocity, ν is the kinematic viscosity and ρ is the fluid density. The quantity τ_w/ρ was determined using the relationship:

$$\frac{\tau_w}{\rho} = \nu \left.\frac{\partial u}{\partial y}\right|_{y \to 0} \qquad \{4.5\}$$

where $\partial u/\partial y\,|_{y\to 0}$ is the velocity gradient near the wall. This quantity was determined experimentally using the data from Figure 43 for $Y/d \leq 0.1$. The values of u_τ determined by this method for De = 125 were 0.083 m/s, 0.068 m/s and 0.061 m/s for Z/d = 5.25, 5.50 and 6.00, respectively. By comparing the data plotted in these coordinates with the theoretical relationship $u^+ = y^+$, errors in the initial radial positions of the probe were determined. Magnitudes of these errors were determined from De = 125 data for each Z/d, then applied to near wall results at all De studied.

Data for De = 170 shown in Figure 45 show better consistency with survey results than the near wall profile at De = 125. However, some differences are still apparent that may be due to shifting of the spanwise position of vortex pairs. The profile for De = 240 in Figure 46 shows good consistency with survey data in Figure 18 for the same De. In both figures, Z/d = 5.50 appears to correspond to an upwash region where velocities are lower and velocity gradients are higher than that at other spanwise locations and Z/d = 6.00 appears to correspond to a downwash region where velocities are generally lower than at other spanwise locations.

Data for De = 401 are presented in Figures 47 through 49. Figure 47 shows a profile that is similar to the turbulent survey results in Figure 19. The data are plotted in wall coordinates in Figures 48 and 49 using a friction velocity for normalization determined from a Clauser [Ref. 25] plot. With the Clauser plot, u^+y^+ is first determined using the equation given by:

$$u^+y^+ = \frac{u\,Y}{\nu} \qquad \{4.6\}$$

y^+ is then determined using the relationship:

$$u^+y^+ = y^+\left[\frac{1}{0.41}\,ln\,y^+ + 5.2\right] \qquad \{4.7\}$$

With y^+ known, the friction velocity is then calculated by:

$$u_\tau = \frac{y^+ \nu}{Y} \qquad \{4.8\}$$

Using this technique, the friction velocity is 0.222 m/s for the De = 401 data at Y/d = 0.1. With this friction velocity used to normalize the streamwise mean velocities, Figures 48 and 49 show good agreement with the law-of-the-wall for $y^+ > 30$-35. For lower y^+, the data deviated from the law-of-the-wall in the buffer region of the boundary layer, as expected.

2. Longitudinal Reynolds Stress

Longitudinal Reynolds stress results are presented in Figures 50 through 63 for the same De and Z/d as the streamwise mean velocity data. Figures 50 through 53 present the dimensional longitudinal Reynolds normal stress. Figures 54 through 57 present the same data normalized by the local mean velocity squared. Figures 58 through 61 present the data normalized by the bulk velocity. Figures 62 and 63 compare the results for De = 401 with results by Kreplin and Eckelmann [Ref. 26], Moser and Moin [Ref. 9] and Morrow [Ref. 27].

As with the mean velocity profiles, the longitudinal turbulence intensity data for De = 125 and 170 are not consistent with the survey data. These inconsistencies probably result for the same reasons that the inconsistencies between the streamwise mean velocity surveys and the streamwise mean velocity profiles are present. At De = 240 and 401, profile results are in good agreement with the data from the surveys.

Figure 62 shows that the present results are in excellent agreement with ones from Kreplin and Eckelmann [Ref. 26] and Moser and Moin [Ref. 9], particularly for $y^+ > 18$. For $y^+ < 18$, the results from the present study are somewhat lower, probably because the data obtained from Refs. 26 and 9 were obtained in channel flows at higher

Reynolds numbers. The magnitude of Re_τ for Ref. 26 is 195, where Re_τ is the Reynolds number base on friction velocity and channel half-height, δ. The magnitude of Re_τ for Ref. 9 is 168. The present measurements correspond to a less developed, or younger, boundary layer at Re_τ = 90.3. In younger boundary layers, the peak in turbulence intensity typically occurs at a greater y^+ than for boundary layers at higher Re_τ.

In Figure 63, the results for De = 401 are compared with results obtained by Morrow [Ref. 27] in a straight channel flow with identical channel cross-section and inlet geometry, and similar flow conditions. Morrow's results are lower than the ones obtained in the curved channel, primarily because of the manner in which electronic signals are sampled and processed in the two studies. In Morrow's study, the output from the hot-wire was sampled at 100 Hz and 200 Hz with appropriately set anti-aliasing filters. Therefore, some of the higher frequency components of the signal are not included in the magnitudes of Morrow's $\overline{u'^2}$ data presented in Figure 63.

C. EFFECT OF CHANNEL CLEANING

Figures 116 through 119 are presented to illustrate the effects of channel cleaning on measured distributions of streamwise mean velocity and longitudinal Reynolds normal stress. These data were obtained at a time when some dirt and dust was present at the channel inlet. As previously discussed, the channel was cleaned immediately prior to the measurement of survey results presented earlier.

Figures 116 and 117 present the dimensional streamwise mean velocity prior to channel cleaning for De = 125.4 and 175.6. Figures 118 and 119 present the longitudinal Reynolds normal stress under the same conditions. By comparing these figures with similar results obtained after the channel was cleaned (Figures 70, 73, 96 and 99, respectively), it is evident that streamwise mean velocity data are very similar, except that

the locations of individual vortex pairs are shifted in the spanwise direction. More significant changes to the qualitative distributions of longitudinal Reynolds normal stress are apparent since magnitudes are reduced by a factor of 10 in the clean channel at $De = 125.4$ and $De = 175.6$. At higher De, channel cleaning had little effect on distributions of streamwise mean velocity or longitudinal Reynolds normal stress.

V. SUMMARY AND CONCLUSIONS

A transparent curved rectangular channel with 40 to 1 aspect ratio was utilized to investigate variations of streamwise mean velocity and longitudinal turbulence intensity that occur at different locations in a spanwise/radial plane located 120 degrees from the start of curvature over a range of Dean numbers. To obtain these measurements, a single-sensor hot-wire probe was traversed over a plane of 328 data points (in a 41 by 8 grid) using an automated two-dimensional traversing apparatus. With a slightly modified version of the same traverse, near-wall profiles of streamwise mean velocity and longitudinal Reynolds normal stress were also obtained.

At a Dean number of 50.2, streamwise mean velocity surveys show spanwise uniform behavior. As the Dean number increases, evidence of Dean vortex pairs is apparent and the flow becomes spanwise periodic due to streamwise velocity deficits at upwash regions located between the two vortices that make up each vortex pair. As the Dean number increases above 263.3, evidence of Dean vortex pairs is less apparent as the flow becomes more or less spanwise uniform.

Longitudinal Reynolds normal stress survey results show locally higher magnitudes for Dean numbers above 60.2 that initially occur at locations corresponding to inflow regions near the concave surface. As the Dean number is increased further, stress magnitudes within the upwash regions continuously increase. As the Dean number becomes greater than 150.6, results show that the stress magnitudes are much greater than at lower Dean numbers. Such increases correspond closely with twisting vortex motions, which is important in regard to transition from laminar to turbulent flow because these variations provide evidence that twisting results in the first important increases in turbulence energy at a given location as the Dean number increases. As the Dean number

exceeds 263.3, regions of locally higher stress merge together to form a fully turbulent flow with spanwise uniform distributions of longitudinal Reynolds normal stress.

Near wall profiles of streamwise mean velocity and longitudinal Reynolds normal stress are in good agreement with survey data and with results from the literature for Dean numbers of 240 and 401. At a Dean number of 401, the streamwise mean velocity profile shows agreement with the law-of-the-wall for $y^+ > 30$. At lower Dean numbers, inconsistencies between profiles and survey data are believed to be due to differences in small scale disturbances resulting from dust build-up on the channel walls and inlet flow management apparatus.

APPENDIX A. FIGURES

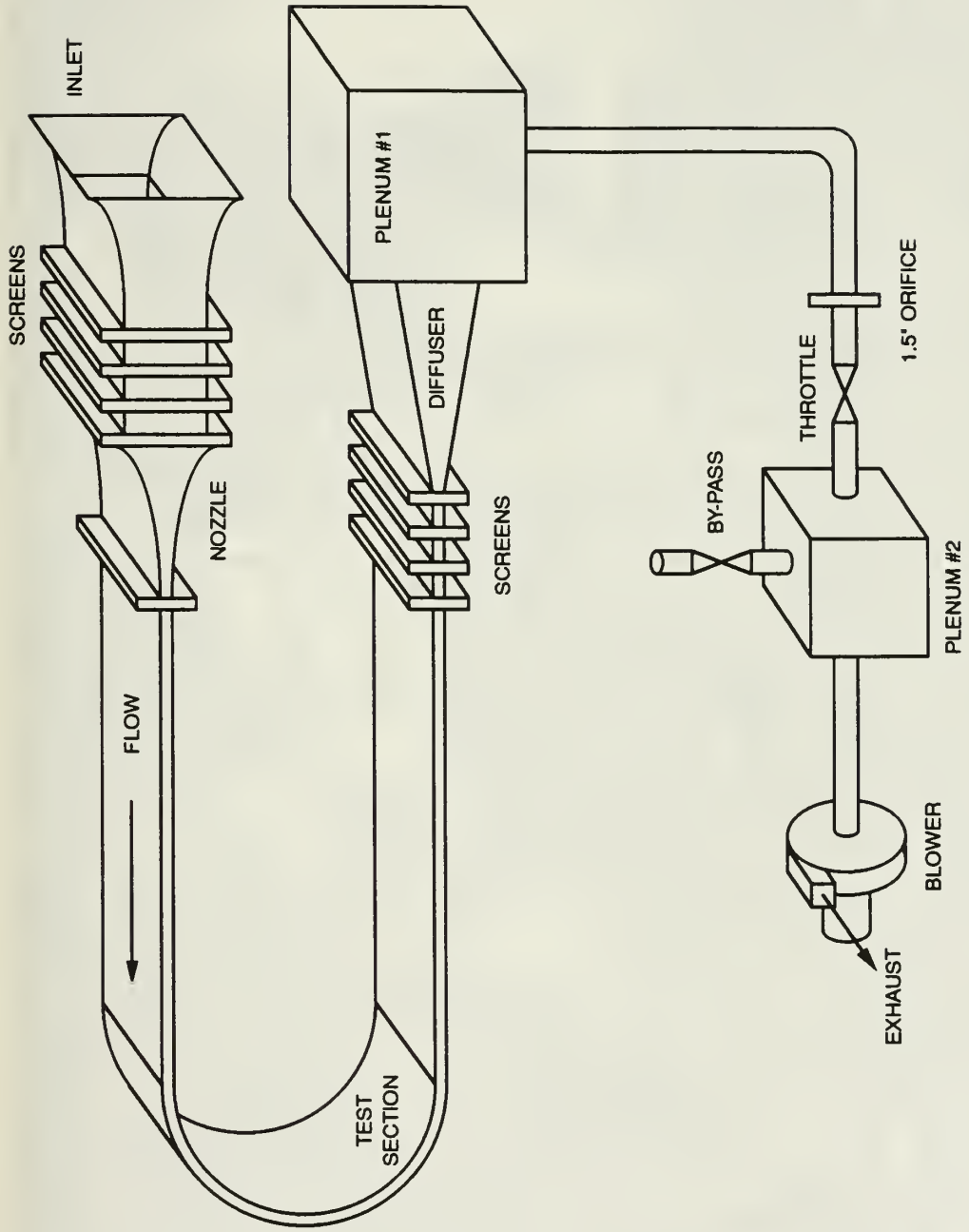

Figure 1. Schematic of Test Facility

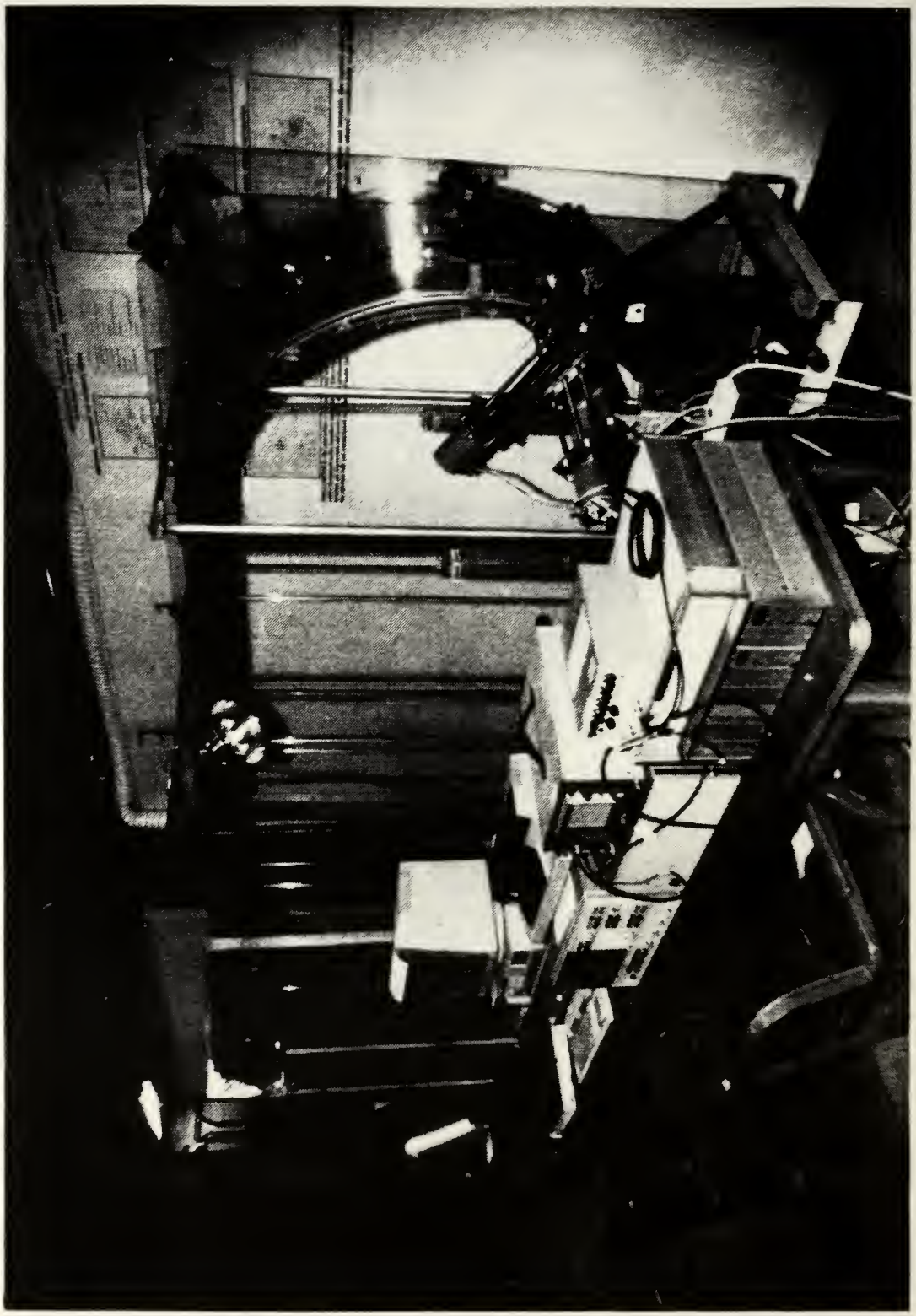

Figure 2. Test Facility (Side View)

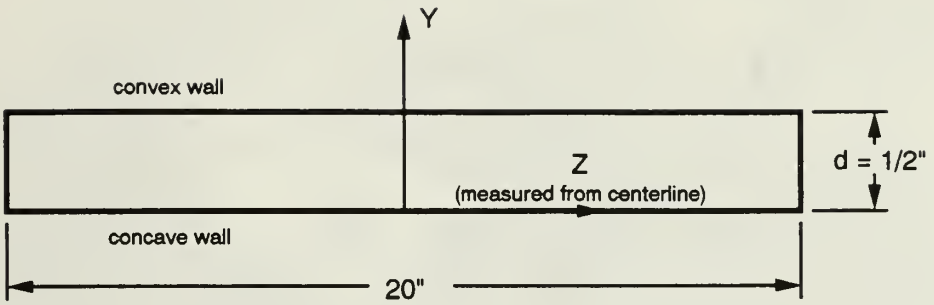

(a) Cross Section (not to scale)

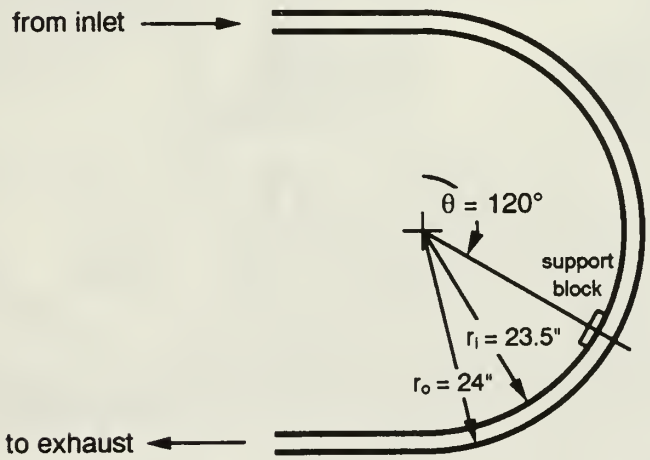

(b) Test Section Geometry

Figure 3. Details of Test Section

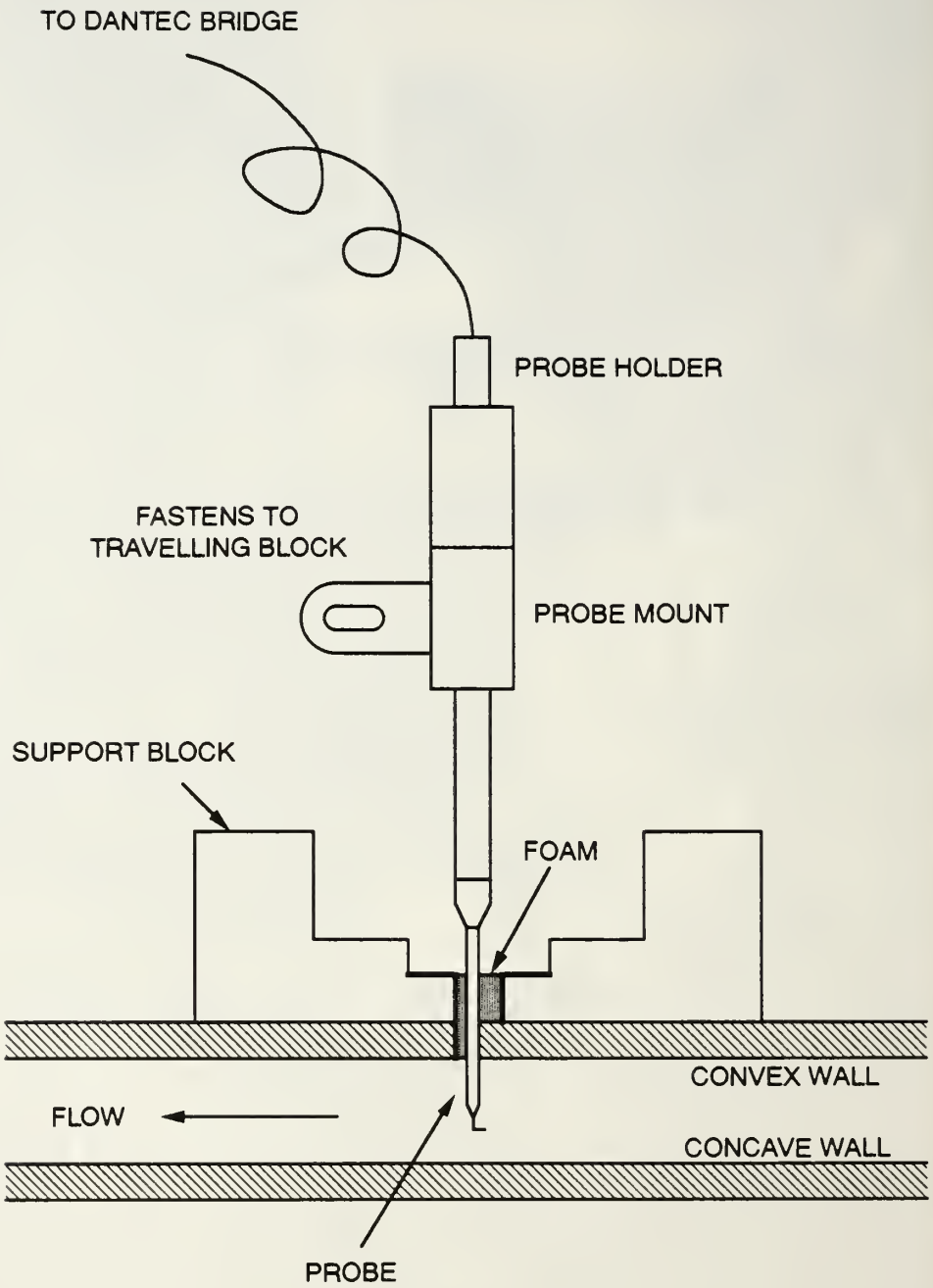

Figure 4. Schematic of Support Block

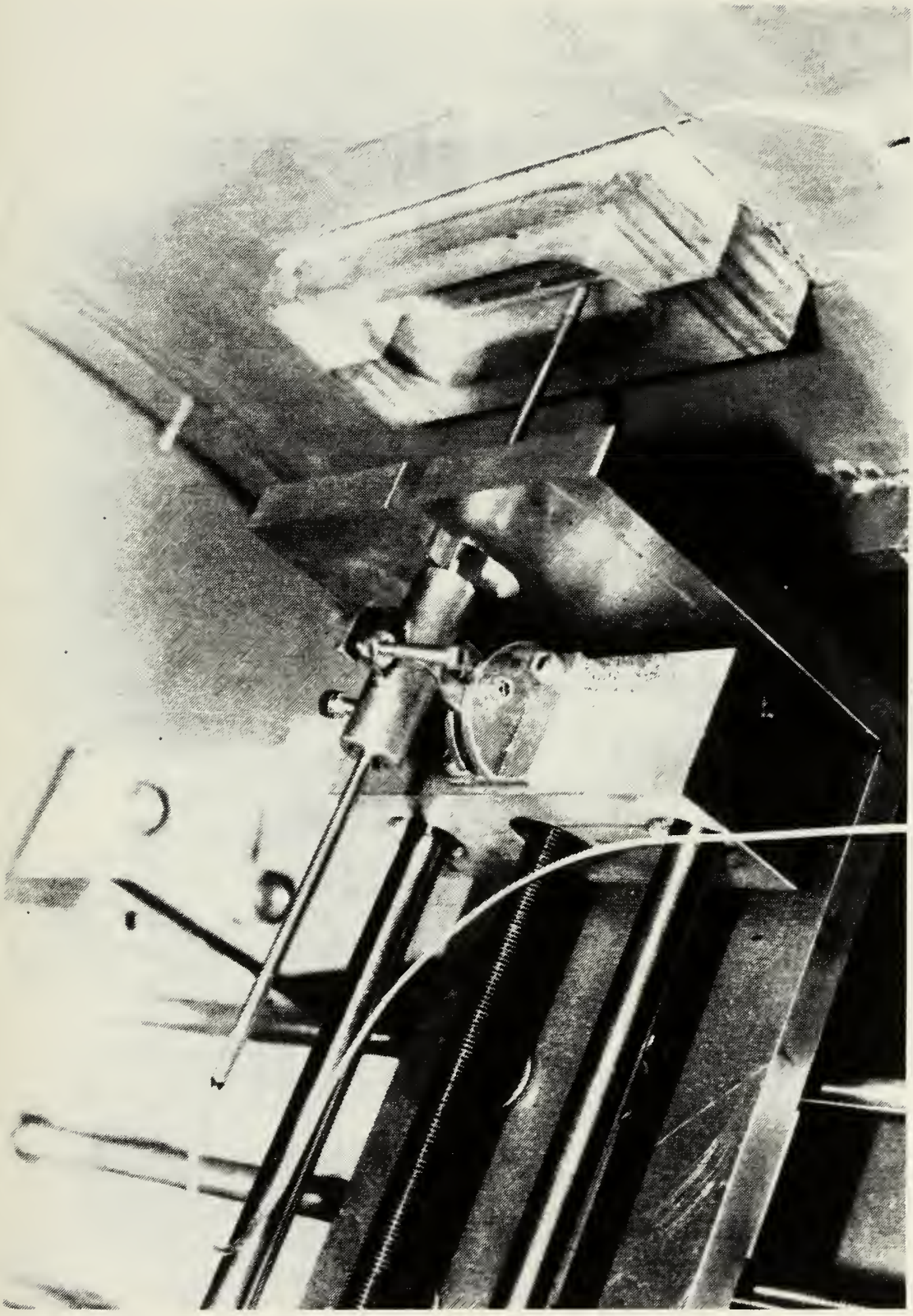

Figure 5. Detail of Support Block and Probe Mount Assembly

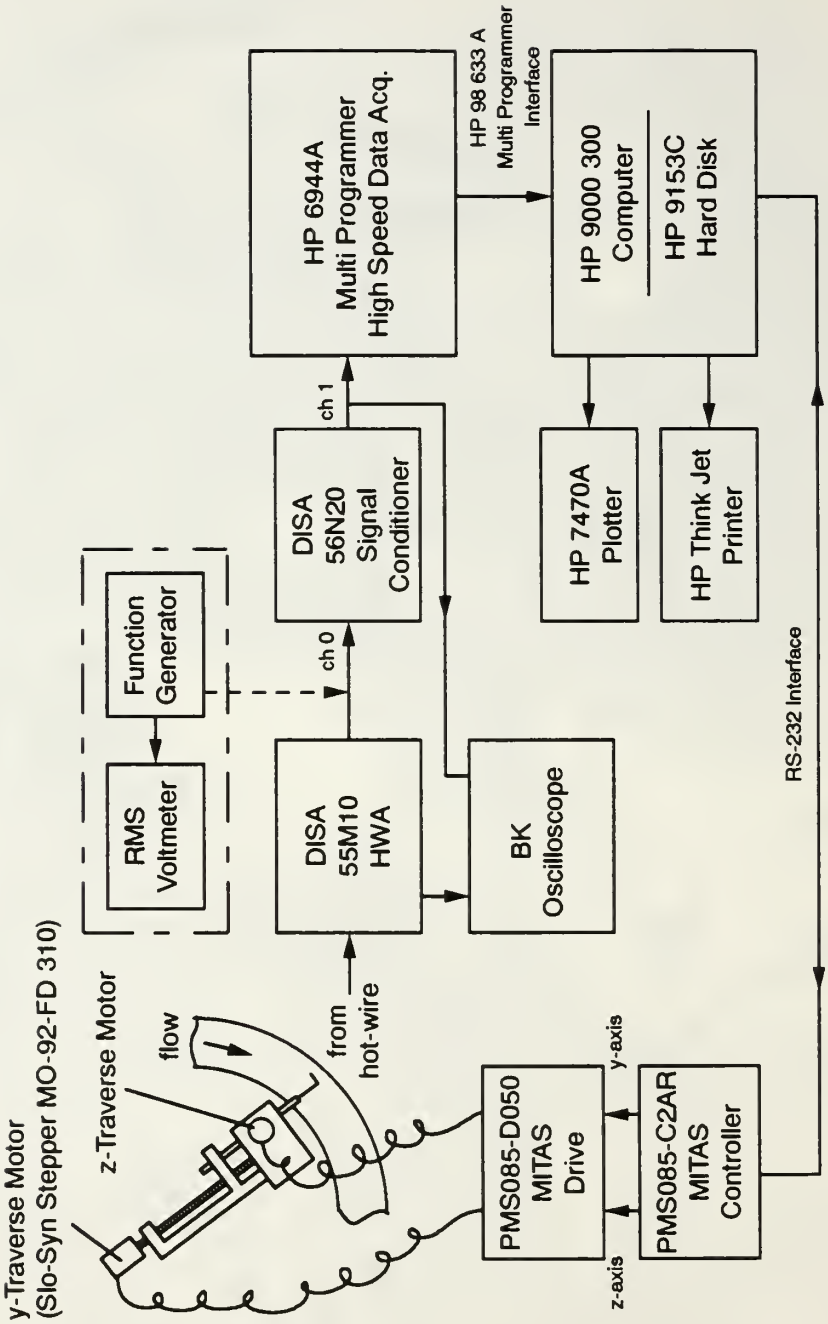

Figure 6. Data Acquisition System

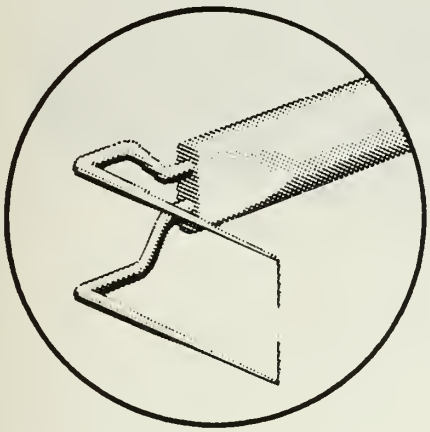

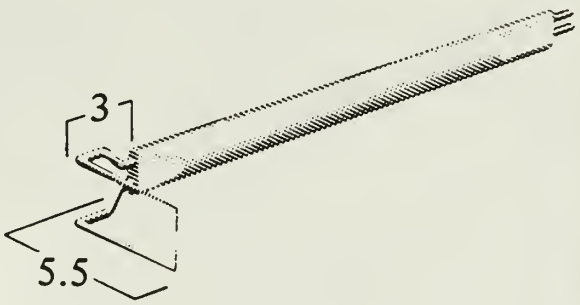

55P04

90°, sensor perpendicular to probe axis

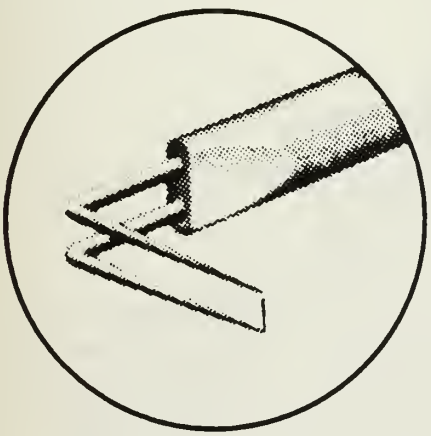

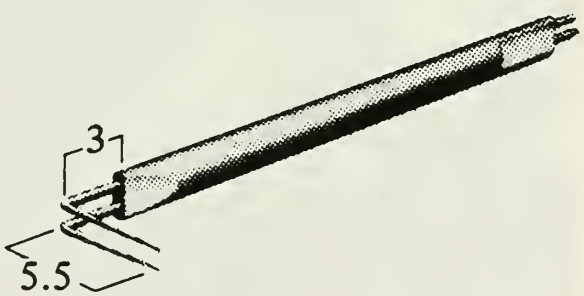

55P14

90°, sensor perpendicular to probe axis

Figure 7. Single-sensor Hot-wire Probes

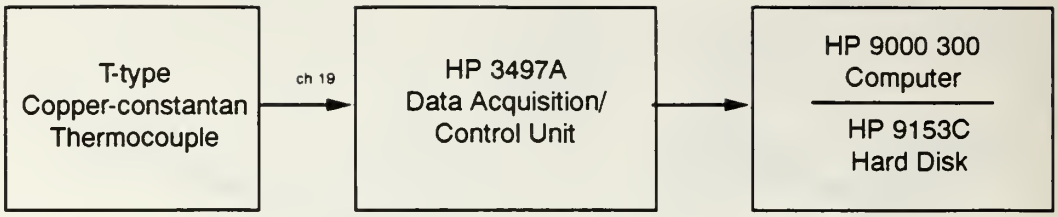

Figure 8. Temperature Measurement System

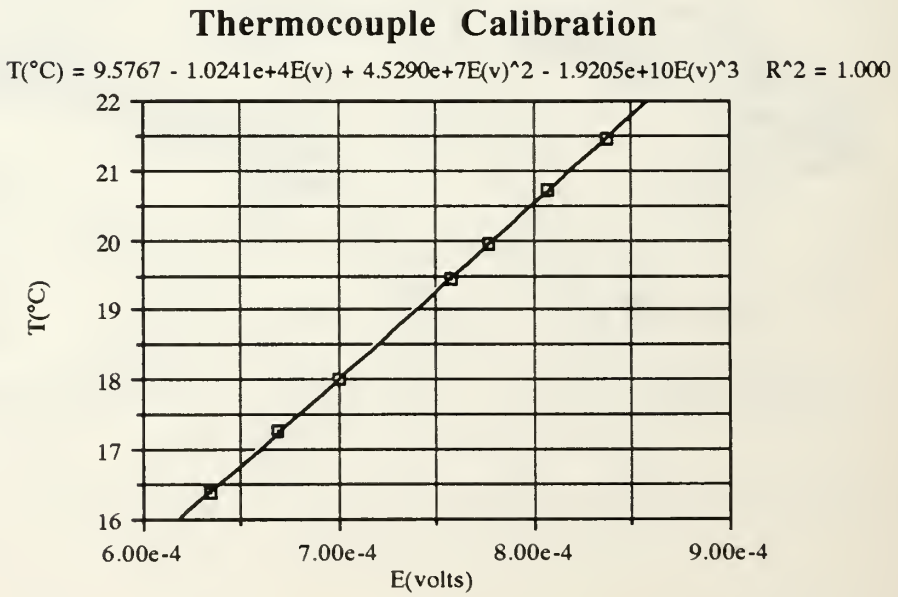

Figure 9. Thermocouple Characteristics

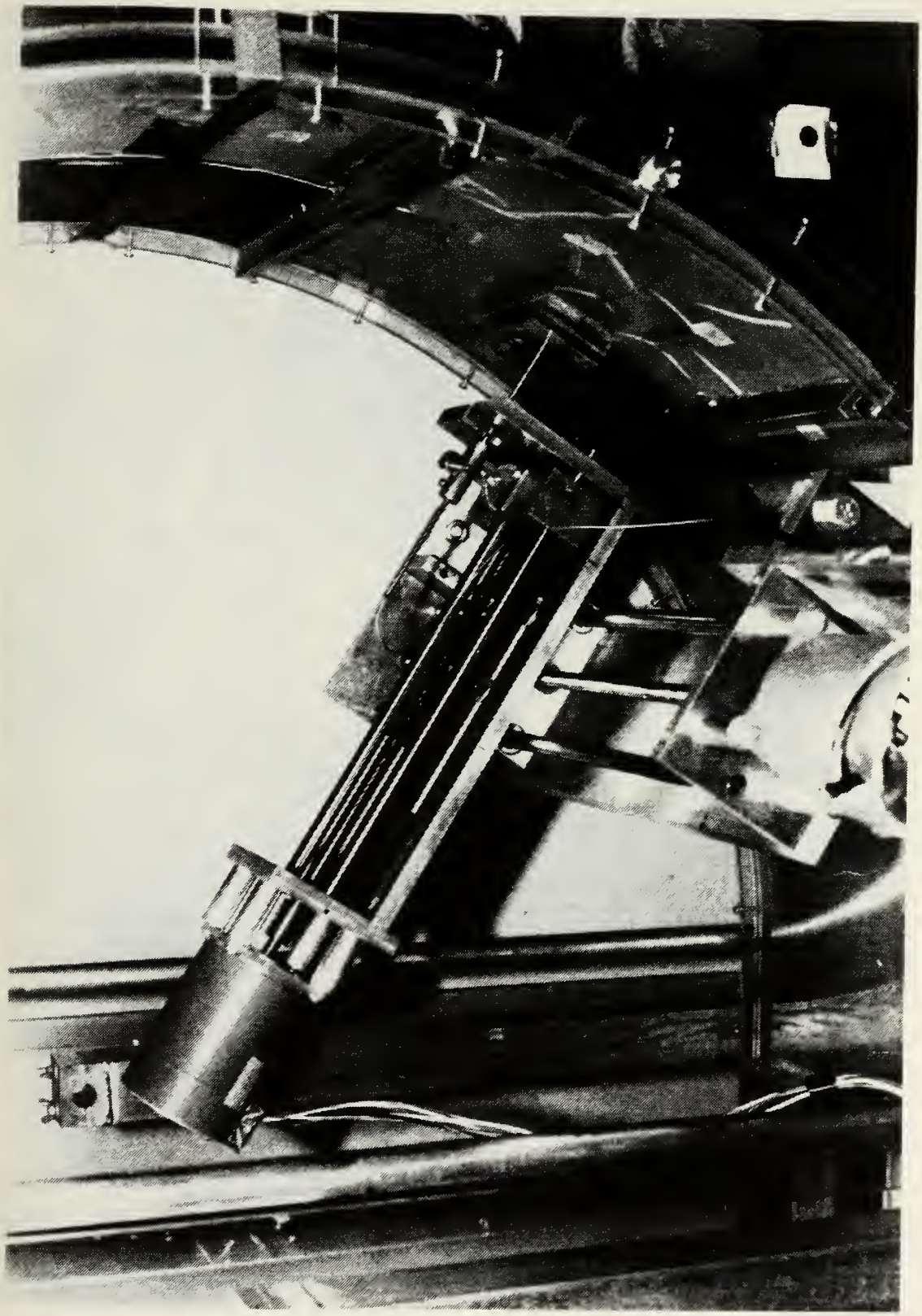

Figure 10. Traverse Used for Velocity Surveys

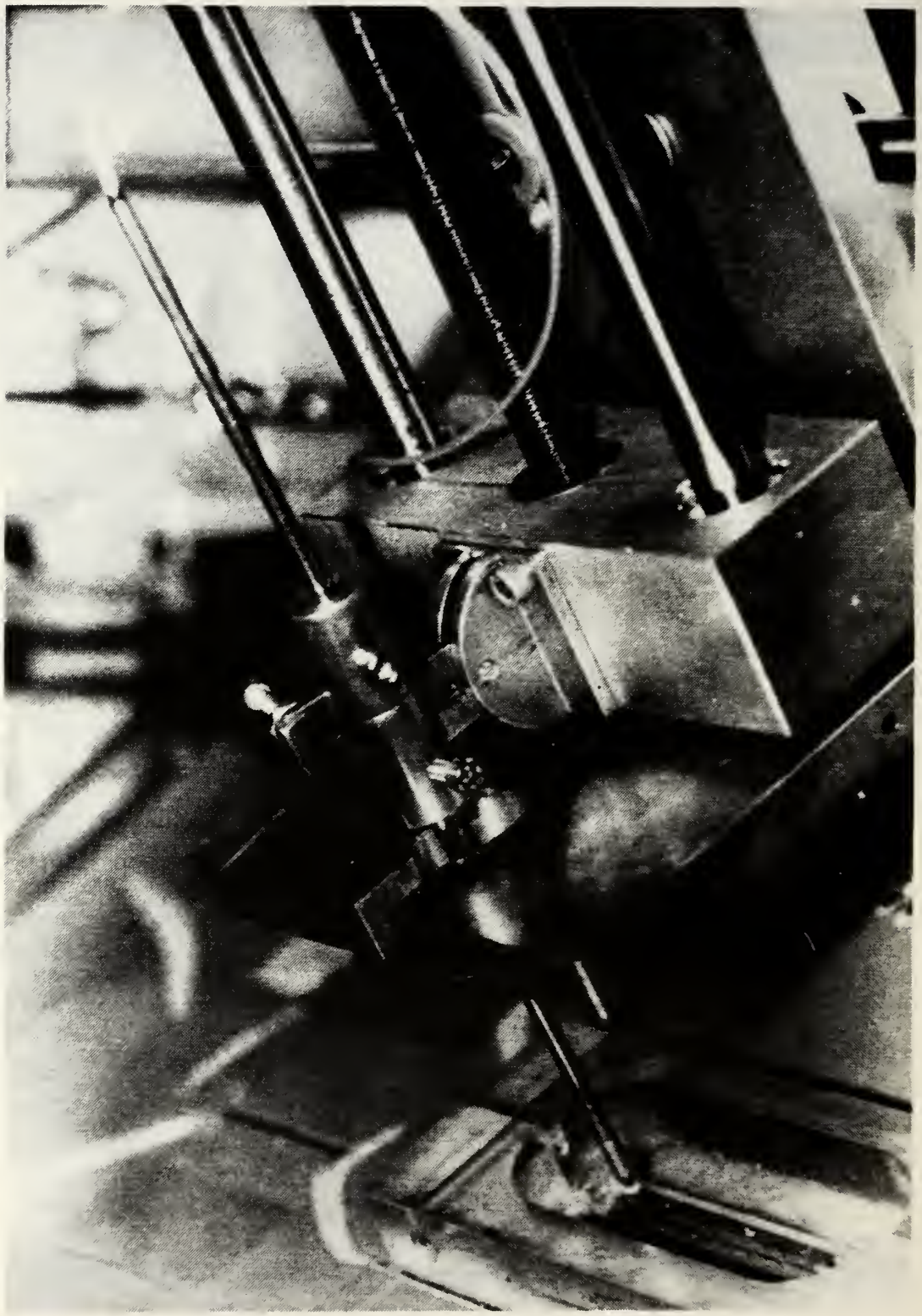

Figure 11. Detail of Traversing Block Used for Velocity Surveys

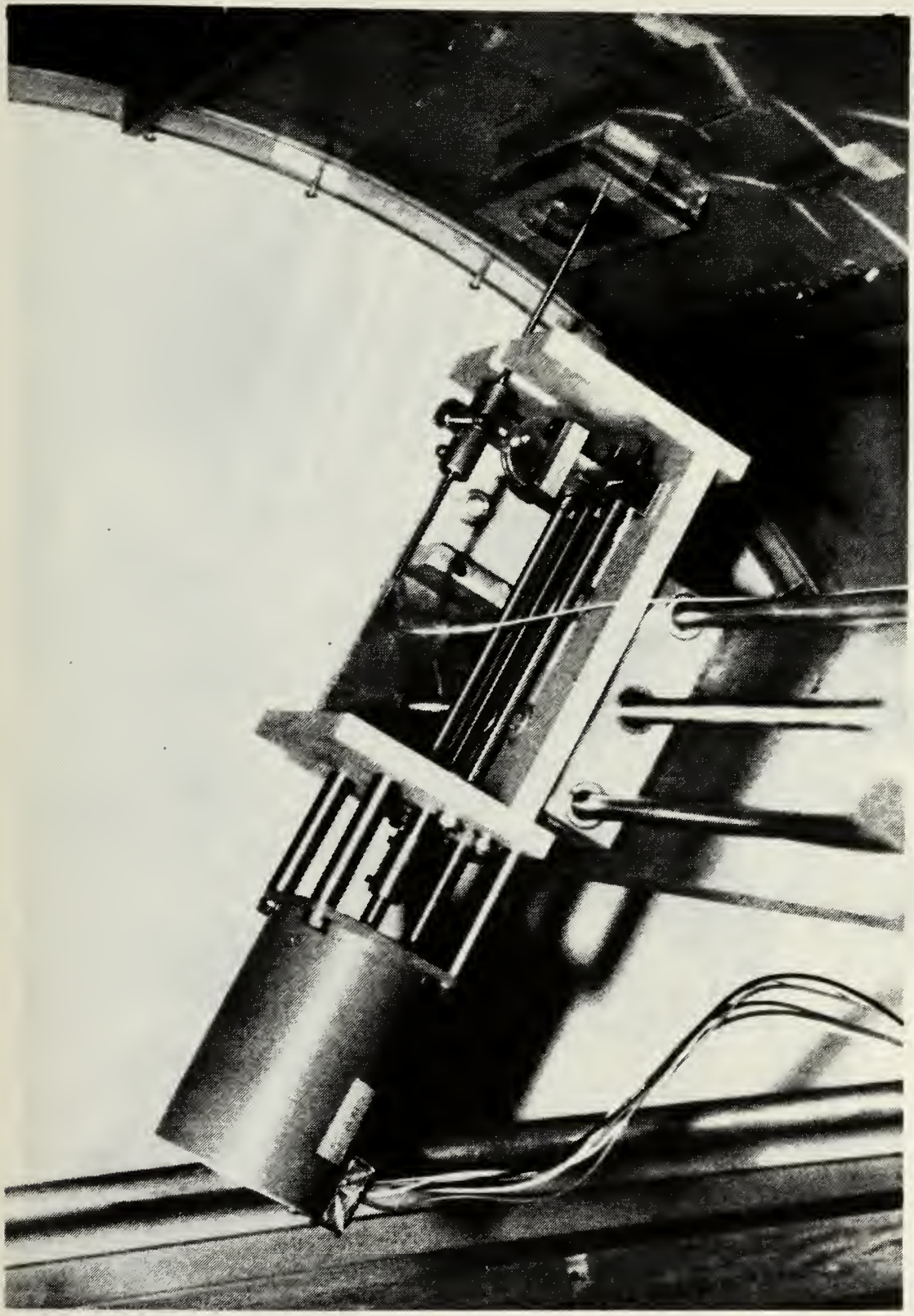

Figure 12. Traverse Used for Near Wall Profiles

Figure 13. Detail of Traversing Block Used for Near Wall Profiles

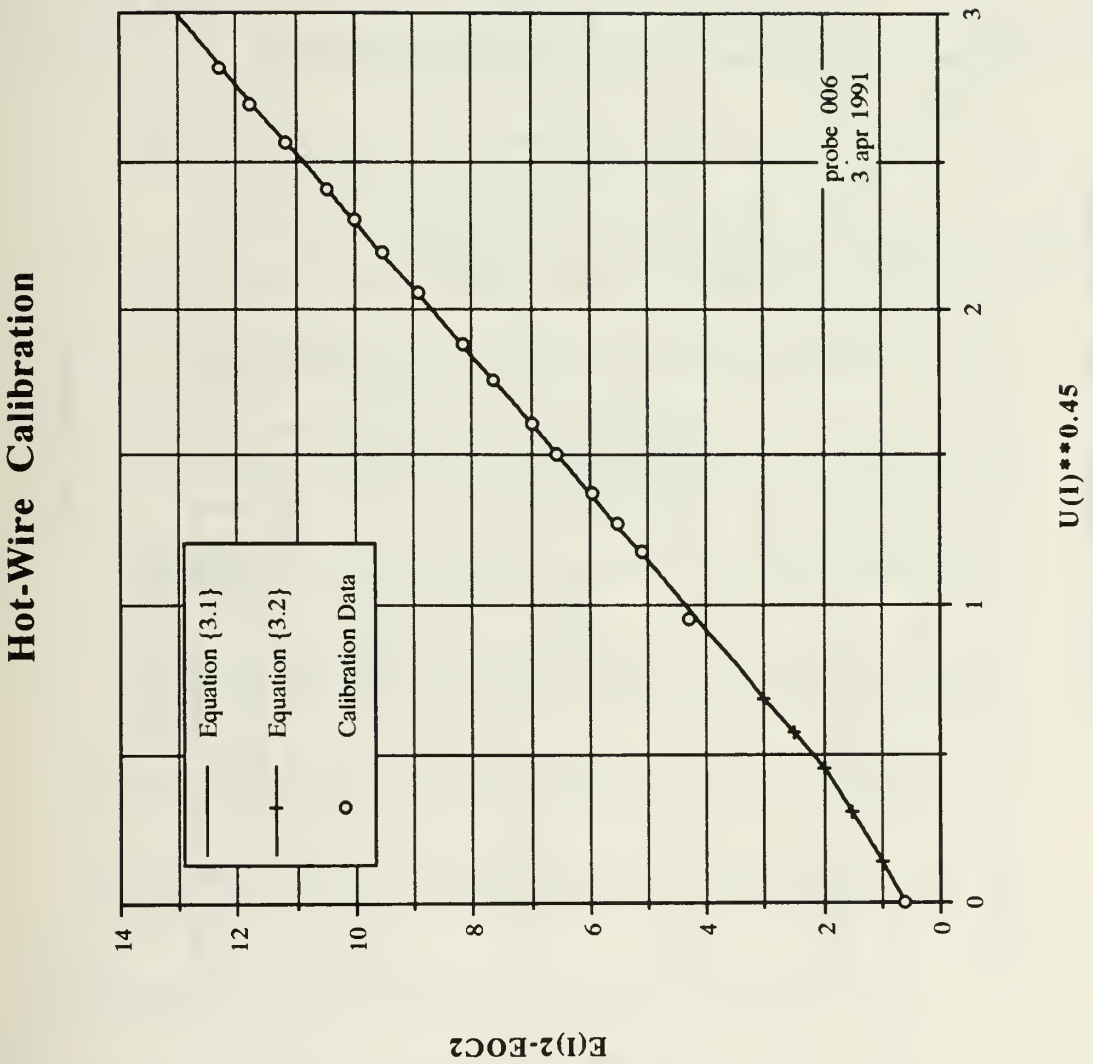

Figure 14. A Typical Hot-wire Calibration

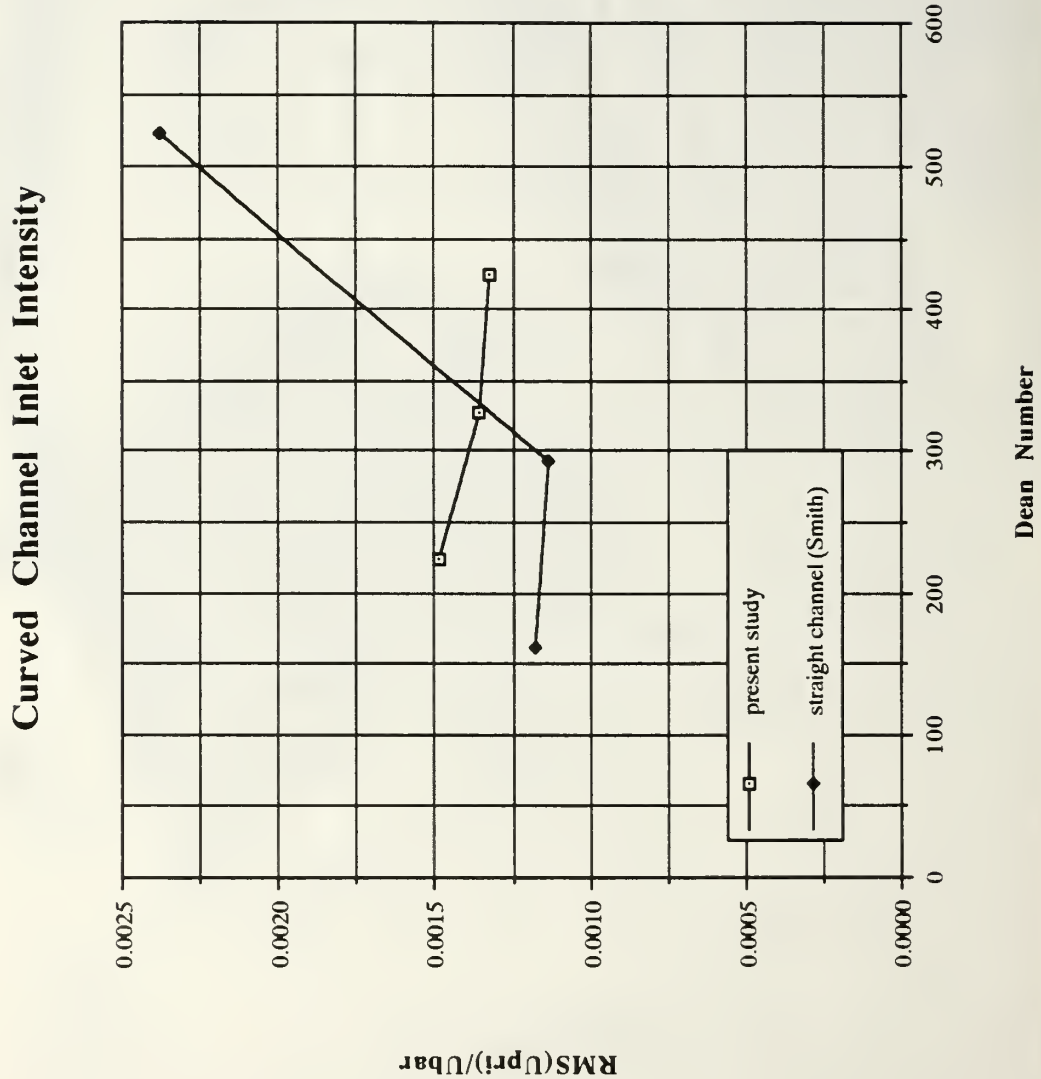

Figure 15. Inlet Turbulence Intensities

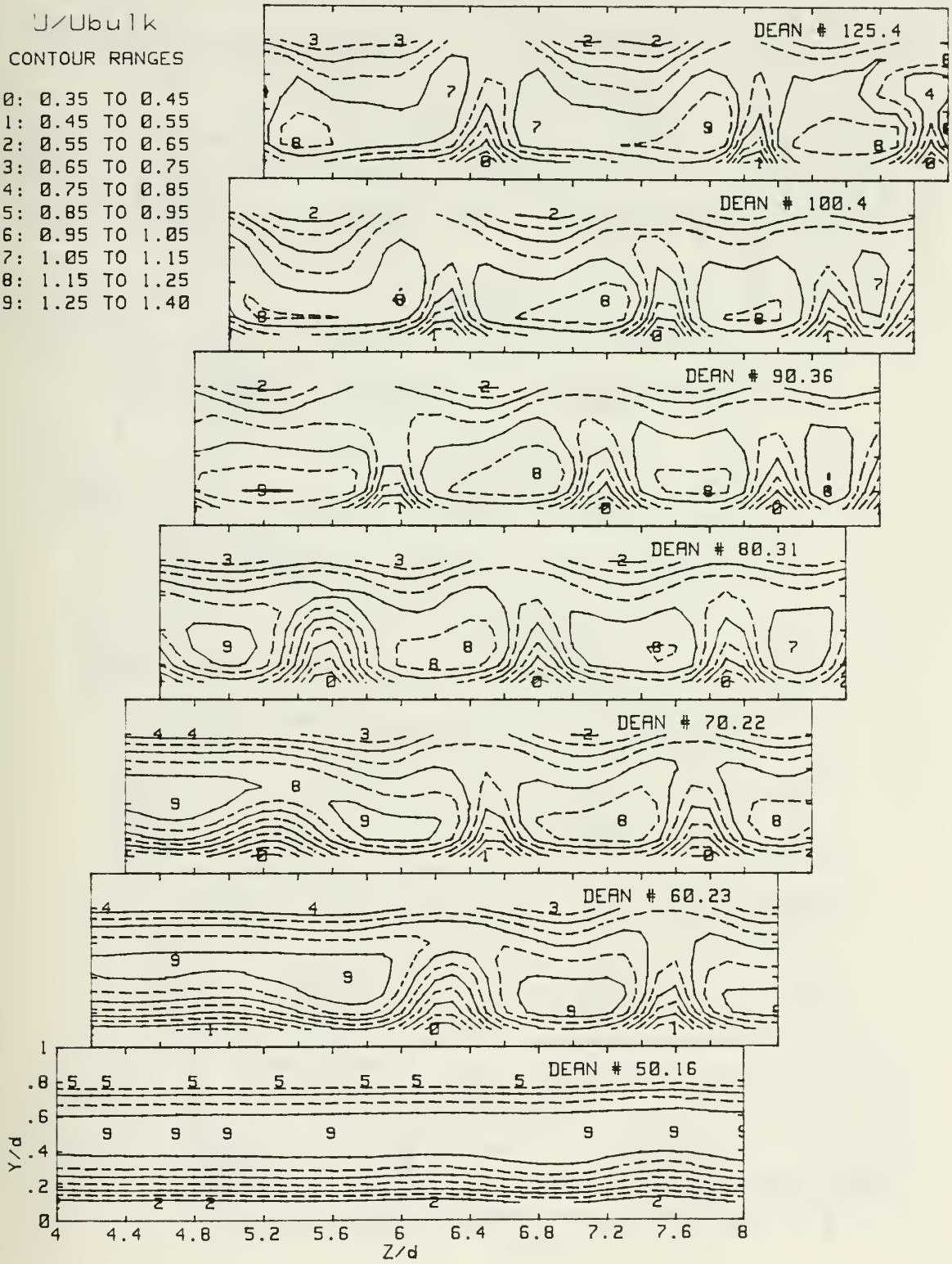

Figure 16. Streamwise Mean Velocity Contours, De=50.2 to De=125.4

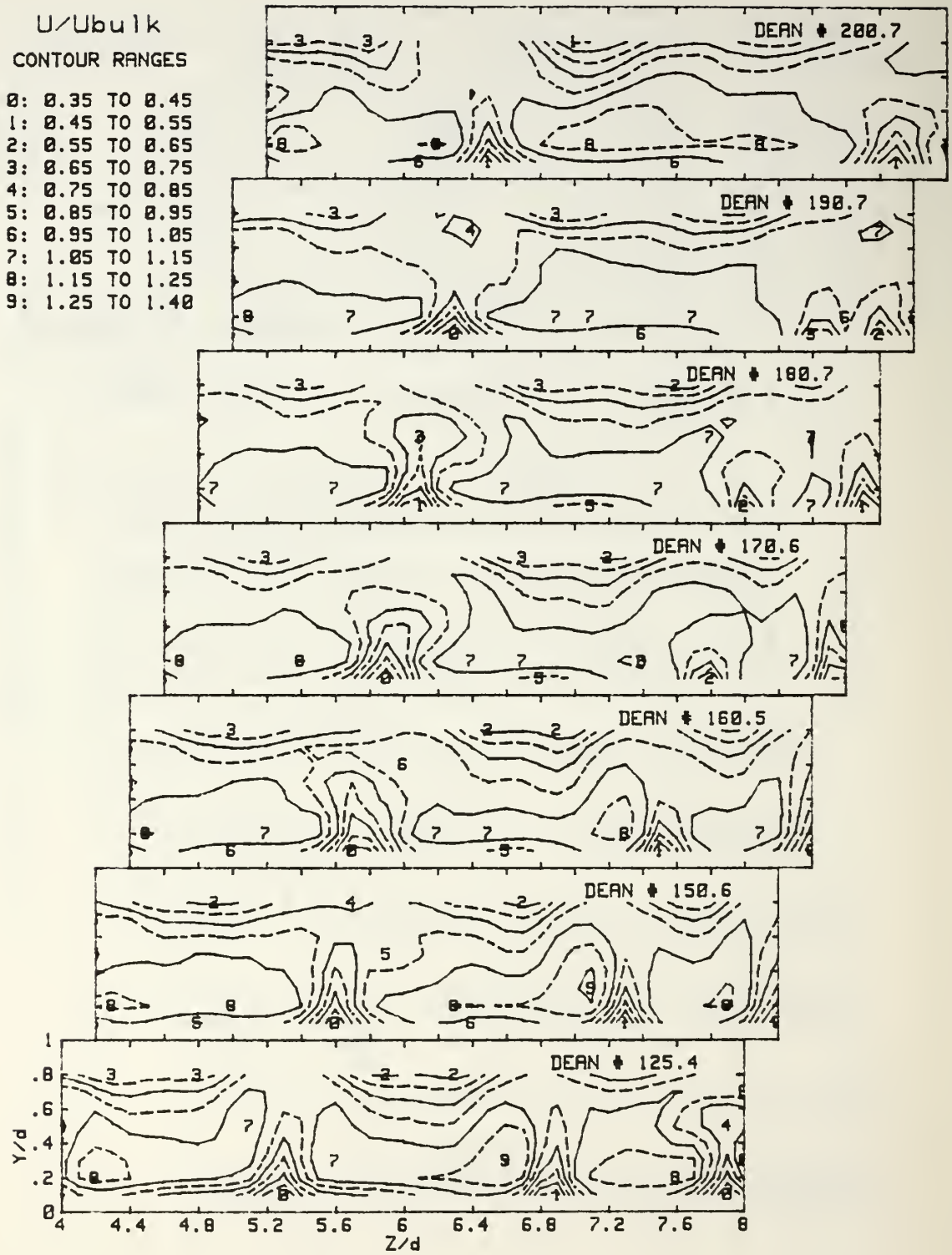

Figure 17. Streamwise Mean Velocity Contours, De=125.4 to De=200.7

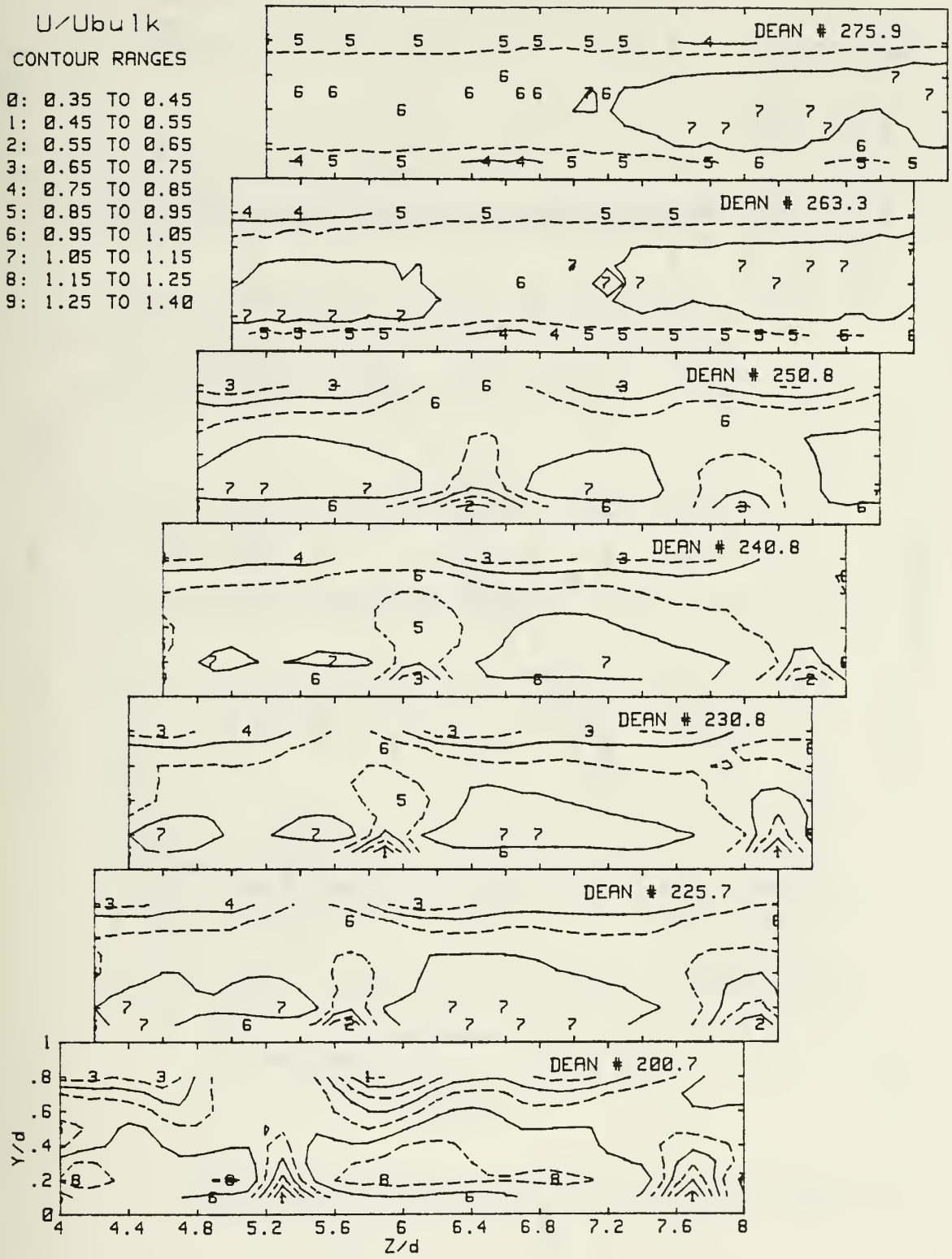

Figure 18. Streamwise Mean Velocity Contours, De=200.7 to De=275.9

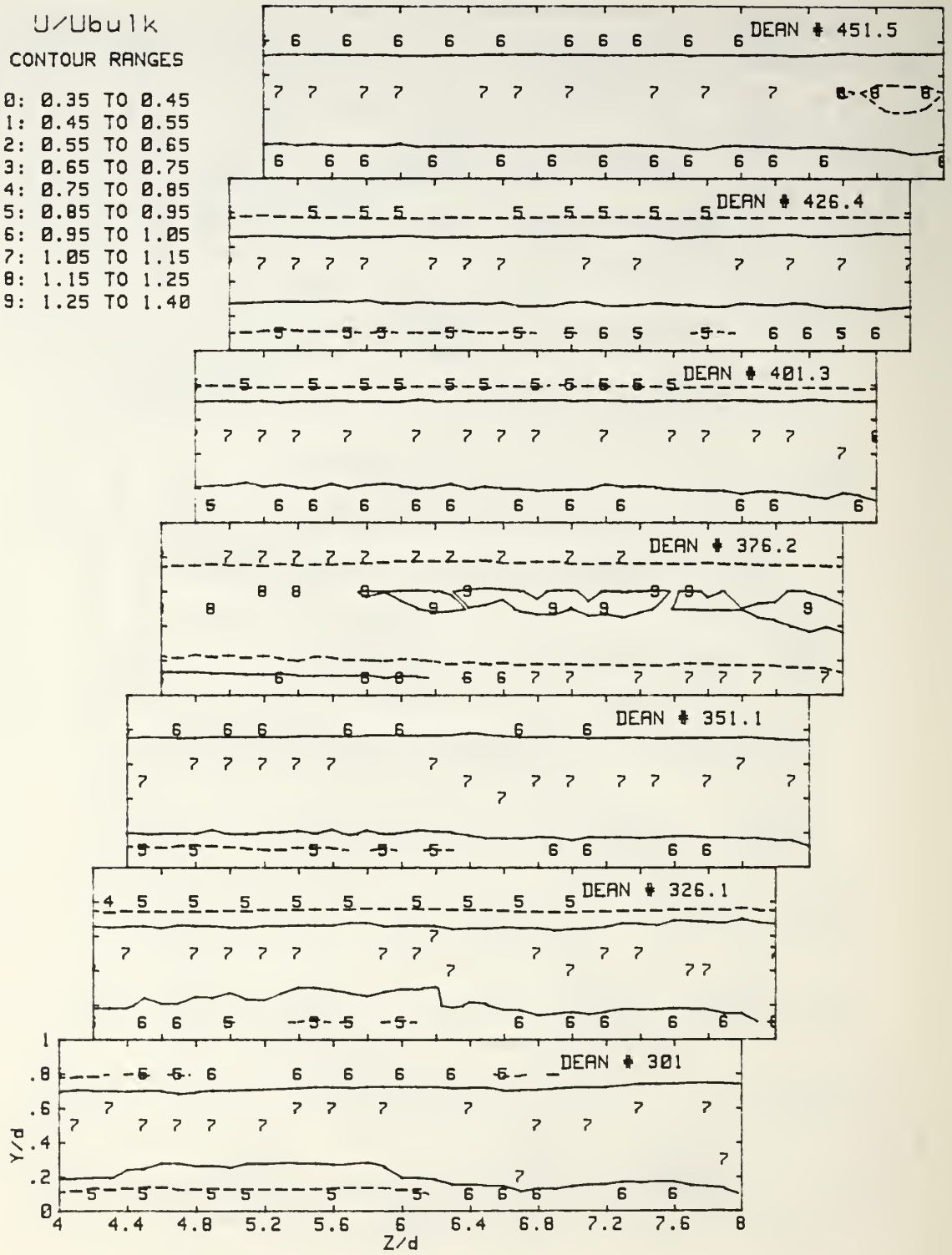

Figure 19. Streamwise Mean Velocity Contours, De=301.0 to De=451.5

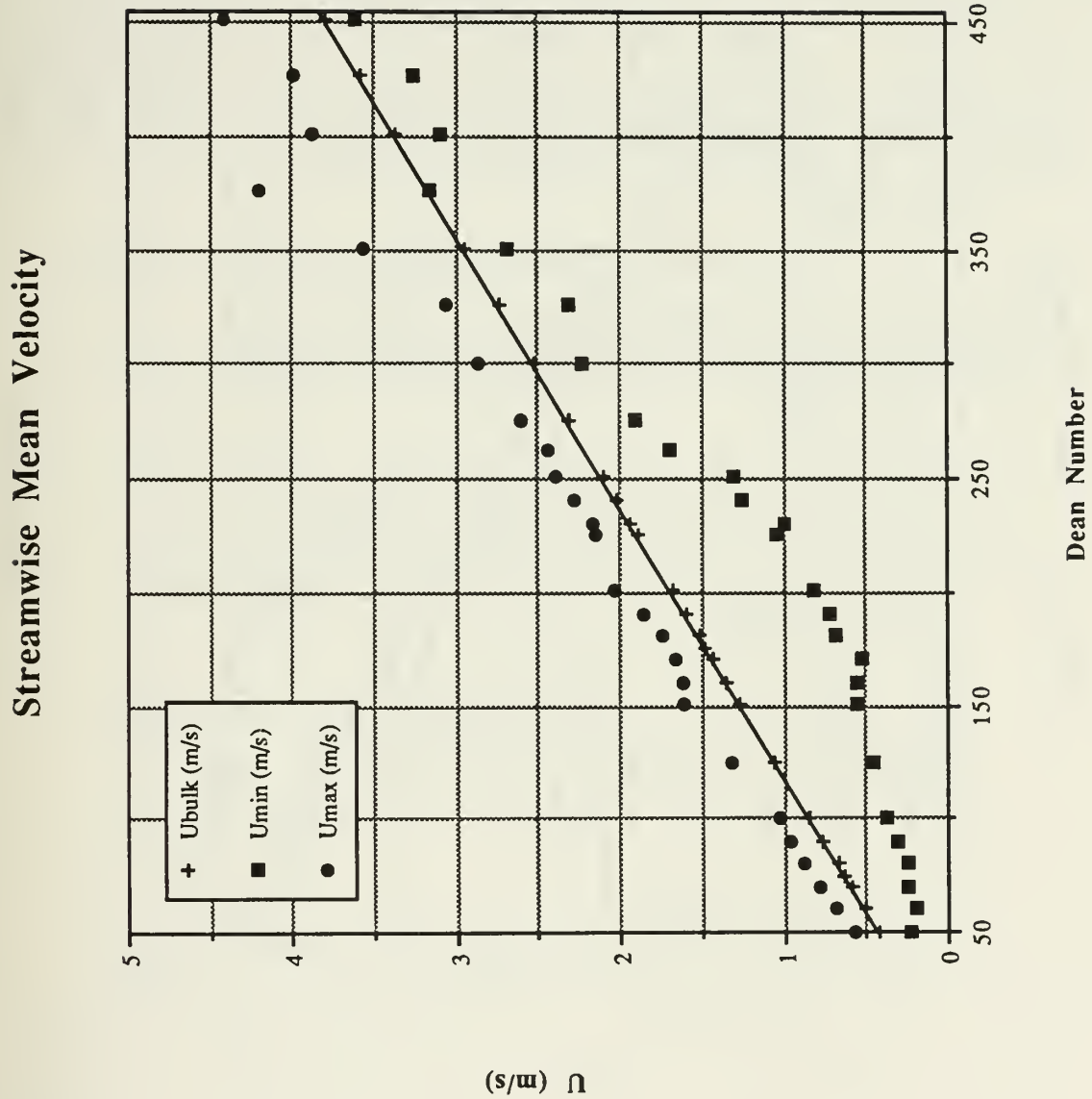

Figure 20. Maximum and Minimum Streamwise Mean Velocities, De=50.2 to De=451.5

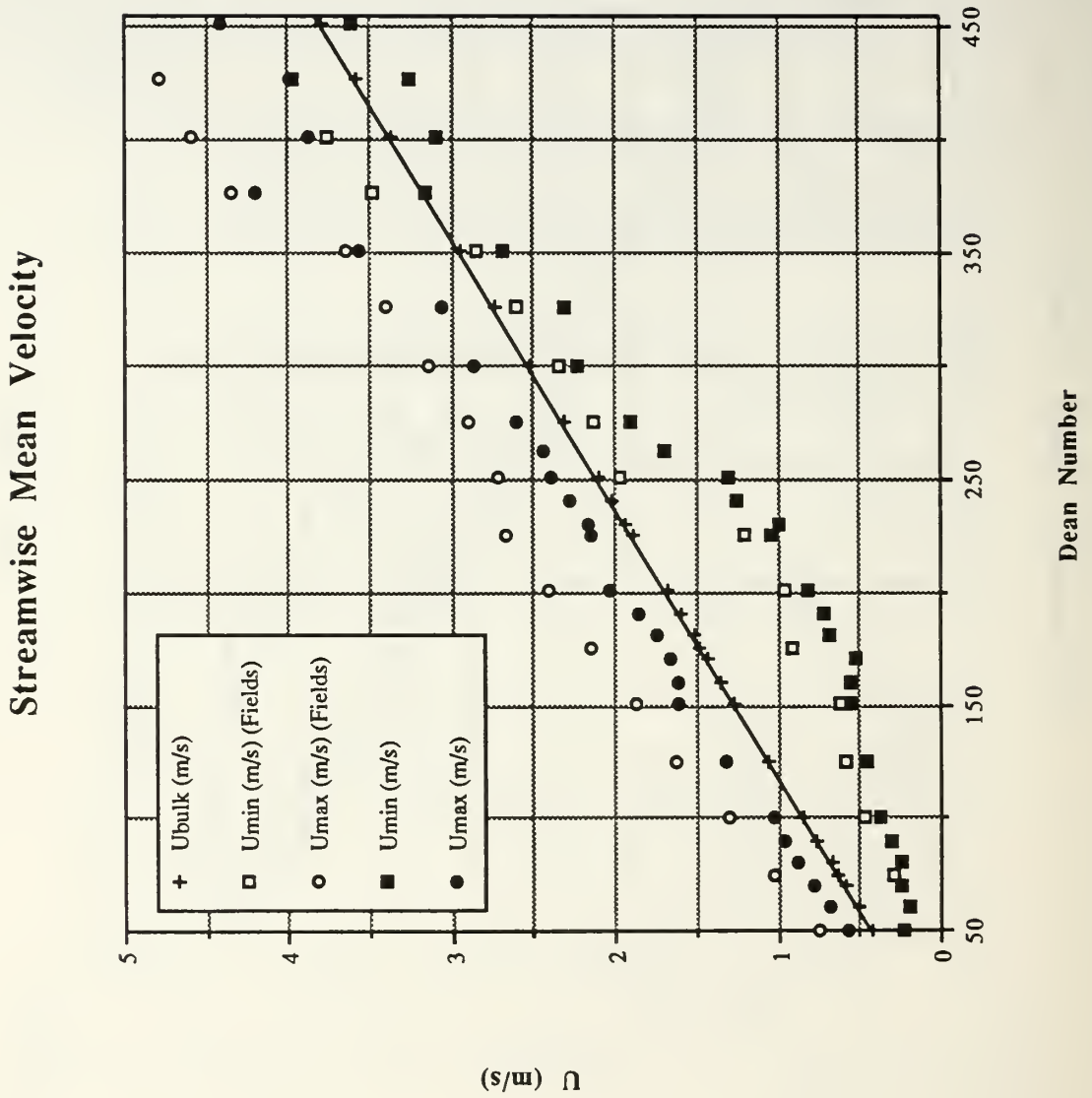

Figure 21. Maximum and Minimum Mean Velocities as Compared With Fields (1990)

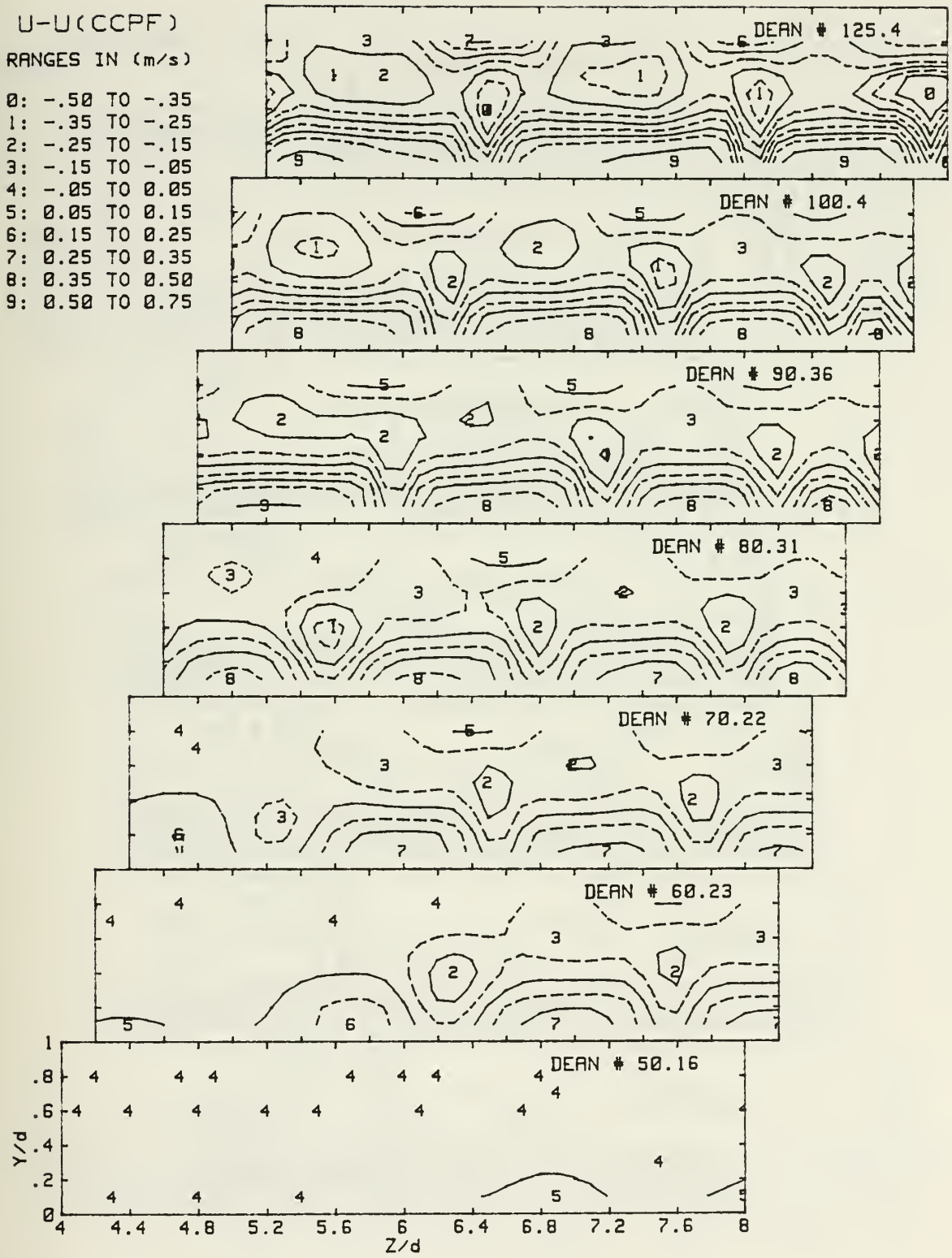

Figure 22. $\bar{u}$ - u_{CCPF} **Contours, De=50.2 to De=125.4**

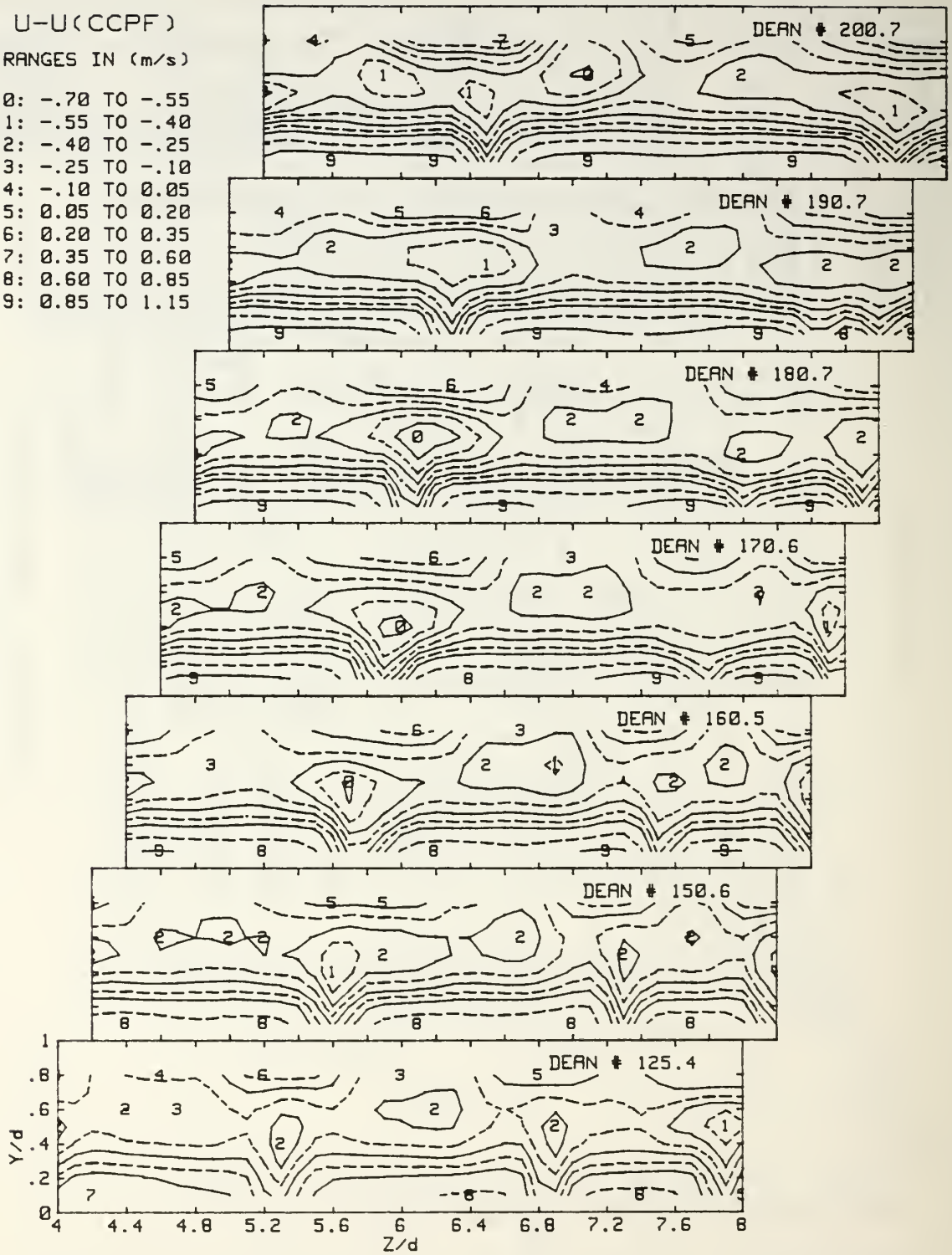

Figure 23. $\bar{u}$ - u_{CCPF} **Contours, De=125.4 to De=200.7**

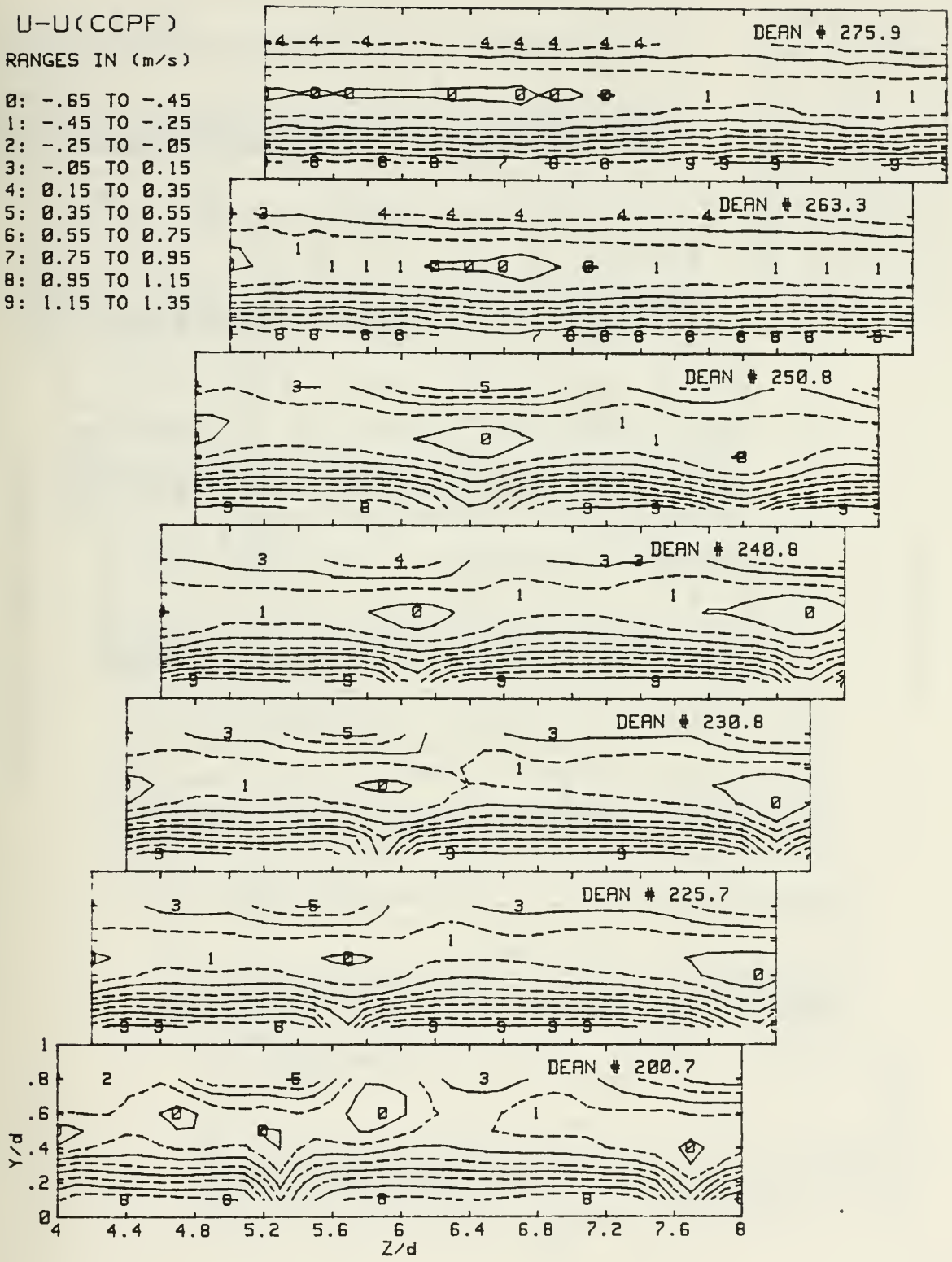

Figure 24. $\bar{u}$ - u_{CCPF} **Contours, De=200.7 to De=275.9**

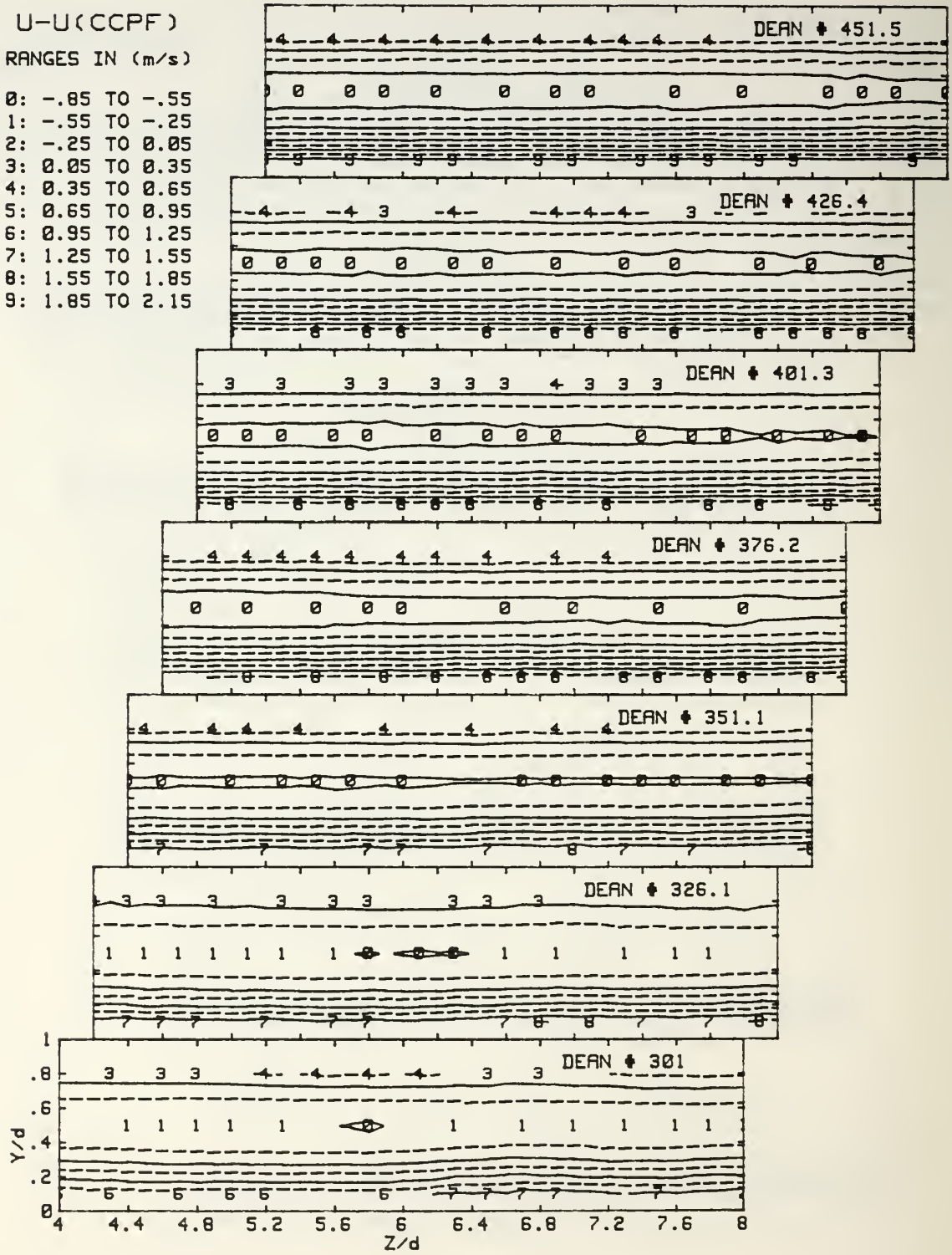

Figure 25. $\bar{u}$ - u_{CCPF} Contours, De=301.0 to De=451.5

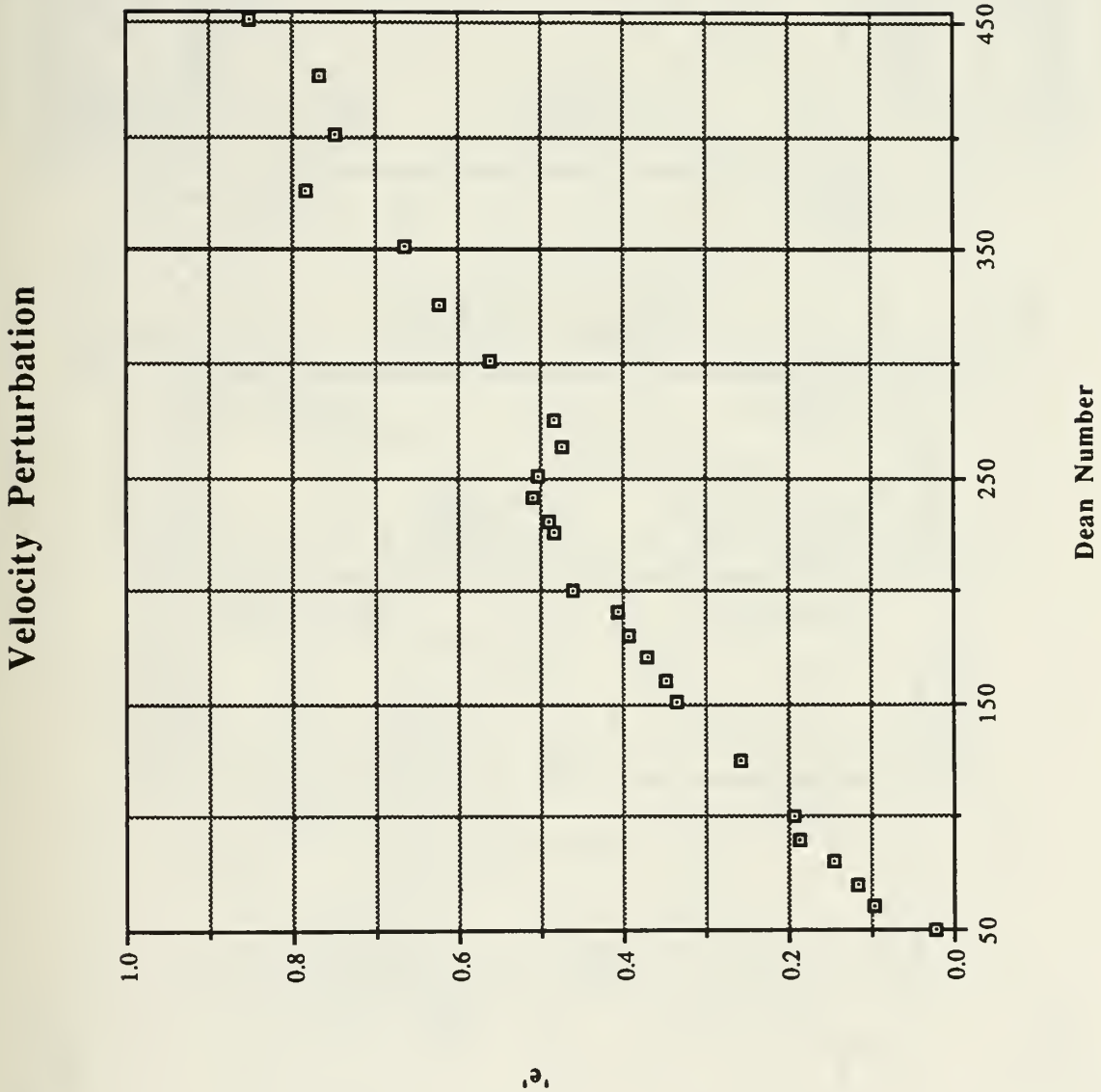

Figure 26. Streamwise Velocity Perturbation, e, vs Dean Number

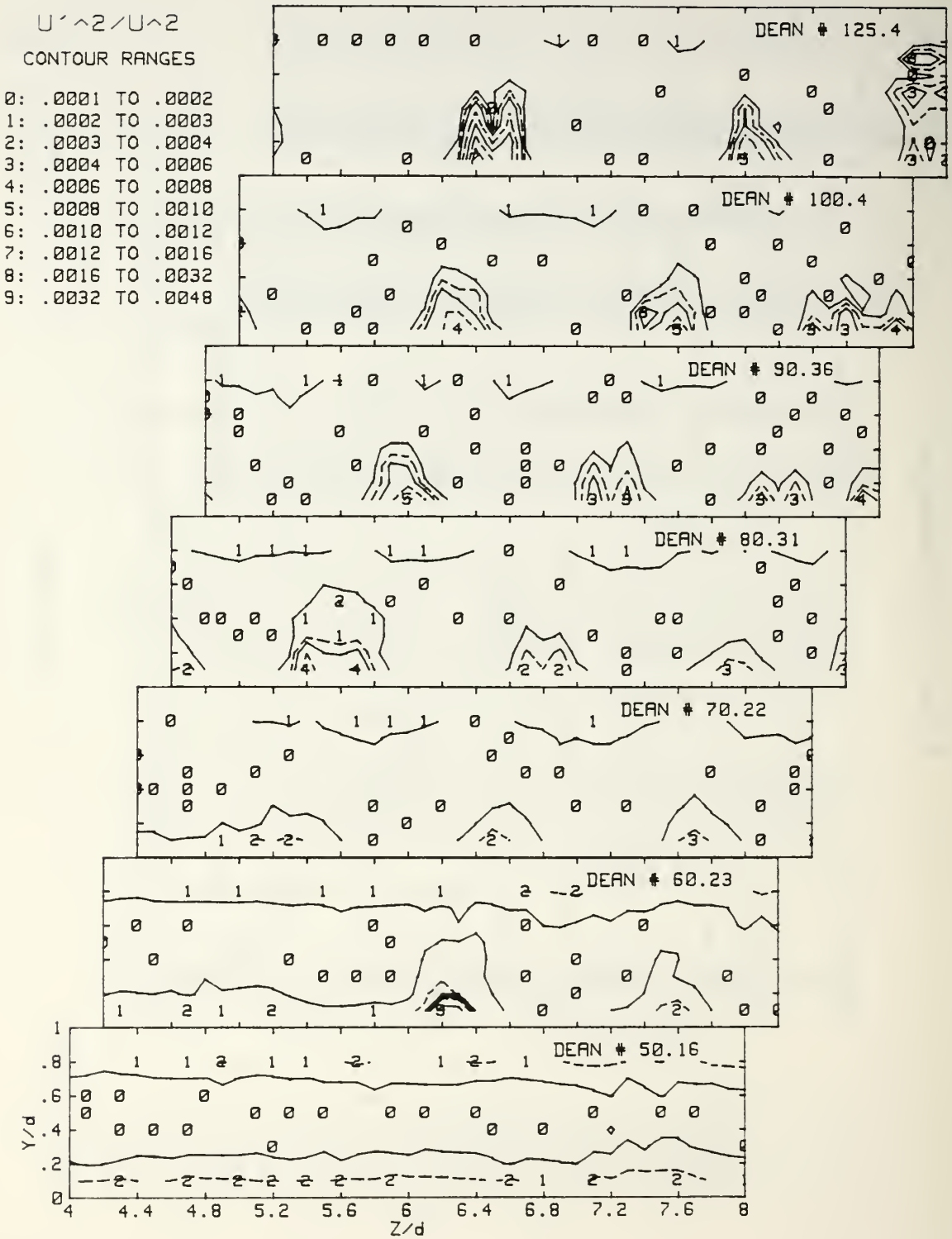

Figure 27. Longitudinal Reynolds Normal Stress Normalized by the Local Mean Velocity Squared, De=50.2 to De=125.4

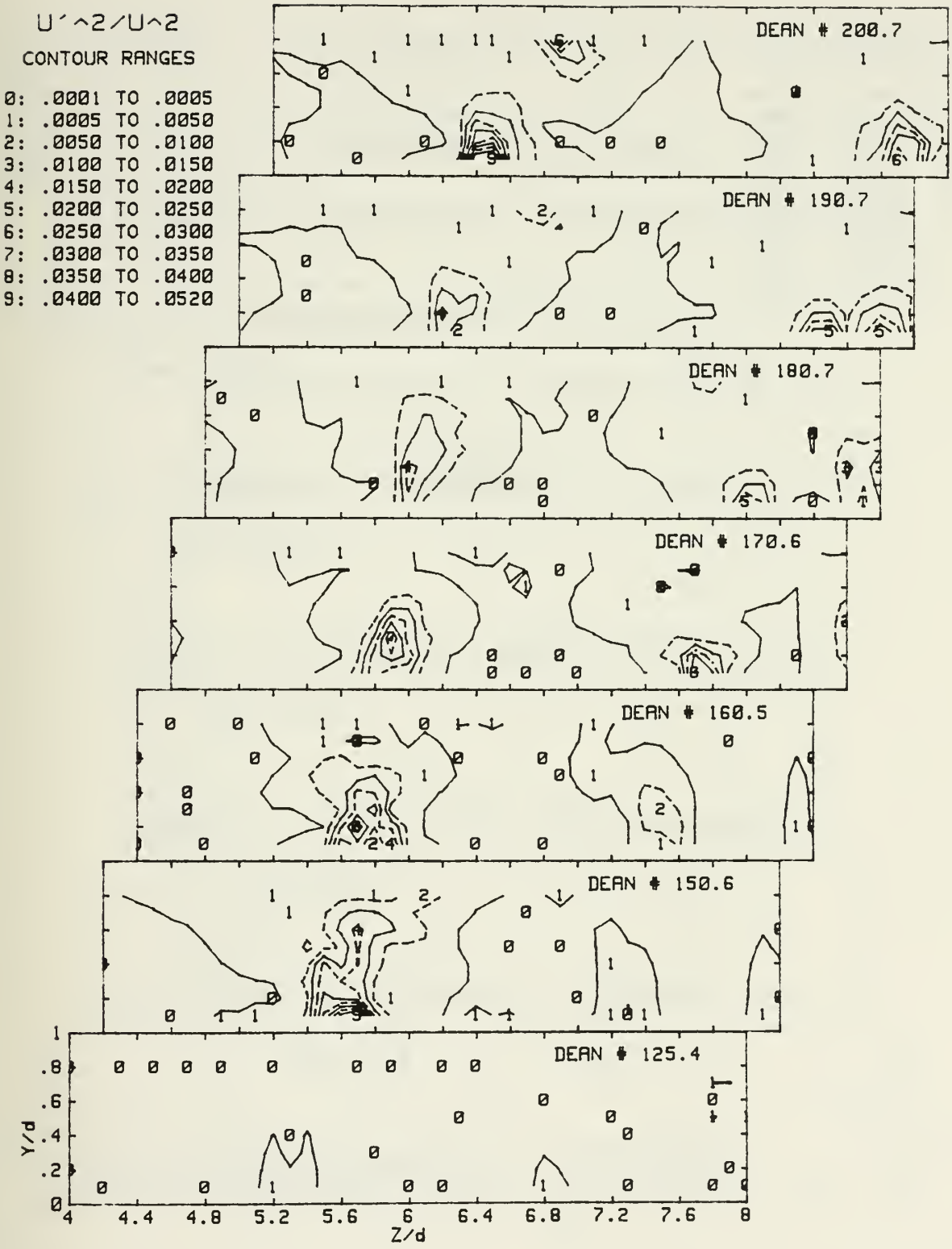

Figure 28. Longitudinal Reynolds Normal Stress Normalized by the Local Mean Velocity Squared, De=125.4 to De=200.7

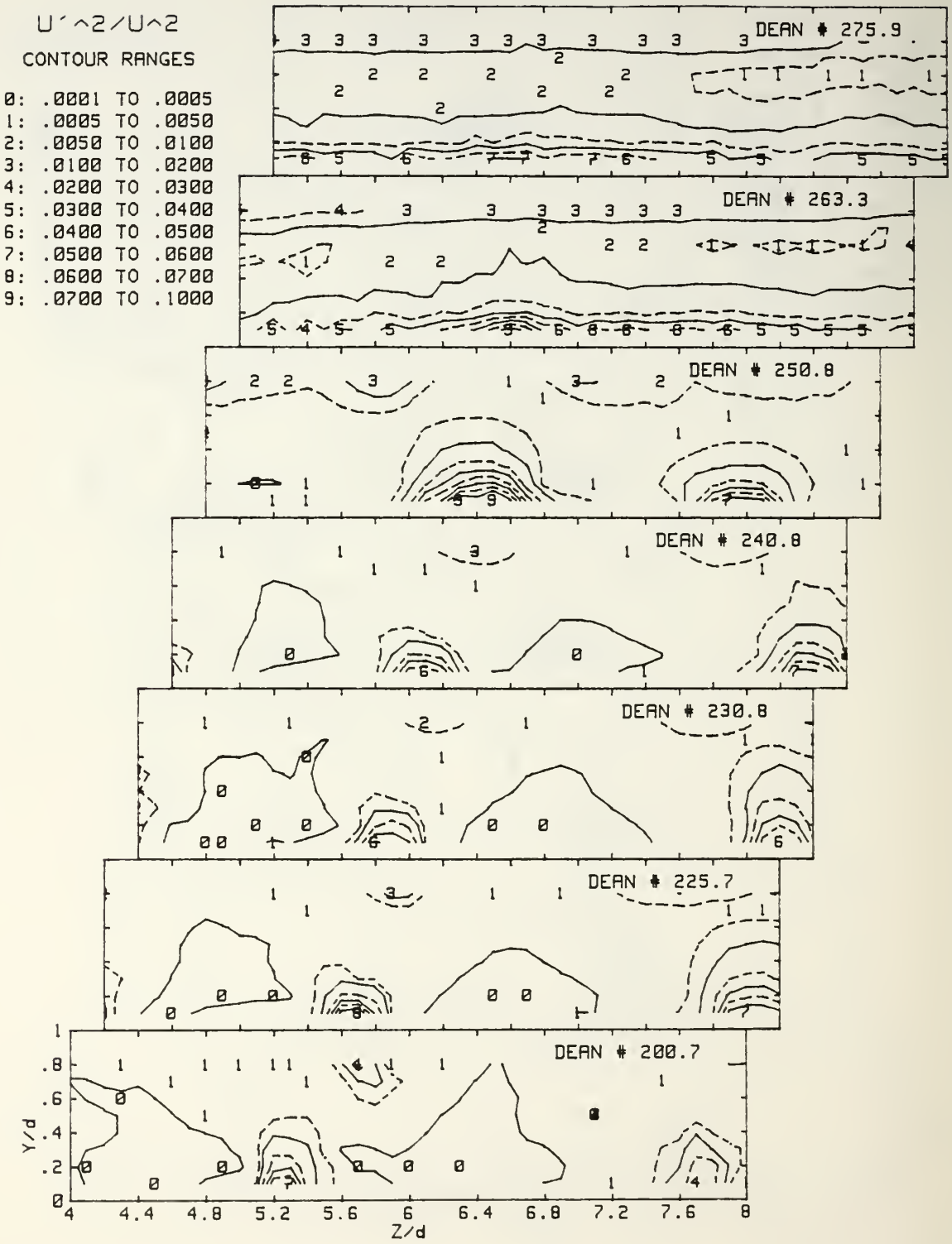

Figure 29. Longitudinal Reynolds Normal Stress Normalized by the Local Mean Velocity Squared, De=200.7 to De=275.9

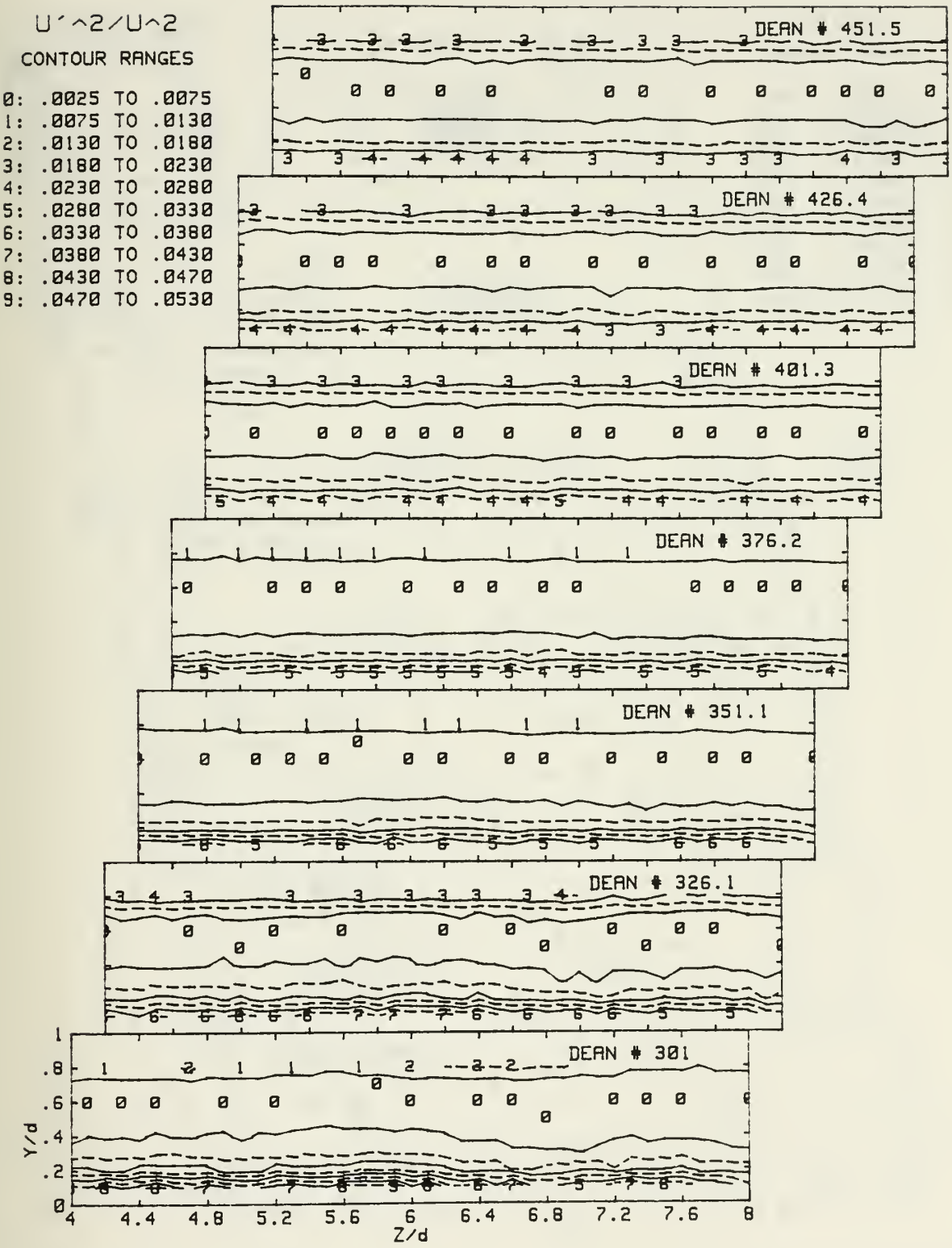

Figure 30. Longitudinal Reynolds Normal Stress Normalized by the Local Mean Velocity Squared, De=301.0 to De=451.5

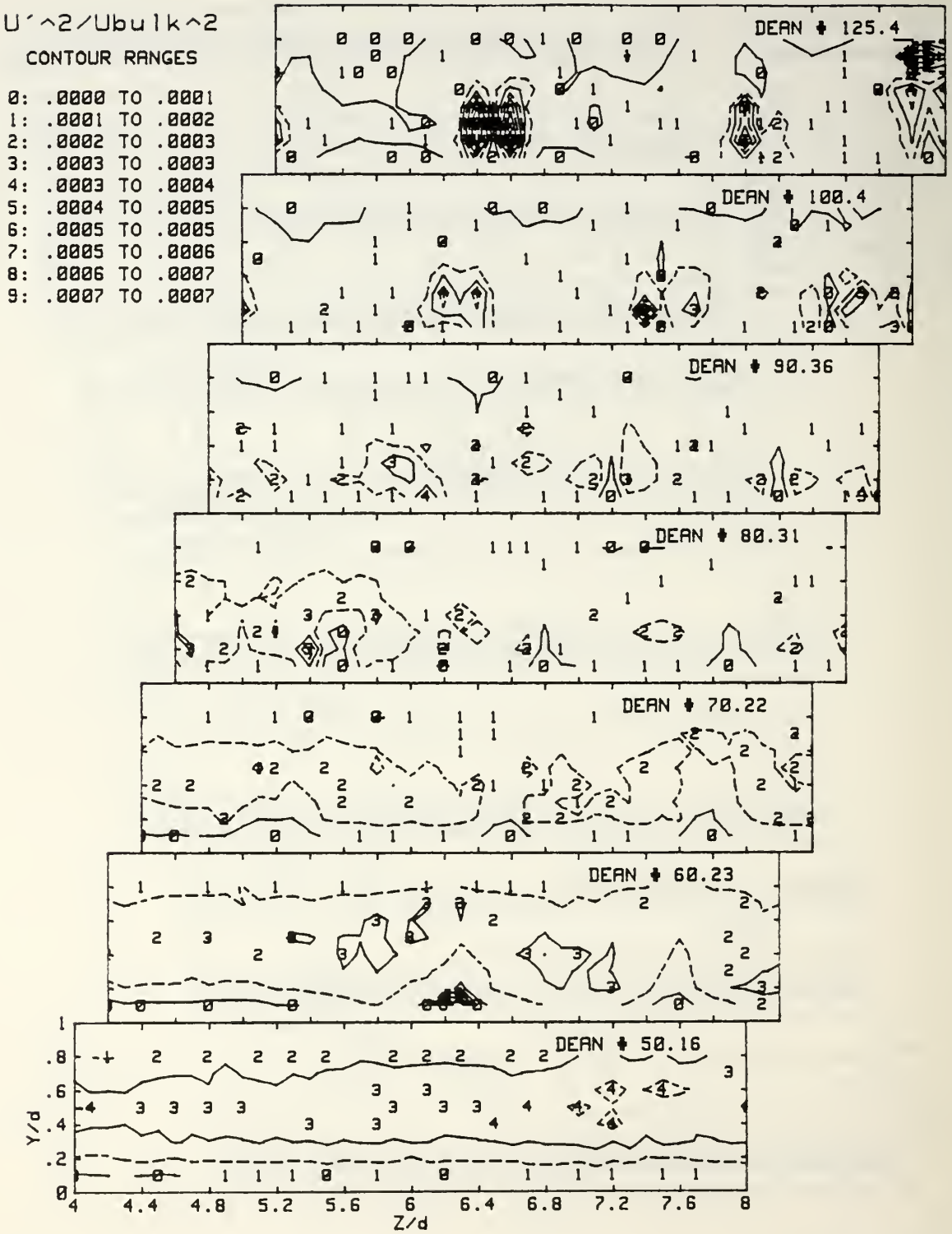

Figure 31. Longitudinal Reynolds Normal Stress Normalized by the Bulk Velocity Squared, De=50.2 to De=125.4

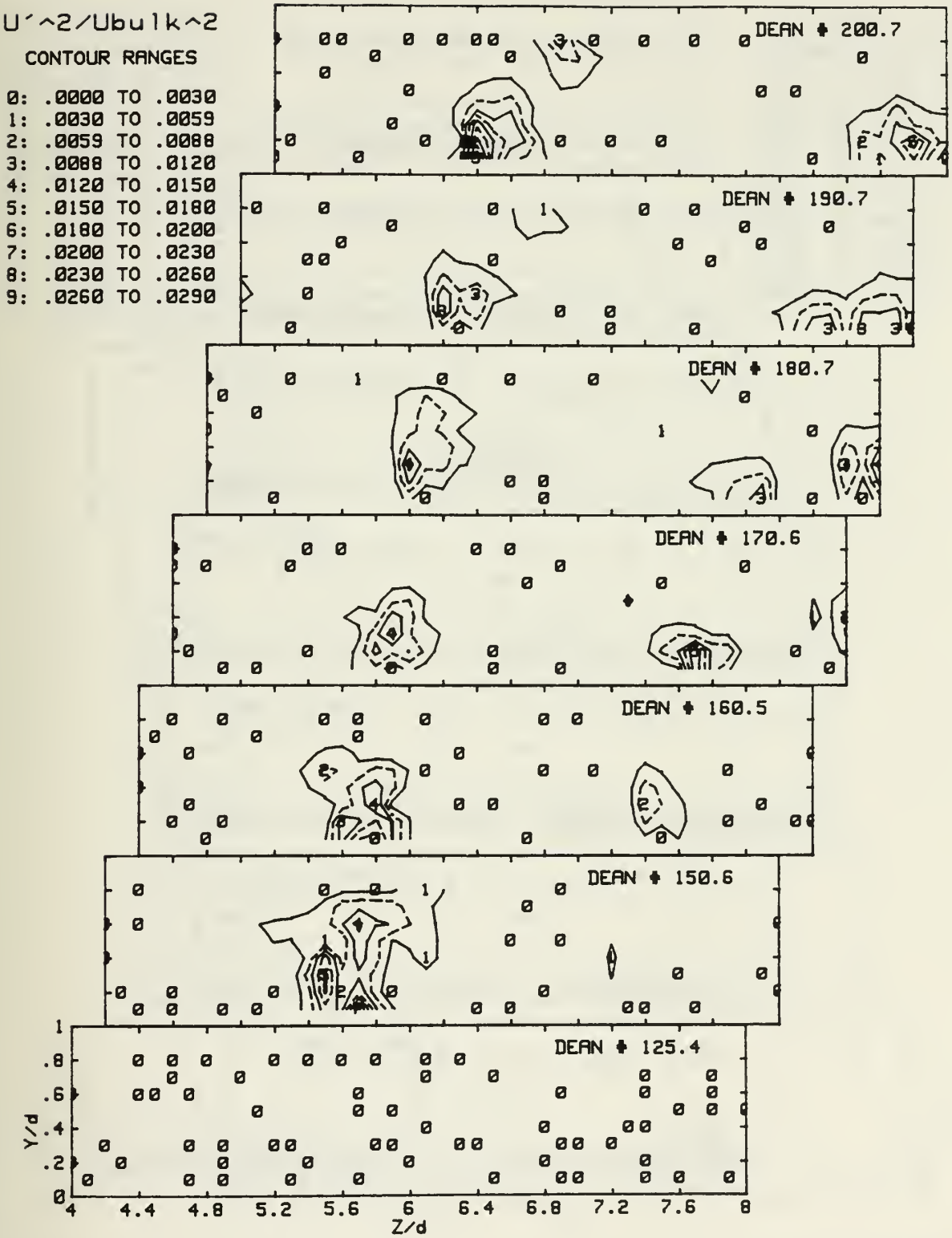

Figure 32. Longitudinal Reynolds Normal Stress Normalized by the Bulk Velocity Squared, De=125.4 to De=200.7

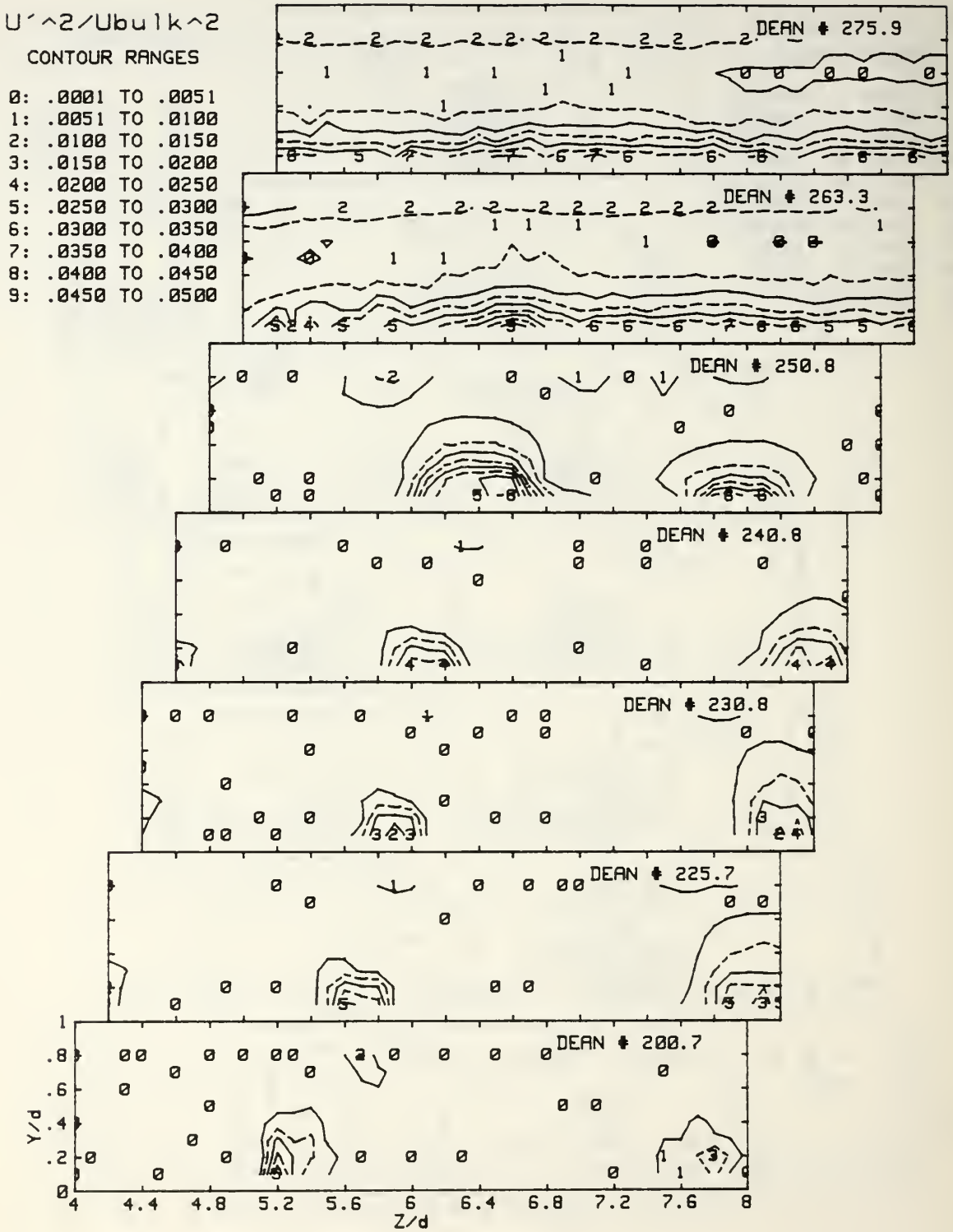

Figure 33. Longitudinal Reynolds Normal Stress Normalized by the Bulk Velocity Squared, De=200.7 to De=275.9

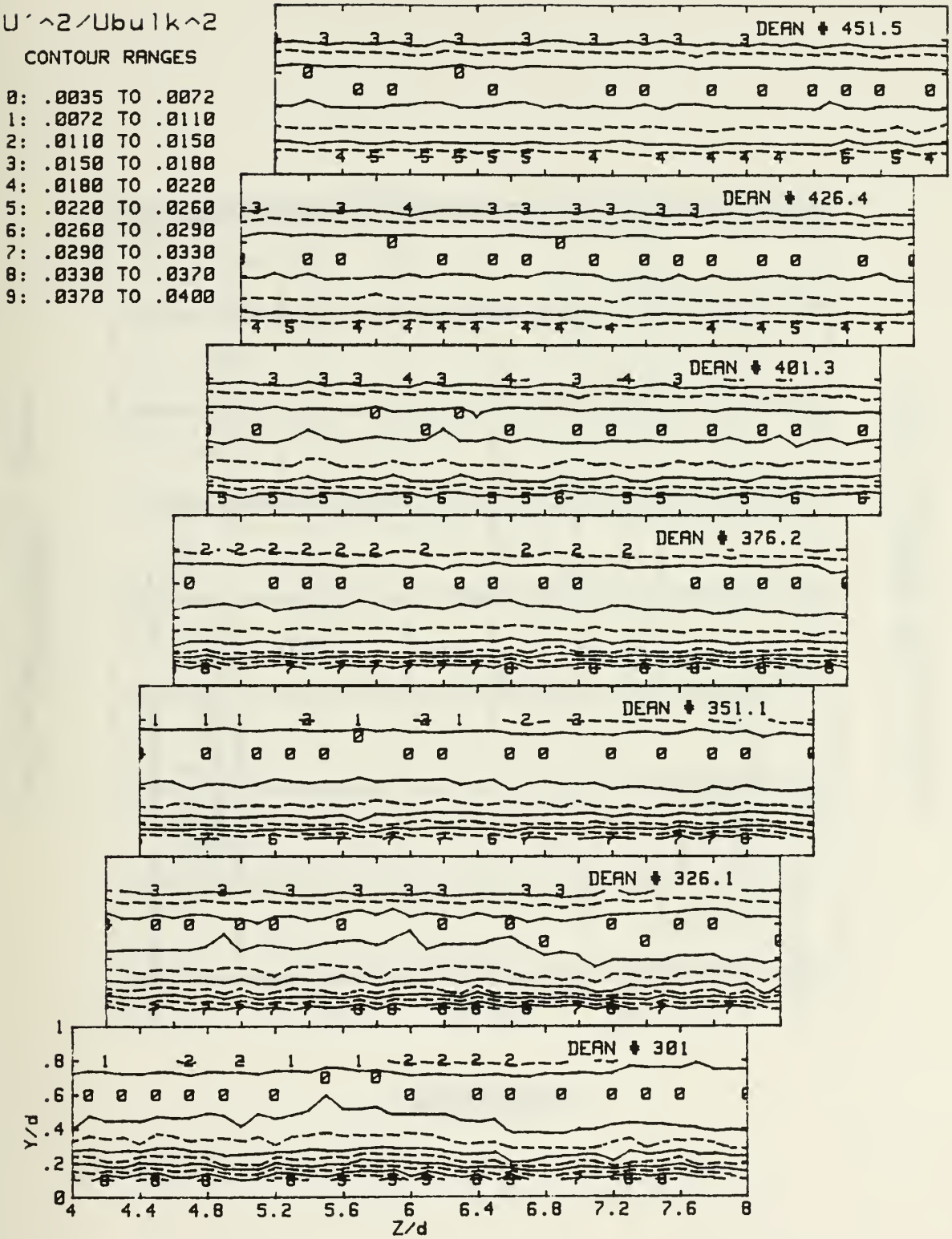

Figure 34. Longitudinal Reynolds Normal Stress Normalized by the Bulk Velocity Squared, De=301.0 to De=451.5

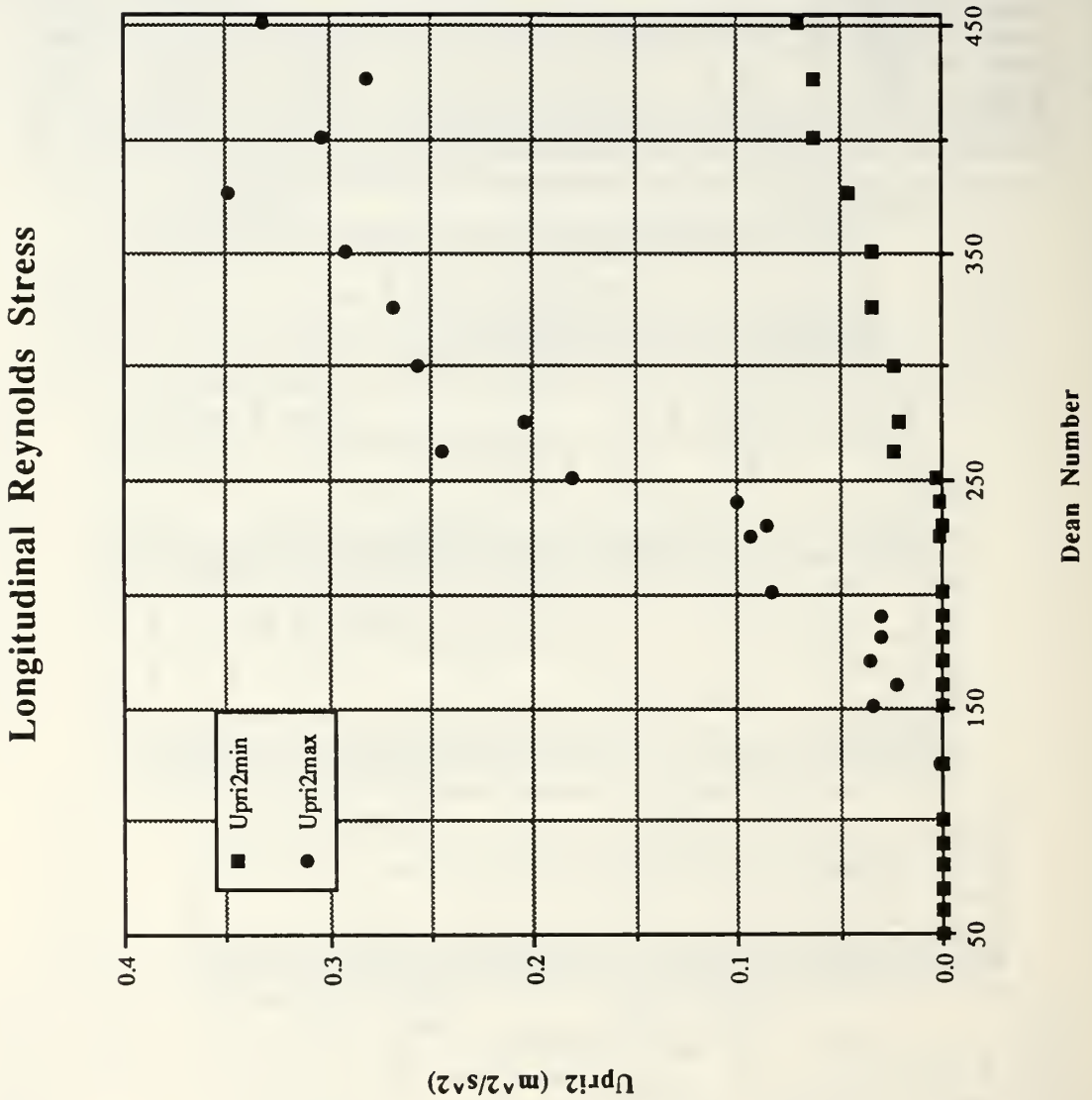

Figure 35. Maximum and Minimum Longitudinal Reynolds Stress, De=50.2 to 451.5

Figure 36. Maximum Value of Longitudinal Reynolds Normal Stress Within Left Most Upwash Region

Figure 37. Longitudinal Reynolds Normal Stress for Y/d=0.1 Within Left Most Upwash Region

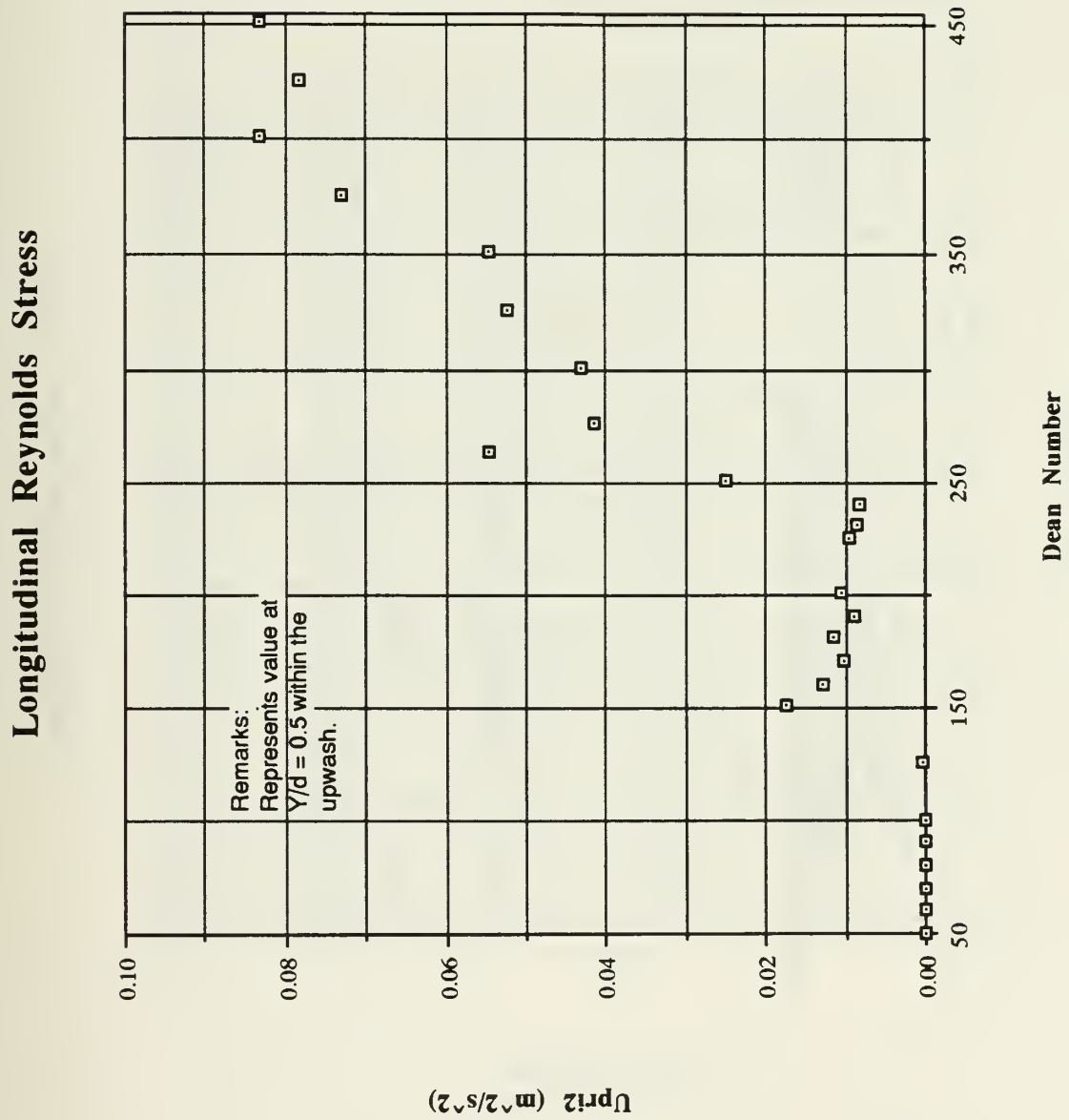

Figure 38. Longitudinal Reynolds Normal Stress for Y/d=0.5 Within Left Most Upwash Region

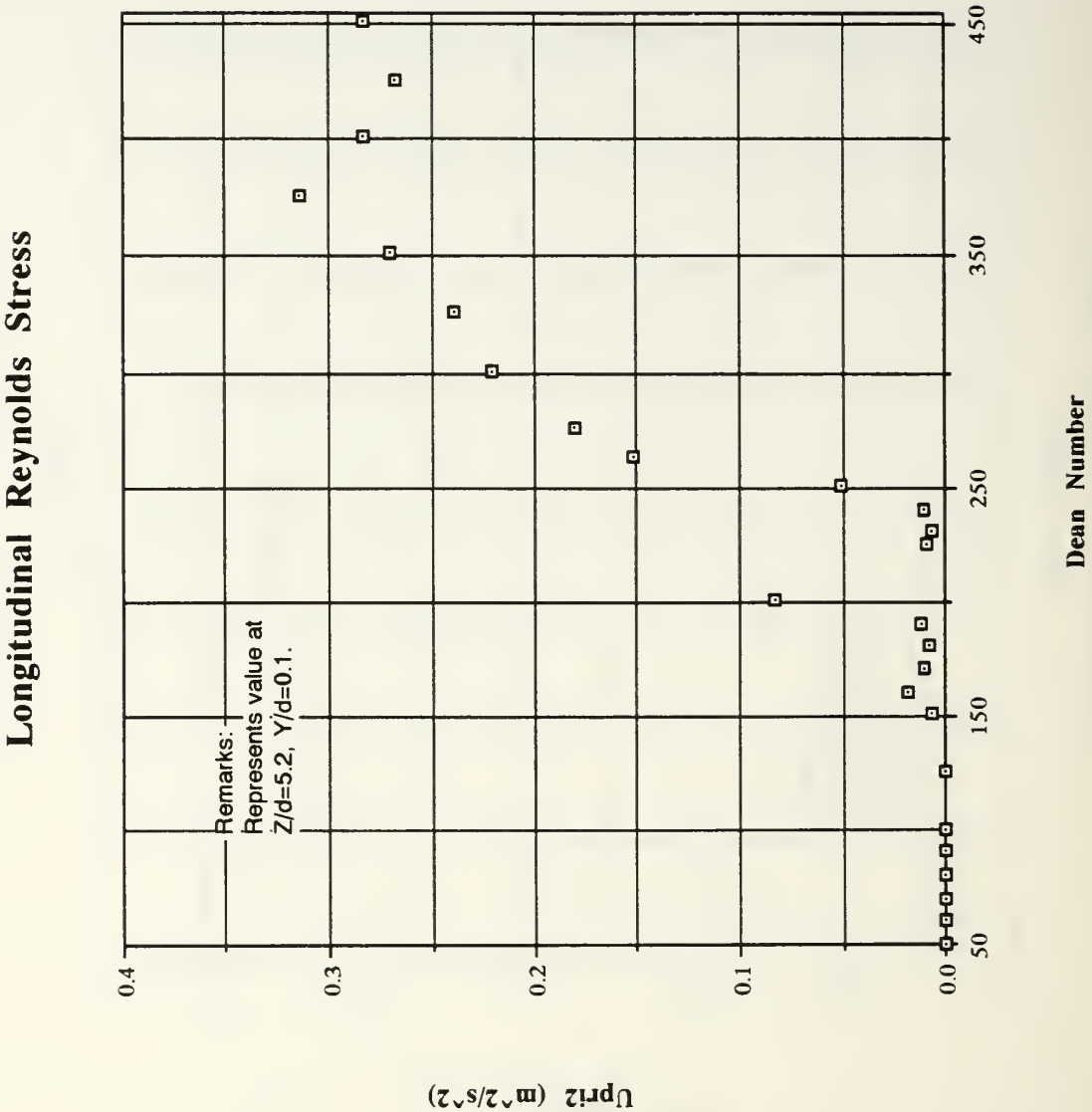

Figure 39. Longitudinal Reynolds Normal Stress for Z/d=5.2, Y/d=0.1 Within Left Most Upwash Region

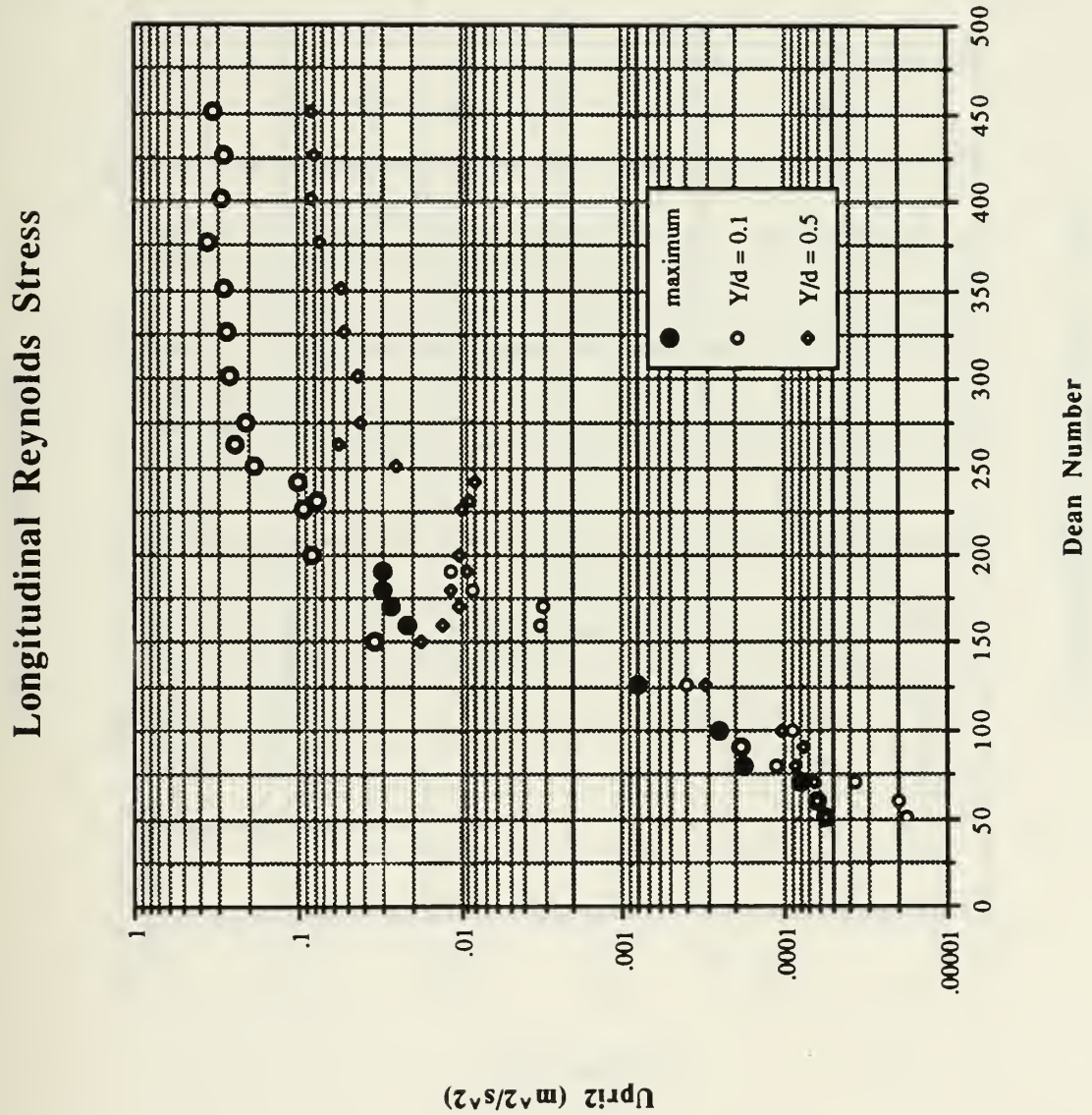

Figure 40. Longitudinal Reynolds Normal Stress Within Left Most Upwash Region, De=50.2 to De=451.5. Data are presented for three positions: maximum value, Y/d=0.1, and Y/d=0.5

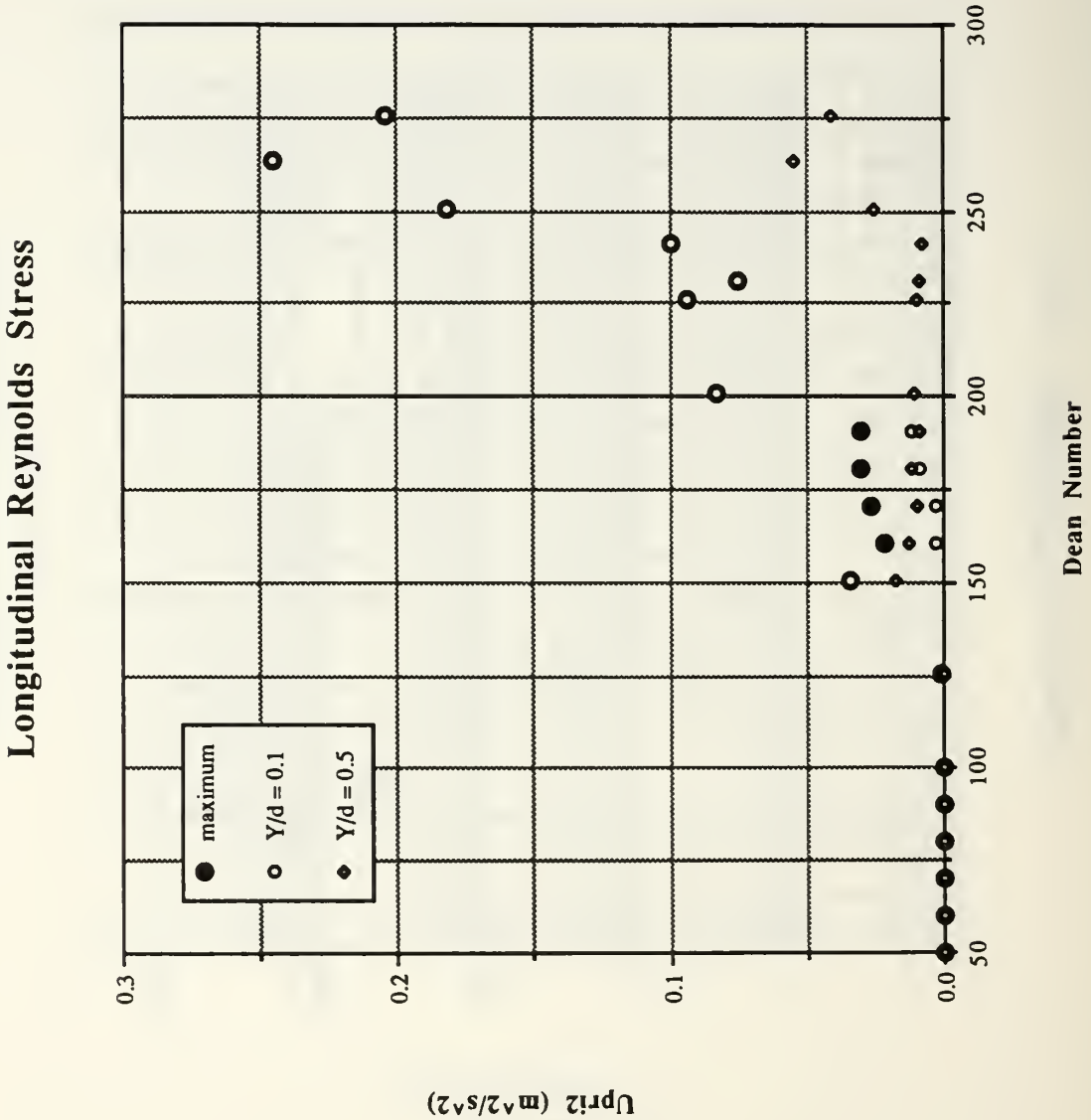

Figure 41. Longitudinal Reynolds Normal Stress Within Left Most Upwash Region, De=50.2 to De=275.9. Data are presented for three positions: maximum value, Y/d=0.1, and Y/d=0.5

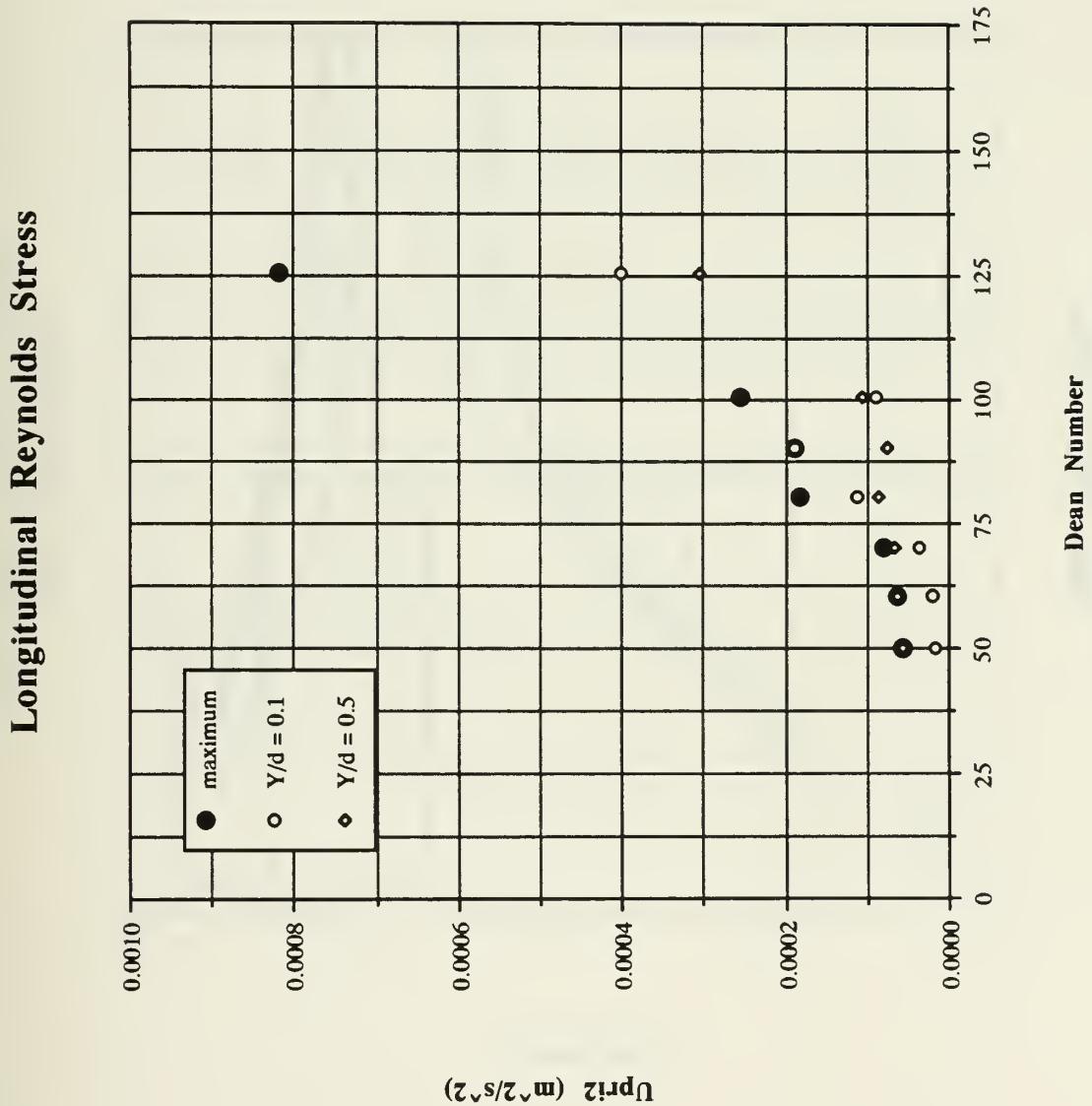

Figure 42. Longitudinal Reynolds Normal Stress Within Left Most Upwash Region, De=50.2 to De=125.4. Data are presented for three positions: maximum value, Y/d=0.1, and Y/d=0.5

Figure 43. Streamwise Mean Velocity Profiles, De=125

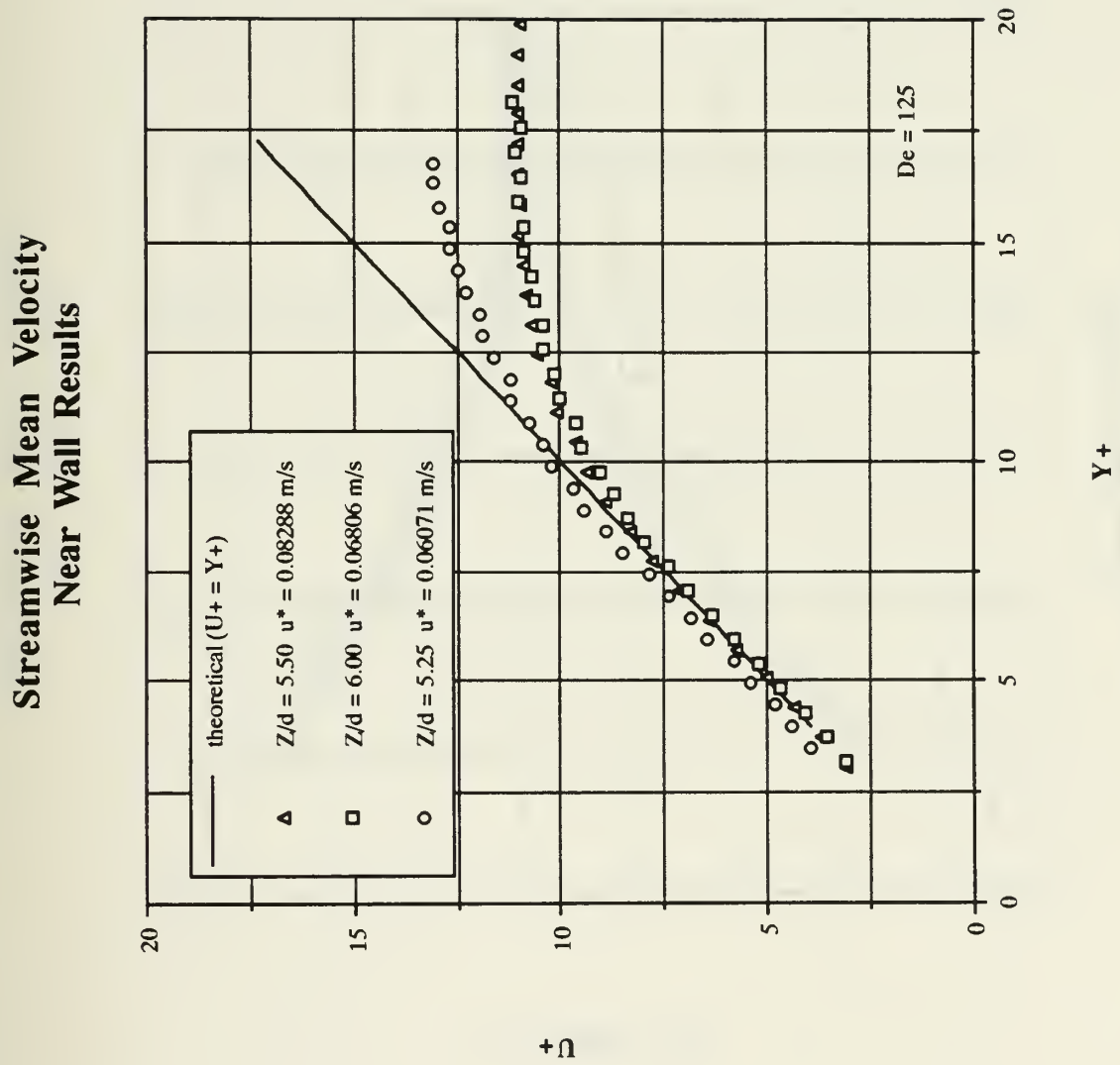

Figure 44. Mean Velocity Profiles in Wall Coordinates, De=125

Figure 45. Streamwise Mean Velocity Profiles, De=170

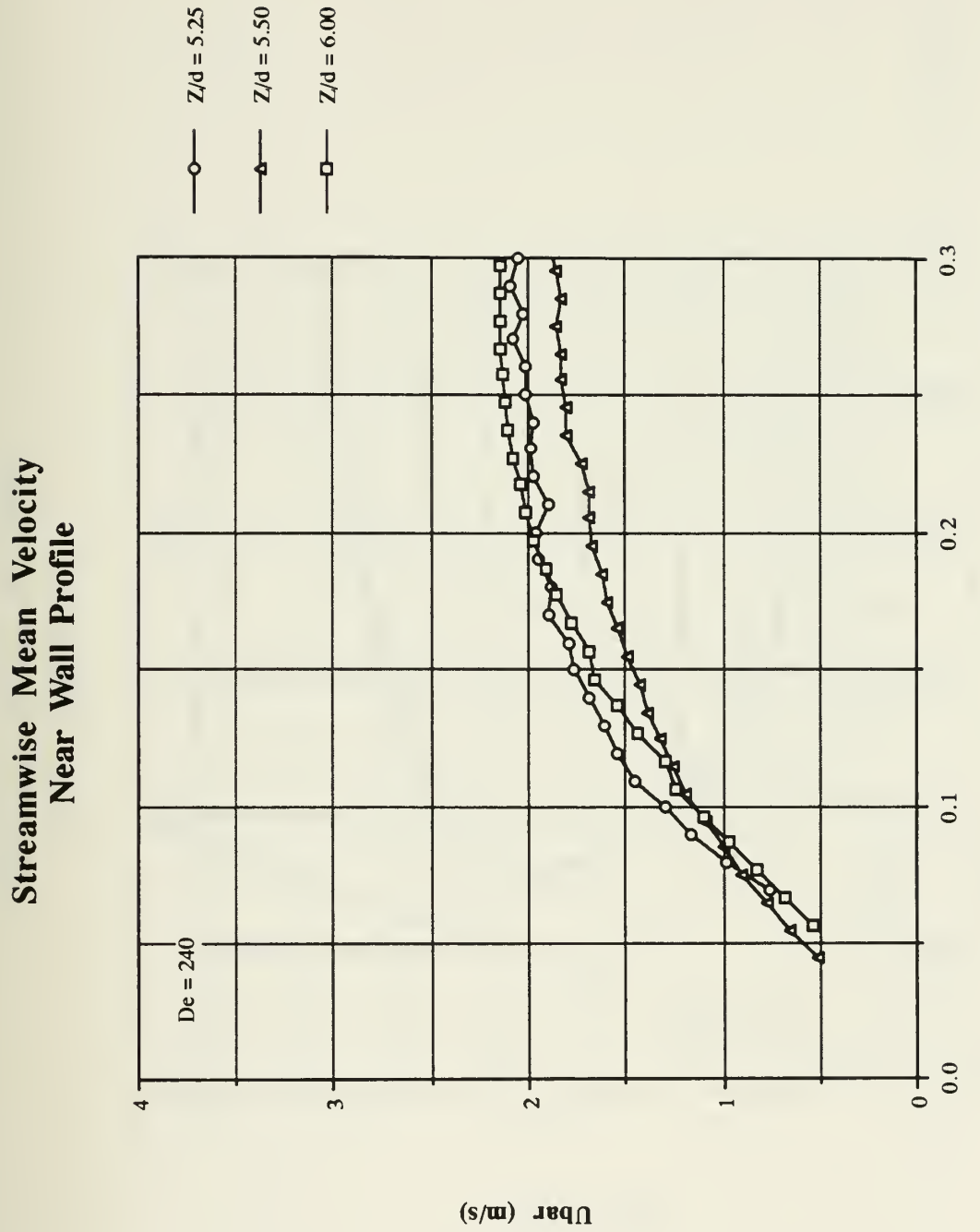

Figure 46. Streamwise Mean Velocity Profiles, De=240

Figure 47. Streamwise Mean Velocity Profile, De=401

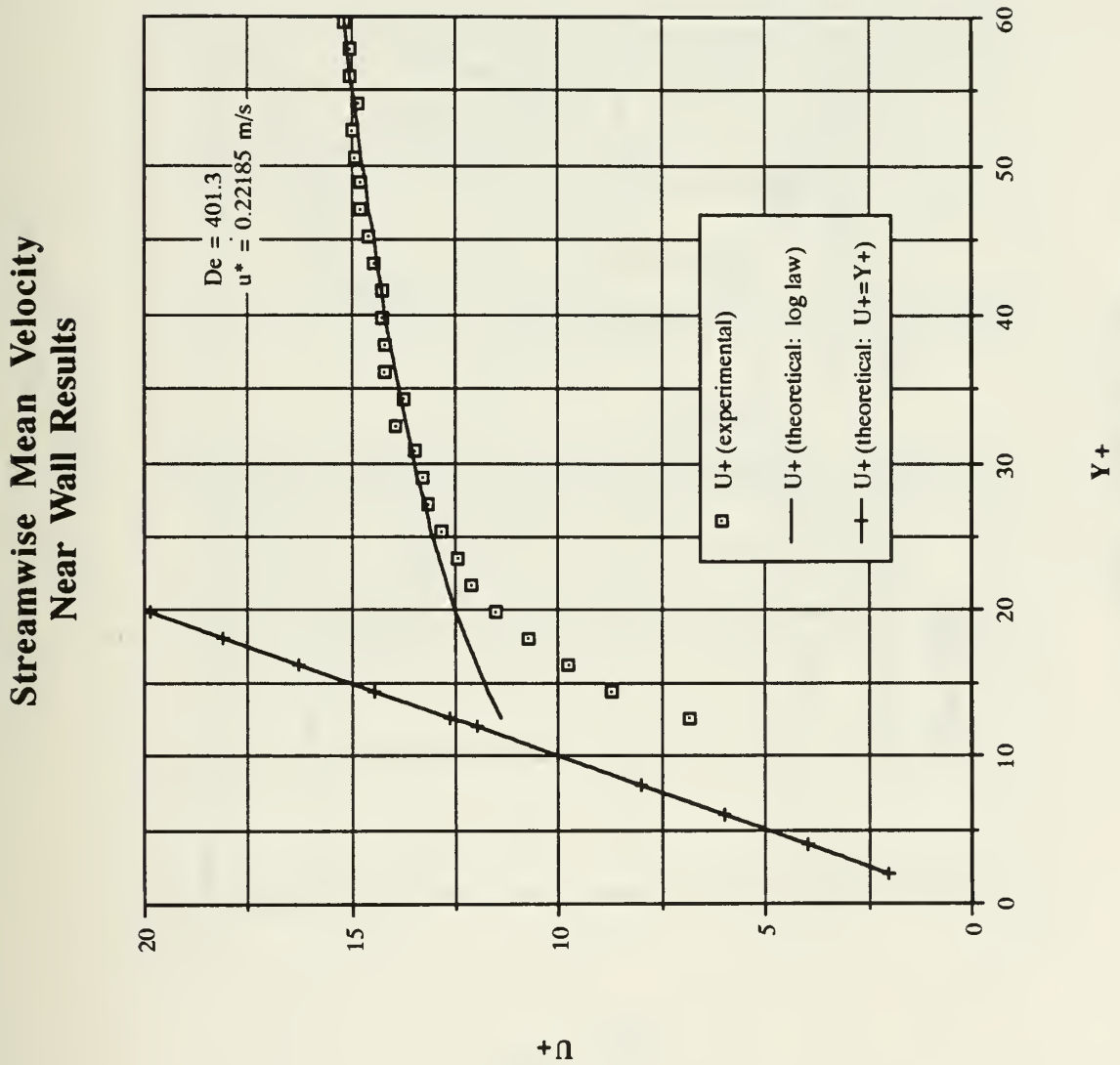

Figure 48. Mean Velocity Profile in Wall Coordinates, De=401

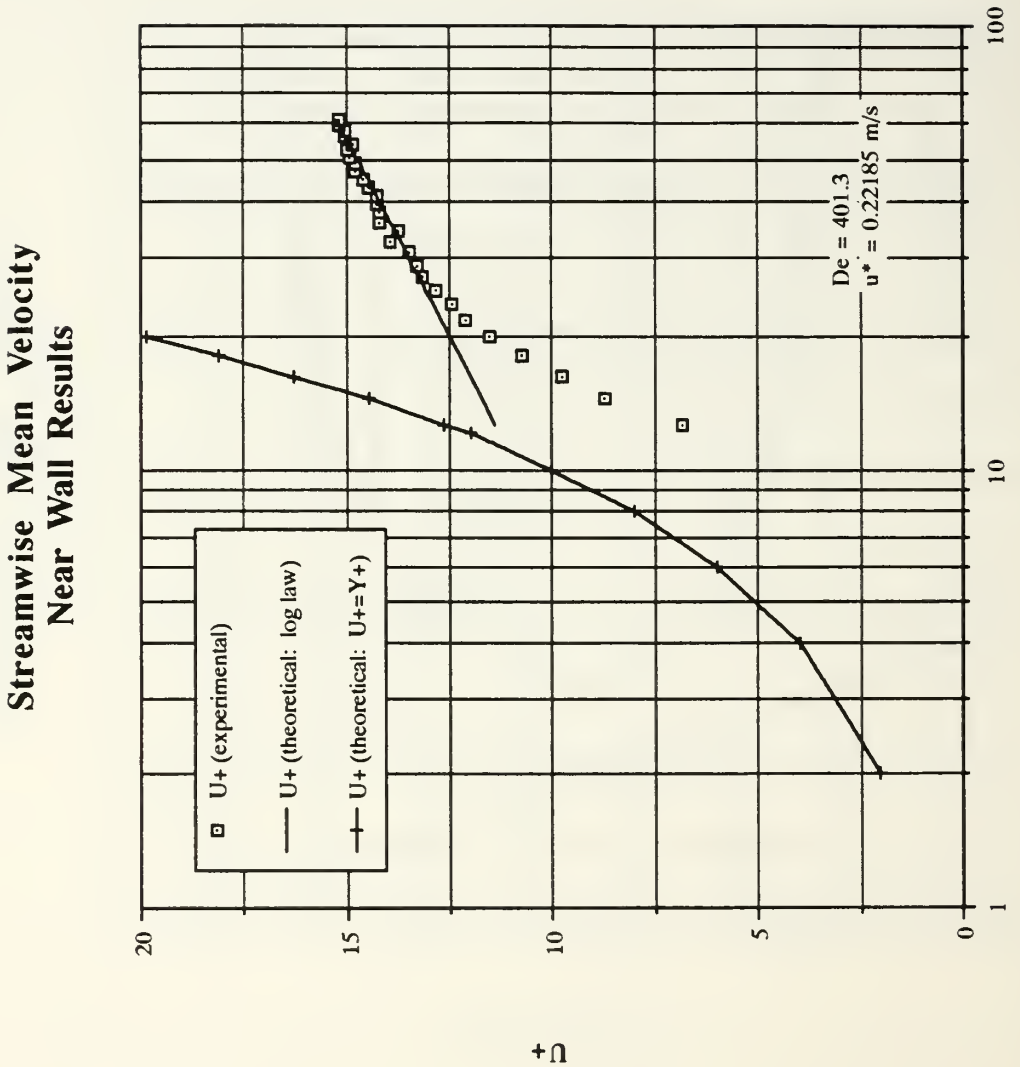

Figure 49. Semi-log Plot of Streamwise Mean Velocity Profile in Wall Coordinates, De=401

Figure 50. Longitudinal Reynolds Normal Stress Profiles, De=125

Figure 51. Longitudinal Reynolds Normal Stress Profiles, De=170

Figure 52. Longitudinal Reynolds Normal Stress Profiles, De=240

Figure 53. Longitudinal Reynolds Normal Stress Profiles, De=401

Figure 54. Normalized Longitudinal Reynolds Stress Profiles, De=125

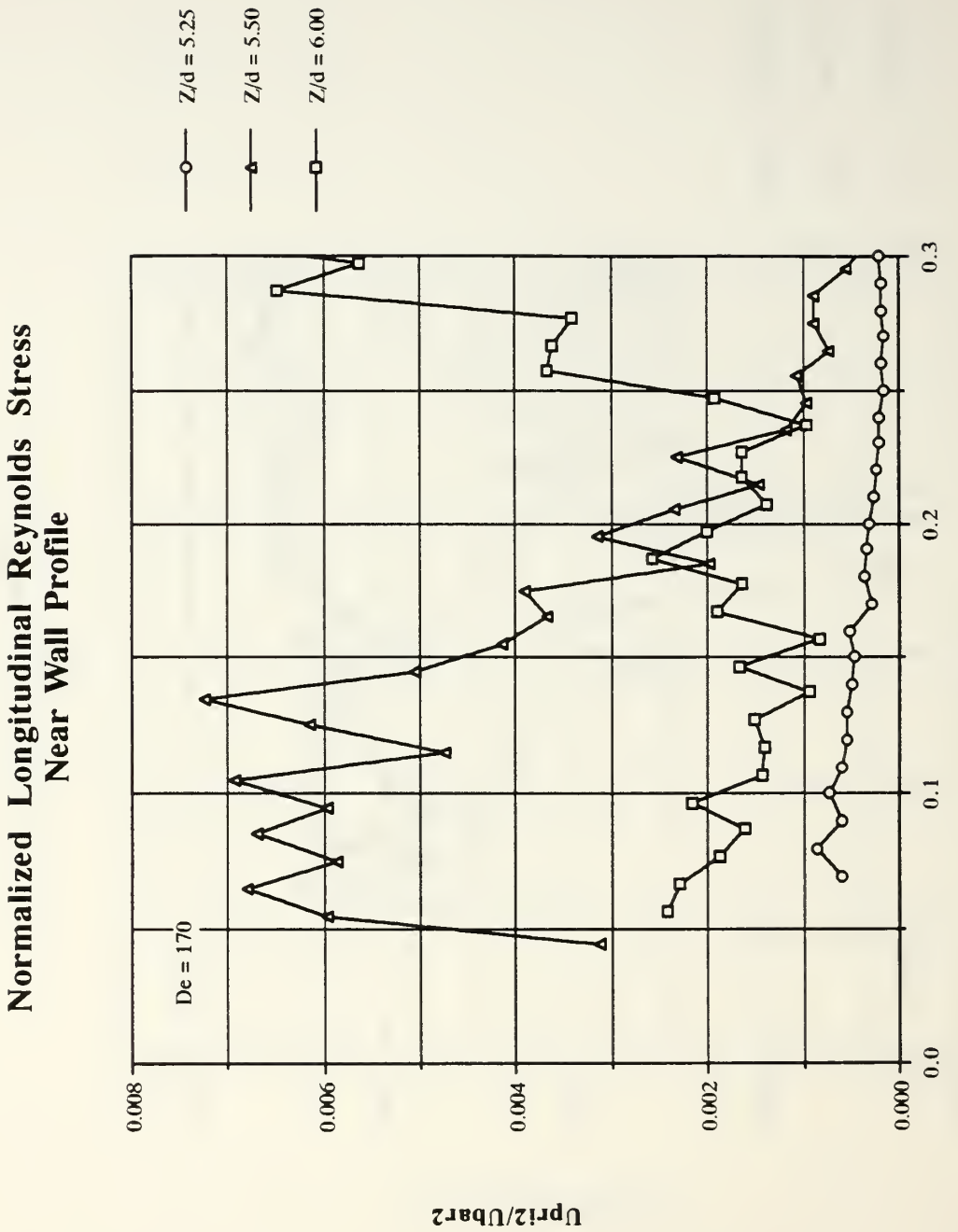

Figure 55. Normalized Longitudinal Reynolds Stress Profiles, De=170

Figure 56. Normalized Longitudinal Reynolds Stress Profiles, De=240

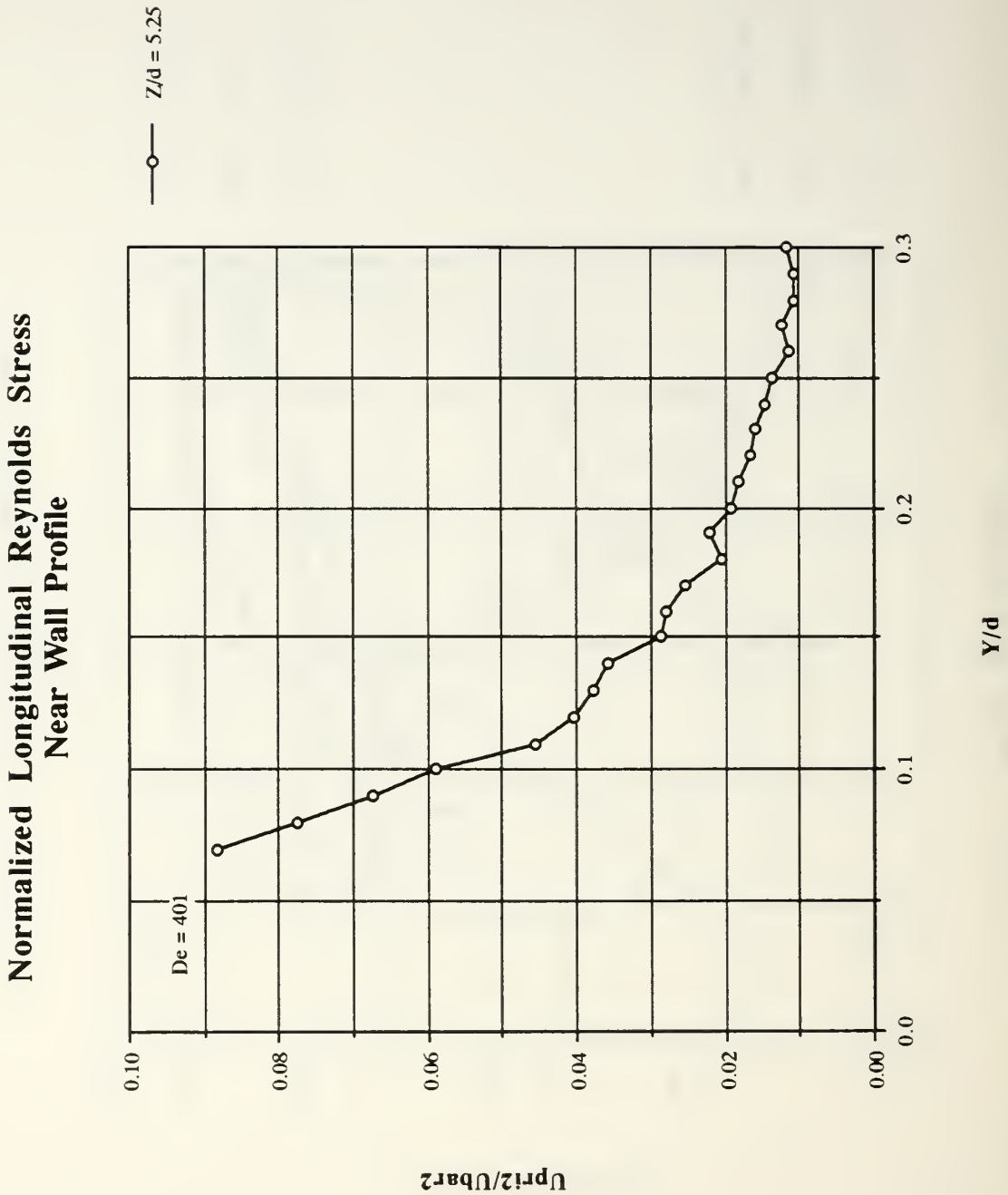

Figure 57. Normalized Longitudinal Reynolds Stress Profiles, De=401

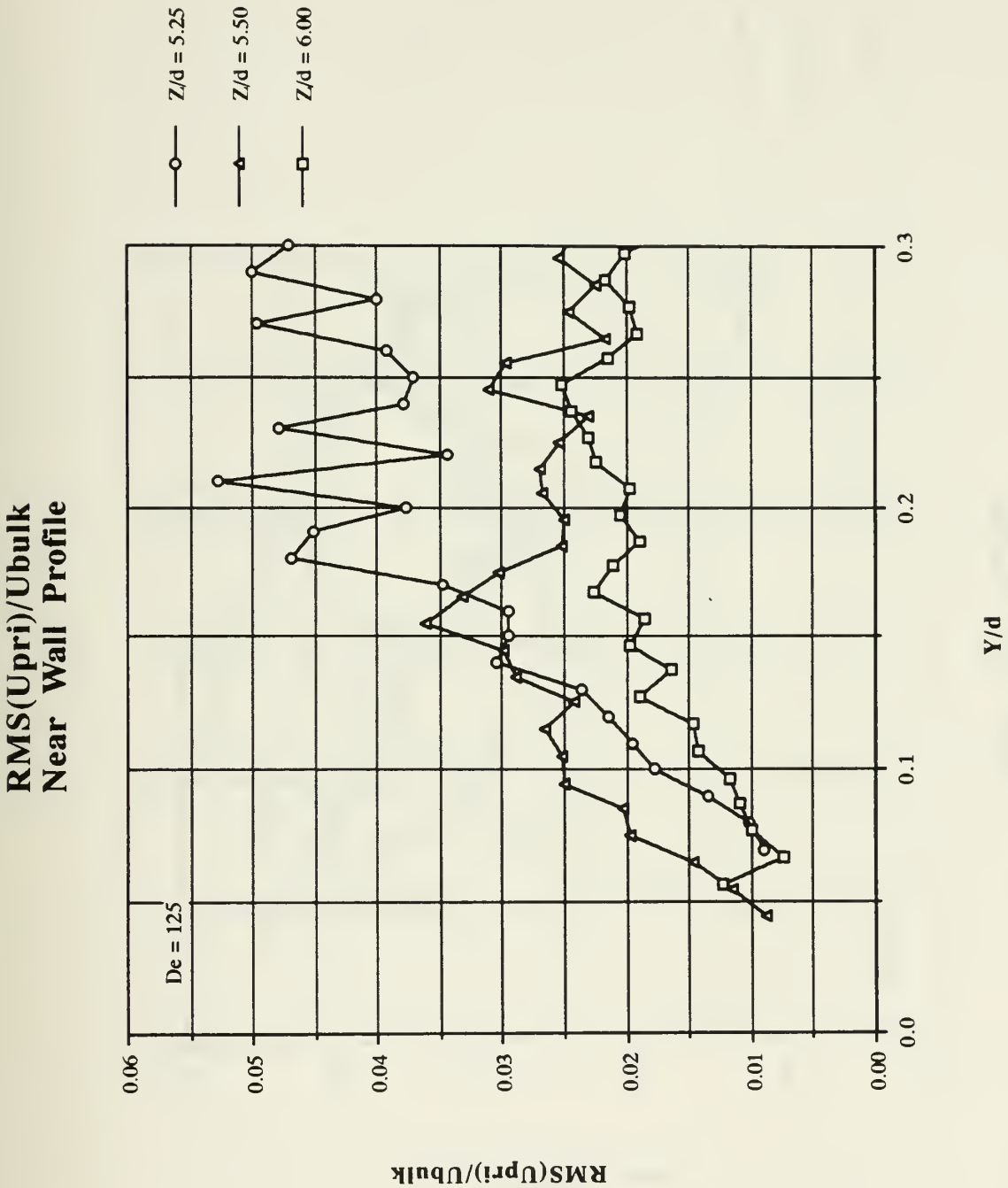

Figure 58. Normalized RMS Intensity, De=125

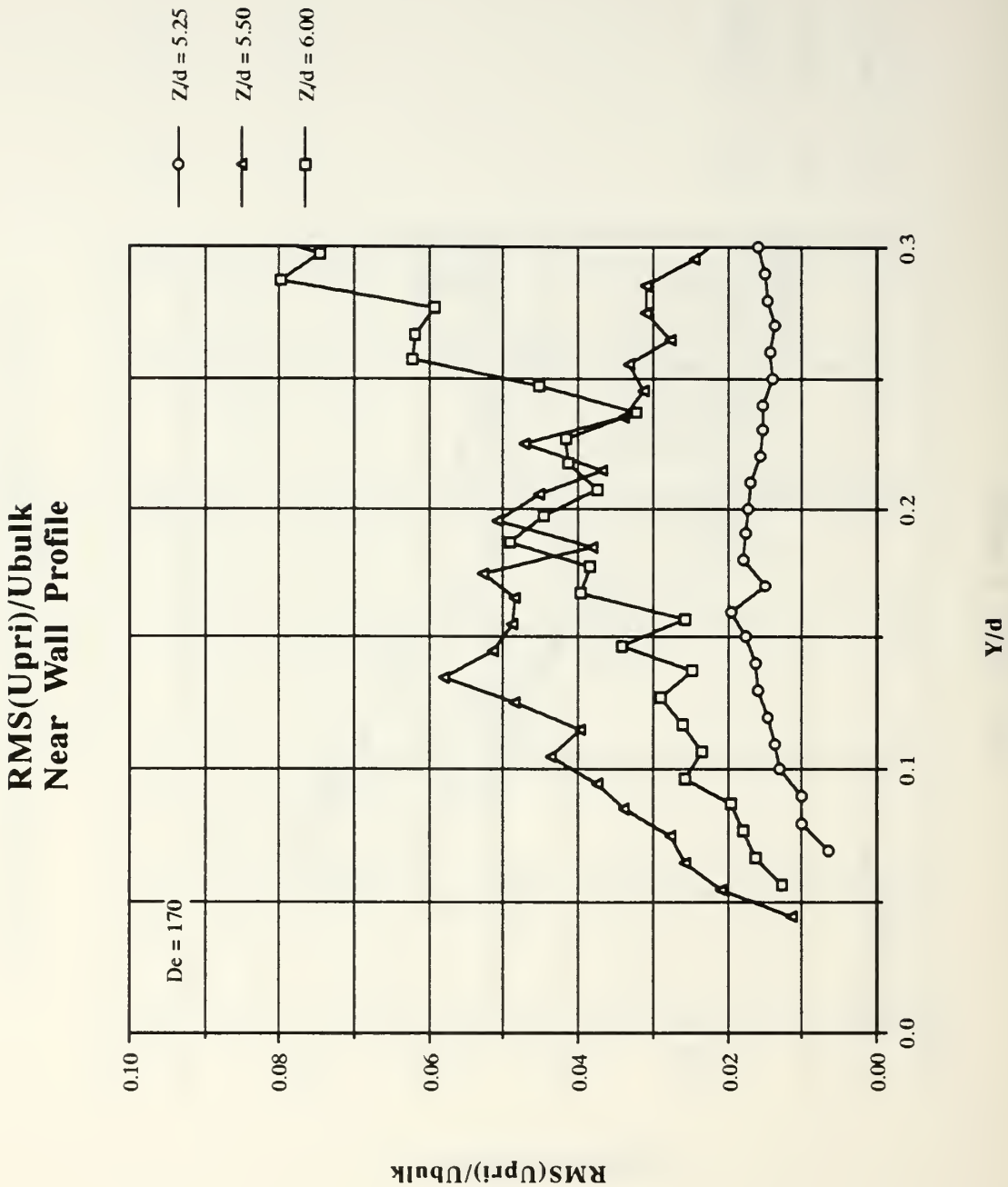

Figure 59. Normalized RMS Intensity, De=170

Figure 60. Normalized RMS Intensity, De=240

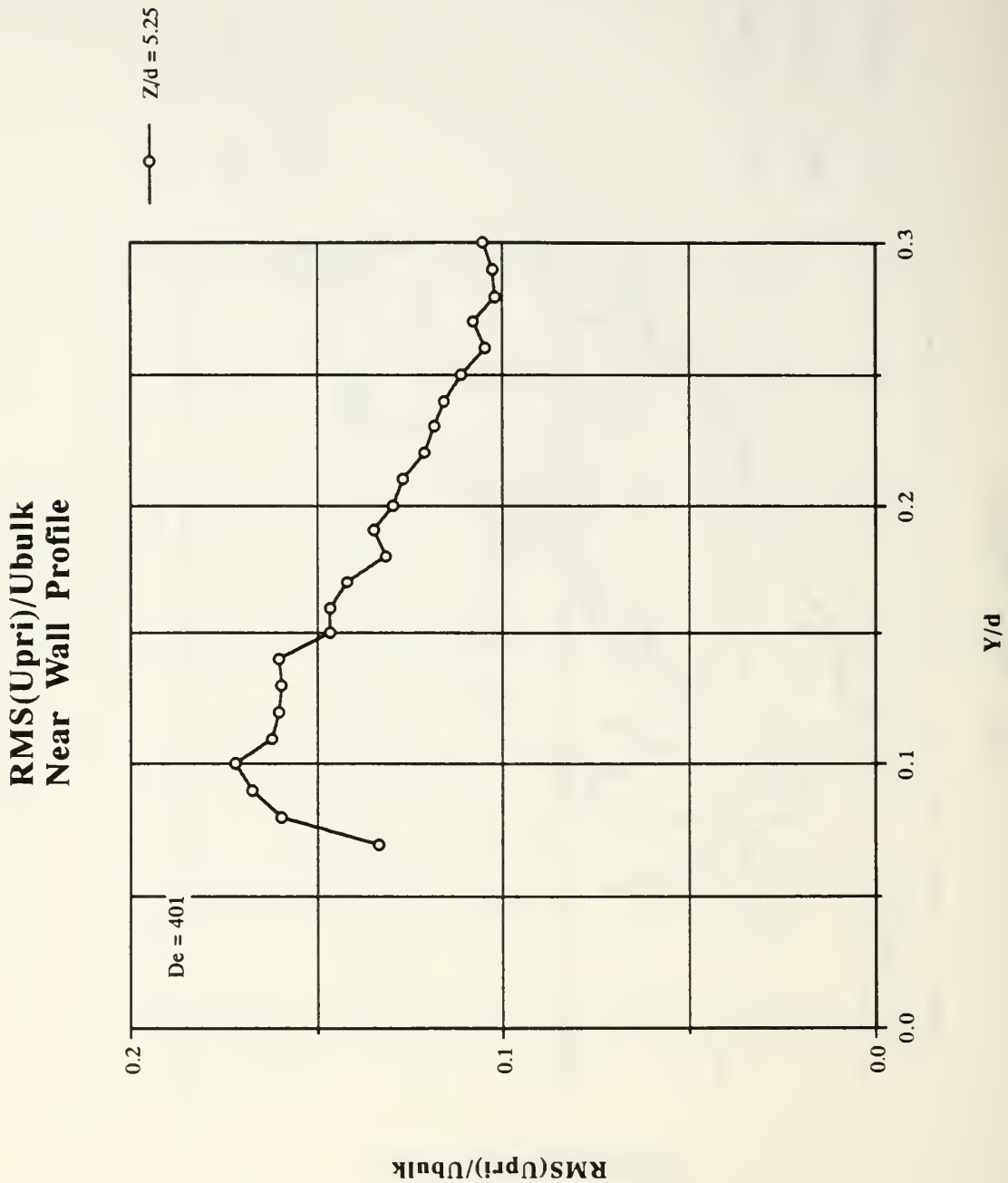

Figure 61. Normalized RMS Intensity, De=401

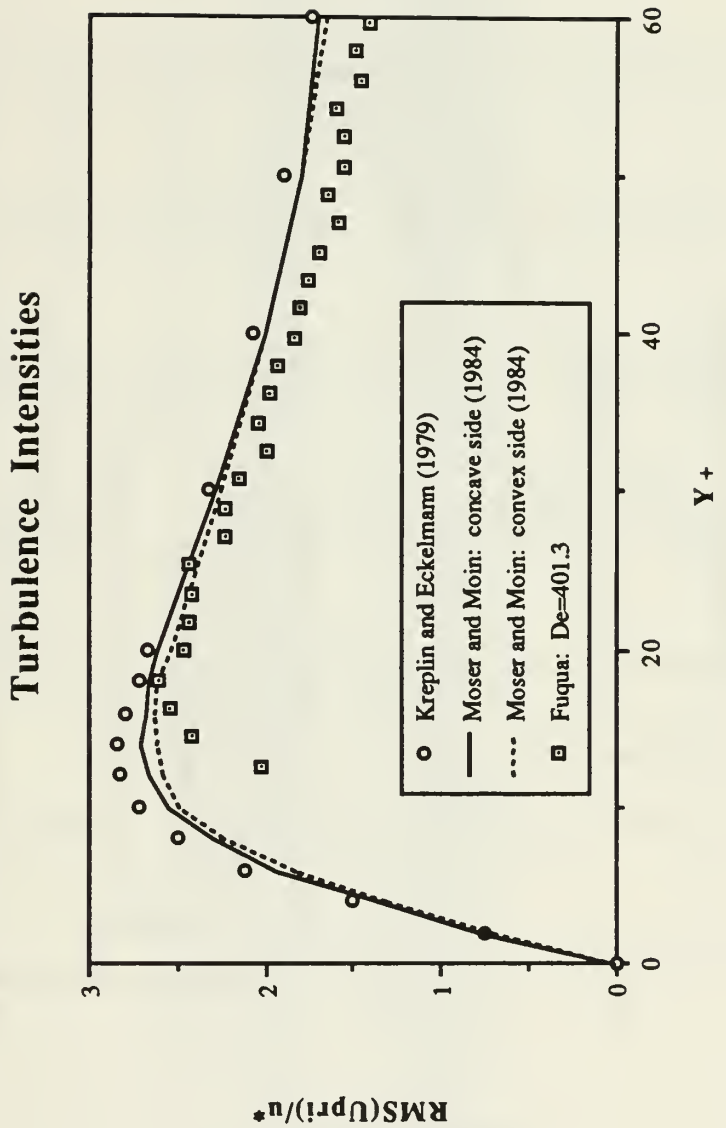

Figure 62. RMS Intensity Normalized by Friction Velocity, De=401

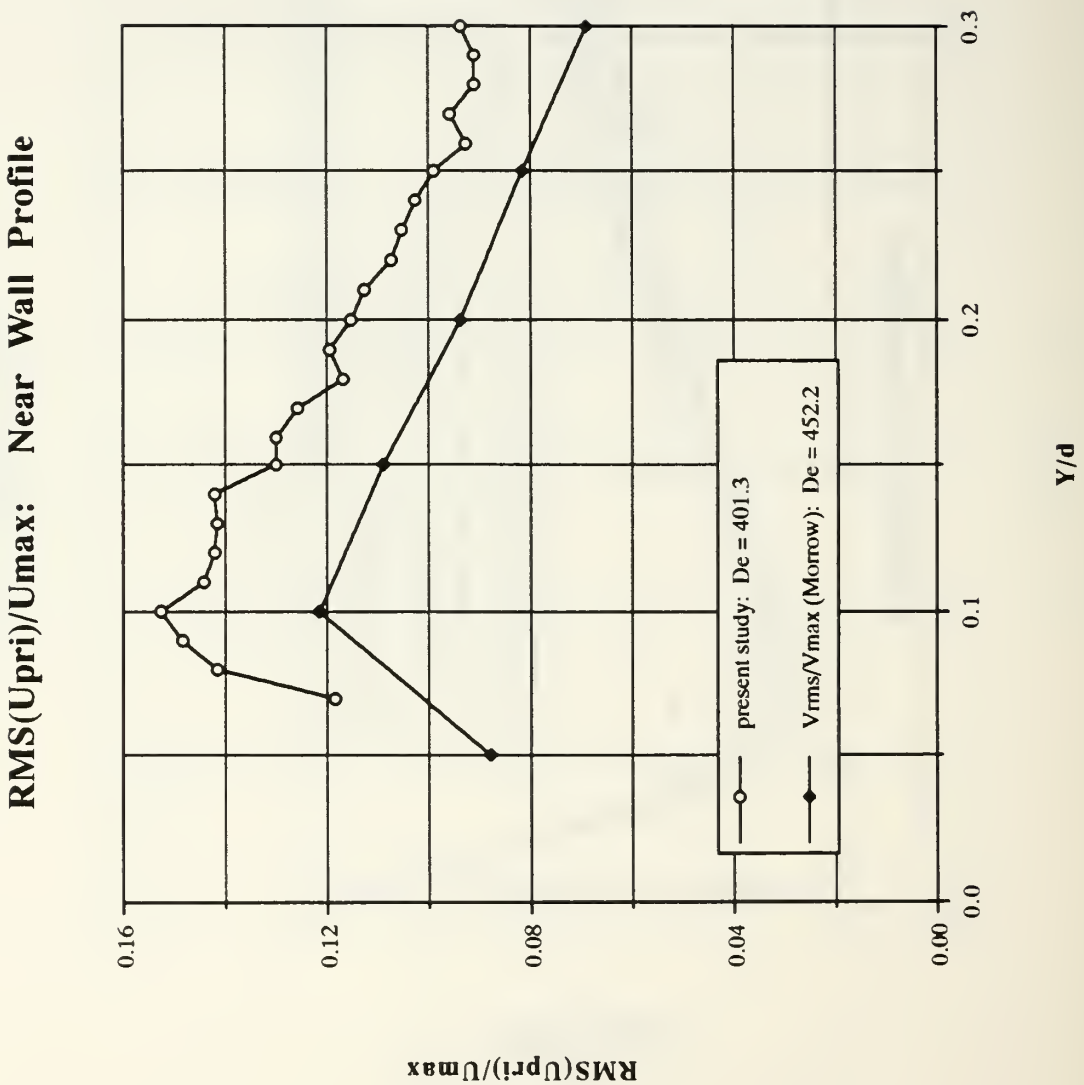

Figure 63. RMS Intensity Normalized by the Maximum Velocity, De=401

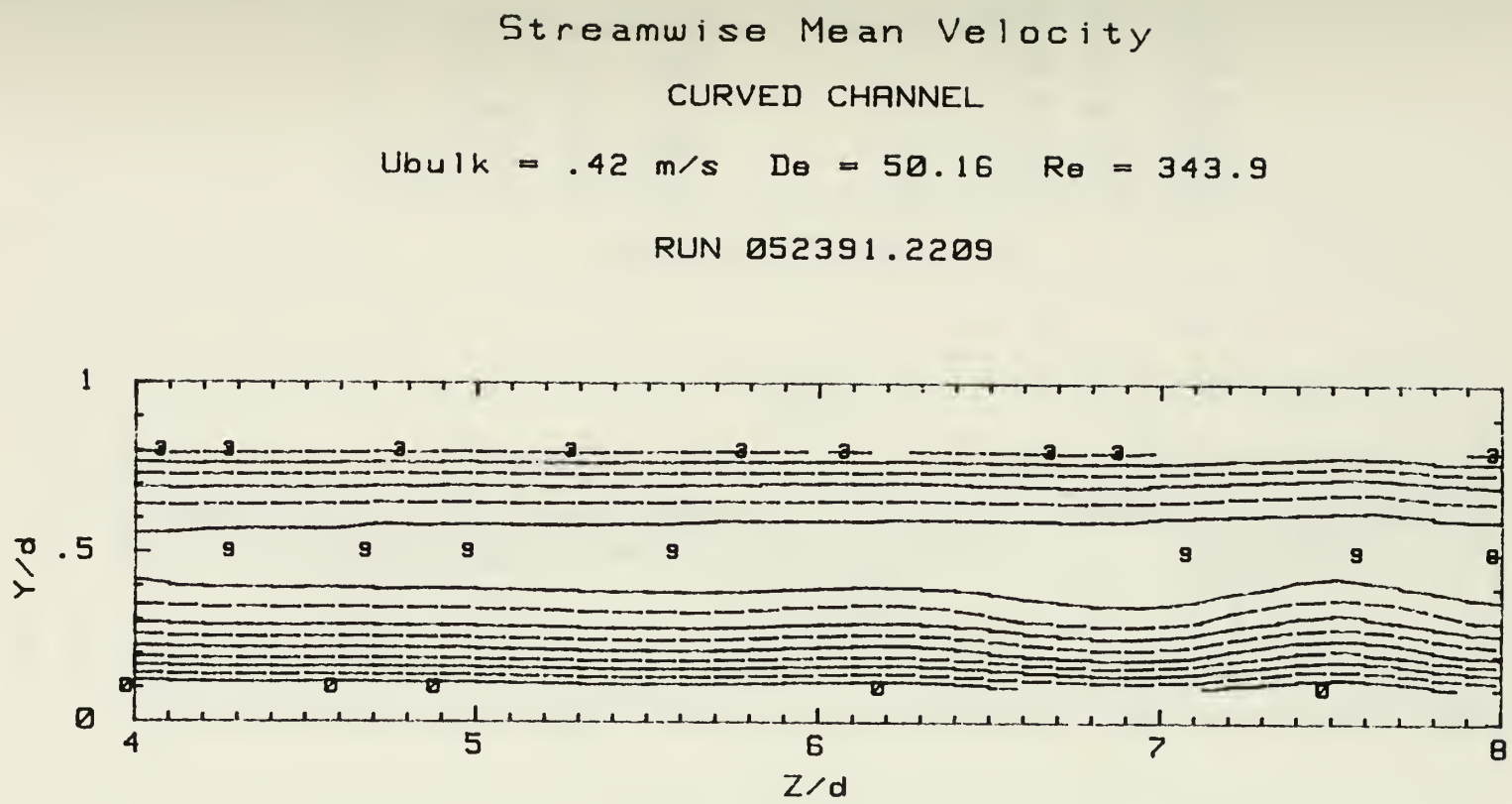

Figure 64. Streamwise Mean Velocity Contour, De=50.2

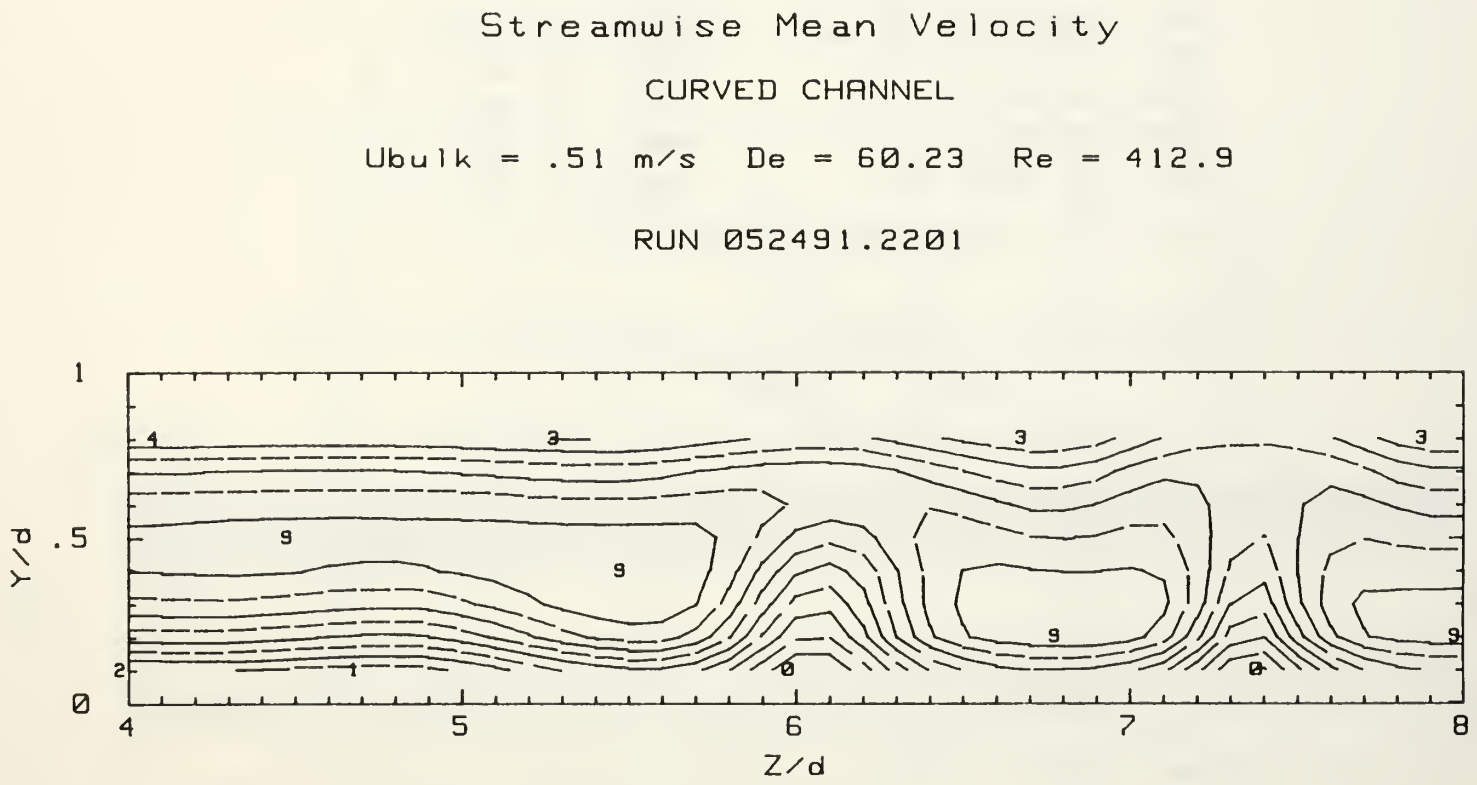

Figure 65. Streamwise Mean Velocity Contour, De=60.2

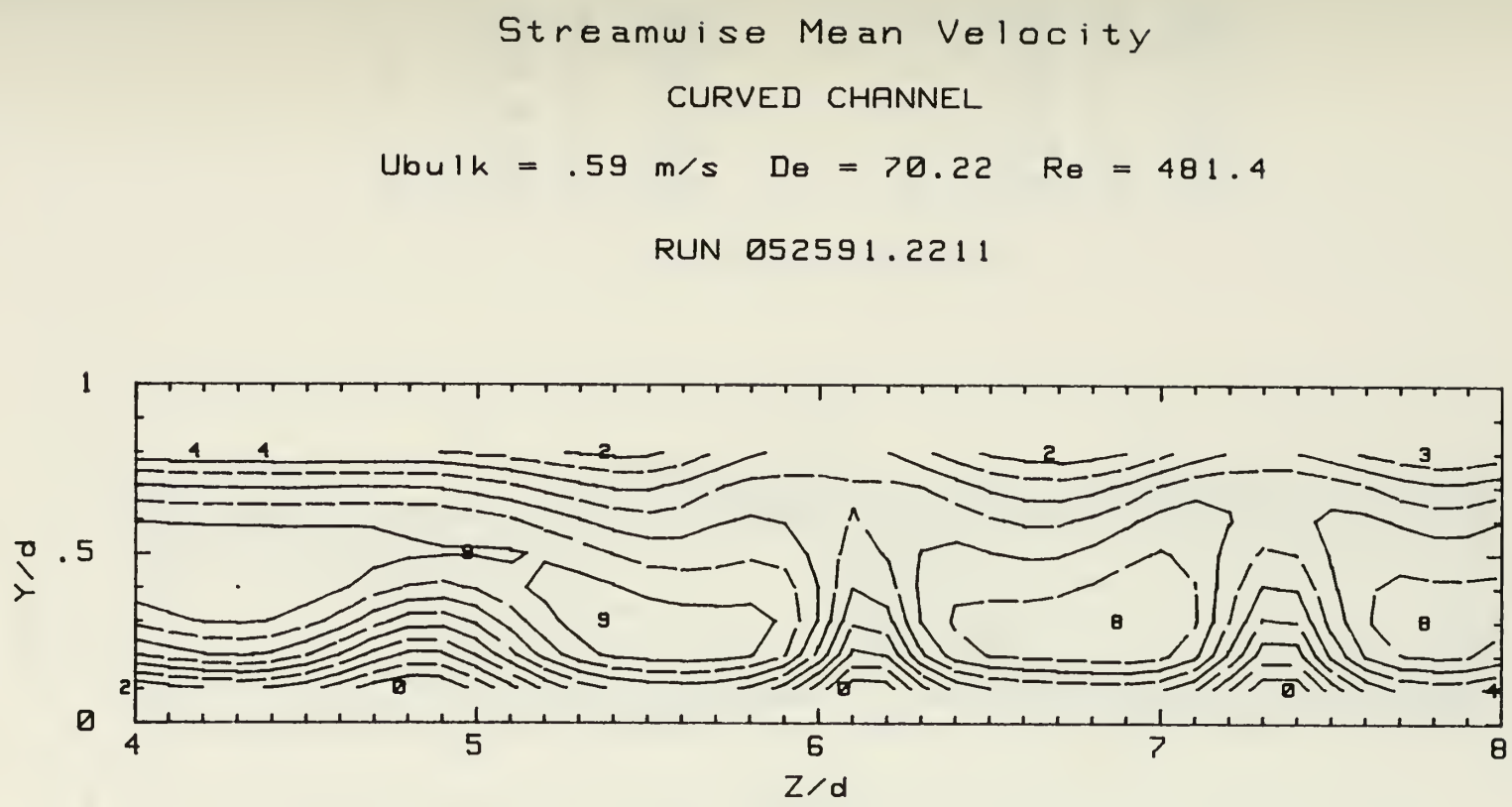

Figure 66. Streamwise Mean Velocity Contour, De=70.2

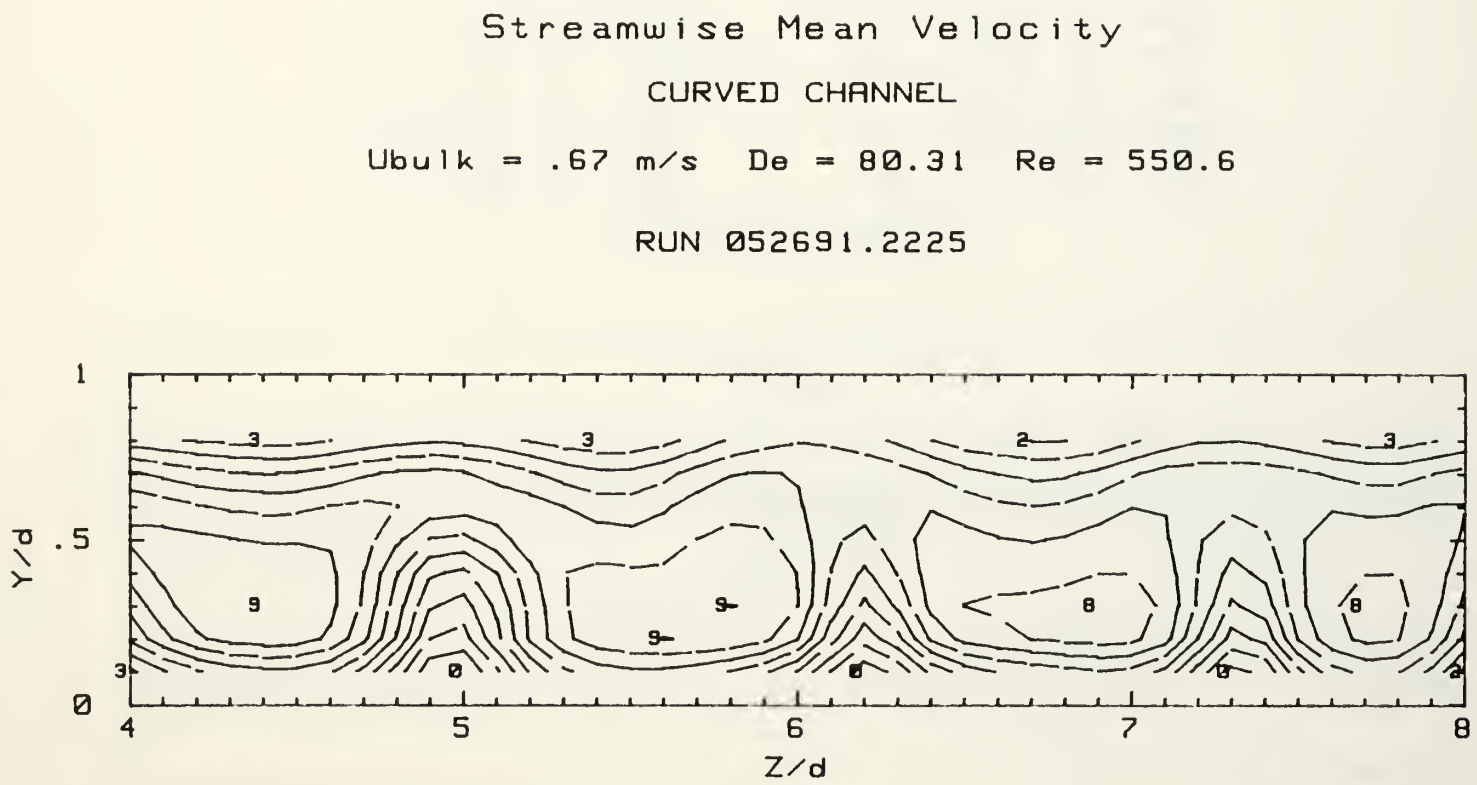

Figure 67. Streamwise Mean Velocity Contour, De=80.3

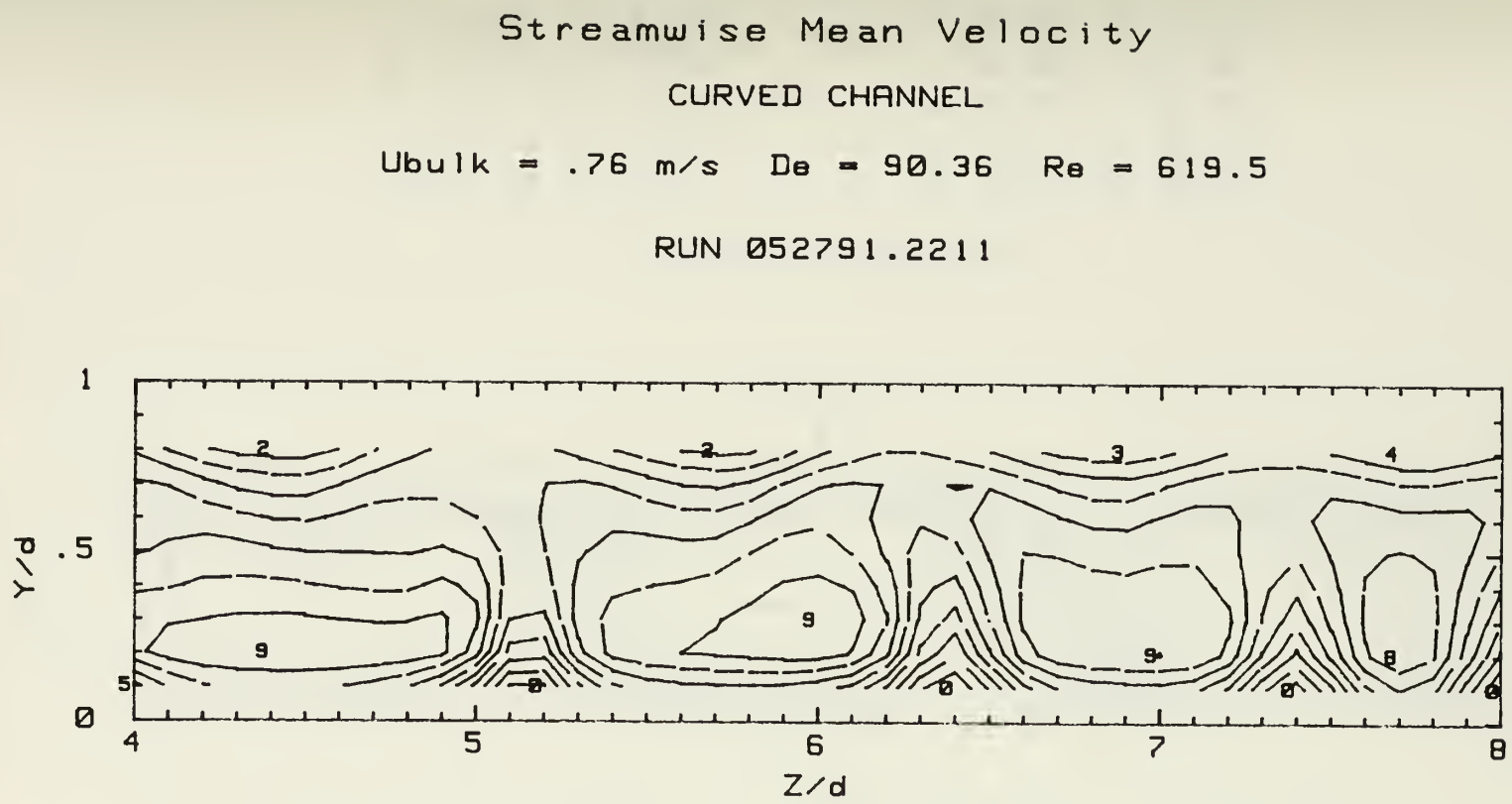

Figure 68. Streamwise Mean Velocity Contour, De=90.4

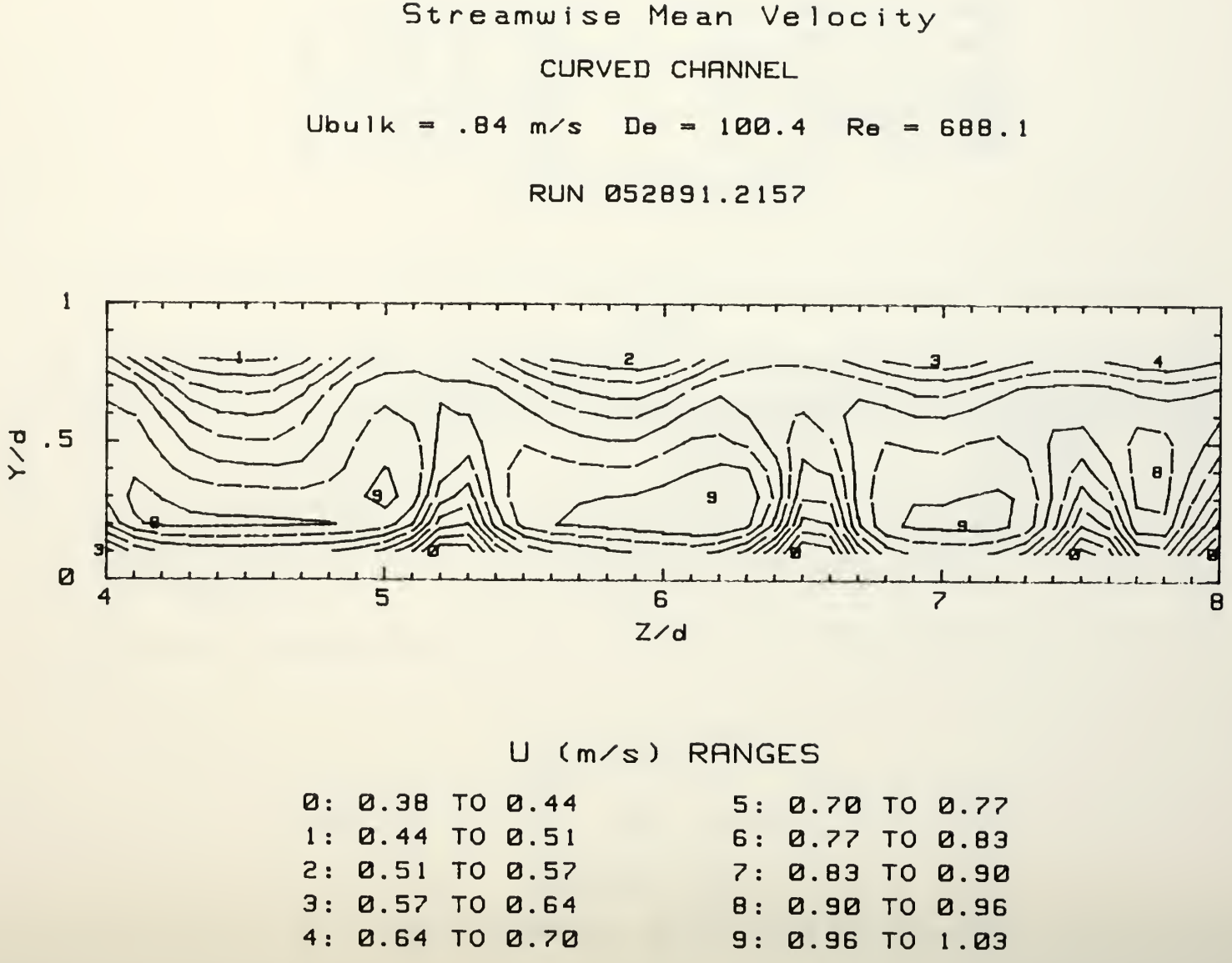

Figure 69. Streamwise Mean Velocity Contour, De=100.4

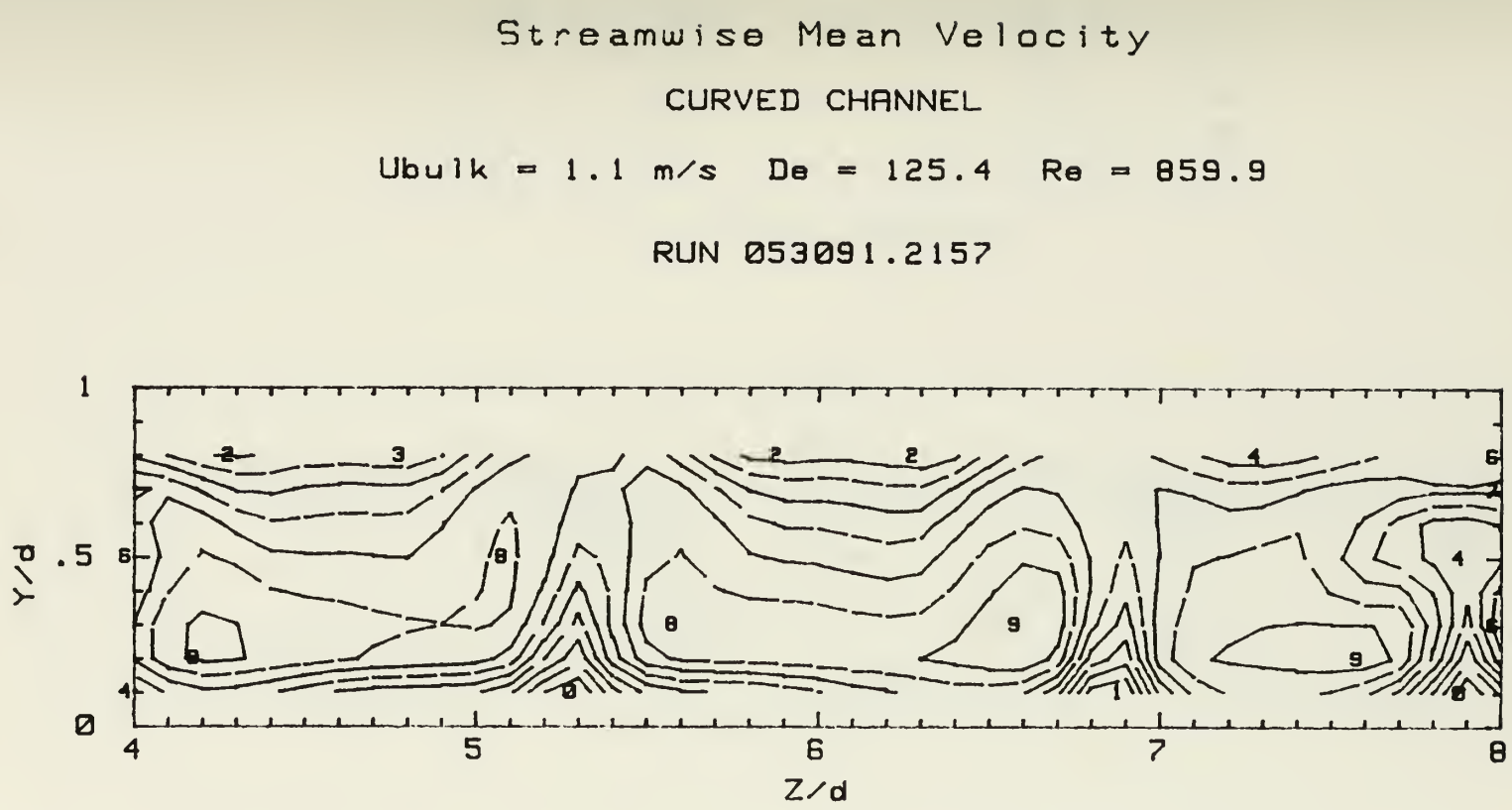

Figure 70. Streamwise Mean Velocity Contour, De=125.4

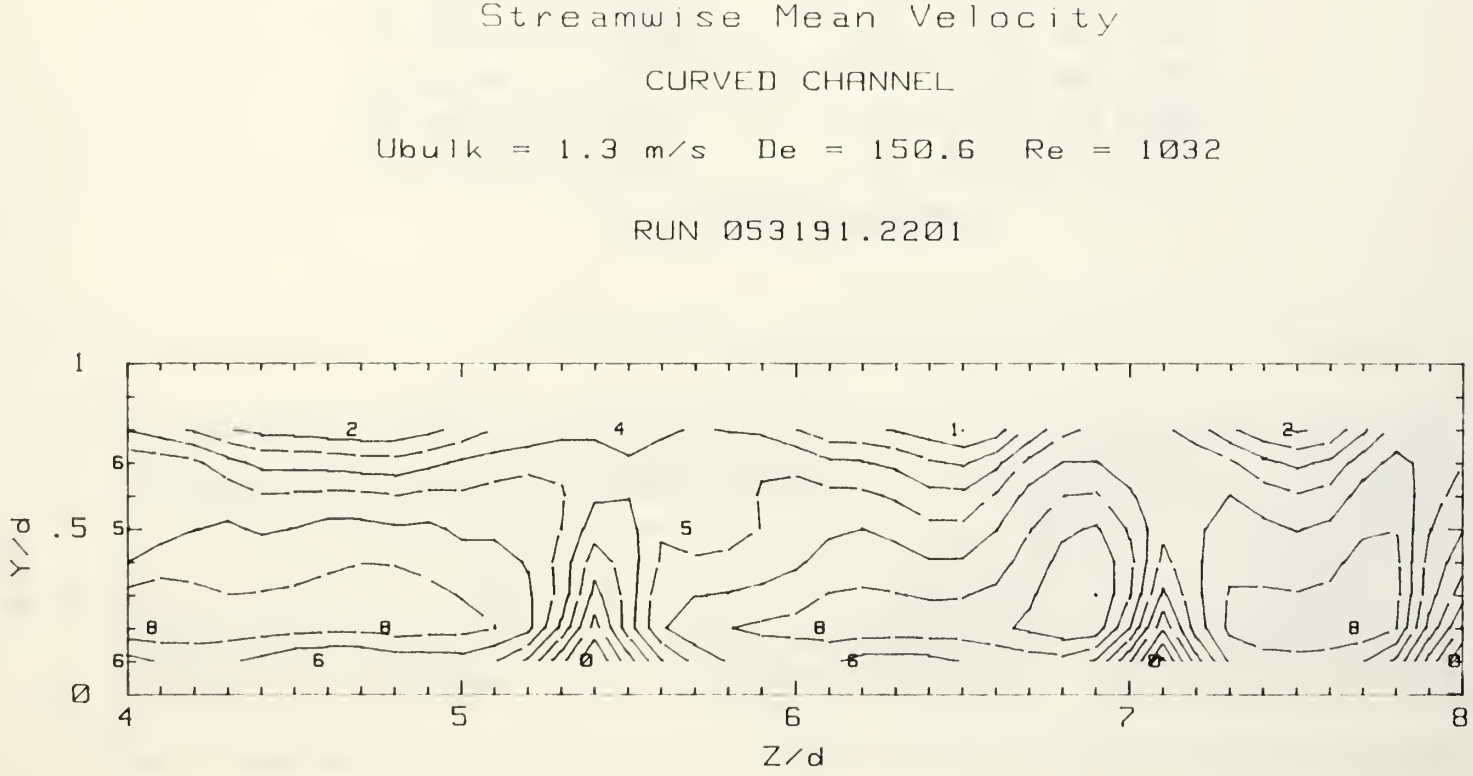

Figure 71. Streamwise Mean Velocity Contour, De=150.6

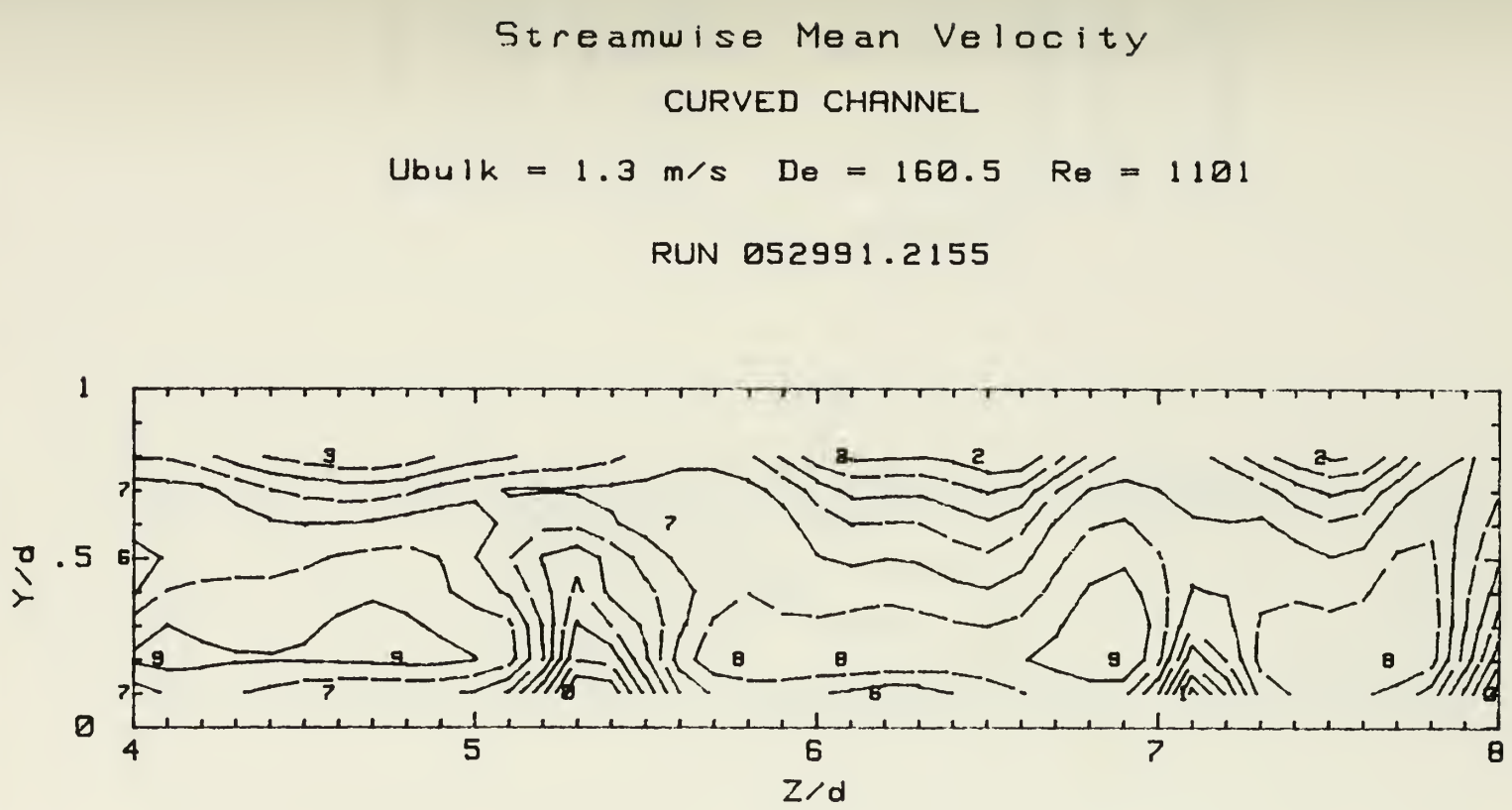

Figure 72. Streamwise Mean Velocity Contour, De=160.5

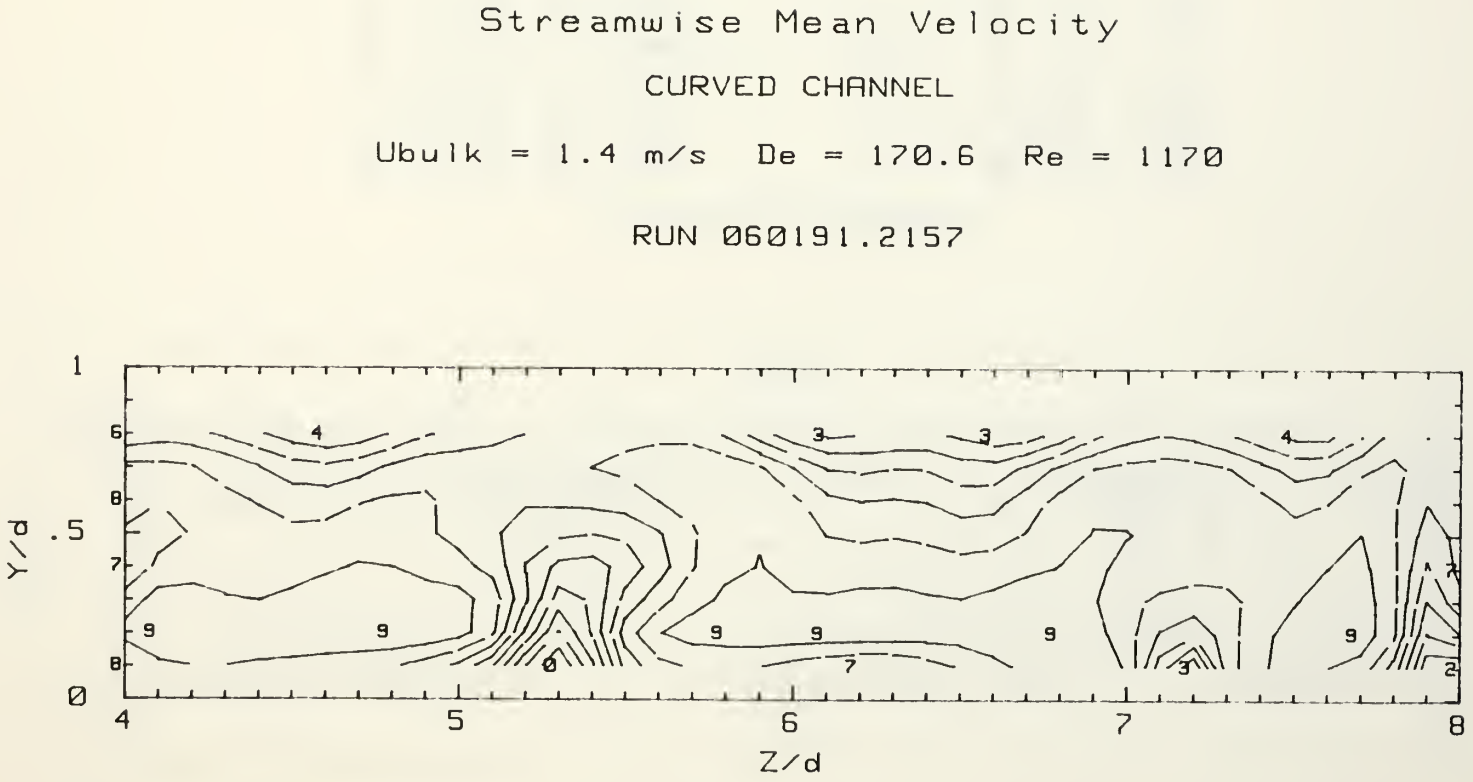

Figure 73. Streamwise Mean Velocity Contour, De=170.6

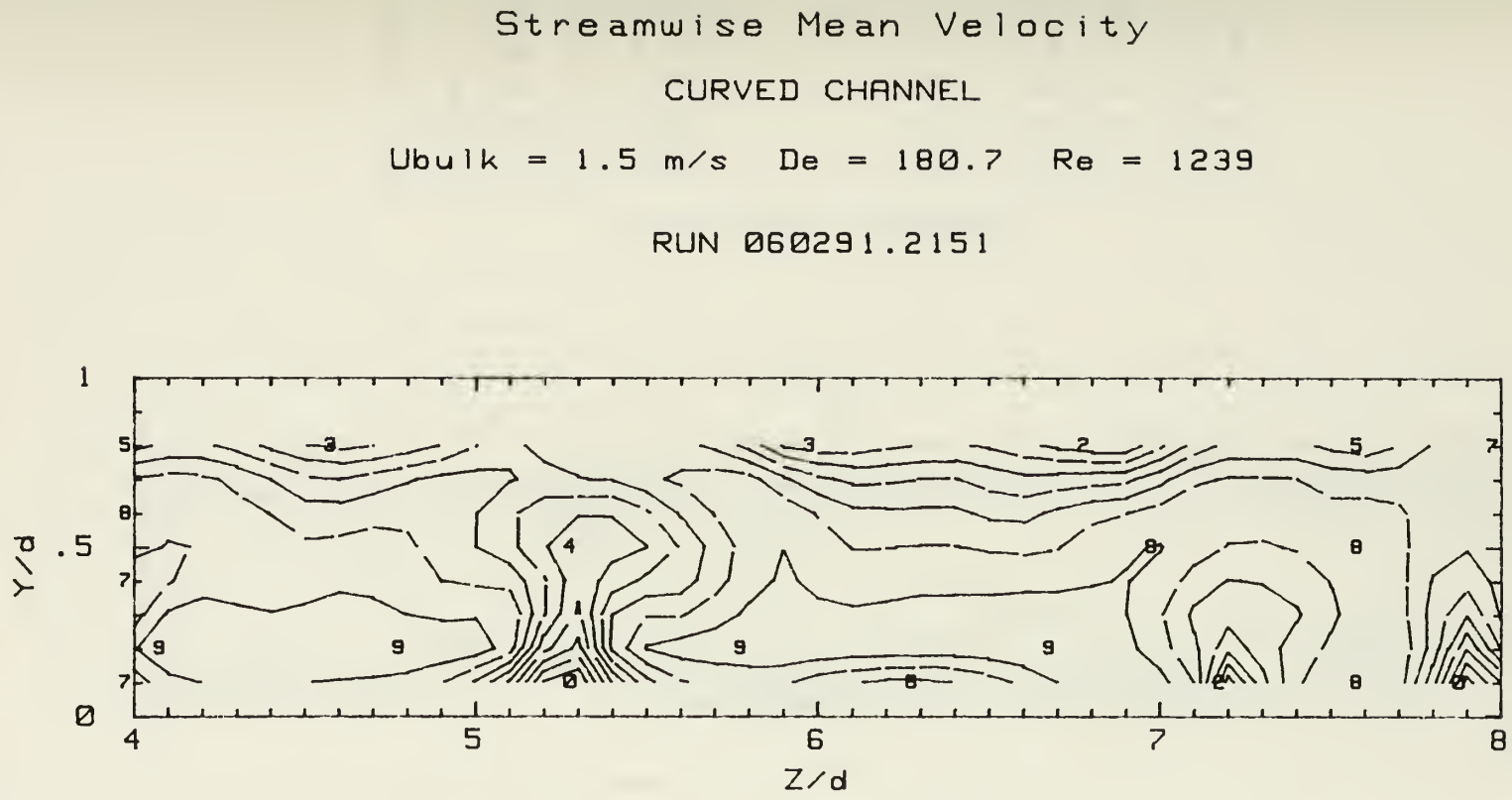

Figure 74. Streamwise Mean Velocity Contour, De=180.7

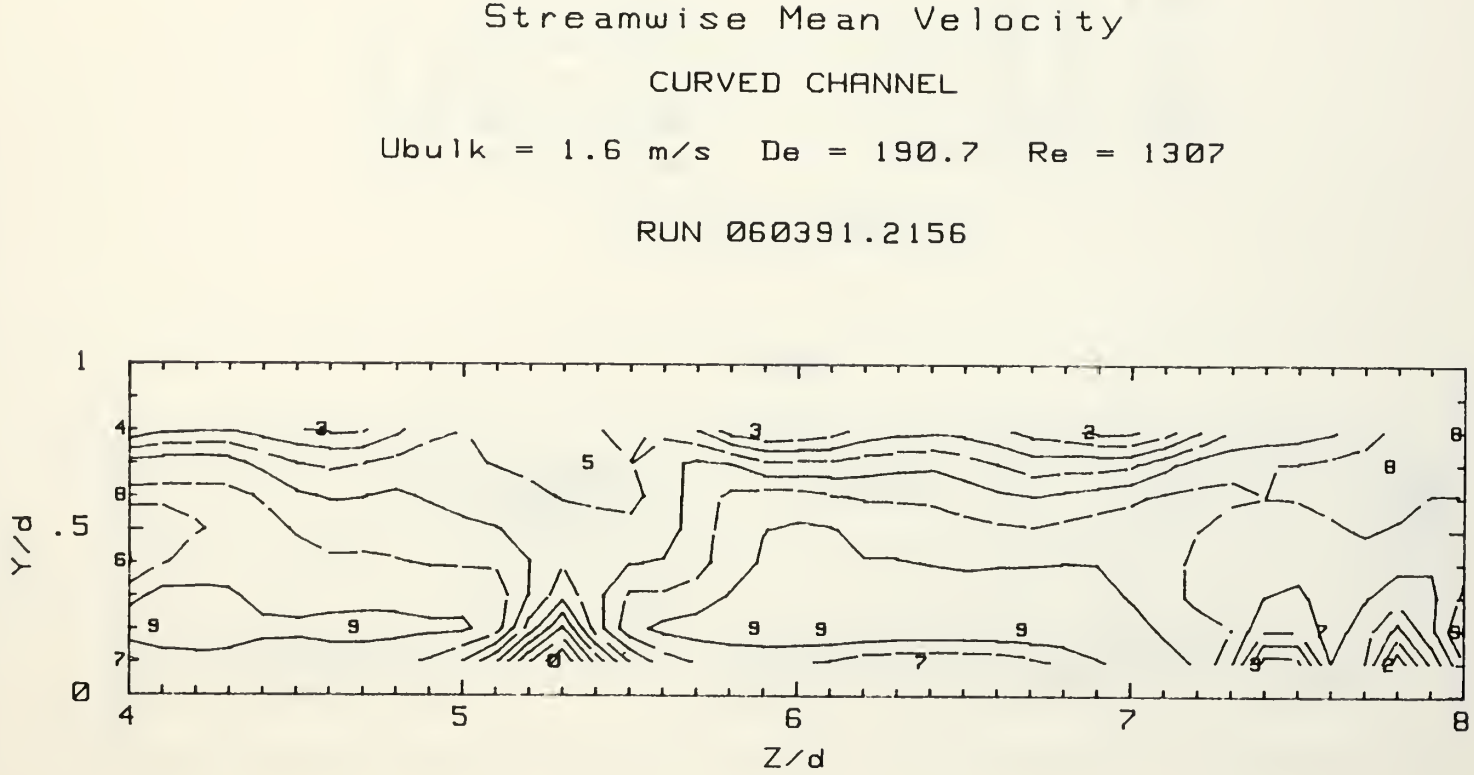

Figure 75. Streamwise Mean Velocity Contour, De=190.7

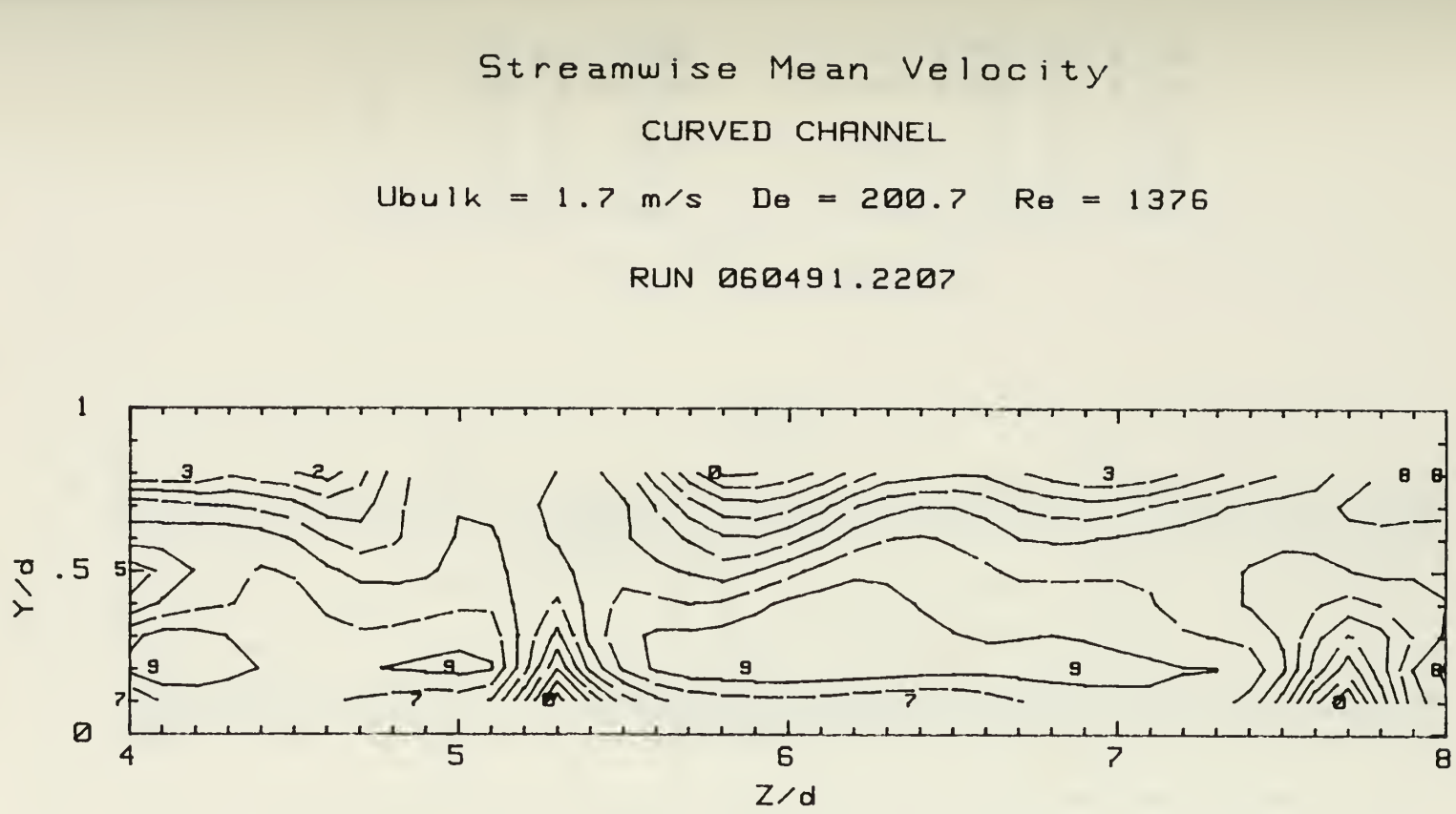

Figure 76. Streamwise Mean Velocity Contour, De=200.7

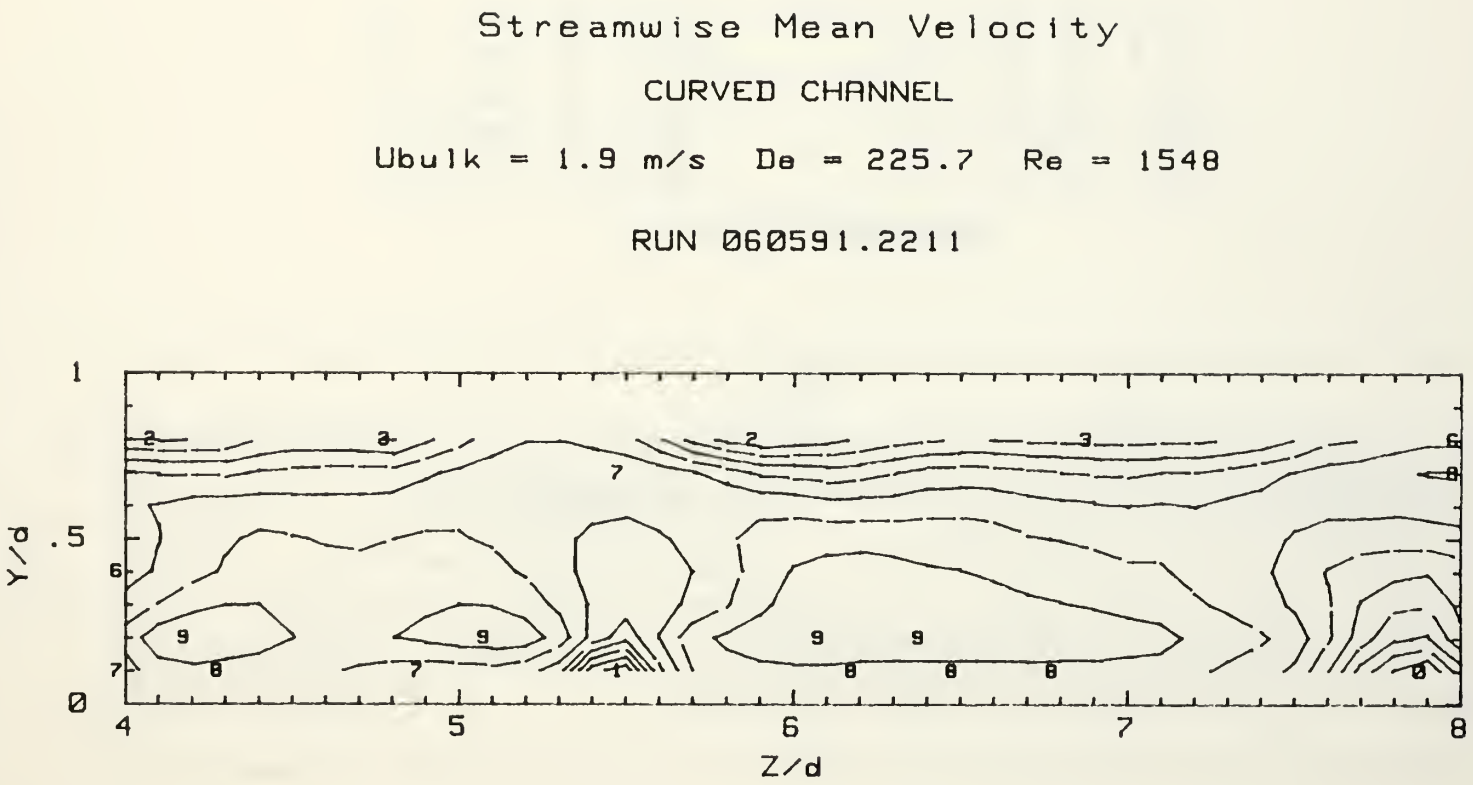

Figure 77. Streamwise Mean Velocity Contour, De=225.7

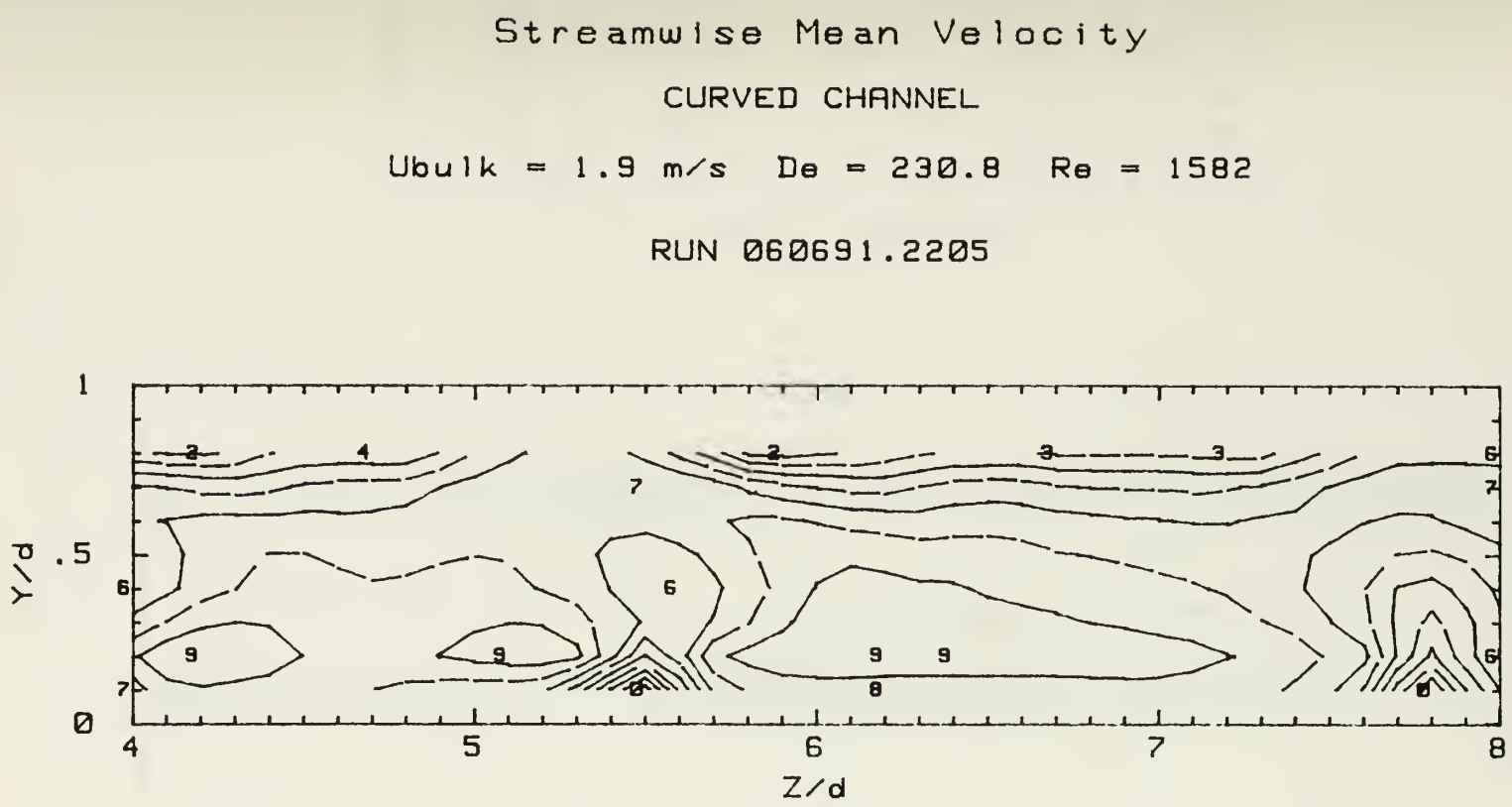

Figure 78. Streamwise Mean Velocity Contour, De=230.8

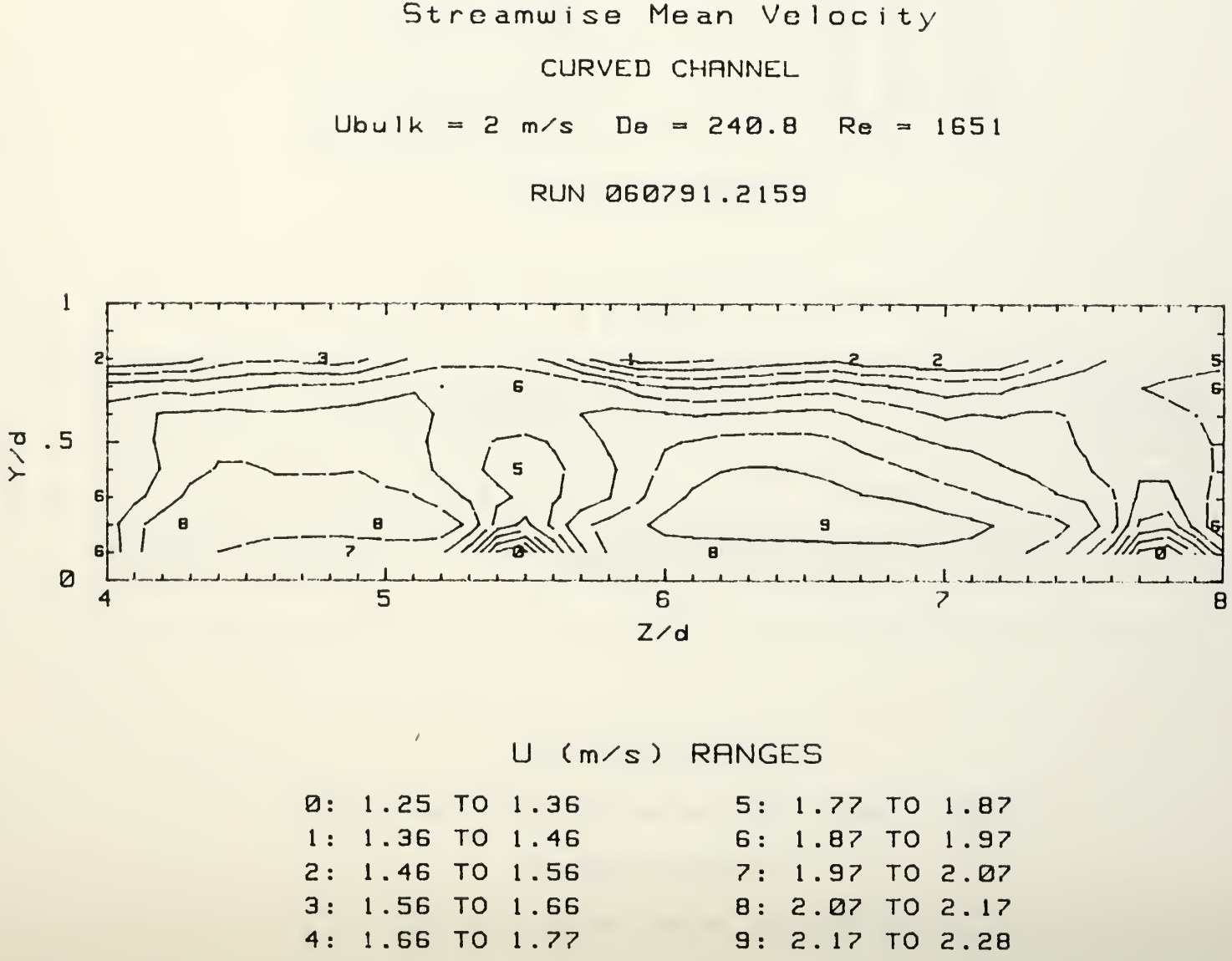

Figure 79. Streamwise Mean Velocity Contour, De=240.8

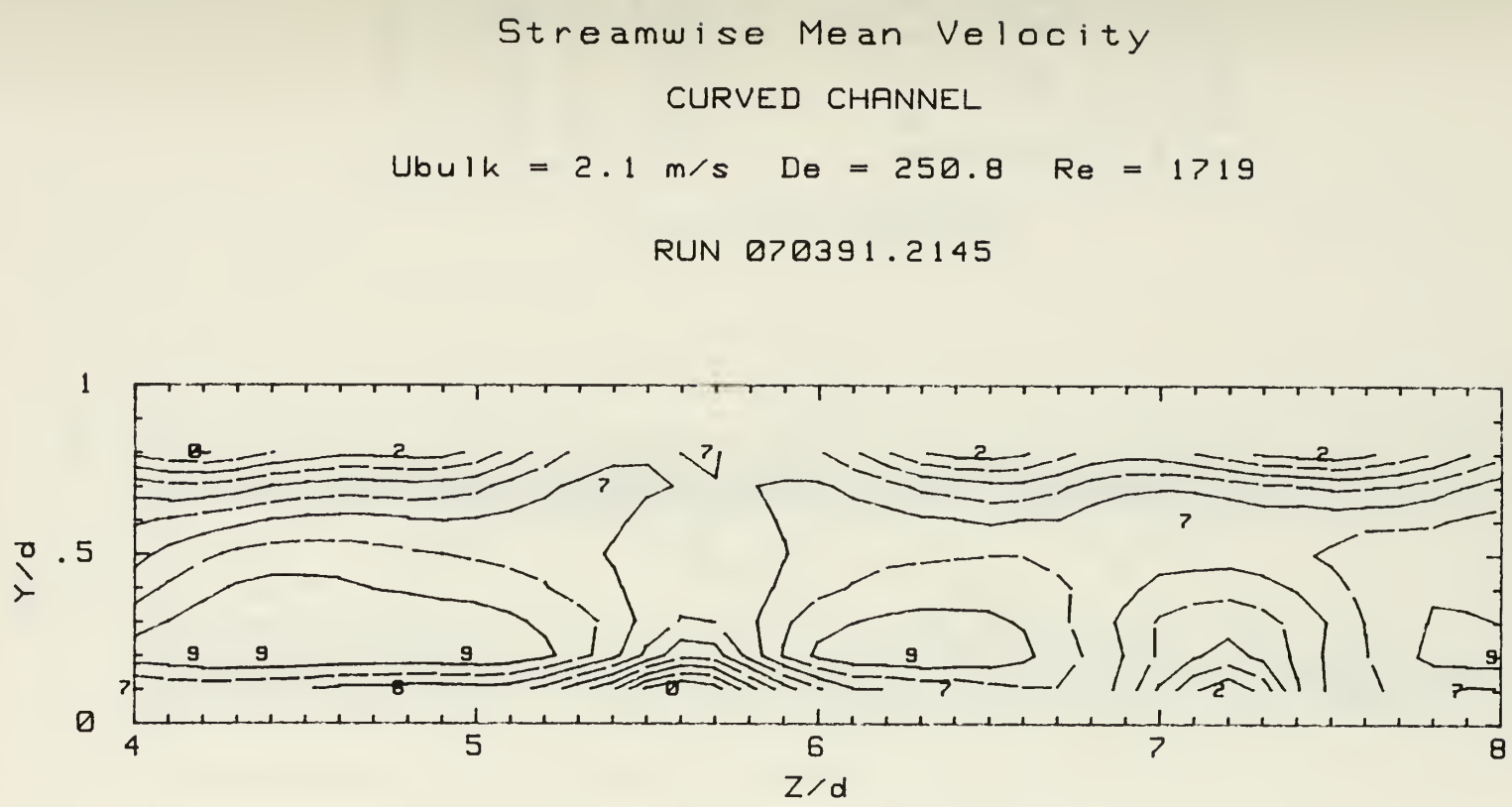

Figure 80. Streamwise Mean Velocity Contour, De=250.8

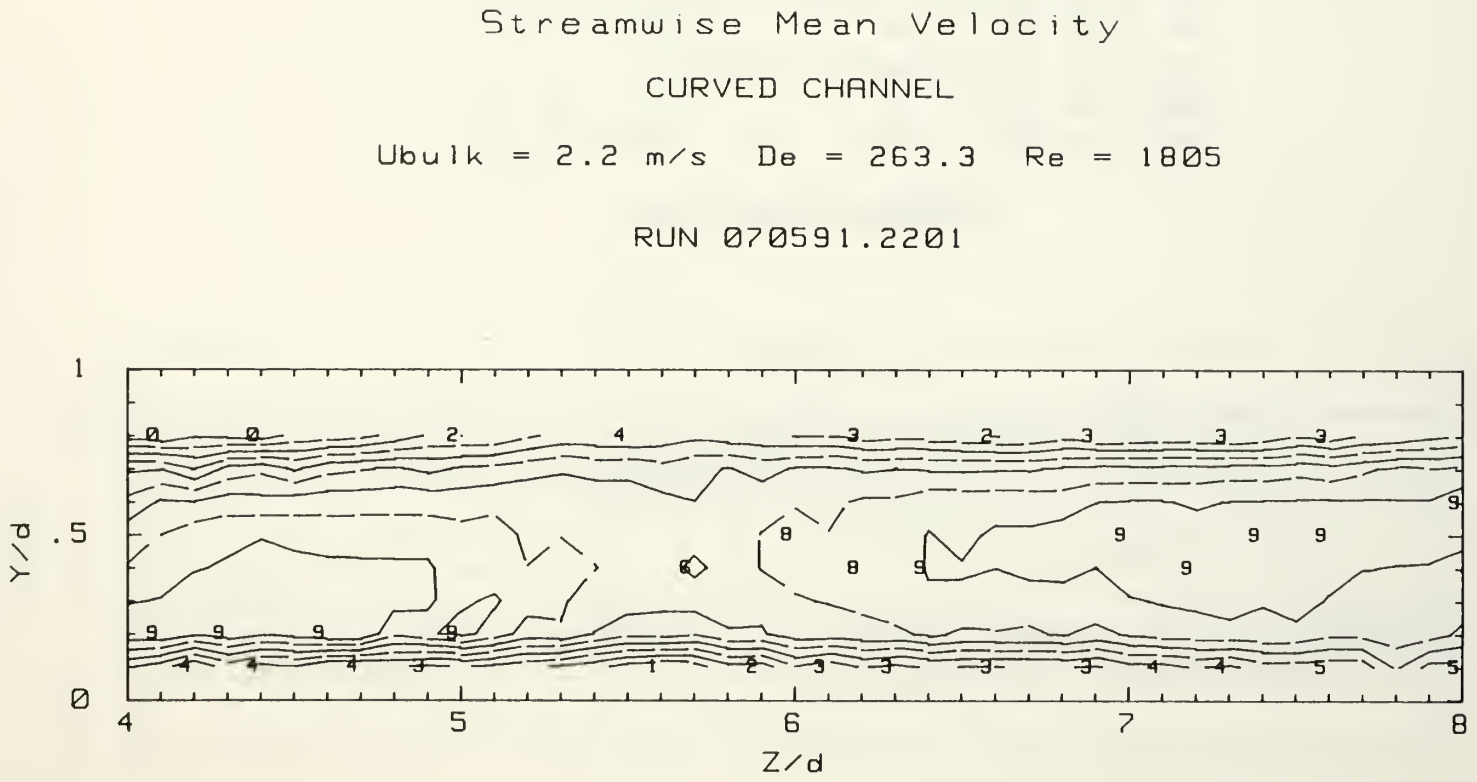

Figure 81. Streamwise Mean Velocity Contour, De=263.3

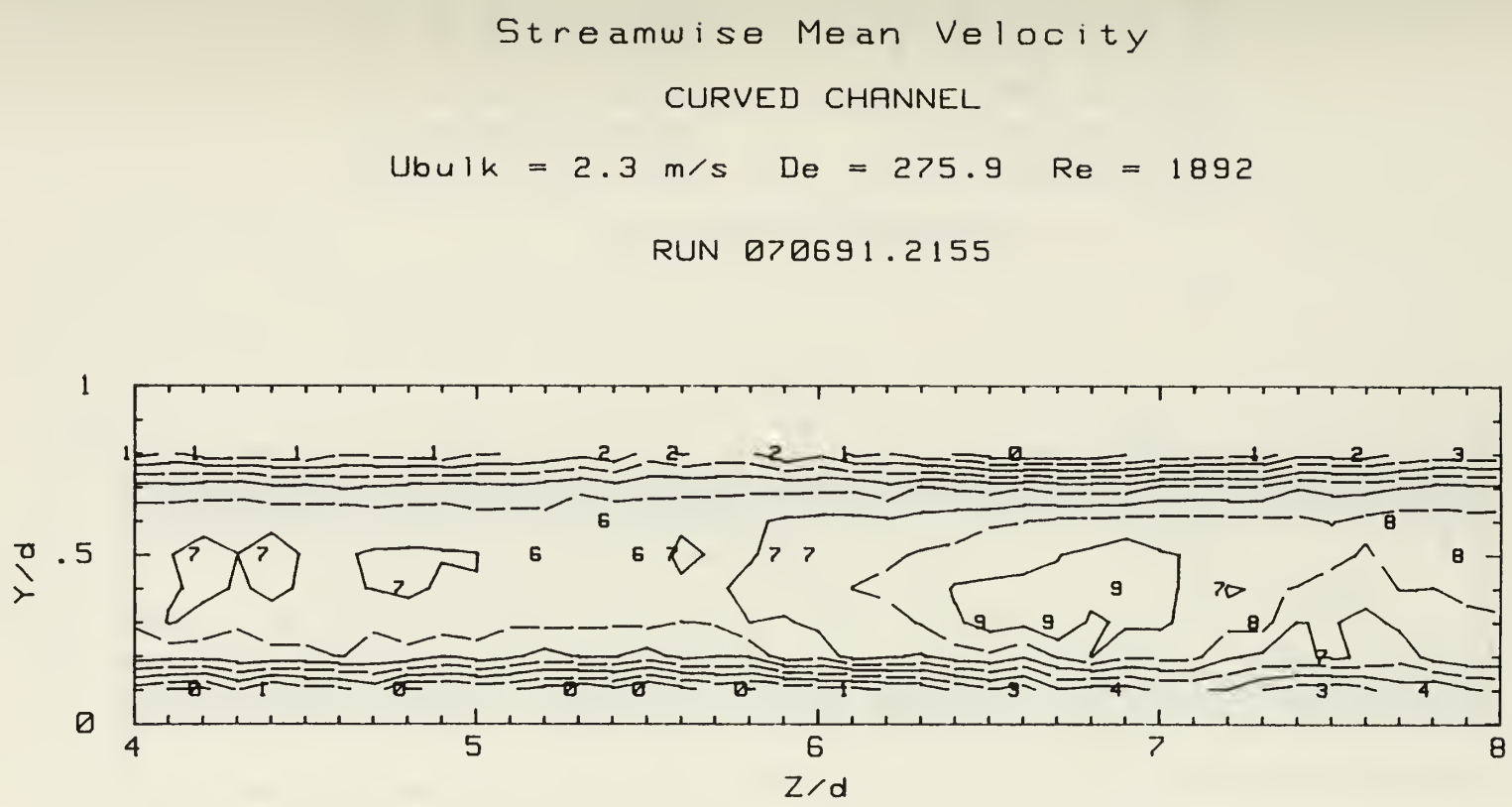

Figure 82. Streamwise Mean Velocity Contour, De=275.9

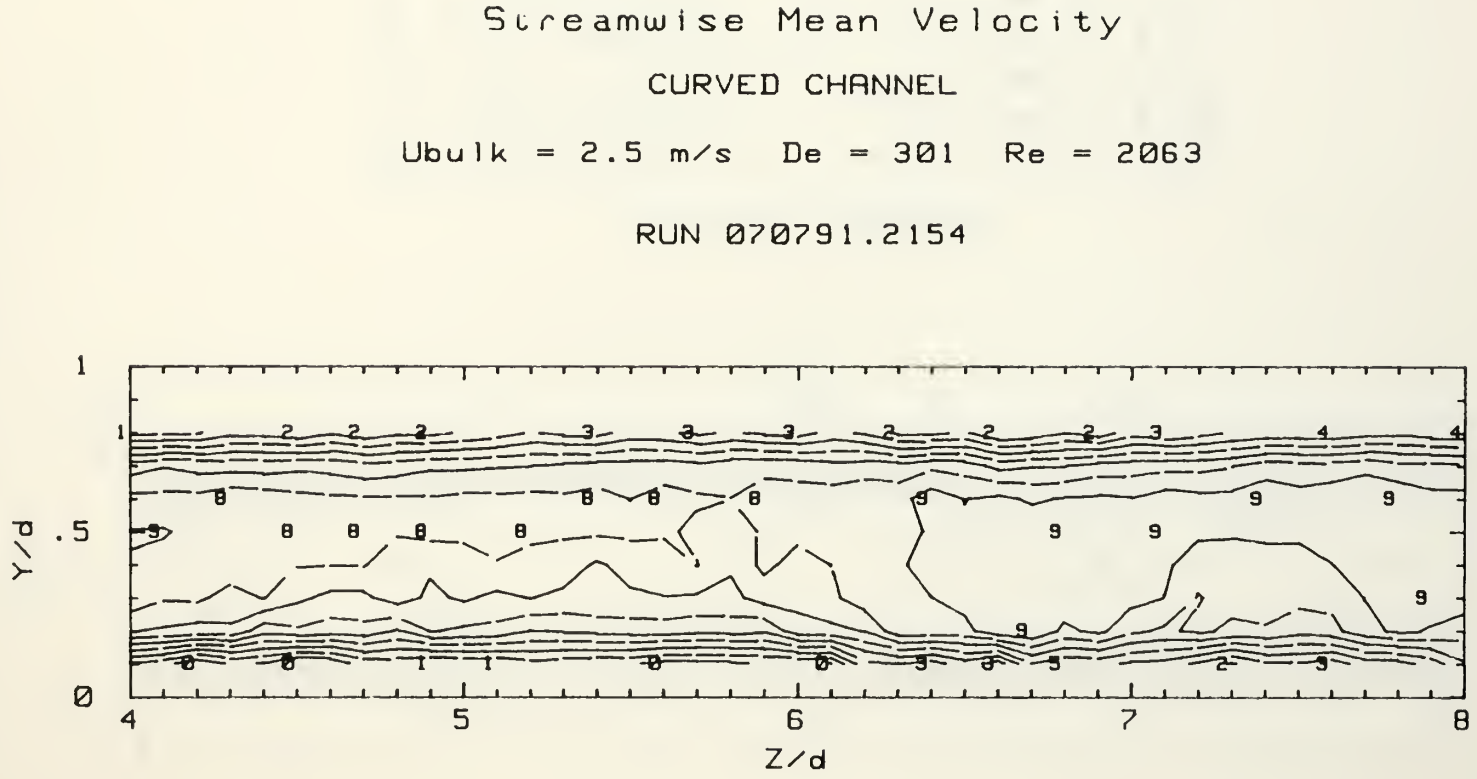

Figure 83. Streamwise Mean Velocity Contour, De=301.0

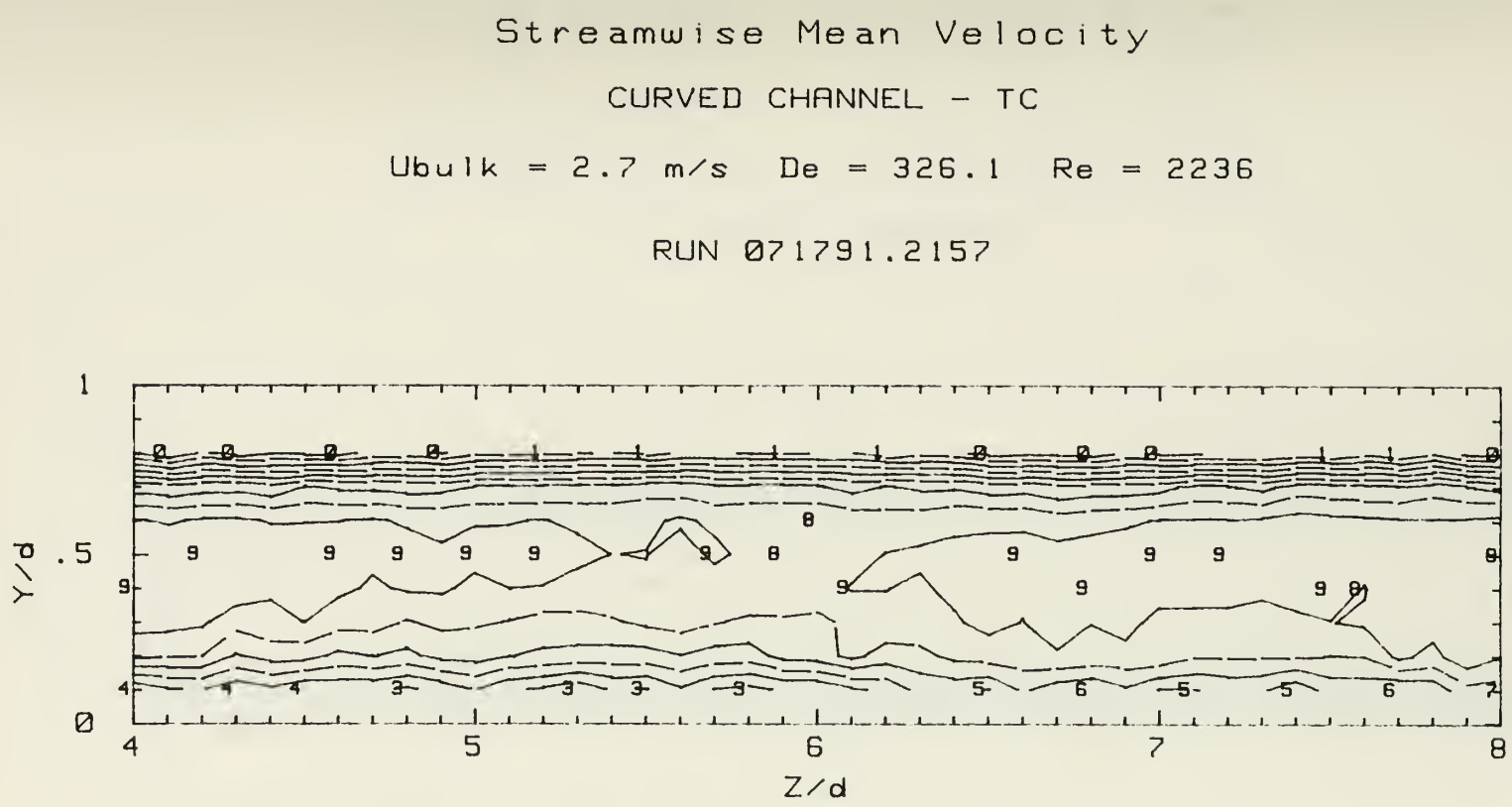

Figure 84. Streamwise Mean Velocity Contour, De=326.1

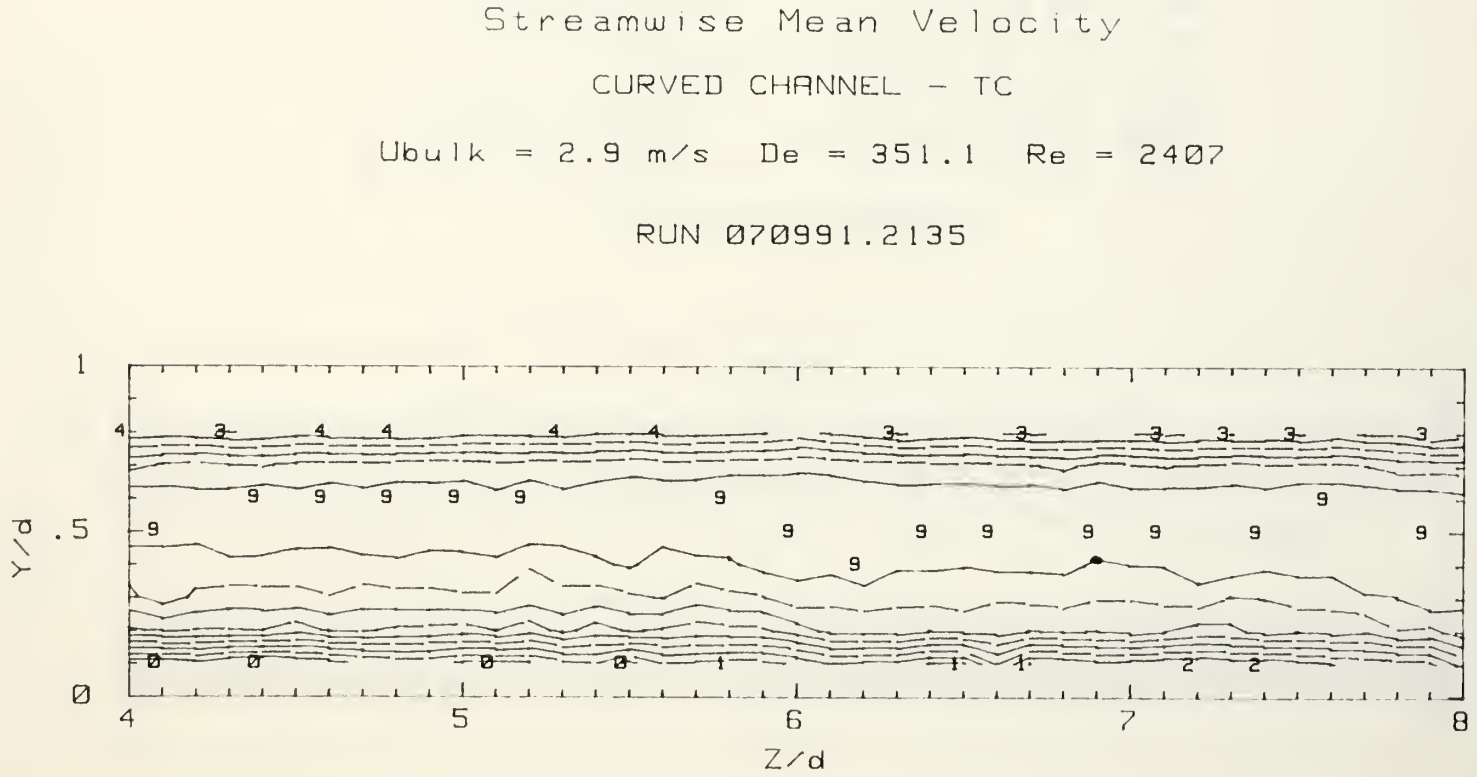

Figure 85. Streamwise Mean Velocity Contour, De=351.1

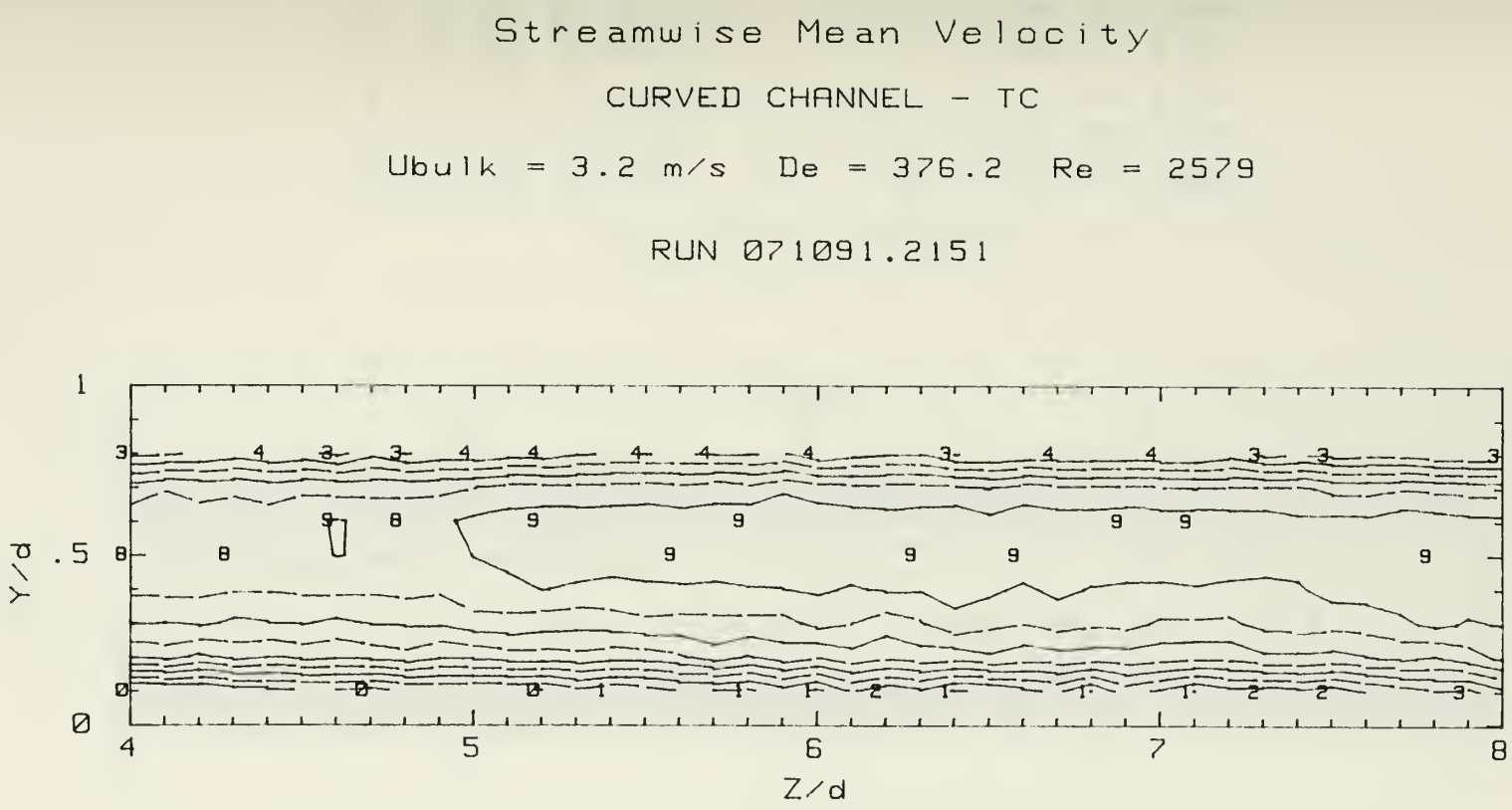

Figure 86. Streamwise Mean Velocity Contour, De=376.2

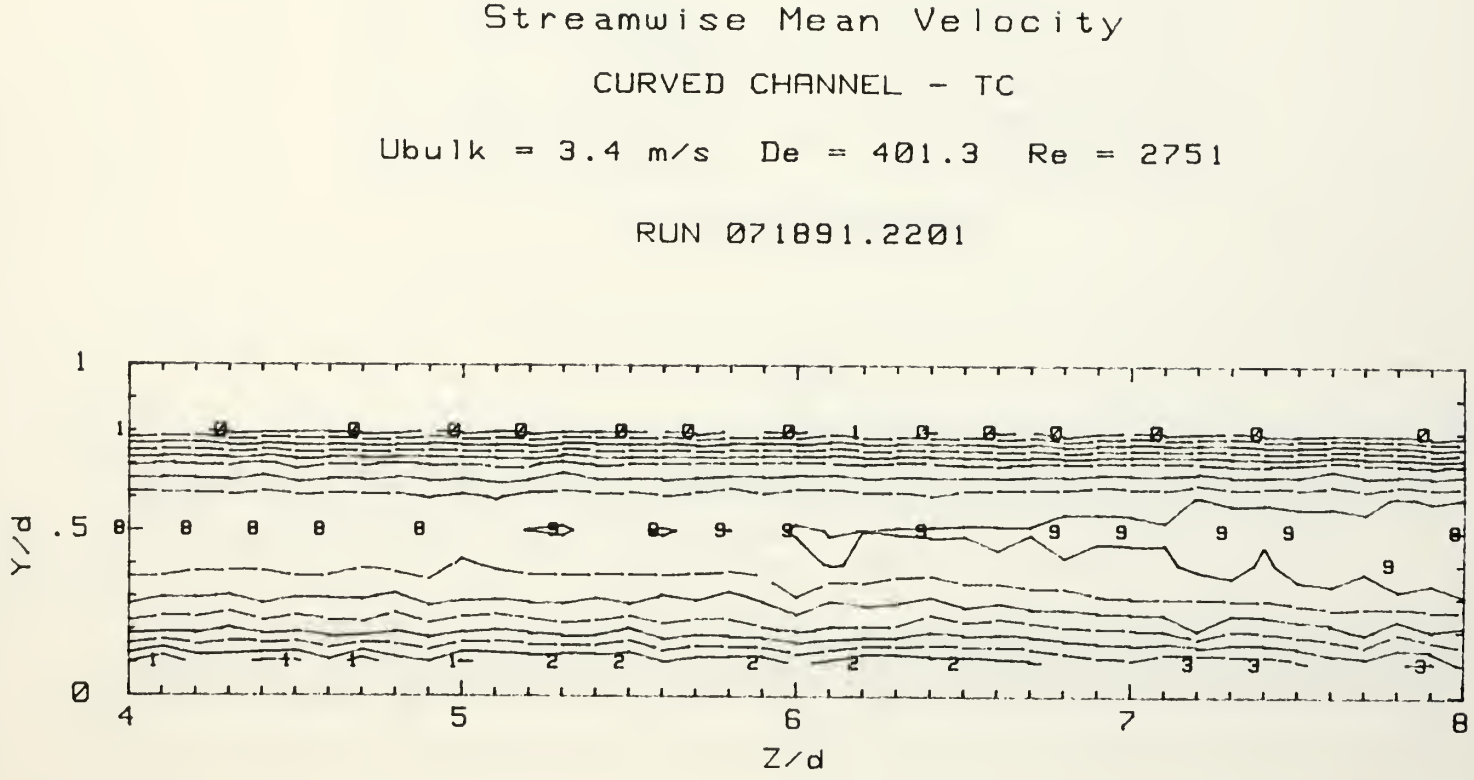

Figure 87. Streamwise Mean Velocity Contour, De=401.3

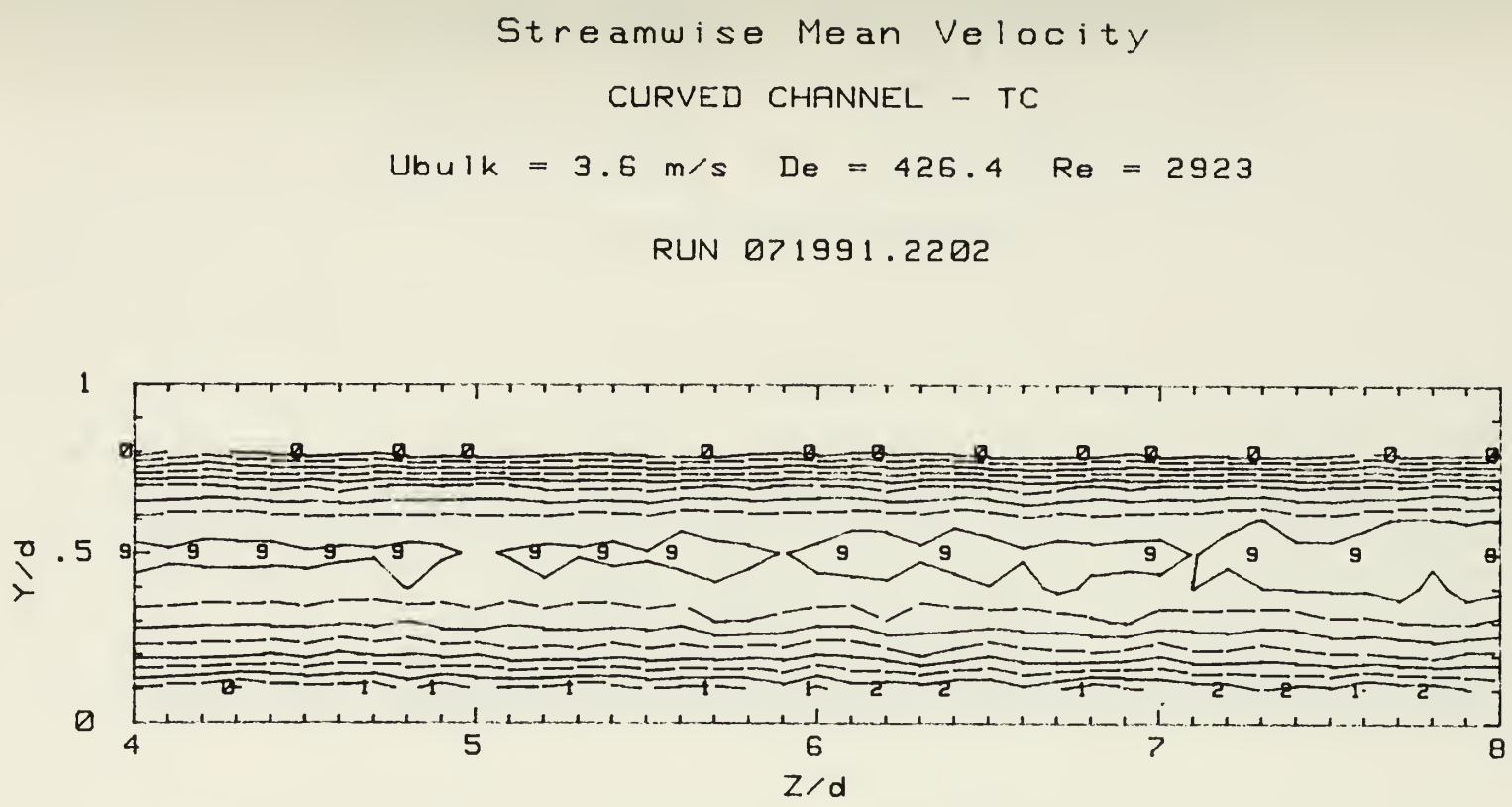

Figure 88. Streamwise Mean Velocity Contour, De=426.4

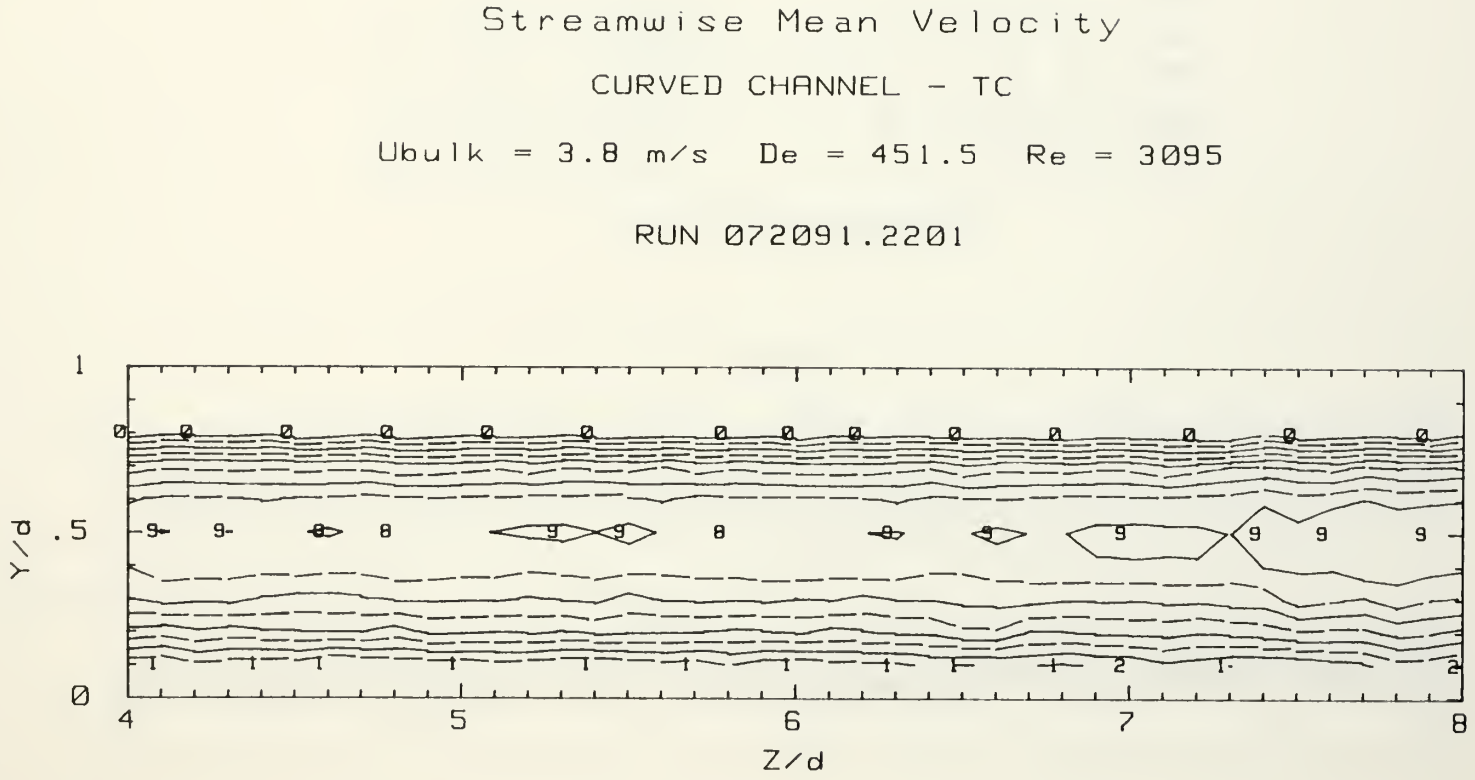

Figure 89. Streamwise Mean Velocity Contour, De=451.5

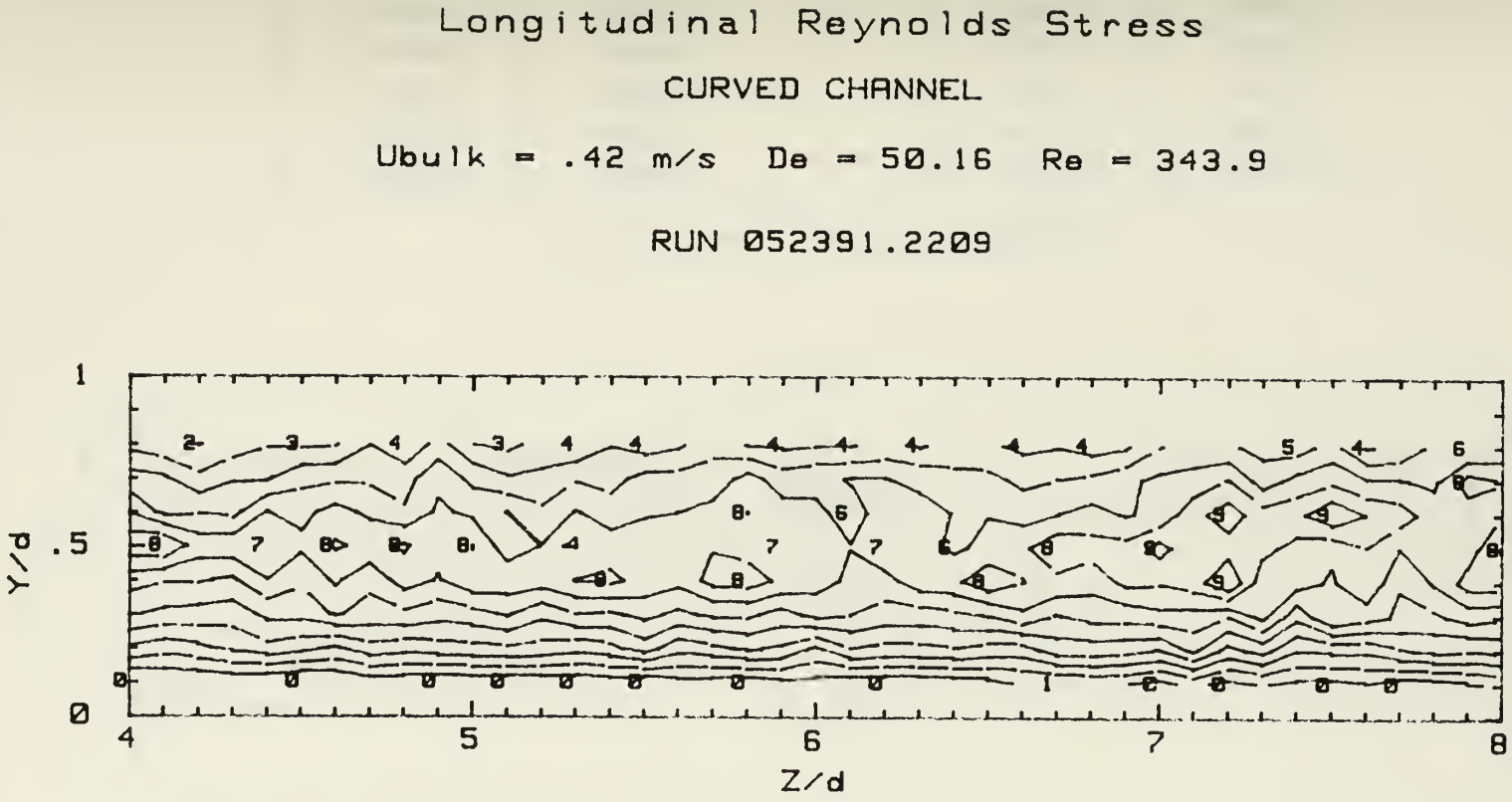

Figure 90. Longitudinal Reynolds Normal Stress Contour, De=50.2

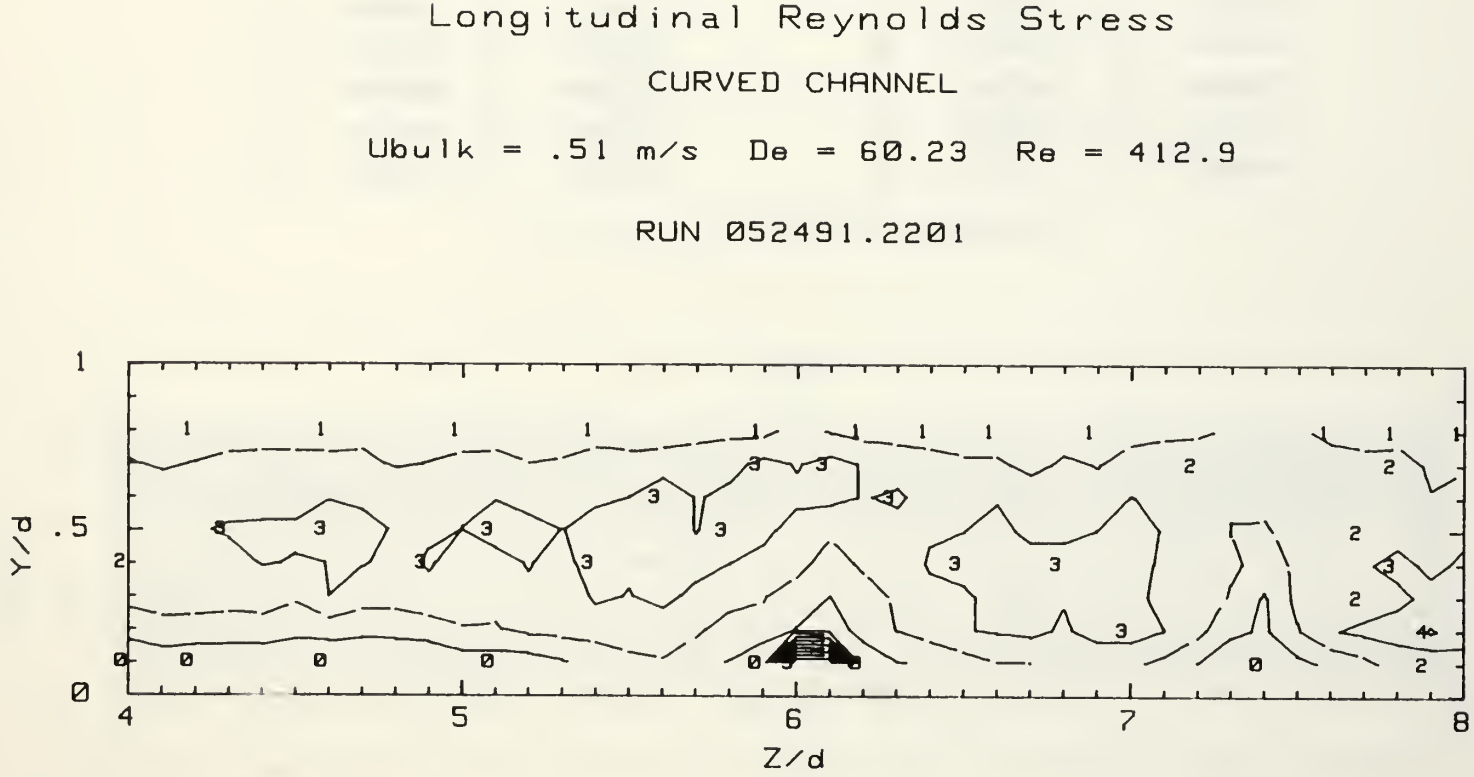

Figure 91. Longitudinal Reynolds Normal Stress Contour, De=60.2

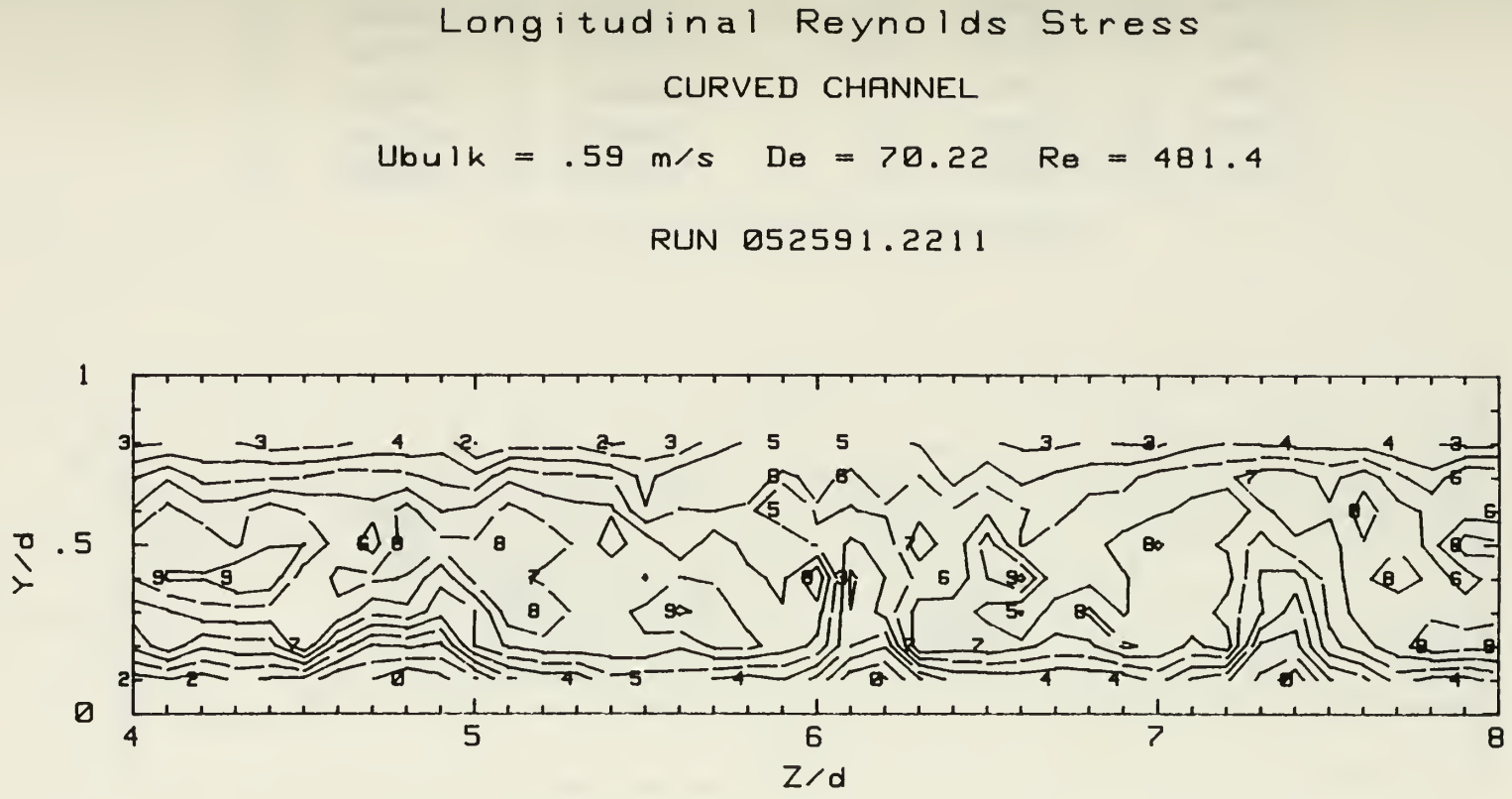

Figure 92. Longitudinal Reynolds Normal Stress Contour, De=70.2

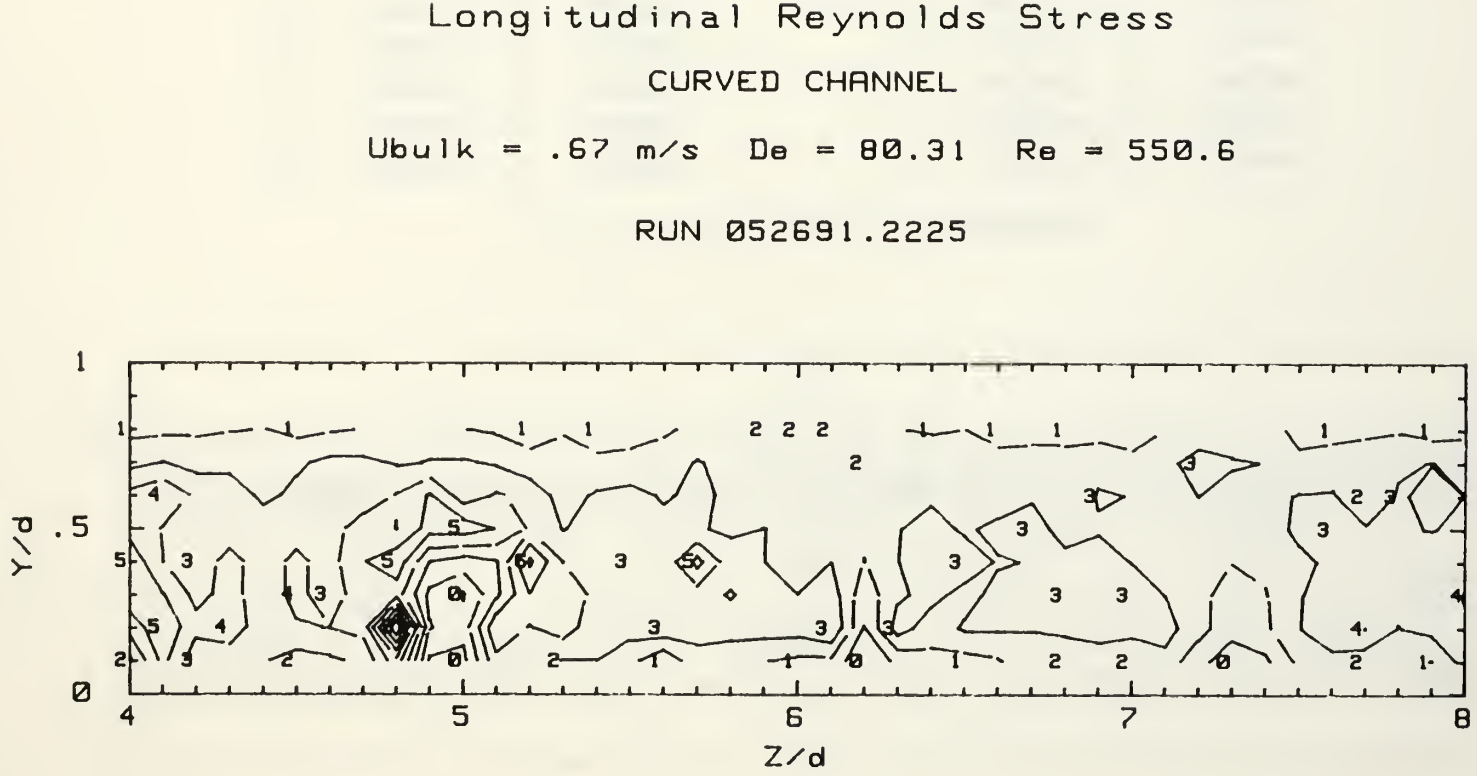

Figure 93. Longitudinal Reynolds Normal Stress Contour, De=80.3

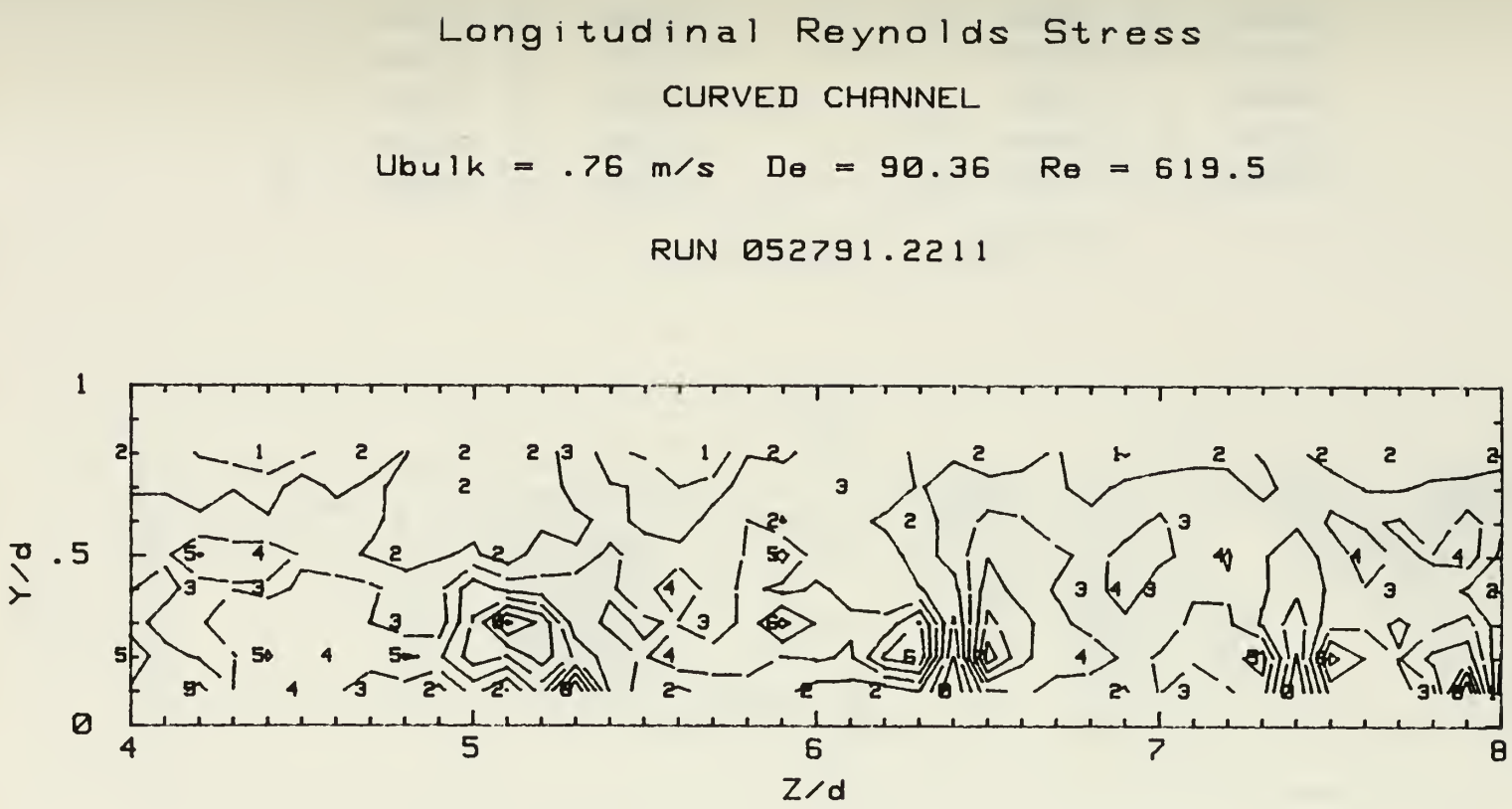

Figure 94. Longitudinal Reynolds Normal Stress Contour, De=90.4

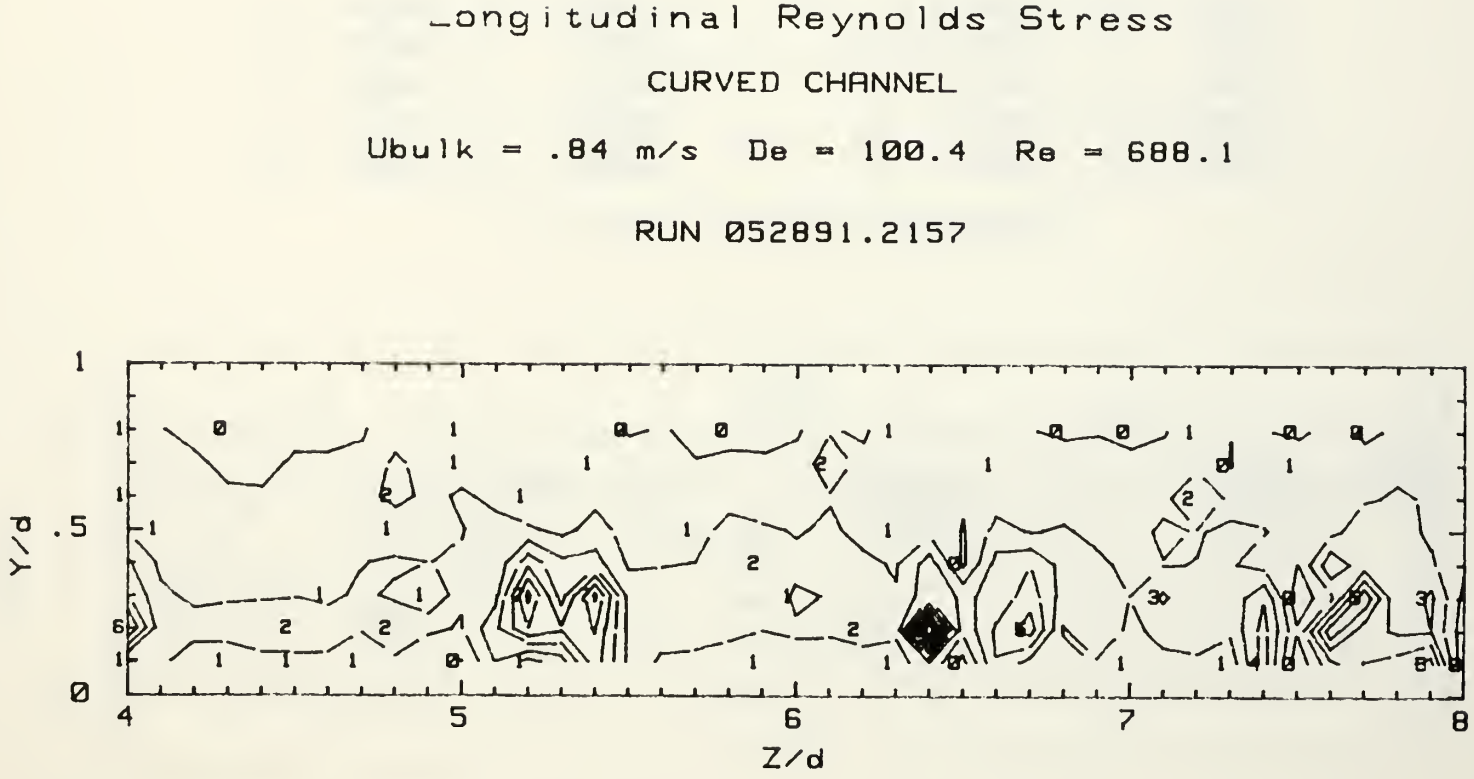

Figure 95. Longitudinal Reynolds Normal Stress Contour, De=100.4

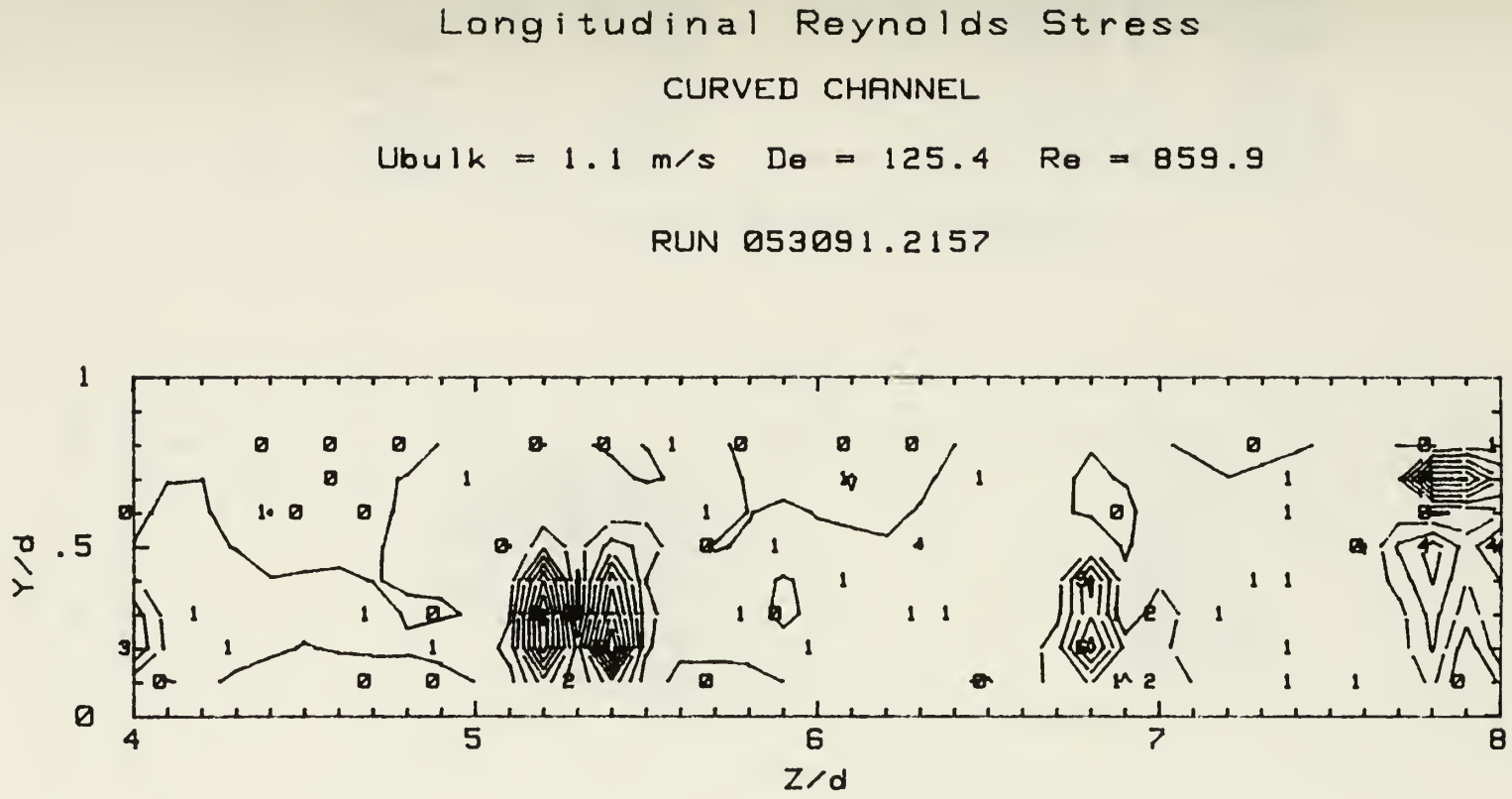

Figure 96. Longitudinal Reynolds Normal Stress Contour, De=125.4

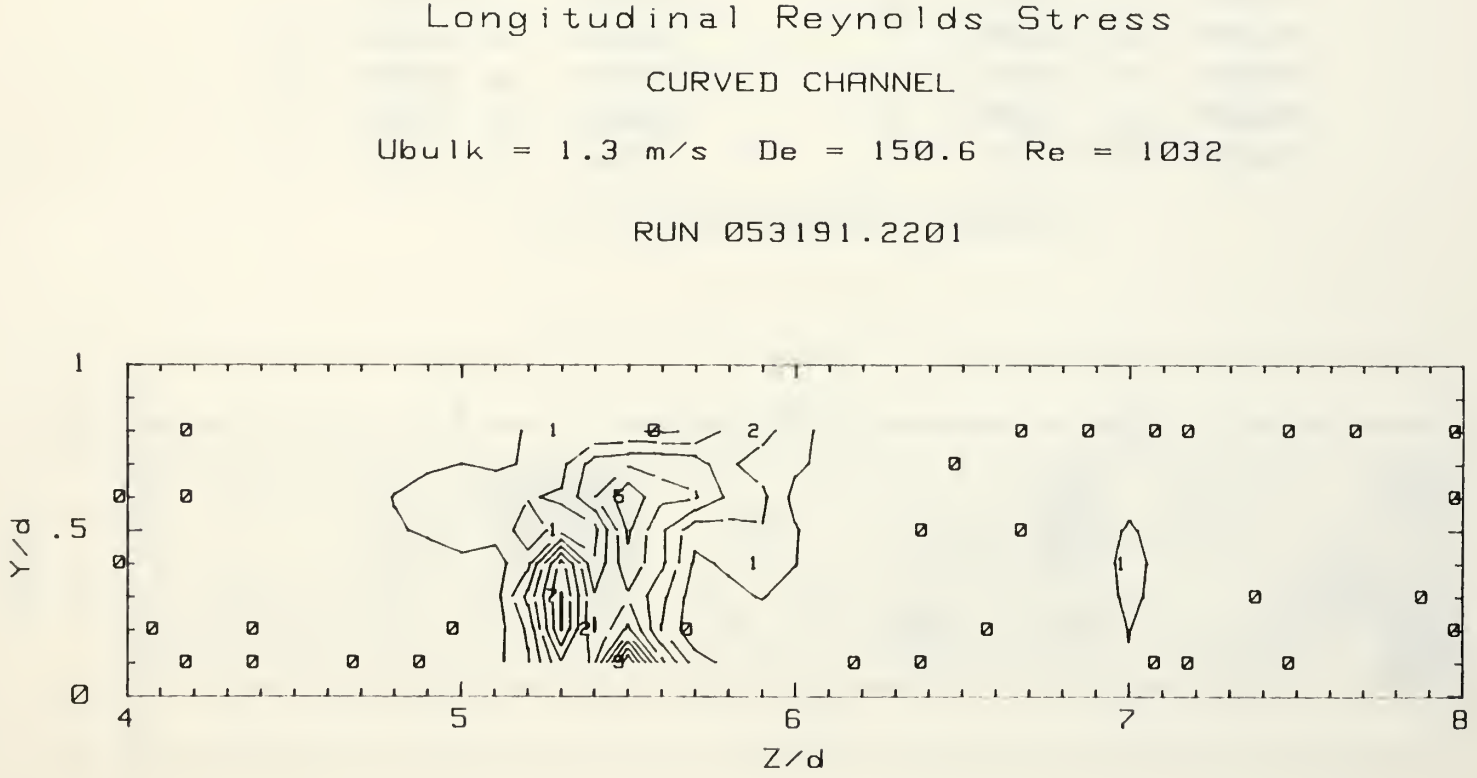

Figure 97. Longitudinal Reynolds Normal Stress Contour, De=150.6

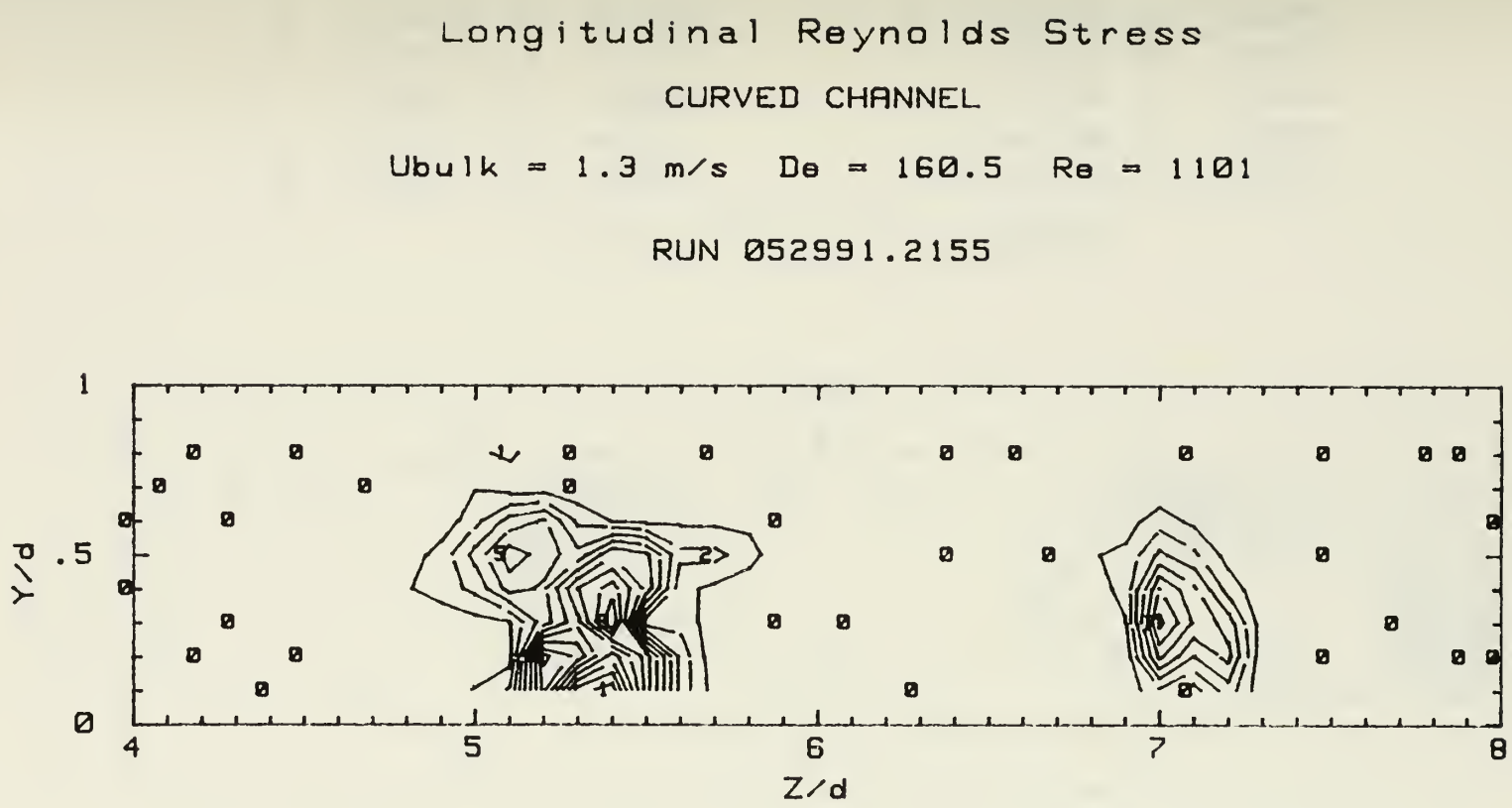

Figure 98. Longitudinal Reynolds Normal Stress Contour, De=160.5

Figure 99. Longitudinal Reynolds Normal Stress Contour, De=170.6

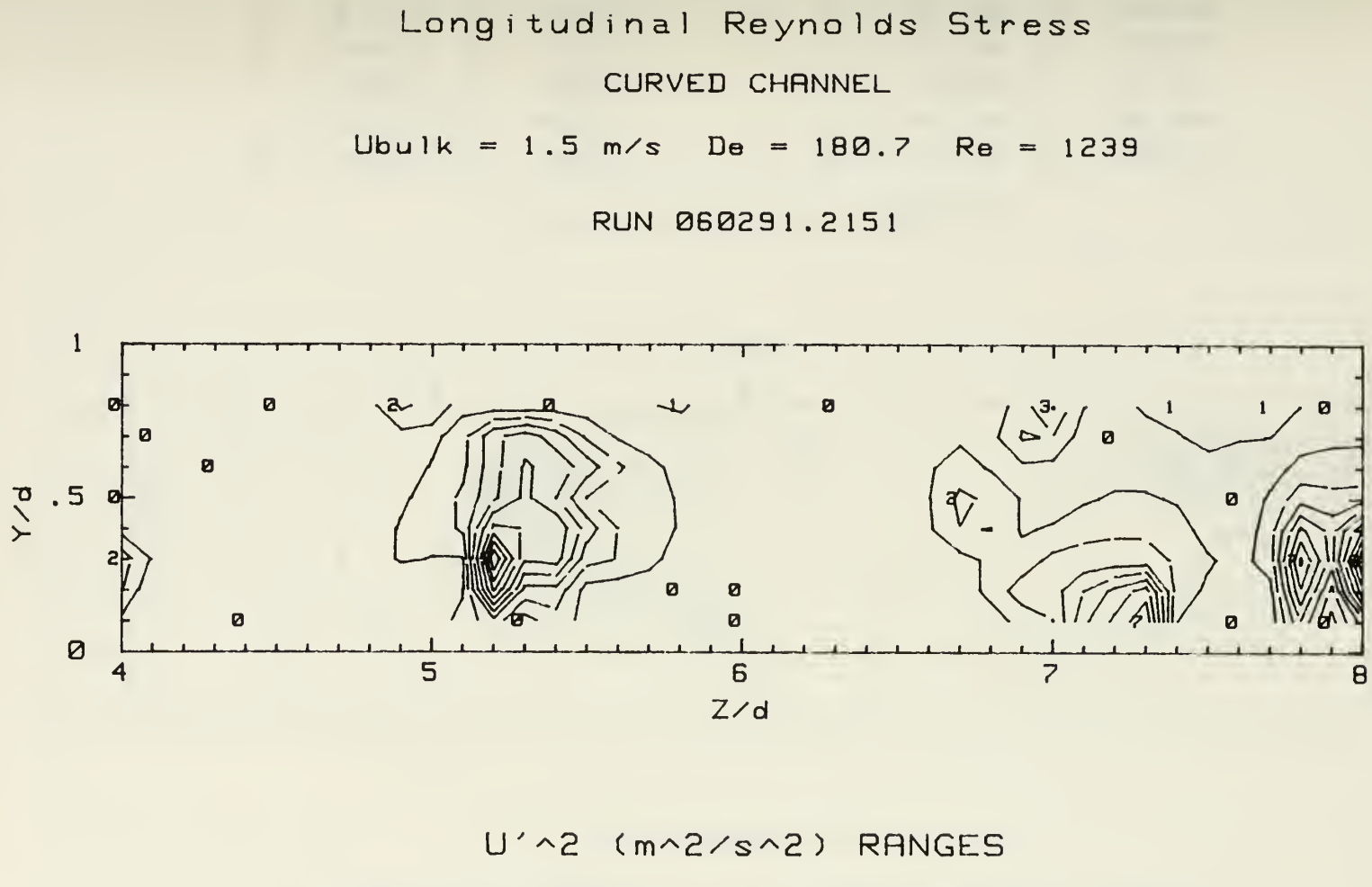

Figure 100. Longitudinal Reynolds Normal Stress Contour, De=180.7

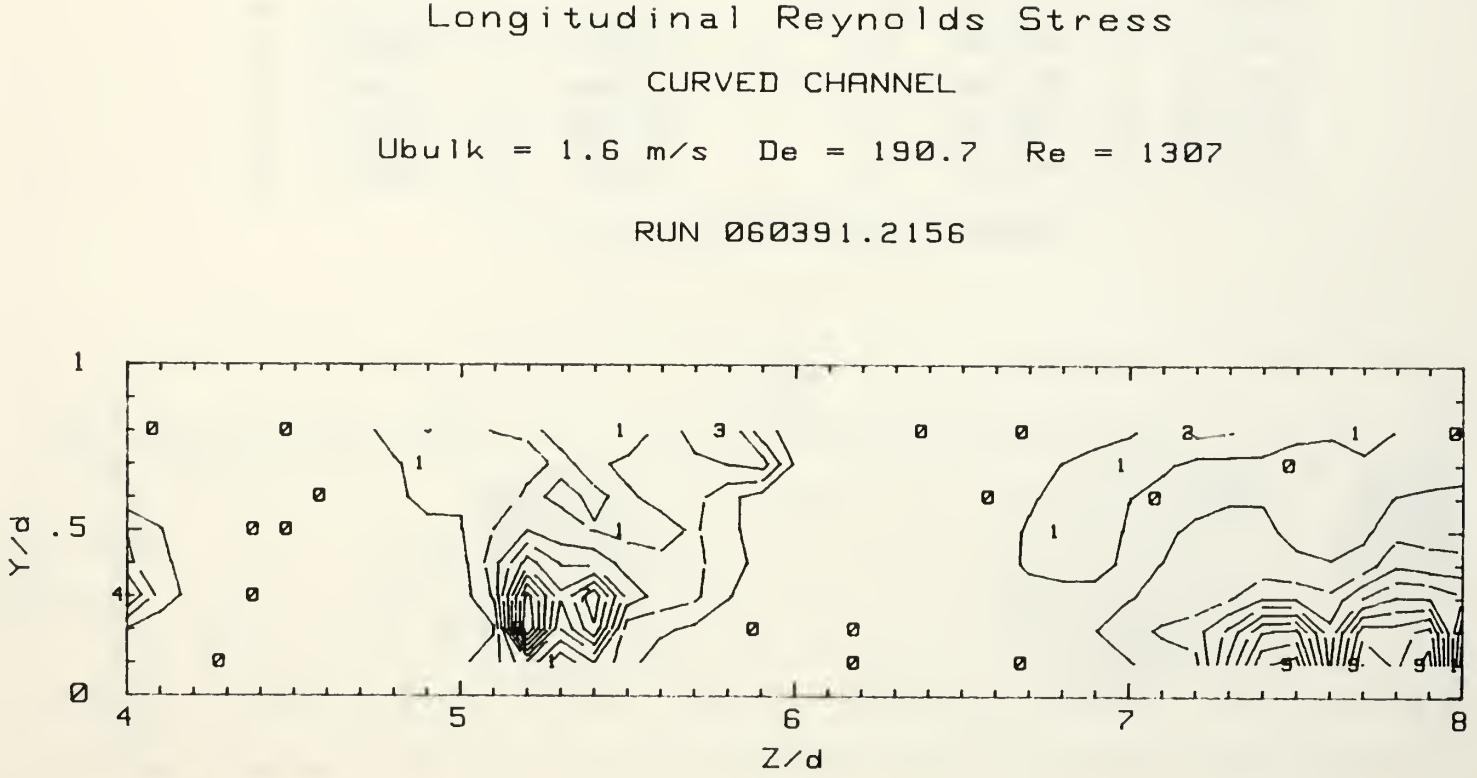

Figure 101. Longitudinal Reynolds Normal Stress Contour, De=190.7

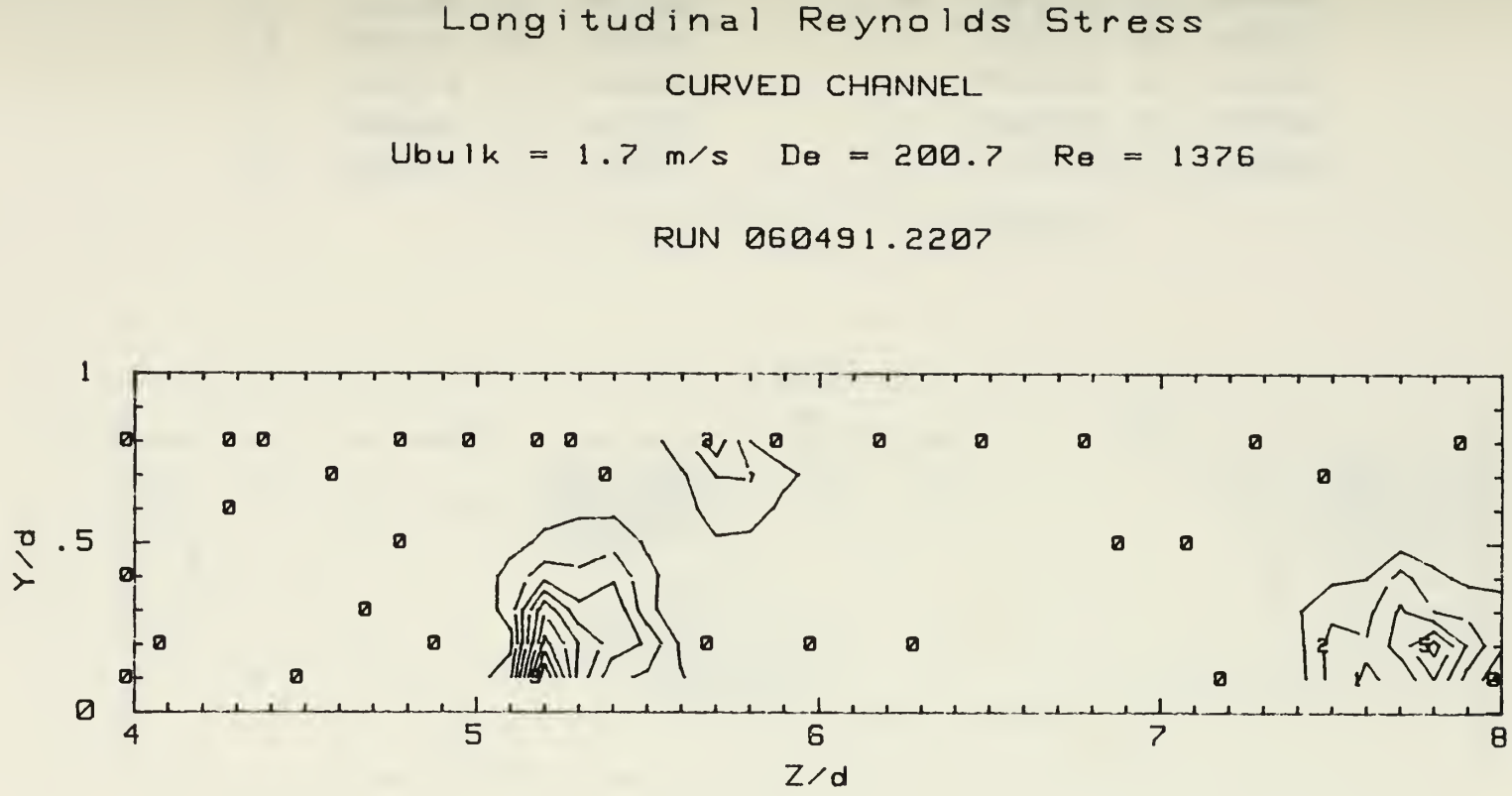

Figure 102. Longitudinal Reynolds Normal Stress Contour, De=200.7

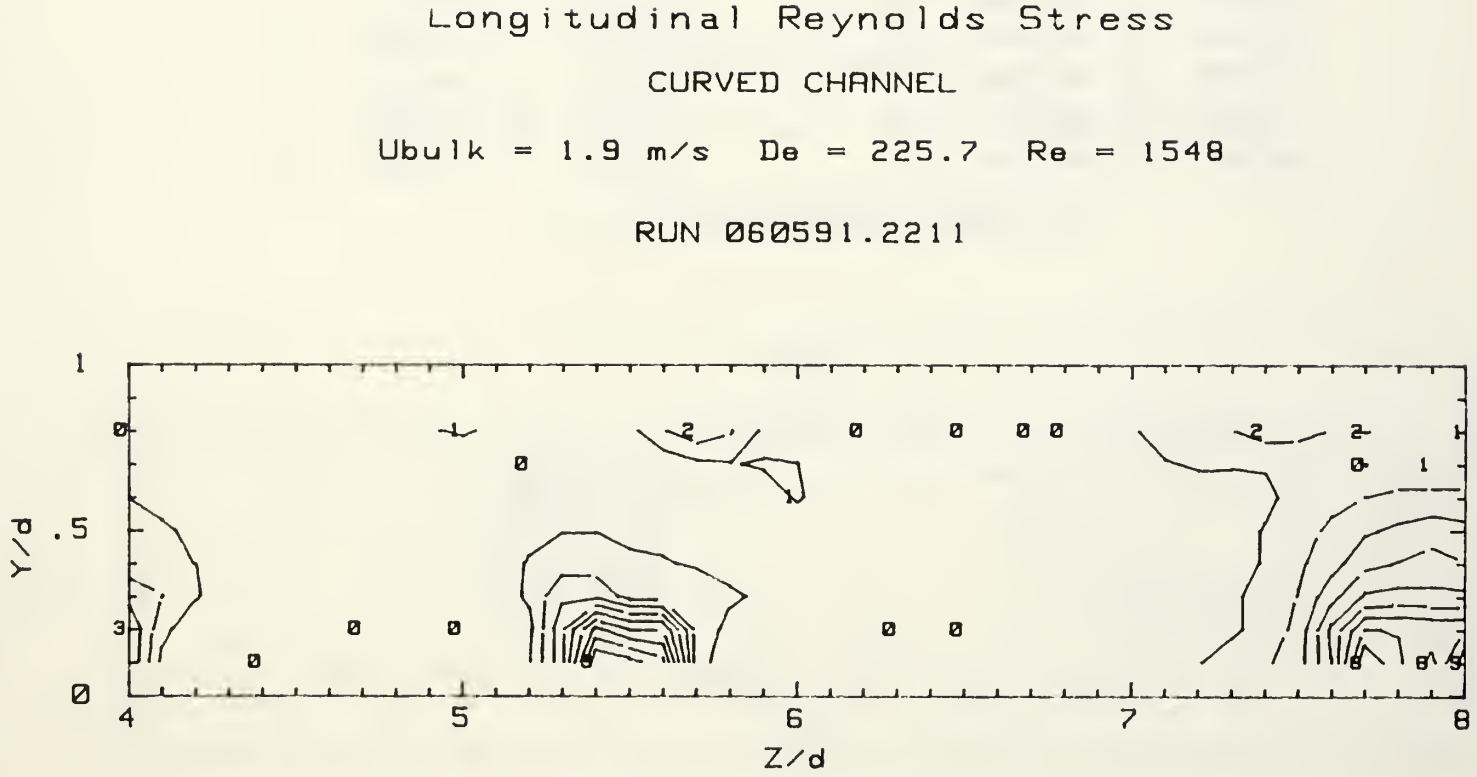

Figure 103. Longitudinal Reynolds Normal Stress Contour, De=225.7

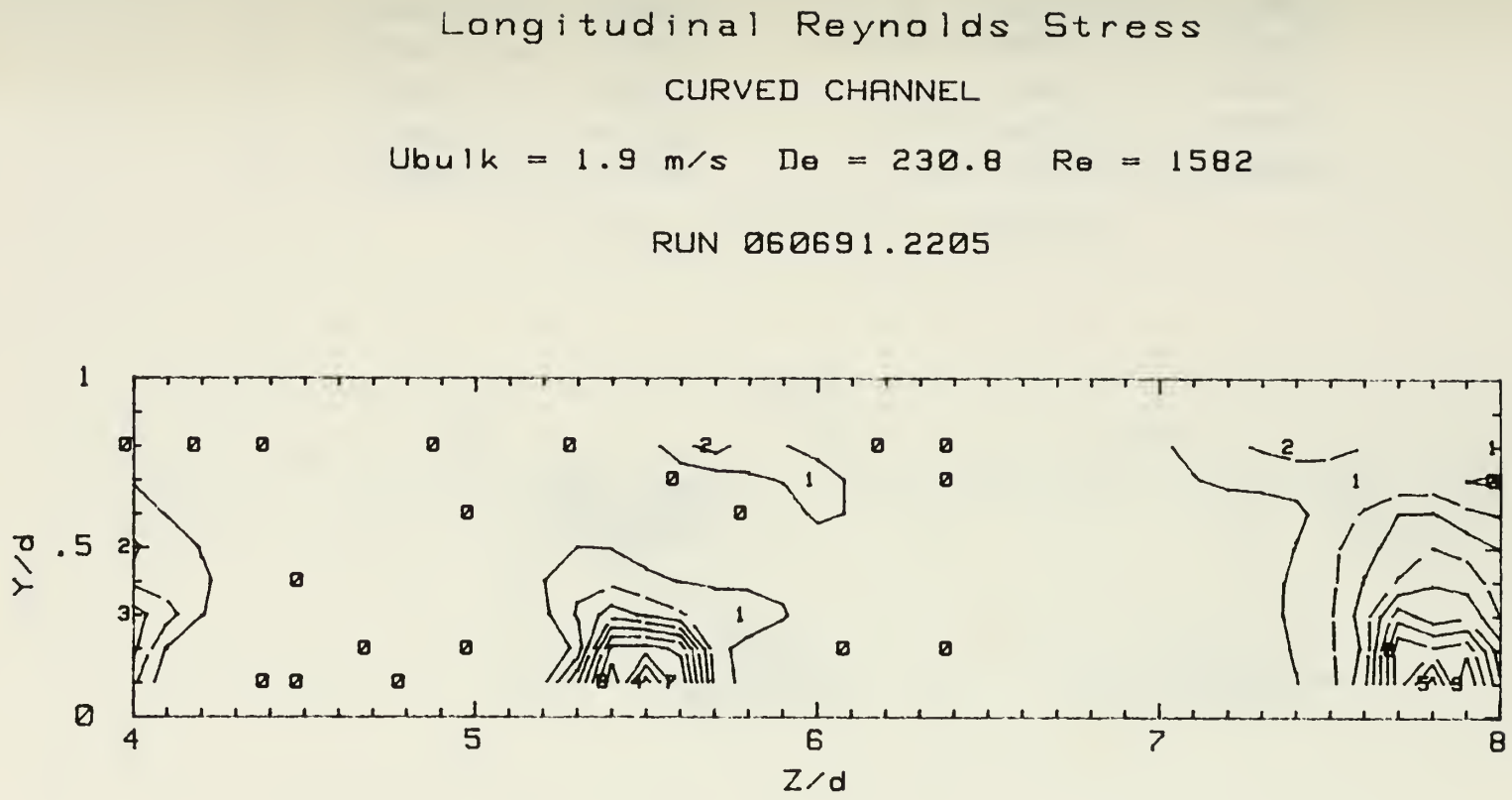

Figure 104. Longitudinal Reynolds Normal Stress Contour, De=230.8

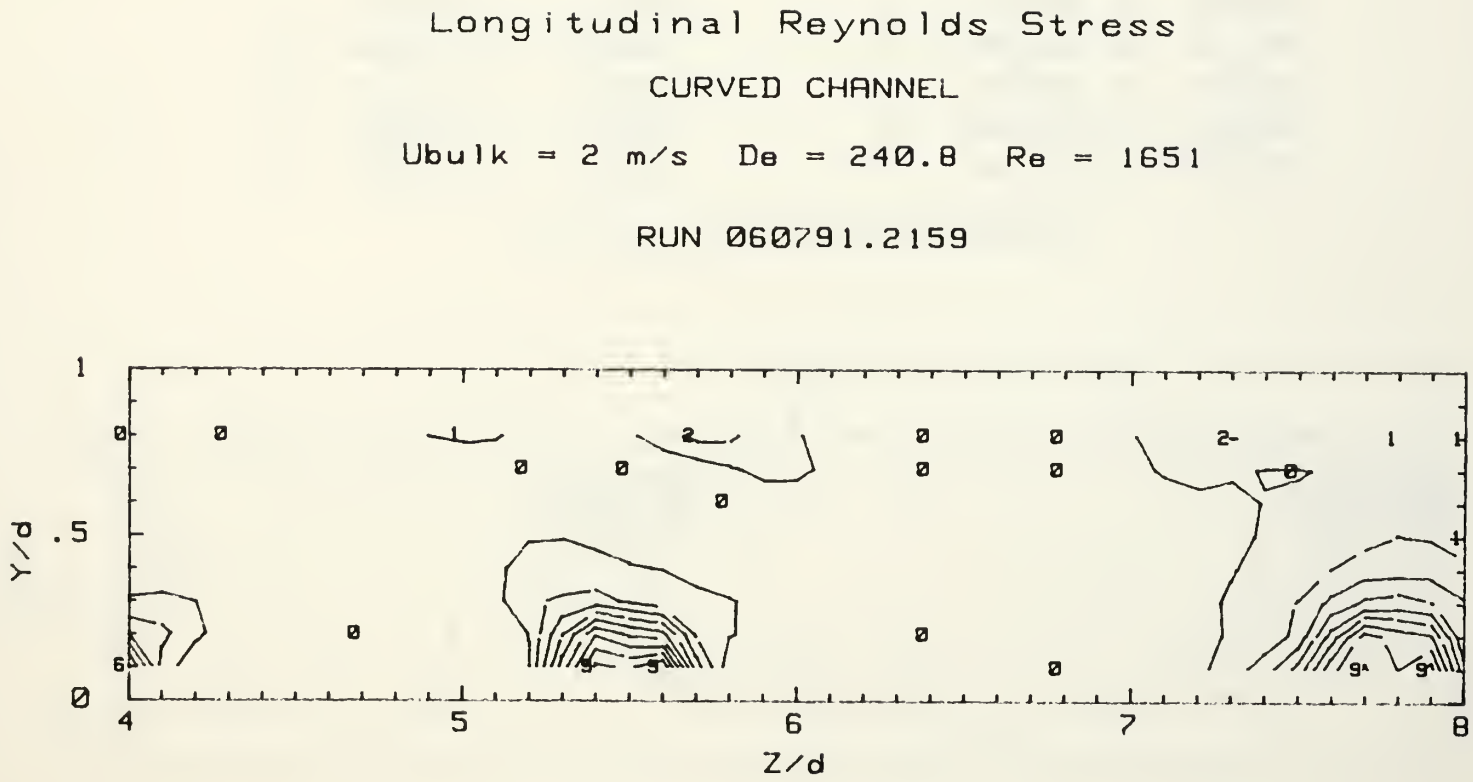

Figure 105. Longitudinal Reynolds Normal Stress Contour, De=240.8

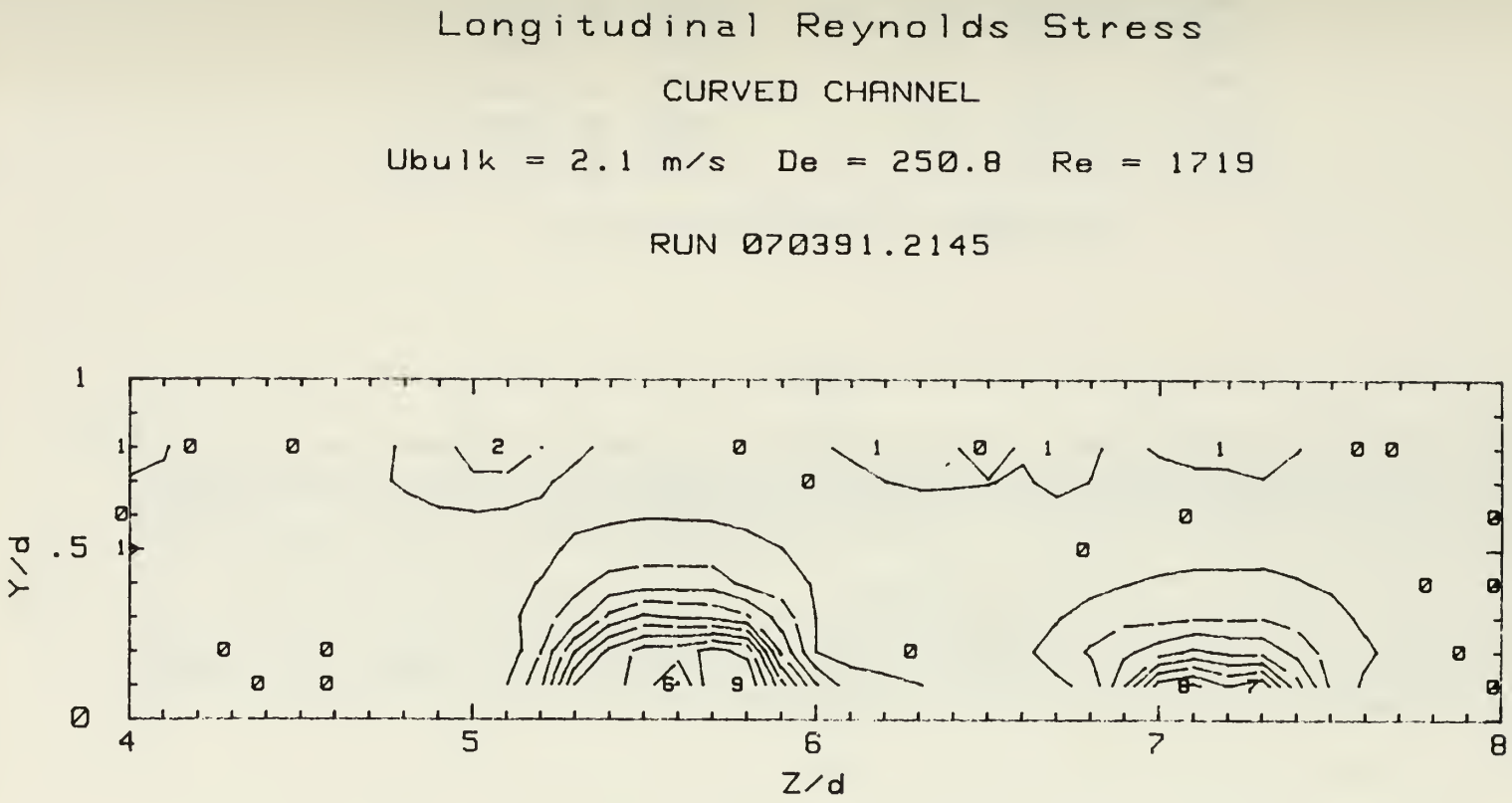

Figure 106. Longitudinal Reynolds Normal Stress Contour, De=250.8

Figure 107. Longitudinal Reynolds Normal Stress Contour, De=263.3

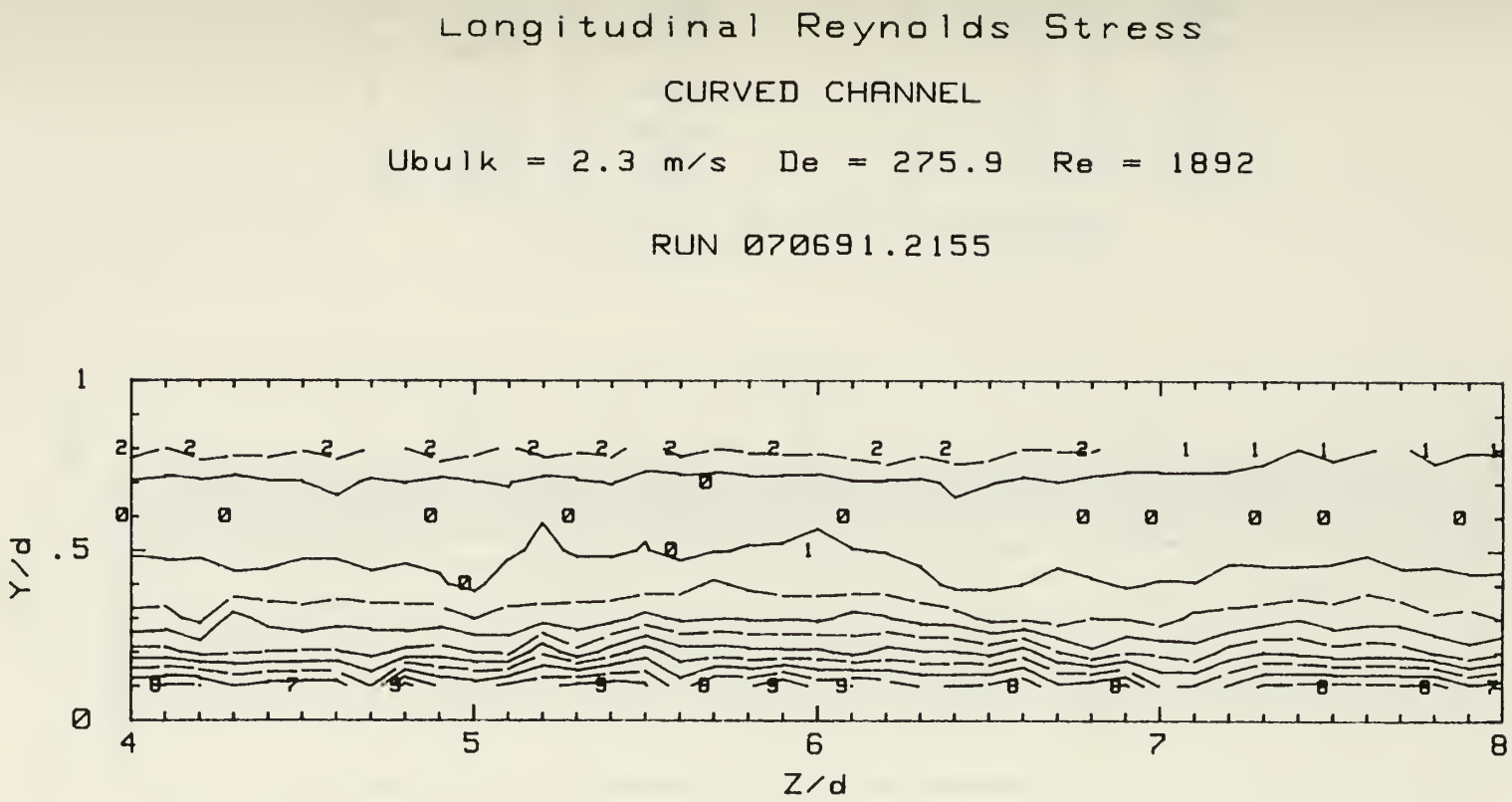

Figure 108. Longitudinal Reynolds Normal Stress Contour, De=275.9

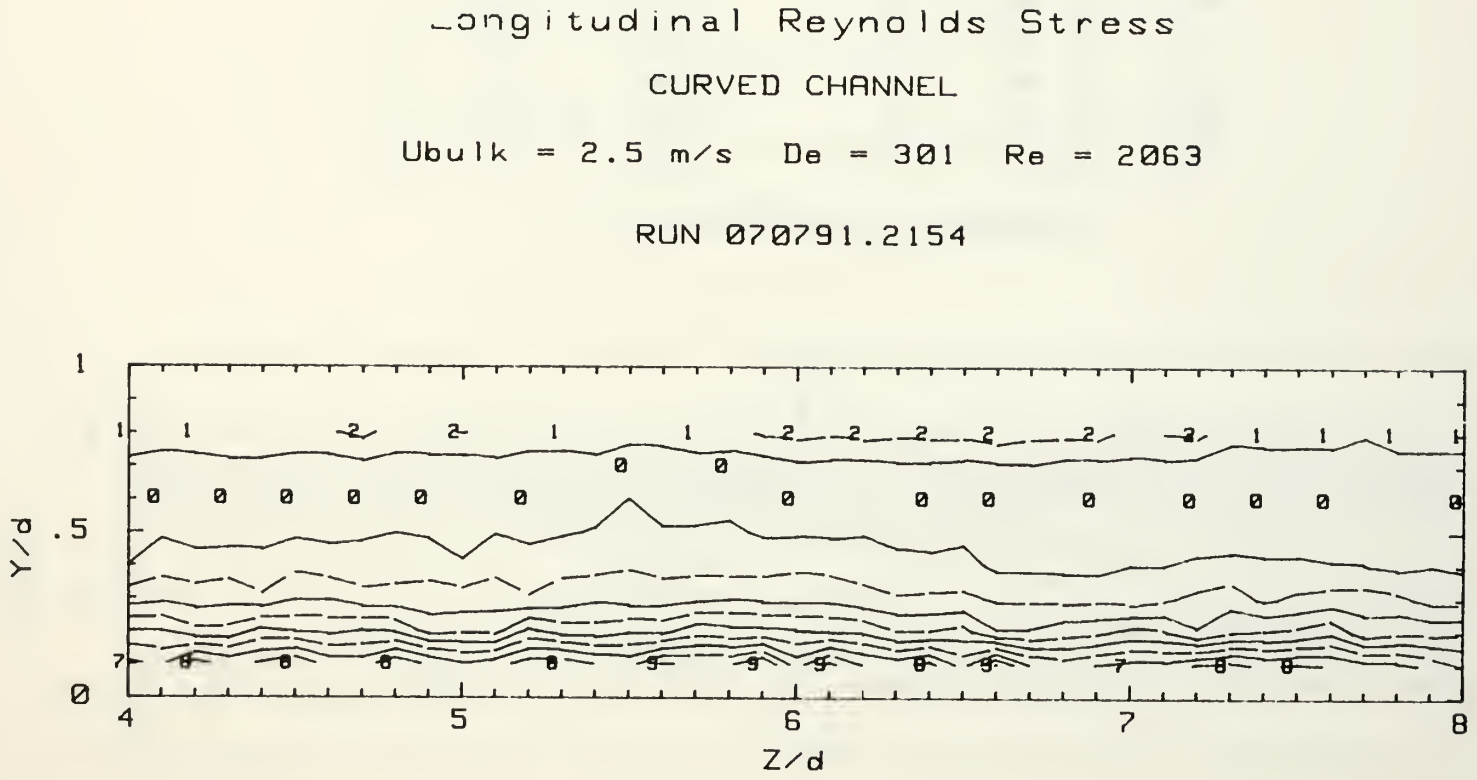

Figure 109. Longitudinal Reynolds Normal Stress Contour, De=301.1

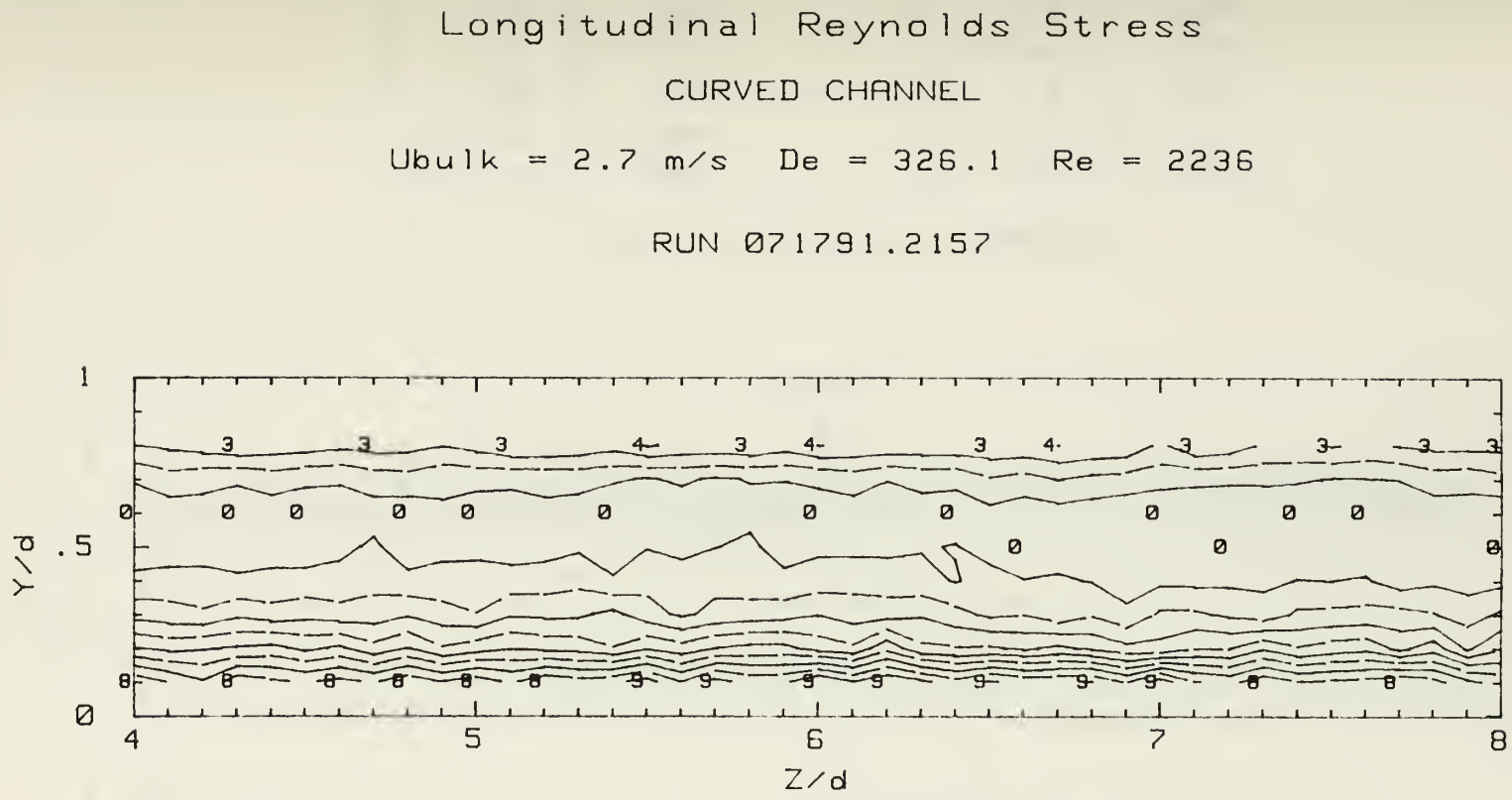

Figure 110. Longitudinal Reynolds Normal Stress Contour, De=326.1

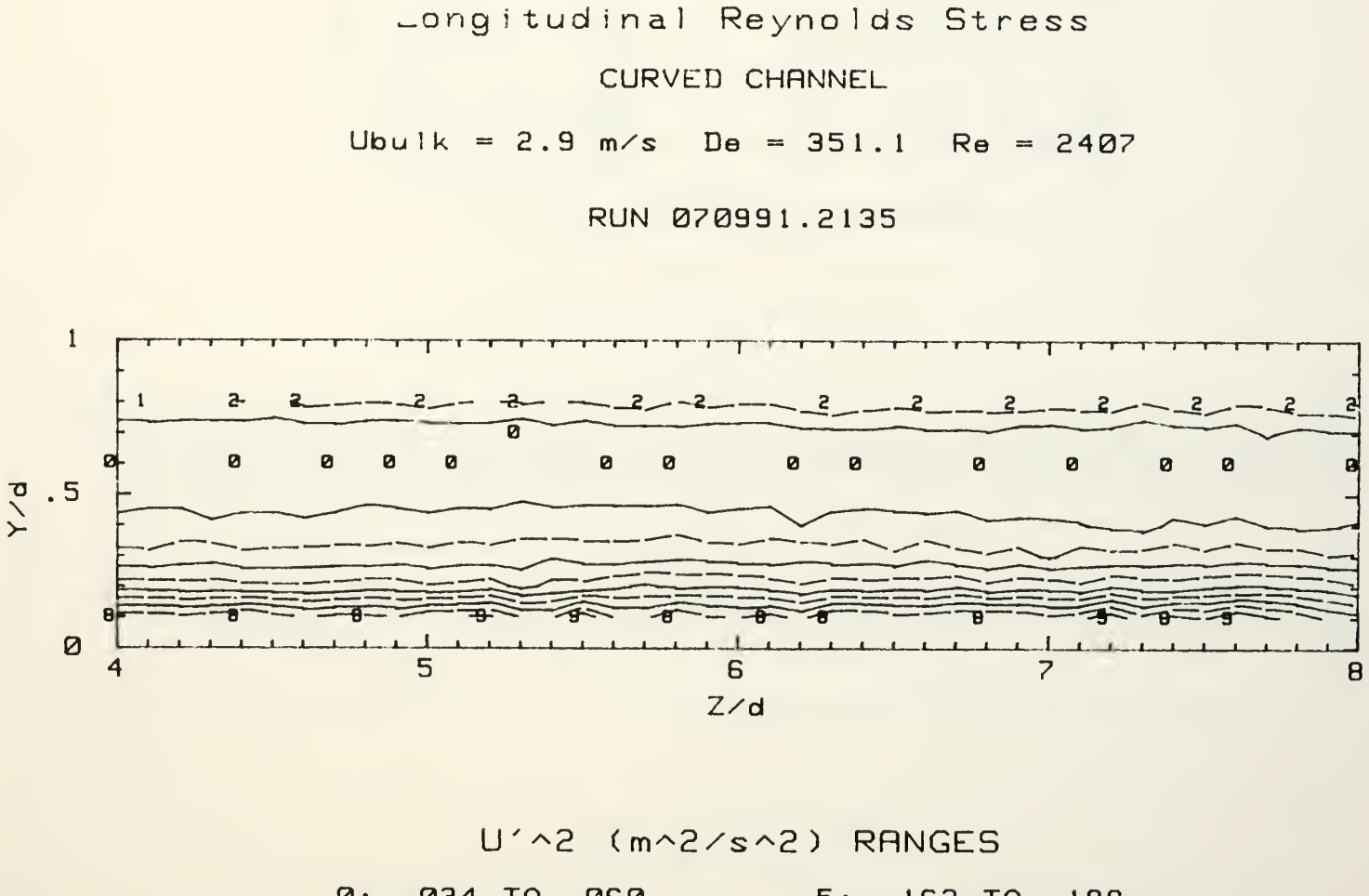

Figure 111. Longitudinal Reynolds Normal Stress Contour, De=351.1

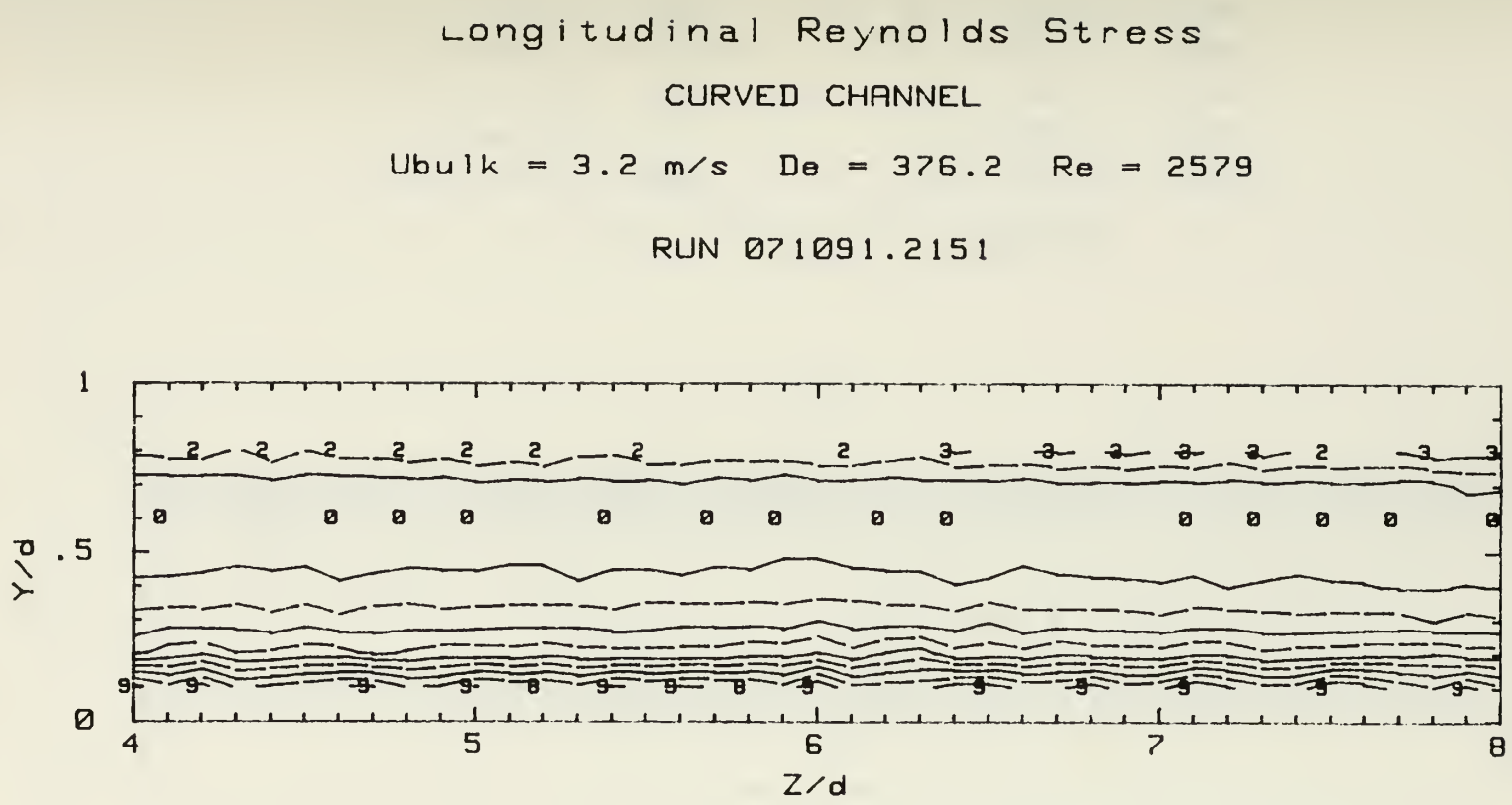

Figure 112. Longitudinal Reynolds Normal Stress Contour, De=376.2

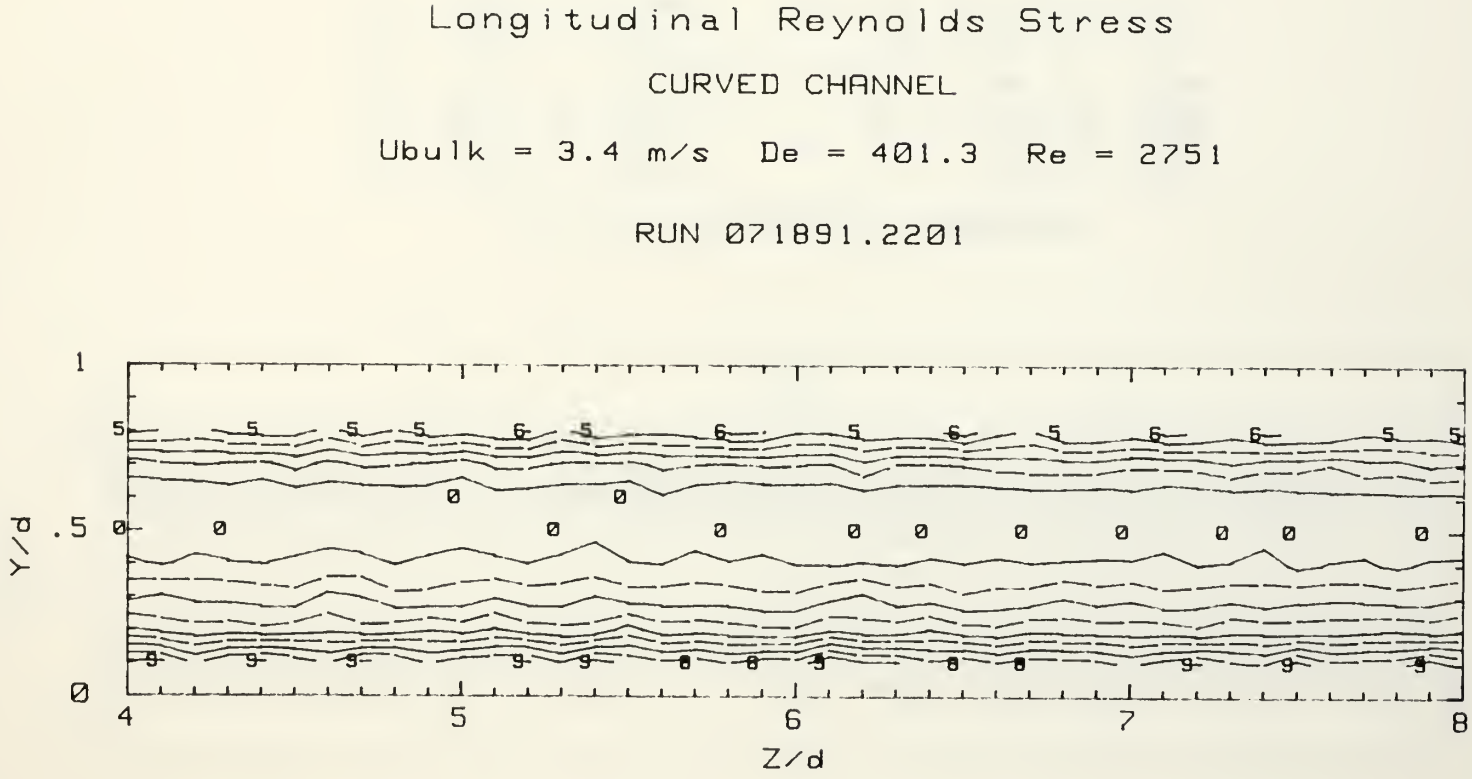

Figure 113. Longitudinal Reynolds Normal Stress Contour, De=401.3

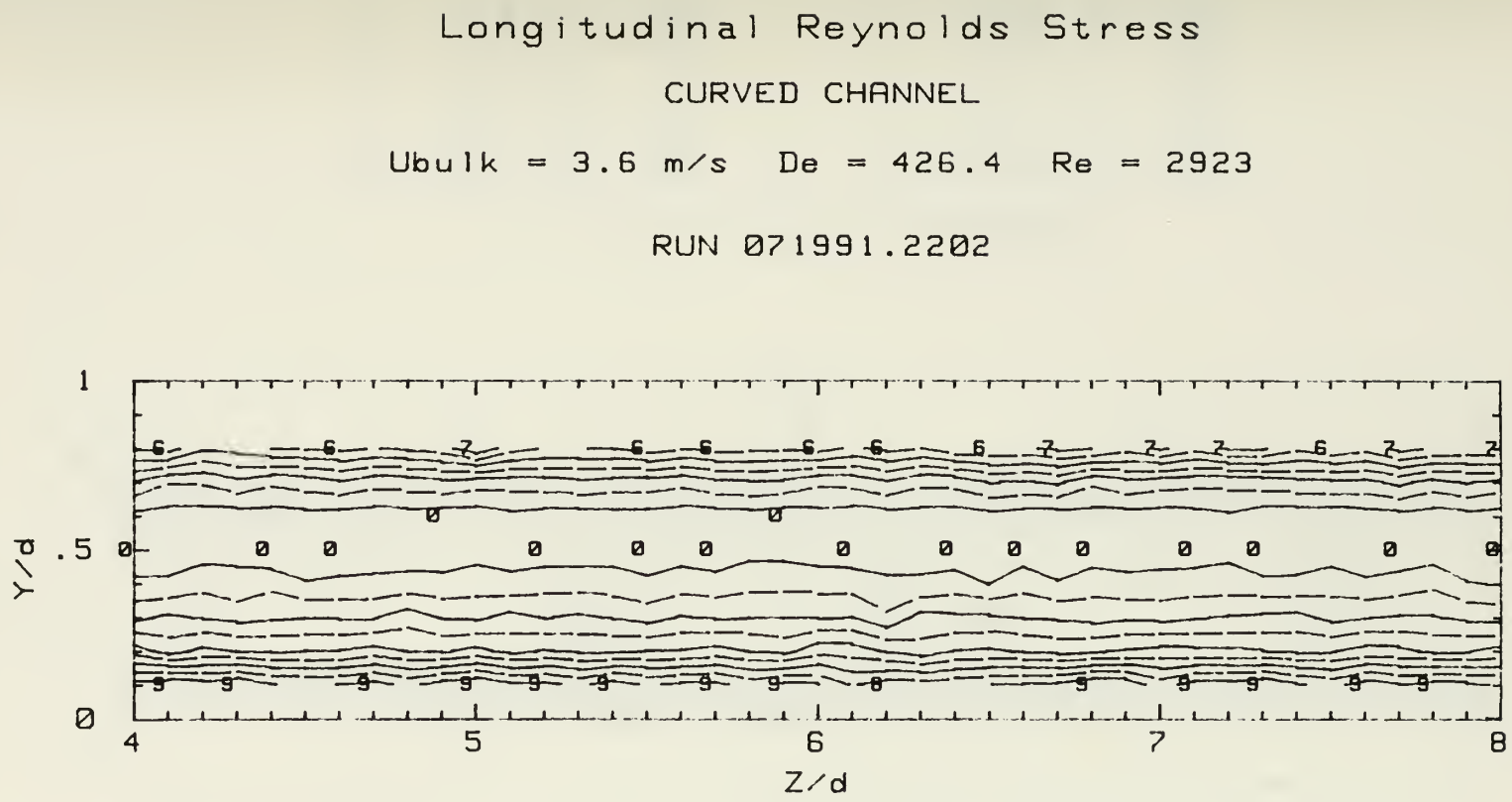

Figure 114. Longitudinal Reynolds Normal Stress Contour, De=426.4

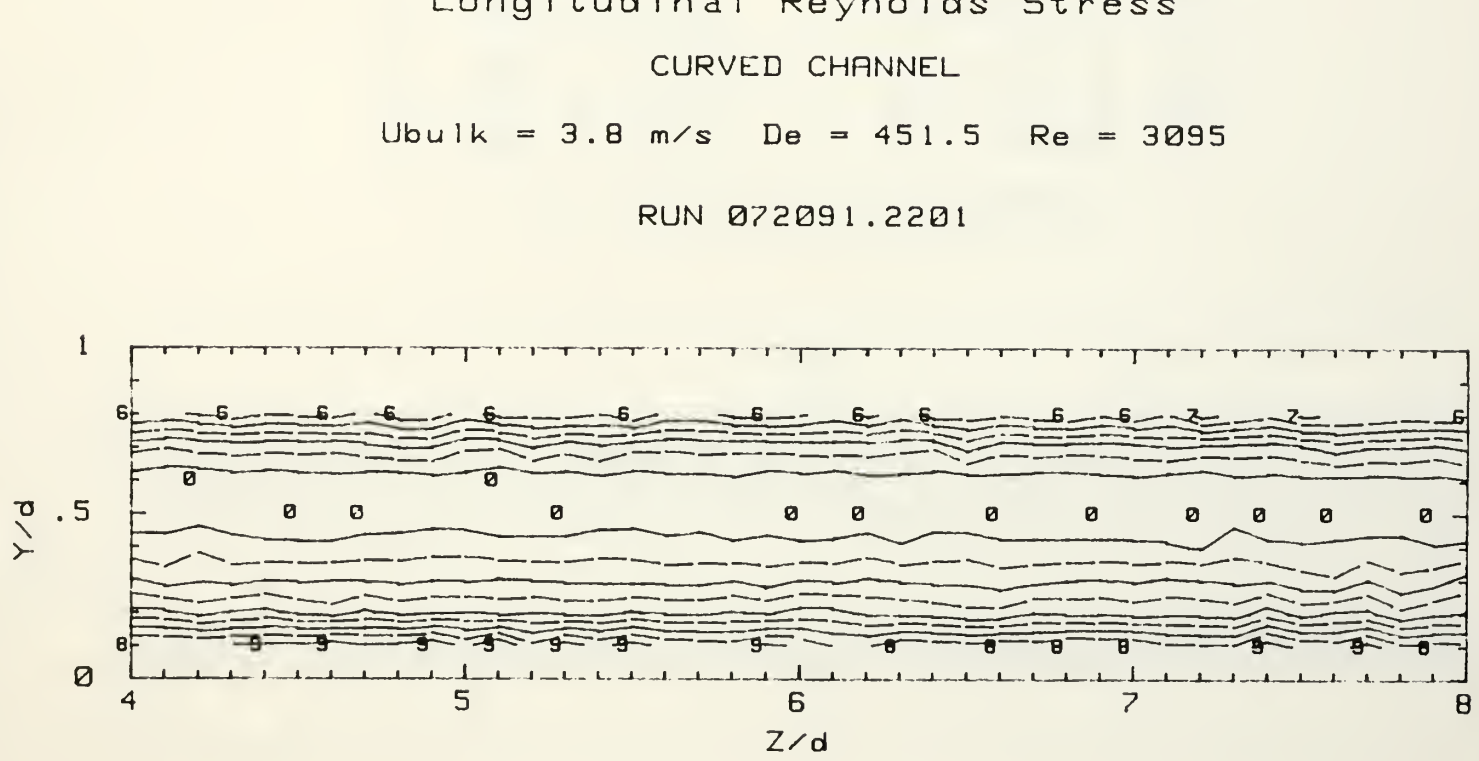

Figure 115. Longitudinal Reynolds Normal Stress Contour, De=451.5

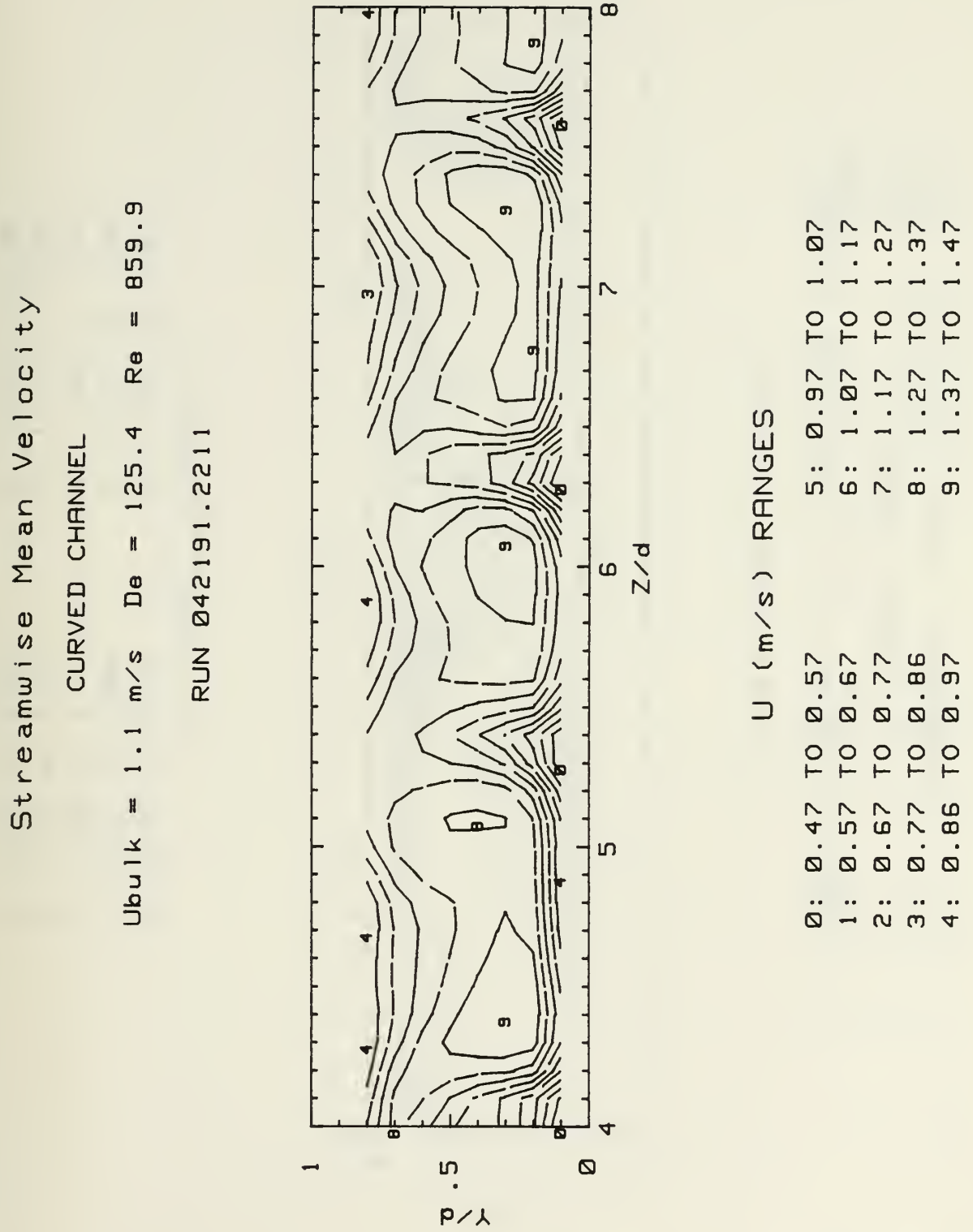

Figure 116. Streamwise Mean Velocity Contour (prior to channel cleaning), De=125.4

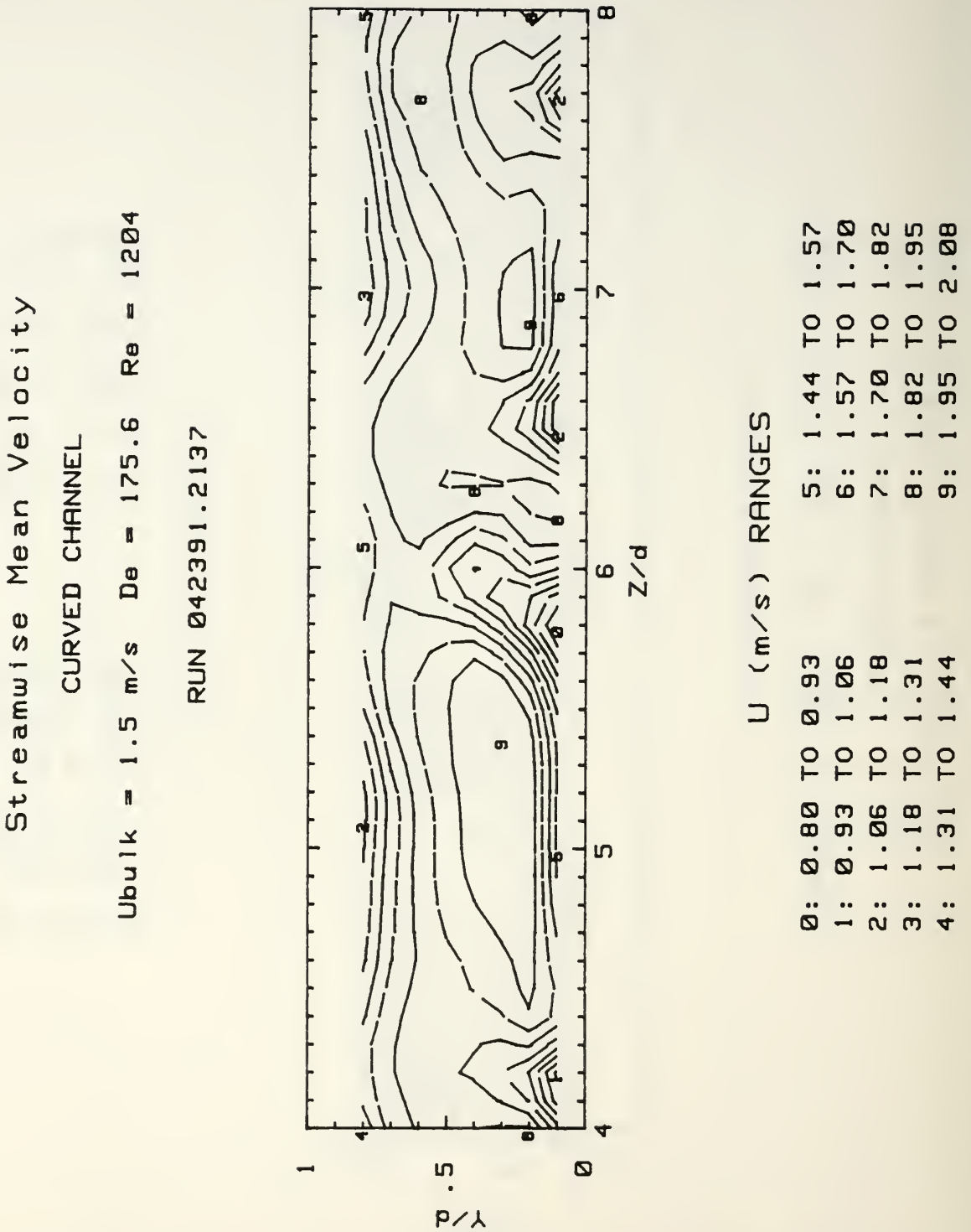

Figure 117. Streamwise Mean Velocity Contour (prior to channel cleaning), De=175.6

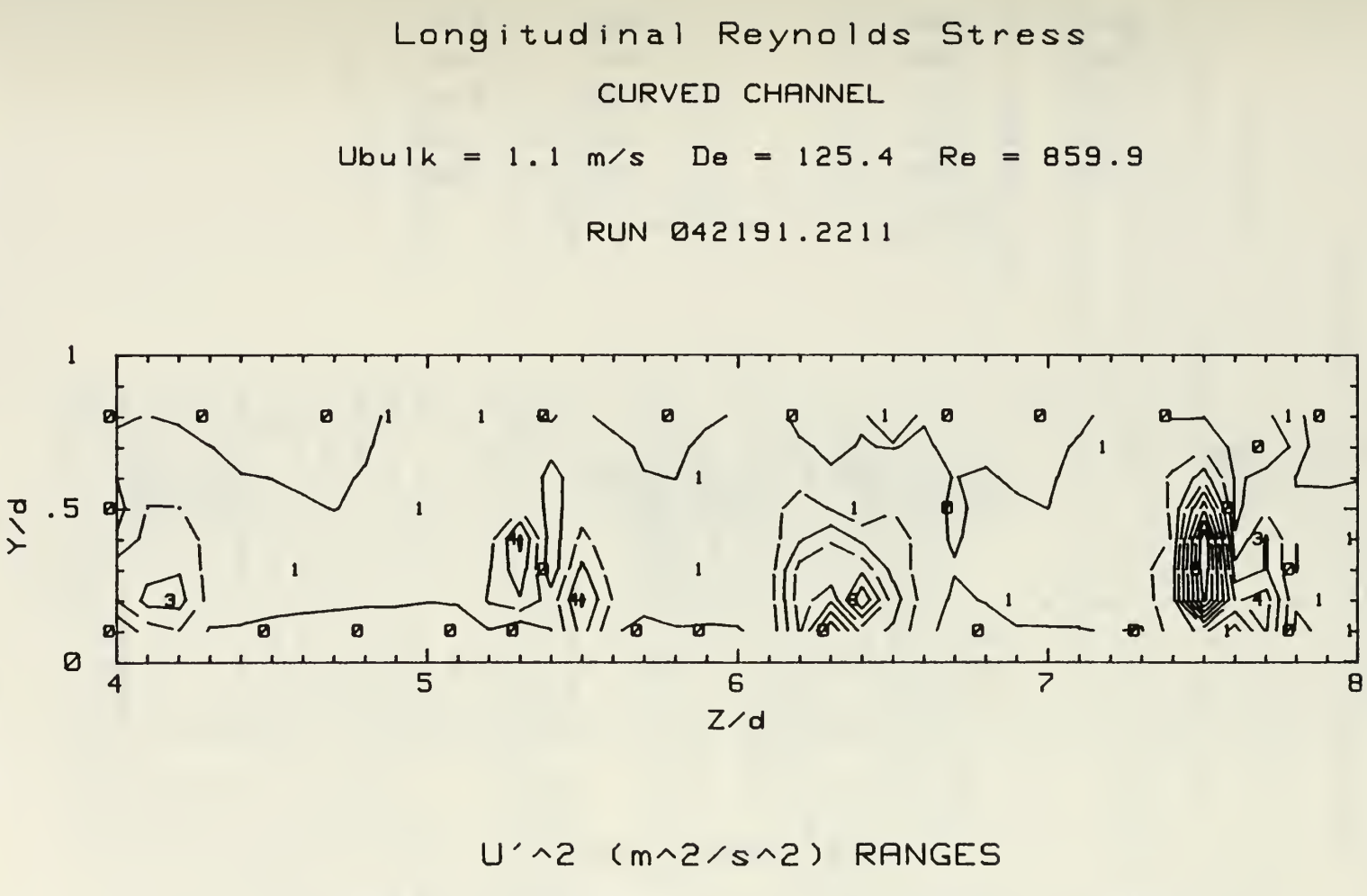

Figure 118. Longitudinal Reynolds Normal Stress Contour (prior to channel cleaning), De=125.4

Figure 119. Longitudinal Reynolds Normal Stress Contour (prior to channel cleaning), De=175.6

APPENDIX B. SOFTWARE DIRECTORY

This appendix lists the various programs use in this study. Accompanying each program listed, is a general description the program . All programs are written/modified in BASIC 4.0 for use on the HP series 9000 model 310 computer unless mentioned otherwise. The programs are listed in order of usage.

Program name	*Description*
HWCAL	This program processes the data obtained during calibration of the single-sensor hot-wire probes. The program determines calibration constants that provide the best straight line fit through the data for $Re_d > 0.07$. For $Re_d < 0.07$, the constants needed in the third-order polynomial approximation previously discussed are determined. This program is written in FORTRAN-77 and was implemented on the Apple Macintosh SE computer.
DEAN15M	This program determines the Dean number in the curved channel based on the pressure drop across an ASME 1.5 inch orifice plate.
TEMPMEAS	This program calculates ambient temperatures at the channel inlet at 10 minute intervals. It requires input from a low-speed data acquisition system and a HP 300 9000 computer independent from that used for hot-wire data acquisition.
HOTWIRE_u	Data acquisition program for measurements in the spanwise/radial plane using single-sensor hot-wire probes. Measures actual system gain and offset, then constructs look-up table using probe calibration constants. The program includes commands to automatically move the probe through the desired number of grid locations at the desired grid spacing. Calculates stream wise mean velocity and longitudinal turbulence intensity at each grid location. The results are written to a data file specified by the user. Three versions of this program are available: 1) HOTWIREu_4 is used for surveys, 2) HOTWIREu_5 is used for profiles, and 3) HOTWIRESP1 is used for inlet turbulence measurements [Ref. 7].

DRFTCORC Data from HOTWIREu is corrected for temperature drift during collection of survey data. The program assumes a linear temperature variation during the run. The user must input the temperature at the start and at completion of the run.

CCPF1M This program calculates the Curved Channel Poiseuille Flow (CCPF) and the maximum and minimum streamwise mean velocity at a given Dean number for Fields [Ref. 6] survey data. A second version, CCPF2M, is used for data from the present study. CCPF2M reads data files created by HOTWIREu.

CONTOURS This program is a general purpose contour plotting program used to graphically present the data files created by HOTWIREu. The following plot types are available: streamwise mean velocity, streamwise mean velocity normalized by U_{bulk}, longitudinal turbulence intensity, longitudinal turbulence intensity normalized by local mean velocity squared, and longitudinal turbulence intensity normalized by U_{bulk}^2.

3DPLOTS This program is similar to CONTOURS except that it plots up to seven plots on one page in a 3-D format. In addition to the five plot types available in CONTOURS, it will produce plots of u-u_{CCPF} and u_{CCPF}. When plotting u-u_{CCPF}, an option is available to determine the velocity perturbation, e.

APPENDIX C. DATA DIRECTORY

This appendix lists the various program files and data files created during this study and their location. The program file names are logical and have been discussed in Appendix B. The data file names are in the following format: *TTNNN_R*, where *TT* indicates the type of data (HW is used for survey data and NW is used for profile data), *NNN* indicates the nominal Dean number, and *R* indicates the run number for a given Dean number. This convention has been relaxed on disks 9 and 10 as this is the data actually used in producing the thesis plots presented in Appendix A.

Disk name	*File name*	*Remarks*
PROGRAM DISK: 1	CNT_BUF_AD	
	DEAN15M	
	HOTWIREu_4	
	HOTWIREu_5	
	CONTOURS	
	PROFILES	
	3DPLOTS	
	DRFTCORC	
PROGRAM DISK: 2	TEMPMEAS	
	CCPF1M	
	CCPF2M	
	HOTWIRESP1	
DATA DISK: 1	HW050_1	
	HW100_0	
	HW050_2	
	HW075_1	
	HW100_1	
	HW200_1	
	HW125_1	
	HW150_1	
	HW175_1	
	HW225_1	
	HW250_1	
	HW150_2	
	HW250_2	

Disk name	*File name*	*Remarks*
DATA DISK: 2	HW250_3	
	HW150_3	
	HW250_4	
	HW275_1	
	HW275_2	
	HW300_1	
	HW325_1	
	HW350_1	
	HW375_1	
	HW400_1	
	HW425_1	
	HW450_1	
DATA DISK: 3	HW060_1	
	HW070_1	
	HW080_1	
	HW090_1	
	HW050_3	
	HW230_1	
	HW240_1	
	HW250_0	
	HW070_2	
	HW070_3	
	HW070_4	
DATA DISK: 4	HW075_2	
	HW075_3	
	HW075_4	
	HW050_4	
	HW050_5	(1)
	HW060_2	(1)
	HW070_5	(1)
	HW080_2	(1)
	HW090_2	(1)
	HW100_2	(1)
	HW160_1	(1)
	HW125_2	(1)
	HW150_4	(1)

Disk name	*File name*	*Remarks*
DATA DISK: 5	HW170_1	(1)
	HW180_1	(1)
	HW190_1	(1)
	HW200_2	(1)
	HW225_2	(1)
	HW230_2	(1)
	HW240_2	(1)
	HW250_6	
	HW275_3	
	HW300_2	
	HW325_2	
	HW350_2	
DATA DISK: 6	HW375_2	
	HW400_2	
	HW425_2	
	HW450_2	
	HW250_R	
	HW250_7	(1)
	HW262_1	(1)
	HW275_4	(1)
	HW300_3	(1)
	HW325_3	
	HW350_3	
	HW375_3	
	HW325_4	
DATA DISK: 7	HW400_3	
	HW425_3	
	HW450_3	
	HW325_5	
	HW325_6	
	HW400_4	
	HW425_4	
	HW450_4	
DATA DISK: 8	HW325_6TC	(1), (3)
	HW400_4TC	(1), (3)
	HW425_4TC	(1), (3)
	HW450_4TC	(1), (3)
	HW350_3TC	(1), (3)
	HW375_3TC	(1), (3)

Disk name	*File name*	*Remarks*
DATA DISK: 9	HW050	
	HW060	
	HW070	
	HW080	
	HW090	
	HW100	
	HW125	
	HW150	
	HW160	
	HW170	
	HW180	
	HW190	
	HW200	
DATA DISK: 10	HW225	
	HW230	
	HW240	
	HW250	
	HW262	
	HW275	
	HW300	
	HW325	
	HW350	
	HW375	
	HW400	
	HW425	
	HW450	
DATA DISK: 11	NW400_1	
	NW400_2	
	NW400_3	
	NW400_4	
	NW125_1	(2), Z/d = 5.25
	NW170_1	(2), Z/d = 5.25
	NW240_1	(2), Z/d = 5.25
	NW400_5	(2), Z/d = 5.25
	NW125_2	(2), Z/d = 5.50
	NW170_2	(2), Z/d = 5.50
	NW240_2	(2), Z/d = 5.50
	NW125_3	(2), Z/d = 6.00
	NW170_3	(2), Z/d = 6.00
	NW240_3	(2), Z/d = 6.00

Remarks: (1) This data is used in preparing thesis plots. The same data are stored using an abreviated file name on data disks 9 and 10.

(2) This data is used in preparing thesis plots.

(3) This data has been corrected for variations in ambient temperature during the survey.

LIST OF REFERENCES

1. Dean, W.R., "Fluid Motion in a Curved Channel," *Proceedings of The Royal Society of London*, Series A, v. 121, pp. 402-420, 01 November 1928.

2. Brewster, D.B., Grosberg, P. and Nissan, A.H., "The Stability of Viscous Flow Between Horizontal Concentric Cylinders," *Proceedings of The Royal Society of London*, Series A, v. 251, pp. 76-91, 15 September 1958.

3. Finlay, W.H., Keller, J.B., and Ferziger, J.H., "Finite Amplitude Vortices in Curved Channel Flow," *Journal of Fluid Mechanics*, v. 194, pp. 417-456, September 1988.

4. Ligrani, P.M., Niver, R.D., "Flow Visualization of Dean Vortices in a Curved Channel with 40 to 1 Aspect Ratio," *Physics of Fluids A,* v. 31, pp. 3605-3617, December 1988.

5. Kelleher, M.D., Flentie, D.L. and McKee, R.J., "An Experimental Study of the Secondary Flow in a Curved Rectangular Channel," *Fluids Engineering*, vol. 102, pp. 92-96, March 1980.

6. Matsson, O.J.E., and Alfredsson, P.H., "Curvature- and Rotation-induced Instabilities in Channel Flow," *Journal of Fluid Mechanics*, vol. 210, pp. 537-563, 1990.

7. Matsson, O.J.E., and Alfredsson, P.H., "Experiments on Instabilities in Curved Channel Flow," *Physic of Fluids A*, 1991.

8. Ligrani, P.M.,Finlay, W.H., Fields, W.A., Fuqua, S.J., and Subramanian, C.S., "Features of Wavy Vortices in a Curved Channel from Experimental and Numerical Studies," *Physic of Fluids A*, 1991.

9. NASA Technical Memorandum 85974, *Direct Numerical Simulation of Curved Turbulent Channel Flow*, by R.D. Moser and P. Moin, October 1984.

10. Bottaro, A., Matsson, O.J.E., and Alfredsson, P.H., "Numerical and Experimental Results for Developing Curved Channel Flow," *Physics of Fluids A*, v. 3, p. 1473, 1991.

11. Niver, R.D., *Structural Characteristics of Dean Vortices in a Curved Channel,* M.S. Thesis, Naval Postgraduate School, Monterey, California, June 1987.

12. Baun, L.R., *The Development and Structural Characteristics of Dean Vortices in a Curved Rectangular Channel*, M.E. Thesis, Naval Postgraduate School, Monterey, California, September 1988.

13. Longest, J.M., *Flow Visualization Studies in (1) A Curved Rectangular Channel with 40 to 1 Aspect Ratio and (2) A Straight Channel with Bulk Flow Unsteadiness,* M.S. Thesis, Naval Postgraduate School, Monterey, California, June 1989.

14. Fields, W.A., *Study of the Effects of Centrifugal Instabilities on Flow in a 40 to 1 Aspect Ratio Rectangular Curved Channel, For Dean Numbers form 35 to Fully Turbulent Conditions*, M.E. Thesis, Naval Postgraduate School, Monterey, California, December 1990.

15. Kendall, M.R., *Effects of Centrifugal Instabilities on Laminar/Turbulent Transition in Curved Channels with 40 to 1 Aspect Ratios,* M.E. Thesis, Naval Postgraduate School, Monterey, California, June 1991.

16. Saric, W.A., conversation with P. Ligrani, May 1991.

17. Perry, A.E., *Hot-Wire Anemometry*, Clarendon Press, Oxford, 1982.

18. DISA, Probe Catalog, p. 10, 1989..

19. Ligrani, P.M. and Bradshaw, P., "Subminiature Hot-Wire Sensors: Development and Use," *Journal of Physics*, Vol. 20, pp. 323-332, 1987.

20. Green, J.G., *Turbulence Structure Resulting from Interaction Between an Embedded Vortex and Wall Jet*, M.S. Thesis, Naval Postgraduate School, Monterey, California, June 1989.

21. Baun, L.R., *The Development and Structural Characteristics of Dean Vortices in a Curved Rectangular Channel*, M.E. Thesis, Naval Postgraduate School, Monterey, California, September 1988.

22. Smith, B.J., *Study of Transition Phenomena in a Straight Channel With 40 to 1 Aspect Ratio With and Without Imposed Pulsations Part Two: Reynolds Number Surveys,* M.S. Thesis, Naval Postgraduate School, Monterey, California, March 1991.

23. Thermosciences Division, Department of Mechanical Engineering, Stanford University Report TF-30, *Instability and Transition in Curved Channel Flow*, by W.H. Finlay, J.B. Keller, and J.H. Ferziger, Stanford, California, May 1987.

24. Finlay, W.H., Keller, J.B. and Ferziger, J.H., "Finite Amplitude Vortices in Curved Channel Flow," *Journal of Fluid Mechanics*, v. 194, pp. 417-456, September 1988.

25. Clauser, F.H., "Turbulent Boundary Layers in Adverse Pressure Gradients," *Journal of the Aeronautical Sciences*, pp. 91-108, February 1954.

26. Kreplin, H. and Eckelmann, H., "Propagation of Perturbations in the Viscous Sublayer and Adjacent Wall Regions", *Journal of Fluid Mechanics*, v. 95, p. 305, 1979.

27. Morrow, D.S., *Transition Phenomena in a Straight Channel With a 40 to 1 Aspect Ratio With and Without Imposed Pulsations Part I: Near-Wall and Central Region Profiles,* M.S. Thesis, Naval Postgraduate School, Monterey, California, March 1991.

INITIAL DISTRIBUTION LIST

		No. Copies
1.	Defense Technical Information Center Cameron Station Alexandria, Virginia 22304-6145	2
2.	Library, Code 0142 Naval Postgraduate School Monterey, California 93943-5002	2
3.	Department Chairman, Code ME Department of Mechanical Engineering Naval Postgraduate School Monterey, California 93943-5000	1
4.	Naval Engineering Curricular Officer, Code ME Department of Mechanical Engineering Naval Postgraduate School Monterey, California 93943-5004	1
5.	Professor Phillip M. Ligrani Code ME/Li Department of Mechanical Engineering Naval Postgraduate School Monterey, California 93943-5000	3
6.	Professor Chelakara S. Subramanian Code ME/Su Department of Mechanical Engineering Naval Postgraduate School Monterey, California 93943-5000	2
7.	Dr. K.C. Civinskas Propulsion Directorate U.S. Army Aviation Research and Technology Activity AVSCOM NASA-Lewis Research Center Cleveland, Ohio 45433	2
8.	LT Steven J. Fuqua 20 Maid Marion Drive Gales Ferry, Connecticut 06335	2

Thesis
F939 Fuqua
c.1 Study of the transition
to turbulence within a
curved rectangular channel
with 40 to 1 aspect ratio.